THE UNIVERSITY *of* EDINBURGH

REDUCTIVE FUNCTIONALISATION OF THE URANYL DICATION

Anne-Frédérique PECHARMAN

A Thesis submitted for the degree of
Doctor of Philosophy
At
The University of Edinburgh
2012

Declaration

The work presented in this thesis is original work of the author, except where specific reference has been made to other sources. It was composed by the author and has not been submitted, in whole or in part, for any other degree.

Anne-Frédérique Pécharman

November 2012

Abstract

This thesis describes the synthesis and reactivity studies of the actinyl dications $[AnO_2]^{2+}$ in a variety of oxidation states.

Chapter one introduces the importance of the chemistry of actinyl cations in nuclear technology and in the environment, and in particular the chemistry of uranyl dication, which is very stable in the higher oxidation state and considered to be chemically-inert.

In Chapter two, on the synthesis of the new macrocyclic Pacman complex $[UO_2(S)(H_2L)]$ is reported and its reactivity with differing amounts of lithium bases evaluated, so providing insight into the single electron reduction of the uranyl dication.

Chapter three is focused on the reactions of the lithiated complexes generated in Chapter two towards acid and silyl sources to obtain complexes in which the oxo-group is further functionalised and to provide mechanistic insight into uranyl immobilisation.

Chapter four evaluates the reactivity of the uranyl(VI) Pacman complex $[UO_2(S)(H_2L)]$ with $[Zn\{N(SiMe_3)_2\}Cl]$ to obtain another routes to form the complex $[(Me_3SiO)UO(THF)(ZnCl)_2(L)]$ and the reactivity with different sources of potassium base, and provides a comparison to the analogues Li-base reactions described in Chapter two. The reactivity of the potassiated and lithiated complexes towards a variety of transition metals are described.

Chapter five contains a summary and conclusions on this work.

Chapter six presents full experimental details and analytical data.

Acknowledgements

I would like to thank my supervisors Prof. Polly L. Arnold and Dr Jason B. Love for the opportunity they gave me to work with them. I would like also to thank them for their support, guidance and encouragements during these three years. I really appreciate the availability that you have to discuss about the subject and to try to answer to the different questions that I could have.

My thanks also go to the past and present members of the Arnold and the Love groups. It has been nice to work and socialise with all of you. You all make the lab a friendly place to work. I would like to thank Dr Jean-Charles Buffet, Dr Aline Devoille, Dr Natalie Potter and Dr James Leeland for the help in the lab and the English lessons.

I would like to thank Prof. Cacciuffo for giving me the opportunity to stay in Karlsruhe and work in his hot laboratory. Thanks also to his group for the welcoming.

I would like to acknowledge Prof Laurent Maron and Dr Ahmed Yahia for the DFT calculations. I would like also acknowledge Mr Juraj Bella and Dr Marika Decremoux for NMR spectroscopy, the Parsons group for the help in crystallography.

My thanks also go to my parents and my family for the support and encouragements in my study and through all my choices.

I would like to thank all my friends I made in Edinburgh, I am so happy that I met you, thanks to Anne for all the parties that we went during three years, thanks to the French Friends that I met here and for the French food that we shared.

Abbreviations

General

°	degrees
°C	degrees Celsius
Å	Angstrom
acac	acetylacetonato
acnac	*β*-ketoiminate, NC(Ph)CHC(Ph)O
^{t}Bu	*tert*-butyl
ca	circa about
CCI	cation cation interaction
Cp	cyclopentadienyl
DHA	dihydroanthracen
DMF	dimethylformaldehyde
DMSO	dimethylsulfoxide
endo	endogenous
Et_2O	diethyl ether
EtOH	ethanol
exo	exogenous
Fc	ferrocene
g	gram(s)
h	hour(s)
IR	infrared
K	Kelvin
LDA	lithium diisopropylamine
Me	methyl
MeOH	methanol
min	minute(s)
mL	millilitre(s)
µL	microlitre(s)
M	$mol.L^{-1}$
mol	mole(s)

mmol	millimole(s)
Ph	phenyl
^{i}Pr	*iso*-propyl
py	pyridine
RT	room temperature
TFA	trifluoroacetic acid
THF	tetrahydrofuran

Nuclear Magnetic Resonance spectroscopic data

δ	chemical shift in ppm
J	coupling constant
Hz	hertz
MHz	megahertz
NMR	nuclear magnetic resonance
ppm	part per million
s	singlet
d	doublet

Table of contents

Chapter 1: Introduction

1.1. Uranyl dication $[UO_2]^{2+}$

The chemistry of the actinyl cation plays a critical role in nuclear technology and in the environmental mobility of actinides. Indeed, over 60 years of nuclear weapon and energy production have lead to a significant amount of radioactive waste.[1] The majority of high oxidation state complexes of the actinides contain the actinyl ion $[AnO_2]^{n+}$ (An = U, Np, Pu; n = 1 or 2). The actinyl dications are essentially linear, that is in contrast to the transition metal dioxo complexes that adopt bent geometries.[2] Actinides such as neptunium, plutonium or americium are stable in the 5+ oxidation state $[AnO_2]^{+}$ form (An = U, Np, Pu) and isolable, however, for the uranium, this form is usually not stable and disproportionates into U(IV) and U(VI) species. The uranyl in the 5+ oxidation state is key to understanding the processes of the transformation of uranyl (VI) to uranium (IV), which is insoluble in water and can be immobilised, Equation (**1**).[3,4]

$$2\,[UO_2]^{+} \longrightarrow [UO_2]^{2+} + U^{IV} \quad \textbf{(1)}$$

Uranium is the only one of the aforementioned actinides to occur naturally in the environment and the least radioactive of the actinyl and so is the most studied. The uranyl dication $[UO_2]^{2+}$ is the prevalent form of uranium. In the 6+ oxidation state the U-O bonds are particularly thermodynamically strong and kinetically inert due to the overlap of a combination of metal 5f and 6d and oxygen 2p orbitals to produce one σ and two π bonds with a formal triple U-O bond order.[3-5] The generation of these hybrid orbitals at uranium for axial bonding leaves few orbitals with which to bind all other ligands at the uranium centre. Also the inverse trans influence effect plays a role in the covalent interactions between the oxo ligands and the metal f orbitals which strengthen the two trans U=O bonds. This is in contrast to transition metal where the metal oxo bond is weakened when a strong ligand is in the *trans* position (trans influence).[6] Almost without exception, these remaining ligands

bind in the equatorial plane perpendicular to the O=U=O axis.[5,7] This is also in contrast to the transition metal dioxo complexes, where the metal oxo bonds are reactive and are involved in a variety of catalytic and stoichiometric reactions such as hydrocarbon oxidation, oxygen atom transfer and cycloaddition reactions (Scheme 1).[8,9]

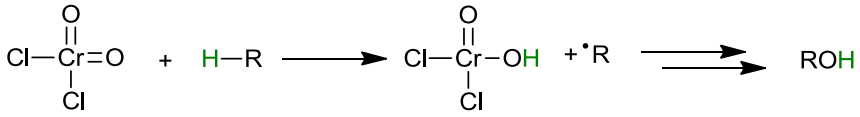

Scheme 1: Oxidation of alkanes

1.2. The uranyl dication in the environment

The chemistry of uranium is dominated by the dioxo uranyl dication $[UO_2]^{2+}$, which is found in aqueous solution and in the solid state. Due to its high solubility and mobility some concerns have been emitted about the long term storage of nuclear waste.[10] In the last ten years, a growing interest in the reduction of the uranyl dication appears and tries to reproduce nature. Researchers are actively investigating ways to take advantage of the vast differences in aqueous solubility between the more soluble $[UO_2]^{2+}$ species and highly insoluble U(IV) species to immobilize uranium, taking examples on the different reduction process present in nature such as metal-reducing microbial organisms,[11-13] natural mineral surfaces[14] and photochemical process.[15-17] Indeed the uranyl dication can undergo bacterial anaerobic reduction where the U(VI) can be reduced to U(IV) by electron transfer by Fe(III)-reducing microorganisms, then the U(IV) precipitates as uranite. These organisms are unable to reduce actinides in the 5+ oxidation state, therefore it is most likely that the reduction of $[UO_2]^{+}$ to U(IV) proceeds via disproportionation.[11-13] This reduction could be interesting for the bioremediation of uranium-contaminated groundwater and to identify a potential mechanism for the biodeposition of uranium ores. In another study, the X-ray absorption spectroscopy shows that a subsurface metal-reducing *bacterium Geobacter sulfurreducens* reduces U(VI) by one electron reduction to form $[UO_2]^{+}$, which is unstable.[13] The final insoluble product U(IV) could be formed from a further reduction of $[UO_2]^{+}$ to U(IV) or from the disproportionation of $[UO_2]^{+}$.

In the case of the natural mineral surfaces, the homogeneous reduction of the uranyl dication by aqueous Fe^{2+} in the presence of hematite particles (α-Fe_2O_3) is quicker. The first step of the reduction is the adsorption of the neutral $UO_2(OH)_2$ species onto the hematite surface schown in Equation (**2**) (≡FeOH symbolises a reactive site).[14]

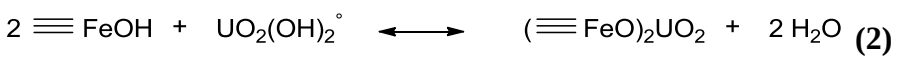

(2)

These adsorbed uranyl ions onto the reactive site are reductively transformed to intermediate unstable U(V) species. These unstable species disproportionate to U(IV) species described as UO_2(s) in the equation and to U(VI) which is adsorbed uranyl species onto reactive sites, Equations **3** and **4**.

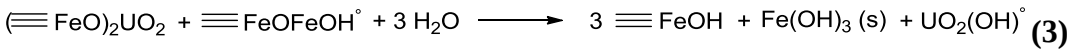

(3)

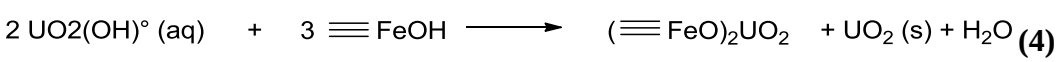

(4)

1.3. Uranyl dication in 6+ oxidation state

1.3.1. Uranyl (VI) dication and ligand design

Due to the *trans*-configuration of the oxo groups of the uranyl dication, the linear uranyl dication is coordinated with four, five or six ligands only in the equatorial plane.[18]

The use of ligands offers an opportunity to synthesise stable macrocyclic complexes of f-block metal ions to explore the bonding parameters and to tap their potential uses. The challenge is to design macrocycles with appropriate ligand design features required to form complexes that can undergo reduction and avoid the disproportionation of the uranyl (V) complexes.

Deshayes and co-workers reported that appropriate crown ethers are able to complex actinyl cation within the compartment. In the case of the uranyl dication, the 18-crown-6 ether cavity has the right size for the uranyl dication.[19] The solid state structure of the complex [UO_2(18-crown-6)] shows that the six equatorial oxygen

atoms are approximately co-planar (Figure 1). The same chemistry has been developed by Clark and co-workers for neptunyl chemistry.[20]

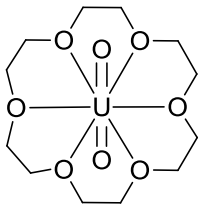

Figure 1: Structure of $[UO_2(18\text{-crown-6})]$

Thuéry and co-workers presented in 1999 the formation of a trigonal coordination of the uranyl dication.[21] The formation of the complex $[UO_2(L)(HNEt_3)].3H_2O$ (LH_3 = p-tert-butylhexahomotrioxacalix[3]arene) has been described and the solid state structure presents a pseudo trigonal axis; the uranium centre is located along this axis and is bonded to the three deprotonated phenolic oxygen atoms in the equatorial plane (Figure 2). The calixarene conformation in this example is a *cone* one.

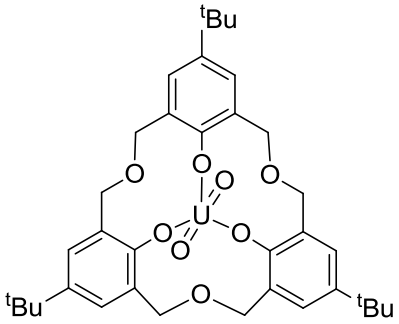

Figure 2: Structure of $[UO_2(L)(HNEt_3)].3H_2O$

We know that porphyrins, phthalocyanines and pyrrole-based macrocycles are used to support reaction chemistry and catalysis by transition metal cations. However, only a few examples for uranyl complexation are known, because of the size of the cavity. The uranium centre is not capable to sit above the plane of the ligand.[22]

The first characterised structurally actinide porphyrin complex was reported in 1975 by Marks and co-workers (Figure 3).[23] The solid state structure shows the complexation of a uranyl cation with an expanded phthalocyanine, so-called superphthalocyanine. The macrocycle has five pyrrole-type subunits; the five-type subunits are coordinated to the uranyl cation in the equatorial plane. This complex was designed to be used in extraction process, but because of the decomposition of the ligand under the conditions of demetallation, its use was limited.

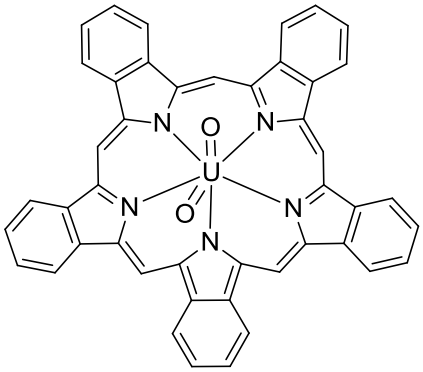

Figure 3: Structure of a uranyl superphthalocyanine complex

Pentaphyrins are derivatives of porphyrin ligands. They are an interesting class of potentially dianionic, pentadentate ligands. Sessler and co-workers reported the synthesis of decaalkyl pentaphyrin.[24] The condensation of this ligand with the uranyl dication leads to the formation of the first structurally characterised actinide complex of pyrrole-derived expanded porphyrins (Figure 4). The complex is obtained as a green solid after purification. The solid state structure shows that the uranyl cation displays a pentagonal bipyramidal geometry and is coordinated in the centre of the pentaphyrin but the macrocycle is distorted from planarity. The uranium atom is located at the centre of the saddle-shaped pentaphyrin, with the distortion from planarity being due to the bonding demands of the uranyl dication. The complex is more soluble in organic solvent and is more stable than the aforementioned uranyl superphthalocyanine complex.

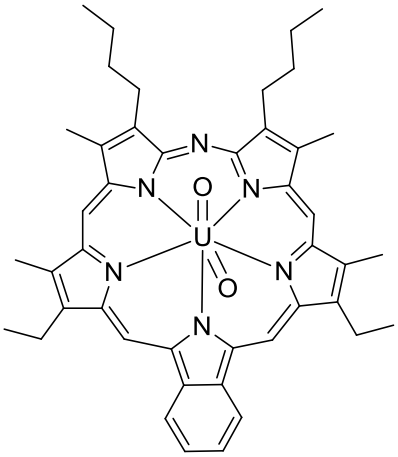

Figure 4: Structure of a uranyl pentaphyrin complex

The ease of the formation of the uranyl pentaphyrin complex, where the macrocycle may be made in the absence of uranyl or template cations, the straightforward synthesis and its stability led Sessler and co-workers to reinvestigate the use of sapphyrin as ligand for the complexation with a uranyl cation.[25] Sapphyrin undergoes a rapid reaction with the uranyl cation in a mixure of methanol, pyridine and triethylamine (Figure 5). The solid state structure confirms the presence of uranyl cation and its complexation with the sapphyrin ligand. The structure shows that the ligand has undergone attack by methoxide anion at the *meso*-carbon resulting in a disruption of the inherent two-fold symmetry of the macrocycle. This addition result also in a loss of overall aromaticity. The uranium centre lies in the plane of the nitrogen donors and is chelated in a saddle-shaped pentagonal planar arrangement.

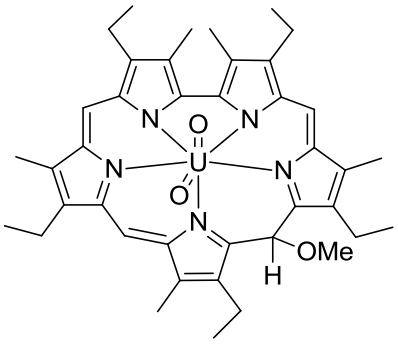

Figure 5: Structure of a uranyl sapphyrin complex

Another example of expanded porphyrin has been reported by Sessler and co-workers. They described the synthesis of the [24]hexaphyrin (1.0.1.0.0.0), which in its oxidised, aromatic form is capable of complexation of actinide ions.[26] The complexation of the ligand with a uranyl dication leads to a dramatic change in the shift of the different resonances (Figure 6). This is consistent with the ring current effect becoming "reversed" as oxidation occurs and aromaticity is induced. The solid state structure confirms the formation of the complex. The uranium centre is bound to the six nitrogen atom from the macrocycle in a planar fashion. The coordination environment of the uranium displays a distorted hexagonal bipyramidal geometry.

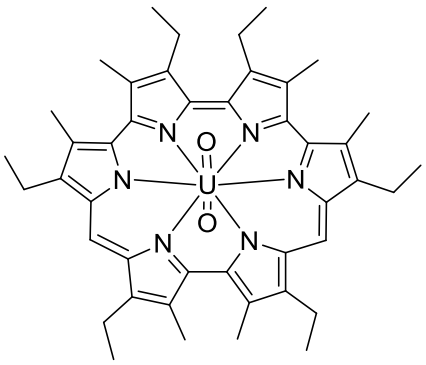

Figure 6: Complexation of an expanded porphyrin, hexaphyrin with a uranyl dictaion

The salen ligand has been known since the mid nineteenth century and is well established in the area of metal coordination chemistry.[27] This ligand forms a tetradentate cleft with two nitrogen and two oxygen atoms. There are a lot of different salen ligands due to the straightforward functionalisation of the precursors.

The formation of uranyl salophen complexes leads to the coordination of small molecules to the uranyl; the uranyl cation adopts usually a pentacoordinate environment. Reinhoudt and co-workers reported the coordination of urea to a uranyl salen complex (Figure 7).[28] The ligand has an attached crown ether as a second cavity, which interacts with urea by hydrogen bonding with the oxygen atom. The carbonyl oxygen of the urea occupies the fifth site of the uranium centre. There is a myriad of asymmetric compartmental ligand where the uranyl dication as a preference to coordinate within the cleft of the Schiff base compartment.[29]

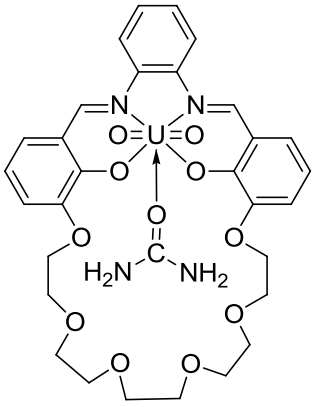

Figure 7: Coordination of urea to a uranyl salen complex

This complex and the derivative complexes have been used to study anion-facilitated transport through supported liquid membranes, or used as dihydrogenphosphate sensors when incorporated into a polymeric membrane.

Sessler and co-workers have considered the possibility to increase the size of the cavity of the ligand and so make other pyrrole-containing "porphyrin-like" systems, incorporating pentagonal planar or hexagonal planar ligand field to stabilize the formation of uranyl (VI) complexes. They reported the first hexadentate pyrrole-derived uranyl Schiff base complex, so-called uranyl-alaskaphyrin (Figure 8).[30] The complex was fully characterised. The solid state structure shows that the uranyl dication is coordinated to all six nitrogen atoms in a planar fashion; the complex is remarkably planar, the maximum deviation from planarity is 0.011(7) Å. The structure is different to those observed in the different "porphyrin-like" systems. As a result, the uranium displays a hexagonal bipyramidal geometry. The complex is stable and does not undergo decomposition or demetallation.

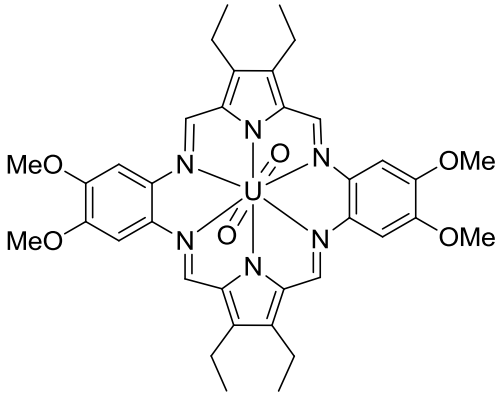

Figure 8: Structure of a uranyl monoxasapharyn complex

The ability of certain expanded porphyrins to stabilise nonlabile, in-plane complexes with the early actinides in their high valent oxo cation is in contrast with tetrapyrrolic congeners (e.g., porphyrins, phthalocyanines). Sessler and co-workers presented the complexation between uranyl and different alaskaphyrin ligands (Figure 9).[31] The condensation between different functionalised diformyl pyrroles and *o*-phenylenediamine derivatives in the presence of proton sponge and uranyl acetate leads to the formation to the complex. These complexes have been used for the application in uranyl containing liquid crystals.

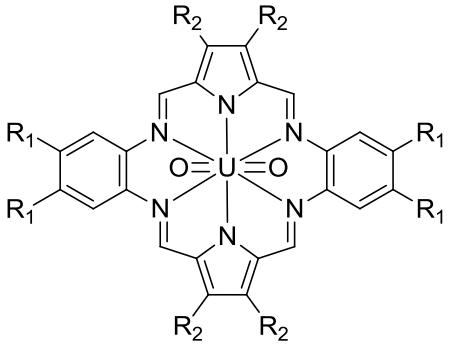

$R_1 = R_2 = O(CH_2)_5CH_3$
$R_1 = R_2 = O(CH_2)_9(CH_3)$
$R_1 = R_2 = O(CH_2)_{13}(CH_3)$

Figure 9: Complexation of uranyl dication with alaskaphyrin ligands

Sessler and co-workers and Love and co-workers reported the use of a polypyrrolic, potentially dinucleating macrocyclic ligand H_4L' forms a dinucleating iron or palladium complex with a well defined molecular cleft, the complex adopts a Pacman structure.[32,33] Arnold, Love and co-workers reported the use of this ligand to form a new uranyl complex $[UO_2(THF)(H_2L)]$ by the reaction of the macrocycle with uranyl silylamide $[UO_2(THF)_2\{N(SiMe_3)_2\}_2]$ (Scheme 2).[34] The complex was characterised by NMR, FTIR spectroscopy and by X-ray diffraction studies. The solid state structure shows that one N4-donor set is sufficiently flexible to accommodate the uranyl dication. The uranium centre is five-coordinate in the equatorial plane with an oxygen atom of a THF molecule occupying the fifth site. The uranium centre displays a pentagonal bipyramidal geometry. The large and flexible macrocycle is able to accommodate the uranyl dication in a way that dinucleating, cofacial diporphyrin ligands cannot, and that the tendency of this ligand set to promote hinged, Pacman topologies could be exploited to study the chemistry of the uranyl ion. The presence of the rigid, bridging aryl group between the two compartments results in the bent structural motif with one group located within the cleft. The complex adopts a Pacman structure with desymmetrisation of the uranyl and a vacant N_4-donor compartment. The oxo groups are in two different environments, the *exo* group is outside the ligand and the *endo* group is in the cleft of the ligand. The lower N4-donor compartment is oriented such that a hydrogen bond is evident between the pyrrole NH group and the *endo*-oxo group.

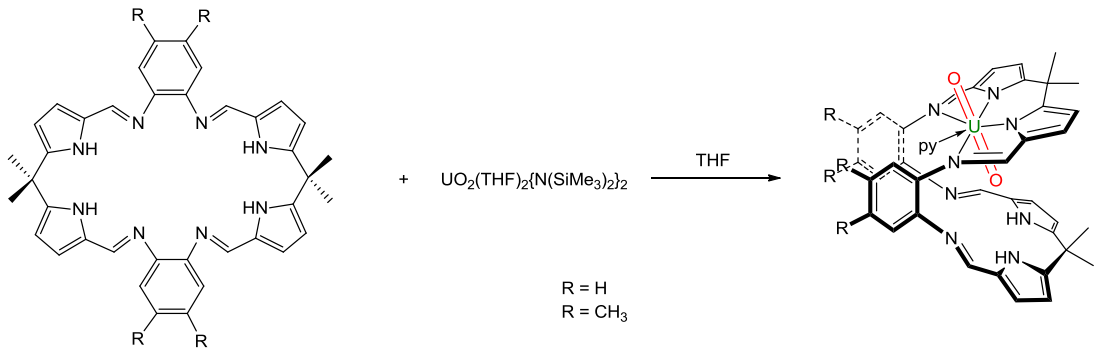

Scheme 2: Synthesis of the uranyl Pacman complexes

1.3.2. Cation-cation interactions of $[UO_2]^{2+}$

Cation-cation interactions are a specific feature of the chemistry of actinyl ions in solution, particularly so for pentavalent ions. Actinyl complexes that display Lewis base interactions between the oxo and a metal counterion, that is $AnO_2^+ \bullet\bullet\bullet M^+$ are called cation-cation interactions. These interactions are important in neptunium and plutonium chemistry, these interactions affect the behaviour of $[NpO_2]^+$ in redox reactions and separation process,[35-39] but are rarely observed for $[UO_2]^{2+}$ (around 1%). The discrepancy between the behaviour of $[NpO_2]^+$ and $[UO_2]^{2+}$ likely arises from the differences in Lewis basicity of their oxo ligand. The neptunium in this cation possesses a $5f^2$ electron configuration which increases the electrostatic repulsion between the metal and the oxo groups, but in the case of the uranyl, the uranium has a $5f^0$ configuration, so lacks in electrostatic interaction.[5,40]

The first cation-cation interaction was observed by Sullivan and co workers in the 1960s. They showed that neptunyl(V) ions in a aqueous perchloric acid media interacts with uranyl(VI).[41] They also showed that neptunyl(V) interacts with chromium(III) ions via the axial oxygen forming the cation-cation complex O-Np(V)-O-Cr(III).[42,43]

The addition of strong σ-donating ligands such as hydroxide, alkoxides, and amines would likely weaken the U=O bond.[44-46] In 1999, Clark and co-workers showed that the addition of hydroxide ligand in the equatorial plane weakens the U=O bond. This phenomenon is confirmed by Raman spectroscopy where a shift of 84 cm^{-1} is observed and by X-ray diffraction studies where a lengthening of the U=O bond is observed.[44] Another example of the weakening of the U=O bond was reported by Burns and co-workers. They reported that the successive addition of silylamide ligands to the uranyl ion leads to a decrease of the U=O symmetric stretching frequency in Raman and IR spectroscopy (Scheme 3).[47]

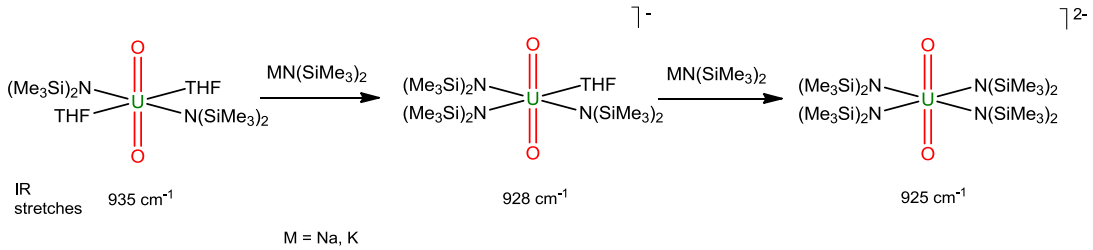

Scheme 3: Successive addition of $[MN(SiMe_3)_2]$ to the uranyl complexes

This weakening increases the basicity of the oxo ligands and so the reactivity of the oxo ligands towards the addition of the metal counter ion is shown by Burns and co-workers.[47] They observed the interaction of the sodium cation with one oxo group and the weakening of the U=O bond in the X-ray diffraction studies. In the solid state structure, the uranium centre displays a relatively undistorted trigonal bipyramidal geometry; the three amido nitrogen occupy the equatorial plane (Figure 10). The U=O length in the complex $[Na(THF)_2][UO_2\{N(SiMe_3)_2\}_3]$ (1.810(5) Å) is elongated in comparison to that in the complex $[UO_2\{N(SiMe_3)_2\}]$ (1.781(5) Å), which implies a weakening of the U=O bond by the interaction with the sodium ion.

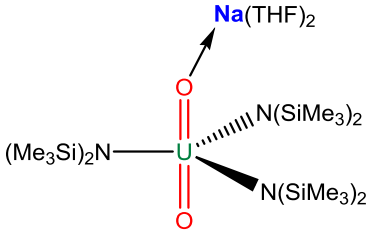

Figure 10: Structure of $[Na(THF)_2][UO_2\{N(SiMe_3)_2\}_3]$

Runde and co-workers reported in 2001 the interaction of alkali metal crown ether with both uranyl oxo groups.[48] The complexes $[Li(12\text{-crown-}4)]_2[UO_2X_4]$ (X = Cl or Br) exhibit interactions between the crown encapsulated lithium ions and the uranyl oxo group, forming a cation-cation complex. The uranium centre has four equatorial halide atoms. The U=O bonds are 1.767(9) Å for the chloride complex and 1.79(1) Å for the bromide complex, and are in the range of the experimental and calculated $[UO_2]^{2+}$ (Figure 11).[36,49,50]

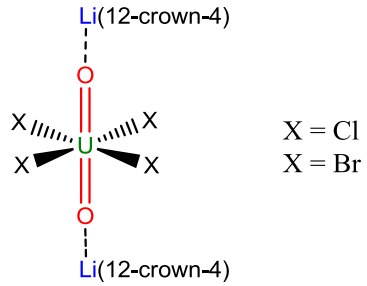

Figure 11: Structure of $[Li(12\text{-crown-4})]_2[UO_2Cl_4]$ and $[Li(12\text{-crown-4})]_2[UO_2Br_4]$.

In 2004, Sarsfield and co-workers reported the synthesis of the first non-metal Lewis acid functionalized uranyl complex.[51] The complex $[UO\{OB(C_6F_5)_3\}(NCN)_2]$ (NCN = $\{(SiMe_3N)CPh(NSiMe_3)\}$) exhibits a significant change in the functionalised U=O bond length (1.898(3) Å), which is longer than the uncoordinated U=O bond length (1.770(3) Å), the U=O−B interaction appears stronger than in the case of cation-cation interaction between the oxo ligands and an alkali metal judging by the changes observed in the U=O bond lengths. This change in bond length can be also observed by Raman spectroscopy by a decrease in the symmetric stretching frequency (780 cm^{-1}) compared to the precursor (803 cm^{-1}). This coordination is maintained in solution; the ^{11}B NMR spectrum exhibits a resonance at −10.6 ppm in C_6D_6 (60 ppm for $B(C_6F_5)_3$) (Figure 12).

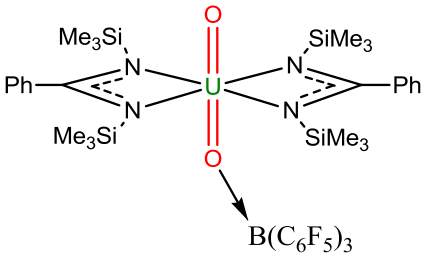

Figure 12: Structure of $[UO\{OB(C_6F_5)_3\}(NCN)_2]$

They have also reported the formation of a cation-cation interaction between a sodium cation and one of the oxo ligands in the complex $[Na(THF)_2(PhCN)_{0.5}][UO_2(NCN)_3]$ (Scheme 4).[46] The complex has three bidentate benzaminato ligands, which are arranged in a propeller-like structure around the

uranyl dication. The UO bonds are unsymmetrical because of the coordination of a sodium ion to an oxo group. They observed a weakening of the oxo ligand by the elongation of the U=O bond interacting with the sodium cation (1.812(3) Å). The IR spectrum shows a shift of the symmetric UO stretch by 61 cm^{-1} from 834 cm^{-1} to 773 cm^{-1}. This weakening suggests that the electron-donating ability of the equatorial ligands influences the Lewis basic properties of the uranyl oxo groups. The addition of water to this complex leads to the formation of a new complex $[Na(THF)UO_2(NCN)_2]_2(\mu_2\text{-}O)$ with cation-cation interaction between all the oxo group and sodium cation. The structure consists of two parallel uranyl units, each coordinated to two NCN ligands, and bridged by an oxide group. The oxo ligands are stabilised in a parallel arrangement with short interatomic contacts to two sodium ions. The X-ray diffraction studies and the IR spectroscopy show the weakening of the UO bond with the elongation of the bonds (1.795(12) Å and 1.828(12) Å) and the shift of the symmetric UO stretch (757 cm^{-1}).

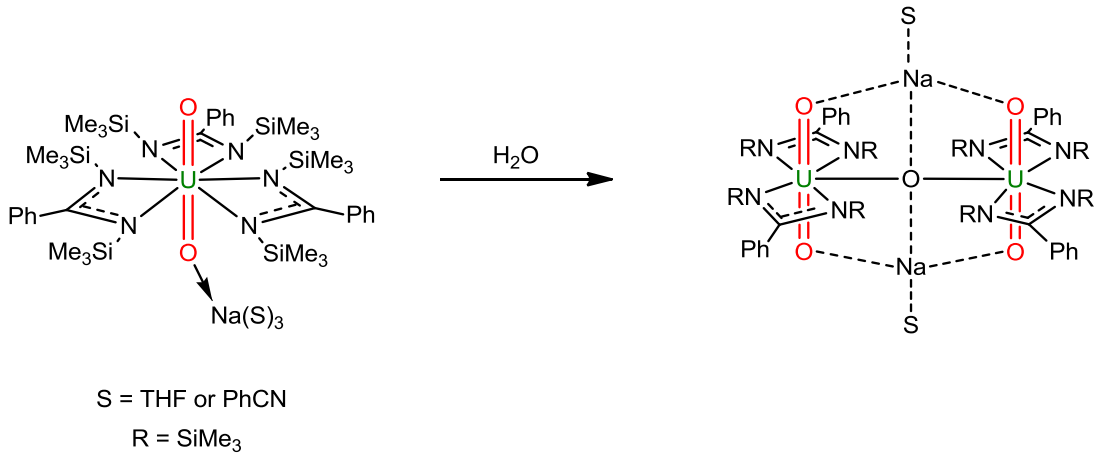

Scheme 4: Structure of $[Na(THF)_2(PhCN)_{0.5}][UO_2(NCN)_3]$ and synthesis of $[Na(THF)UO_2(NCN)_2]_2(\mu_2\text{-}O)$

Another example of borane interaction has been reported by Hayton and co-workers, where the addition of two equivalents of $B(C_6F_5)_3$ to a solution of $[UO_2(^{Ar}acnac)_2]$ (Ar = 3,5 $^{t}BuC_6H_3$) leads to the formation of the complex $[UO\{OB(C_6F_5)_3\}(^{Ar}acnac)_2]$ (Figure 13).[52] The solid state structure shows that the uranium centre displays a octahedral geometry, with one $B(C_6F_5)_3$ coordinated to one

oxo group. The U=O(B{C_6F_5}$_3$) bond is elongated (1.890(4) Å) and is in the range of the one observed in the complex [UO{OB(C_6F_5)$_3$}(NCN)$_2$].[51] The complex also exhibits a U=O stretch at 845 cm^{-1}, which is shifted by 56 cm^{-1} in comparison to the starting complex and is also in the range of the IR stretch in the complex [UO{OB(C_6F_5)$_3$}(NCN)$_2$] (Figure 12). The X-ray diffraction studies and the IR spectroscopy confirm the weakening of the UO bond.

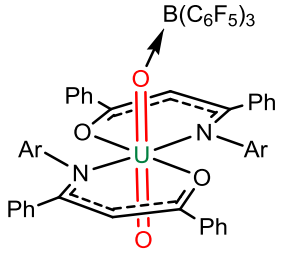

Figure 13: Structure of [UO{OB(C_6F_5)$_3$}(^{Ar}acnac)$_2$]

Wilkerson and co-workers reported the formation of a CCI between the uranyl dication and another uranium in the tetrameric complex [UO_2{OCH(^{i}Pr)$_2$}$_2$]$_4$ (Figure 14).[45] The spectroscopic data show that the U=O bond is weakening in comparison to other uranyl dication. Indeed, the coordination geometry around each uranium centre can be considered as a distorted octahedron and the study of the bond length shows an elongation of the U=O bond (1.846(4) Å) interacting with another uranium centre. This length is in the same range than the one described in the precedent complex [Na(THF)UO_2(NCN)$_2$]$_2$(μ_2-O). The symmetric stretch of U=O bond observed in the Raman spectrum is shifted drastically at 713 cm^{-1} in comparison to the average of the uranyl group (~ 860 cm^{-1}).

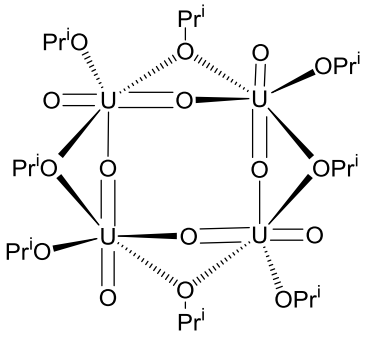

Figure 14: Structure of $[UO_2\{OCH(^iPr)_2\}_2]_4$ showing T-shaped complexation

In 2006, our groups reported the selective functionalisation of the uranyl ion with a transition metal.[36] The reaction between the uranyl(VI) macrocycle $[UO_2(THF)(H_2L')]$ and $[M\{N(SiMe_3)_2\}_2]$ (M = Mn, Fe, Co) leads to the formation of $[UO_2(THF)M(THF)(L')]$ in a moderate yield (Scheme 5). The manganese and cobalt complexes have been characterised in the solid state by X-ray diffraction studies and are essentially isostructural. The uranium centre is seven coordinate and displays a distorted pentagonal bipyramidal geometry with the oxo groups retaining a *trans* arrangement. The *endo*-oxo group is bounded to the transition metal by a direct donor bond. The *endo* U=O bond for the complex $[UO_2(THF)Mn(THF)(L')]$ (1.808(4) Å) is elongated in comparison the uranyl Pacman complex $[UO_2(THF)(H_2L')]$ (1.790(4) Å). The IR and Raman spectra are complicated by overlapping ligand absorptions. In the Raman spectrum, the absorption of each complexes at 811cm^{-1} (Mn), 804cm^{-1} (Fe), 807cm^{-1} (Co) is absent in the similarly Pacman-shaped complex Cu_2L. They are the first molecular complexes that exhibit a cation-cation interaction between the uranyl dication and a transition metal cation that is retained in solution and the solid state (Scheme 5).

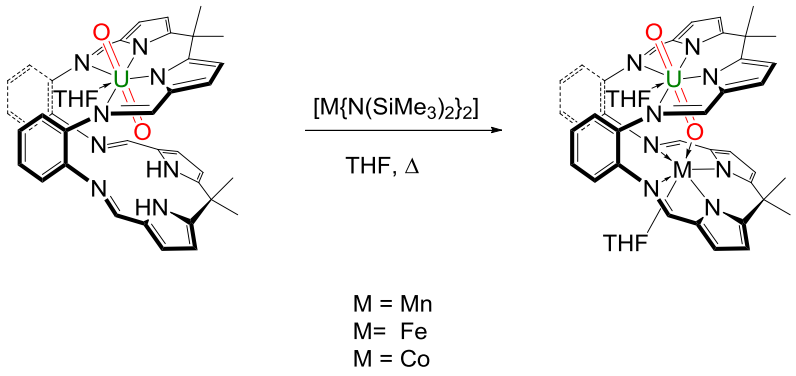

Scheme 5: Synthesis of a complex containing a CCI between uranyl and a transition metal cation

1.4. Reduction of uranyl $[UO_2]^{2+}$

The reduction of the uranyl dication can be done by electrochemical reactions, photochemical reactions or chemical reactions. Here we will show a few examples of each reaction.

1.4.1. Reduction of the uranyl dication by electrochemical reactions

The reduction potentials of many uranyl complexes are known and show that the ligands coordinated in the equatorial plane have an effect on the observed U(VI)/U(V) redox potentials.[40,53-56] Indeed, the biggest reduction potentials belong to the complexes containing strongly electron donating ligands (Figure 15).[54,55] As a result, strong reducing agents, such as Cp_2^*Co (−1.94 V *vs* Fc^+/Fc) can reduce the uranyl complexes with high redox potentials as observed by Hayton and co-workers. Weaker donors tend to have a small effect on the reduction potential of $[UO_2]^{2+}$ as seen in the acetate or DMSO uranyl complexes.

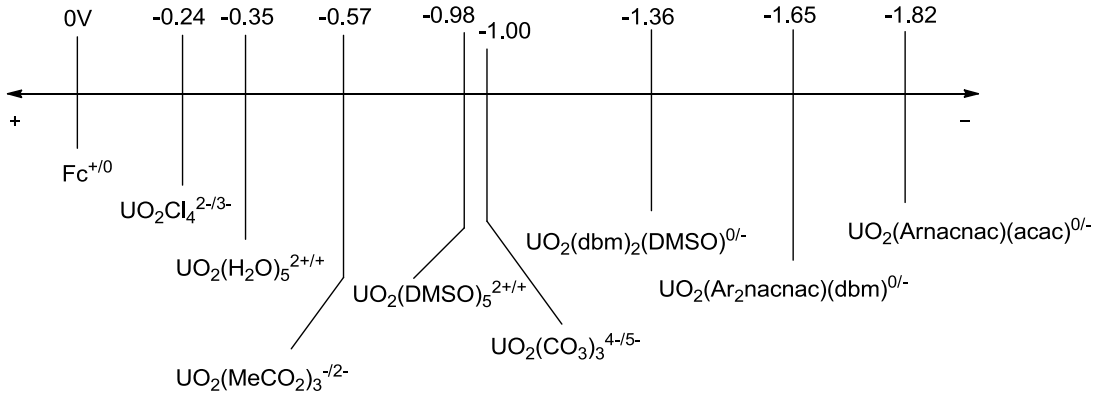

Figure 15: U(VI)/U(V) reduction potentials (*vs* Fc^+/Fc) of selected uranyl complexes

Electrochemical reactions of the uranyl complexes have been studied in aqueous and non-aqueous solutions. Ikeda and co-workers have studied the chemical properties of the actinyl ions in basic media because of the weak alkalinity of deep ground water (pH = 9).[57] They reported that the uranyl dication in carbonate and bicarbonate media is in the $[UO_2(CO_3)_3]^{4-}$ form. The reduction of this complex in bicarbonate media results in the formation of U(IV) from the disproportionation. In the carbonate media (at pH > 11), the complex undergoes quasi-reversible reduction and forms a stable uranyl complex, Equation (**5**).

$$\left[UO_2(CO_3)_3\right]^{4-} + e^- \rightleftharpoons \left[UO_2(CO_3)_3\right]^{5-} \qquad E^0 = -0.85\ V\ (vs\ Ag/AgCl) \quad \textbf{(5)}$$

In the case of the aqua uranyl complex in acidic perchlorate solution, the complex is quasi-reversibly reduced at the Pt electrode. Then the uranyl species in the 5+ oxidation state is further reduced irreversibly to U(IV) (Figure 16).

$$UO_2^{2+} + e^- \rightleftharpoons UO_2^+ \qquad \text{(quasi-reversible)}$$

$$UO_2^+ + H^+ + e^- \longrightarrow UOOH^+ \qquad \text{(irreversible)}$$

$$UOOH^+ + 3\,H^+ \longrightarrow U^{4+} + 2\,H_2O \qquad \text{(irreversible)}$$

Figure 16: Electrochemical reduction of aqua uranyl complex

Ikeda and co-workers reported also the importance in the choice of the ligand in the equatorial plane. Indeed, in 1996, they studied the electrochemical reduction of the complex $[UO_2(acac)_2(DMSO)]$.[58] They showed that the complex is reduced quasi-reversibly and suggested that the electrochemical reduction of $[UO_2(acac)_2(DMSO)]$ proceeds through electron transfer followed by chemical reaction as shown in the equation (Figure 17).

$$[U^{VI}O_2(acac)_2(DMSO)] + e^- \rightleftharpoons [U^{V}O_2(acac)_2(DMSO)]$$

$$[U^{V}O_2(acac)_2(DMSO)] + x\ DMSO \longrightarrow [U^{V}O_2(acac)(uni\text{-}acac)(DMSO)_{x+1}]$$

$$[U^{V}O_2(acac)(uni\text{-}acac)(DMSO)_{x+1}] + DMSO \longrightarrow [U^{V}O_2(acac)(DMSO)_{x+2}] + acac^-$$

Figure 17: Electrochemical reduction of $[UO_2(acac)_2(DMSO)]$

They also studied the stability of the uranyl in the 5+ oxidation state against the different ligands. They demonstrated that the use of salophen (N,N'-disalicylidene-o-phenylenediaminate) as ligand can stabilise the uranyl(V) and that the basic electrochemical reaction of $[UO_2(saloph)(L)]$ (L = DMSO or DMF) in non-aqueous solvents is reduced quasi-reversibly and is accompanied by L dissociation as shown in the scheme 6.[59]

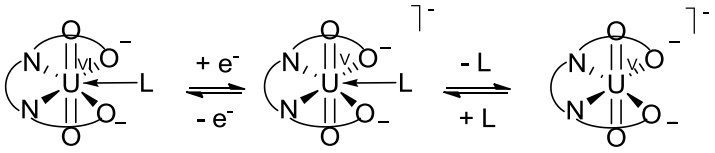

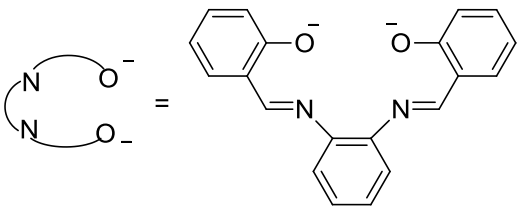

L = DMSO

Scheme 6: Electrochemistry of the complex $[UO_2(saloph)(L)]$

These studies confirm that uranyl complexes with tetradentate ligands in the equatorial plane of the uranyl are more stable than those with uni- or bidentate ligands.

They showed also that the uranyl complexes with high U(VI)/U(V) reduction potential (E^0 values become negative in order of complexes with uni-, bi-, tri- and tetradentate ligand) have more difficulty in the electrochemical reduction and are found to form stable uranyl complexes in the 5+ oxidation state.[60]

They also showed that the use of pentadentate Schiff base ligand avoids the coordination of a solvent molecule in the equatorial plane by fully chelation of the ligand around the uranyl. This phenomenon prevents cation-cation interaction and preserves the stable U(V) species.[18]

1.4.2. Reduction of the uranyl dication by chemical reactions

1.4.2.1.Reduction to uranium(IV)

A few examples of the direct reduction of the uranyl dication into uranium in the 4+ oxidation state are known. Berthet and co-workers showed that the addition of an excess of Me_3SiX (X = Cl, Br, I) to a solution of $UO_2I_2(THF)_3$ in acetonitrile leads to the formation of $UX_4(MeCN)_4$ (Scheme 7).[61] Total deoxygenation of the uranium is observed; this is in contrast to the reaction of $MoOX'_2$ (X' = $\{S_2CN(C_2H_5)_2\}_2$) or CrO_3 with Me_3SiX where only partial deoxygenation occur and lead to the formation of $MoOX'_2X_2$ or CrO_2Cl_2.[62,63] The IR spectrum displays strong stretches for the coordinated nitrile CN and no UO stretch.

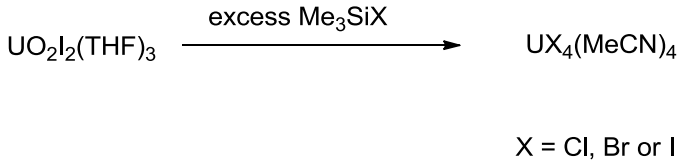

Scheme 7: New routes to tetrahalide $UX_4(MeCN)_4$

Another example is the reduction of $[UO_2]^{2+}$ by U(III). The reaction between $[UO_2(OTf)_2]$ and $U(OTf)_3$ in a mixture pyridine/MeCN affords the U(IV) oxide cluster $[U_6(\mu_3\text{-}O)_8(\mu_2\text{-}OTf)_8(py)_8]$.[64] The structural features of the uranyl moiety are

not preserved upon the reduction, as indicated by the long U-O bond length (average 2.25(3) Å), Equation (**6**).

$$UO_2(OTf)_2 + 2\ U(OTf)_3 \xrightarrow[20\ °C]{py/MeCN} 0.5\ [U_6(\mu_3\text{-}O)_8(\mu_2\text{-}OTf)_8(py)_8] \quad (\mathbf{6})$$

1.4.2.2.Reduction to uranyl(V)

A few uranyl (+V) forms are known but the chemistry is very limited by the instability of the uranium (V). Recent advances have lead to the formation of new and isolable uranyl complexes in the 5+ oxidation state.

Berthet and co-workers reported in 2003 the first uranyl complex in the 5+ oxidation state characterised only in the solid state made serendipitously during the synthesis and crystallisation of anhydrous uranyl triflate compounds. Crystals of $[UO_2(OPPh_3)_4][OTf]$ were obtained from the recrystallisation of $[UO_2(OPPh_3)_4][OTf]_2$ (Figure 18). The uranium centre in the complex $[UO_2(OPPh_3)_4][OTf]$ displays an octahedral geometry; the UO distances 1.817(6) Å and 1.821(6) Å are elongated in comparison to the uranyl(VI) complex $[UO_2(OPPh_3)_4][OTf]_2$ (1.7632(16) Å and 1.7603(15) Å) and are slightly longer than the NpO bond (1.797(2) Å) in the isostructural neptunium ion $[NpO_2(OPPh_3)_4]^+$,in agreement with the variation in the radii of $[UO_2]^+$ and $[NpO_2]^+$ ions.[65]

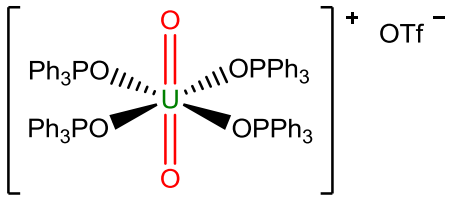

Figure 18: Structure of $[UO_2(OPPh_3)_4][OTf]$

Uranyl in the 5+ oxidation state can be synthesised by electron transfer from a reducing agent. In 2008 Hayton and Wu isolated uranyl(V) complexes by reduction of uranyl (VI) complexes stabilised by equatorial ligands such as phosphine oxide or β-diketonate.[54,66] In the case of the phosphine oxide ligand, the complex was isolated

in a good yield as an orange powder (Scheme 8). The stabilisation of the uranyl (V) complex is due to the bulk of the $[Ar_2nacnac]^-$ ligands anion ($[Ar_2nacnac]^-$ = $[(2,6\text{-}^iPr_2C_6H_3)NC(Me)N(2,6\text{-}^iPr_2C_6H_3)]^-$), which provide steric effect in the equatorial plane and along the O=U=O axis and prevents the formation of CCI that are supposed to be at the origin of disproportionation reactions.[66] The ^1H NMR spectrum of $[UO_2(Ar_2nacnac)(Ph_2MePO)_2]$ indicates the formation of a paramagnetic complex. This complex was characterised in the solid state by X-ray diffraction studies, the uranium centre displays a distorted octahedral geometry. The structure shows a lengthening of the U=O bond (1.810(4) Å and 1.828(4) Å) by 0.05 and 0.08 Å in comparison to the uranyl(VI) complex $[UO_2(Ar_2nacnac)(Ph_2MePO)_2][OTf]$. This is similar to other reported uranyl complexes in the 5+ oxidation state, the IR stretch band of the asymmetric U=O bond observed at 800 cm^{-1} confirms the formation of a uranyl (V) complex with a decrease of 118 cm^{-1} in comparison to the precursor uranyl complex. The UV-vis of $[UO_2(Ar_2nacnac)(Ph_2MePO)_2]$ has an absorption at 755 nm (ε = 56 $L.mol^{-1}.cm^{-1}$) consistent with a *f-f* transition.

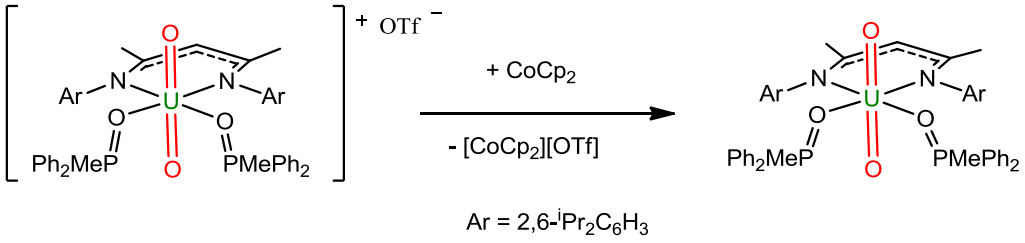

Scheme 8: Synthesis of $[U^VO_2(Ar_2nacnac)(Ph_2MePO)_2]$

The replacement of the phosphine oxide ligands by different β-diketiminate ligands could play a role in the potential reduction of the uranyl dication.[54] Indeed, electrochemical analysis of the uranyl(VI) complexes $[UO_2(Ar_2nacnac)\{RC(O)CHC(O)R\}]$ (R = Me, Ph or CF_3) shows a systematic decrease in the U(VI)/U(V) complex with the variation of the R group on the ligand (R = Me, U(VI)/U(V) = −1.82 V; R = Ph, U(VI)/U(V) = −1.59 V; , R = CF_3, U(VI)/U(V) = −1.39 V (*vs* Fc^+/Fc)). These accessible reduction potentials allow the chemical reduction with Cp'Co (Cp = C_5H_5 or C_5Me_5) in toluene and result in the formation of uranyl(V) complexes $[Cp'Co][UO_2(Ar_2nacnac)\{RC(O)CHC(O)R\}]$ (R

= Me, Cp' =C_5Me_5; R = Ph, Cp' = C_5Me_5; R = CF_3, Cp' = C_5H_5) (Scheme 9). The crystal structure of the complex [UO_2(Ar_2nacnac){RC(O)CHC(O)R}] (R = Ph) consists of a discrete cation/anion pairs; the uranium centre displays a distorted octahedral geometry. Due to the low quality of the crystal, comparisons of the bond lengths are not possible. The IR stretch band of the asymmetric U=O bond observed in the different diketonate ligands (R =Me, ν = 838 cm^{-1}; R = Ph, ν = 844 cm^{-1}; R = CF3, ν = 864 cm^{-1}) are shifted in comparison to their uranyl(VI) analogues. The UV-vis spectra exhibit absorptions at 791 nm (ε = 75 $L.mol^{-1}.cm^{-1}$) and 644 nm (ε = 210 $L.mol^{-1}.cm^{-1}$) for R = Me, 743 nm (ε = 170 $L.mol^{-1}.cm^{-1}$) and 634 nm (ε = 220 $L.mol^{-1}.cm^{-1}$) for R = Ph, 677 nm (ε = 430 $L.mol^{-1}.cm^{-1}$) for R = CF_3. These absorptions are consistent with f-f transition and the presence of $5f^1$ ion.

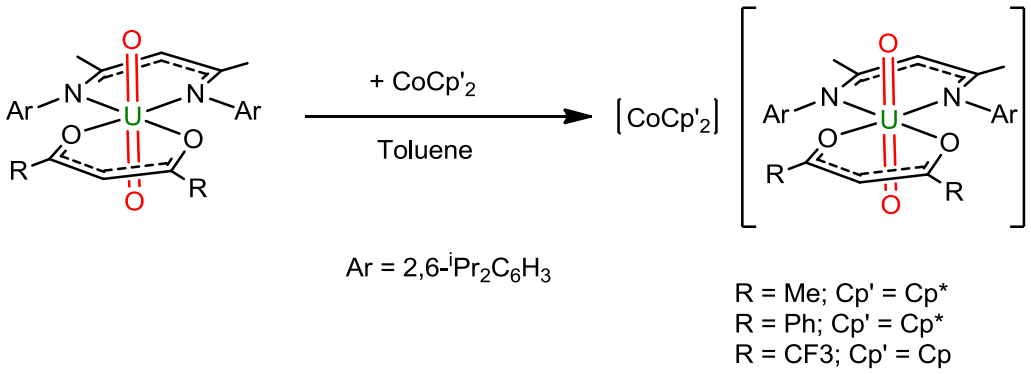

Scheme 9: Synthesis of uranyl (V) complexes by electron transfer

Due to the thermally instability of the aforementioned complexes, Hayton and co-workers have used diphenyl-β-diketoiminate instead of the β-diketiminate ligands.[52] The potential reduction of the complex [UO_2(^{Ar}acnac)$_2$] (Ar = 3,5-^{t}Bu$_2$C$_6$H$_3$) is −1.35 V (*vs* Fc^+/Fc) as measured by cyclic voltammetry. This value is similar to the one observed with the β-diketiminate ligands and allows chemical reduction of the uranyl(VI) complex. The addition of decamethylcobaltocene to the complex [UO_2(^{Ar}acnac)$_2$] leads to the formation of the complex [Cp*$_2$Co][UO_2(^{Ar}acnac)$_2$] in the 5+ oxidation state (Scheme 10). The complex is characterised by ^{1}H NMR spectroscopy and indicates the presence of a paramagnetic uranyl moiety. The solid state structure consists of a discrete cation/anion pair; the uranium centre displays a distorted octahedral geometry. The UO bond lengths are

elongated in comparison with the uranyl(VI) complex (1.838(5) Å/ 1.755(5) Å respectively). In the IR spectrum, no band corresponding to the asymmetric UO stretch could be assigned, because of overlaps with the ligand. However, in a similar complex $[Cp^*_2Co][UO_2(^{Ar}acnac)_2]$ (Ar = 2,4,6-$Me_3C_6H_2$), the asymmetric UO stretch is assigned to a band at 784 cm^{-1} and is in the range of the $[UO_2]^+$. The UV-vis spectrum exhibits absorptions at 620 nm (ε = 250 $L.mol^{-1}.cm^{-1}$), 725 nm (ε = 460 $L.mol^{-1}.cm^{-1}$) and 846 nm (ε = 520 $L.mol^{-1}.cm^{-1}$). These absorptions are consistent with *f-f* transition and the presence of $5f^1$ ion.

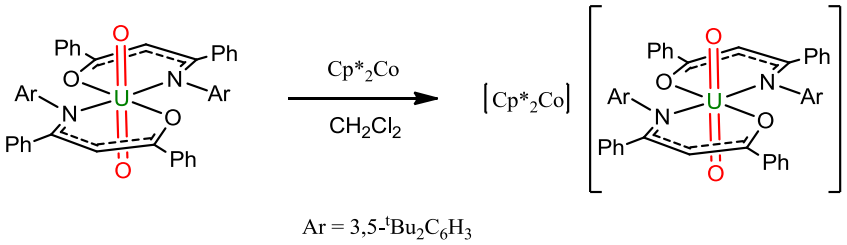

Scheme 10: Synthesis of uranyl complexes in the 5+ oxidation state

Mazzanti and co-workers[67] and Berthet and co-workers[68] reported the formation of $\{[UO_2(py)_5][KI_2(py)_2]\}_n$ by two routes (Figure 19). Mazzanti and co-workerd reported the synthesis of $\{[UO_2(py)_5][KI_2(py)_2]\}_n$ by the oxidation of $[UI_3(THF)_4]$ (U^{III}) with pyridine-N-oxide and water; the compound exhibits pentagonal bipyramidal coordination geometry around the uranium. The oxo groups are axial with five pyridine molecules in the equatorial plane. Each oxo group is bound to a potassium ion, forming a 1D chain. The U=O bonds (1.834(2) Å and 1.843(2) Å) are longer than the U=O bonds in the uranyl(VI) compound. The IR spectrum shows an absorption at 797 cm^{-1} for the U=O asymmetric bond stretch. The second route, described by Berthet and co-workers, is the reduction of $[UO_2I_2(THF)_3]$ (U^{VI}) with K_5R_5 (R=H or Me) in pyridine, where the complex is obtained in 50 % yield. The complex is only characterised by X-ray diffraction studies.

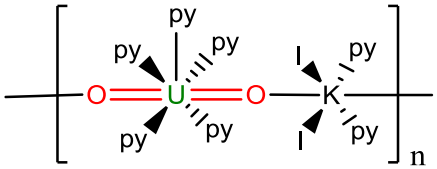

Figure 19: Structure of $\{[UO_2(py)_5][K(I)_2(py)_2]\}_n$

The ability of this complex to undergo ligand substitution reaction has been exploited by Mazzanti and co-workers and leads to the formation $\{[UO_2(dbm)_2]_4[K_6(py)_{10}]\}.I_2.(py)_2$ by addition of dibenzoylmethanate to the complex $\{[UO_2(py)_5][KI_2(py)_2]\}_n$ (Figure 20).[66,69] The complex crystallises as a tetrameric cation-cation uranyl complex in the 5+ oxidation state. Each $[UO_2]^+$ moiety coordinates two adjacent uranyl groups and is involved in two T-shaped cation-cation interaction and also in a cation-cation interaction with a potassium ion. The uranium centre is seven coordinate, which results in a pentagonal bipyramidal geometry. The interaction between the uranyl groups results in lengthening of the UO group in the U=O−U fragment (1.923(10) Å and 1.934(8) Å). In the fragment U=O−K the UO length (1.828(10) Å and 1.811(9) Å) are similar to that observed in the complex $\{[UO_2(py)_5][KI_2(py)_2]\}_n$. The weakening of the UO bond can be observed in the IR spectrum by the shift of the UO stretch in comparison to the starting material (782 cm^{-1}/ 797 cm^{-1} respectively). The complex dissociates completely in DMSO to lead to the formation of the stable monomeric complex $[UO_2(dbm)_2(DMSO)_x]K$. The use of this ligand in the electrochemical reduction of the uranyl(VI) was reported previously by Ikeda and co-workers.[70]

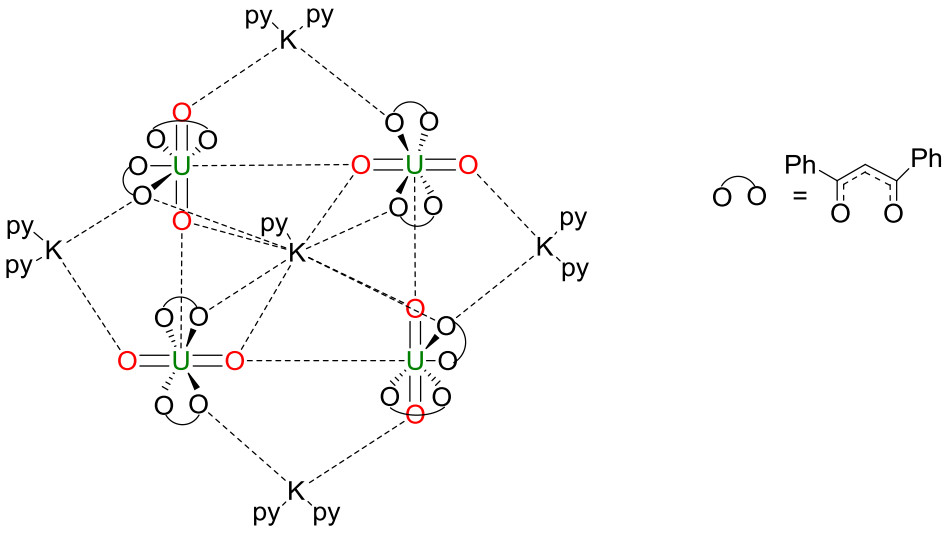

Figure 20: $\{[UO_2(dbm)_2]_4[K_6(py)_{10}]\}.I_2.(py)_2$

The choice of the different ligands plays an important role in the stabilisation of the uranyl moiety in the 5+ oxidation state and in avoiding decomposition of the complexes by disproportionation. During the course of this thesis work, other members of our groups reported the reduction and selective oxo group silylation of the uranyl dication.[71] The reaction between the uranyl(VI) Pacman complex $[UO_2(THF)(H_2L)]$ and $KN(SiMe_2R)_2$ (R = Me or C_6H_5) in the presence of transition metals (Fe, Zn) leads to the reductive silylation of the uranyl and formation of the cation-cation complexes with a transition metal $[(Me_3SiO)UO(THF)M_2I_2(L)]$ (Scheme 11). The Schiff-base pyrrole macrocycle, which on metal complexation folds to form a Pacman structure has two non identical N_4-donor compartments, one of which is occupied by a linear uranyl ion and the other is vacant. The vacant compartment is ideally placed to coordinate reagents that can react with the uranyl dication. The complexes $[(Me_3SiO)UO(THF)Fe_2I_2(L)]$ and $[(Me_3SiO)UO(THF)Zn_2I_2(L)]$ have been characterised by single crystal X-ray diffraction studies and show that the Pacman structural motif of the precursor remains intact. The uranium centre is seven coordinate and displays a distorted pentagonal bipyramidal geometry with the oxo groups retained in a *trans* arrangement. The equatorial sites are occupied by the nitrogen atoms of the macrocycle and an oxygen atom from THF sitting between the macrocyclic aryl

rings. The U=O bonds are longer than in the precursor, for $[(Me_3SiO)UO(THF)Fe_2I_2(L)]$ the *endo*-oxo bond is lengthened by 0.083 Å and the *exo*-oxo bond by 0.223 Å. For $[(Me_3SiO)UO(THF)Zn_2I_2(L)]$ the *endo*-oxo bond is lengthened by 0.08 Å and the *exo*-oxo bond by 0.205 Å. The IR spectra of these complexes are complex in the region of U=O absorption because of contributions from the macrocycle ligand and the O-SiR_3 groups. They have shown that placing the uranyl ion in a rigid and asymmetric coordination environment allows the generation of a reactive and highly oxidising uranyl complex.

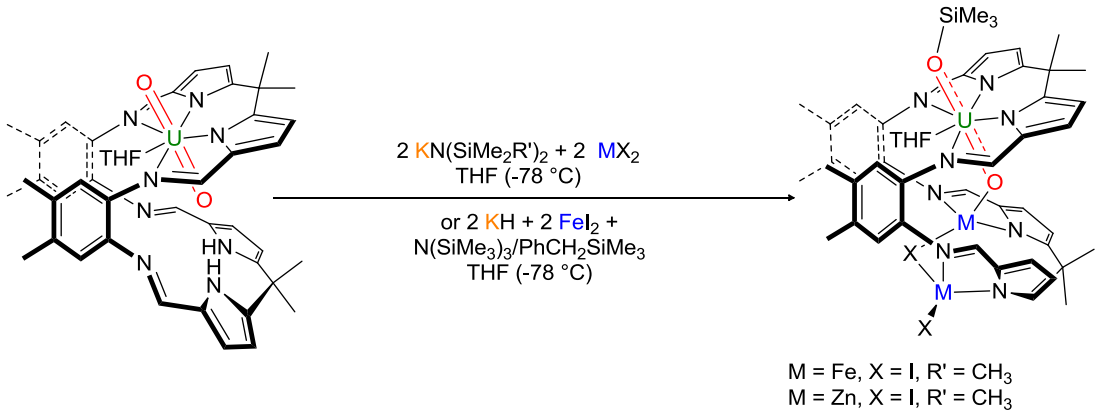

Scheme 11: Reductive oxo silylation of the uranyl Pacman complex

They have recently reported that the addition of $UO_2\{N(SiMe_3)_2\}_2(py)_2$ (in slight excess) to the uranyl Pacman complex $[UO_2(THF)(H_2L)]$ results in the formation of an unprecedented butterfly-shaped U(V) oxo dimer $[(Me_3SiOUO)_2(L)]$ and is similar to the one predicted by DFT calculation by Schreckenbach and co-workers (Scheme 12).[72,73] This compound displays a new structural motif in which one of the inert uranyl oxo groups has moved in cis position, affording a tightly bound U_2O_2 core; the two *exo*-oxo groups are silylated. The ^1H NMR spectrum is very simple due to the high symmetry of the molecule and confirms the presence of a uranyl complex in the 5+ oxidation state. The complex is a C_{2v}-symmetrical diamond shape with an average U−O distance of 2.094 Å. The U−O(silyl) distances are also elongated (2.034(4) Å and 2.040(4) Å). Each uranium centre adopts a pentagonal bipyramidal geometry and affords a U(V)U(V) dimer with a very short U···U separation.

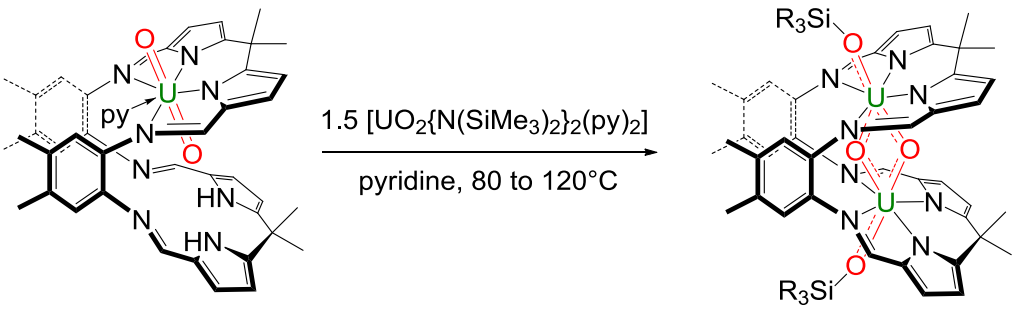

R_3 = Me_3 or Me_2Ph

Scheme 12: Synthesis of the butterfly-shaped binuclear U(V) complex

Another oxo silylation has been reported by Hayton and co-workers.[74] They showed that the reaction of the uranyl(VI) complex $[UO_2(^{Ar}acnac)_2]$ (^{Ar}acnac = Ar*N*C(Ph)CHC(Ph)*O*, Ar = 3,5-$^{t}Bu_2C_6H_3$) with an excess of Me_3SiI results in the formation of the uranyl complex $[U(OSiMe_3)_2(^{Ar}acnac)I_2]$ in the 5+ oxidation state and the loss of one ligand (Scheme 13). The uranium centre adopts a distorted octahedral geometry with one ^{Ar}acnac ligand and two iodide ligands in the equatorial plane. The two oxo groups are silylated and the UO bond lengths (1.996(5) Å and 1.986(5) Å) are elongated in comparison to the uranyl(VI) precursor. The NIR spectrum confirms the presence of $5f^{1}$ ion. The magnetic moment (μ_{eff} = 1.52μ_B at 298 K) supports this.

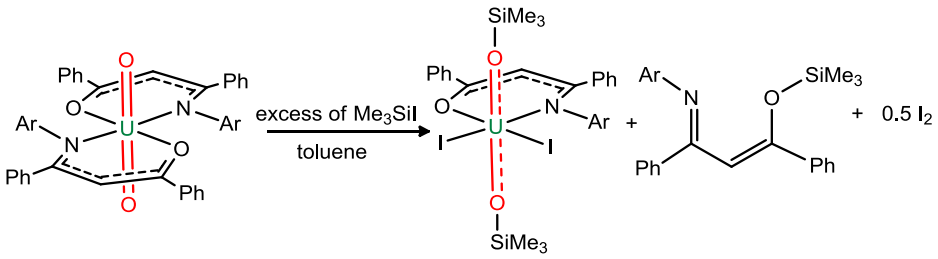

Scheme 13: Synthesis of $[U(OSiMe_3)_2(^{Ar}acnac)I_2]$

They reported another example of reductive silylation of the uranyl moiety.[75] In particular, the reaction of $UO_2(^{tBu}acnac)_2$ with ten equivalents of Me_3SiI in the presence of Ph_3P results in the formation of the complex $[Ph_3PI][U(OSiMe_3)_2I_4]$ (Scheme 14). In the solid-state structure, the uranium centre adopts an octahedral

geometry. The two oxo groups are functionalised by a silyl group and are elongated (1.990(6) Å). The formation of the paramagnetic complex has been confirmed by the measurement of the magnetic moment via Evans' method (μ_{eff} = 1.4μ_B at 295 K). This value is lower than the theoretical (2.54μ_B).[76] The NIR spectrum is consistent with the presence of $5f^1$ ion. This complex can undergo further reduction to obtain U(IV) complexes.

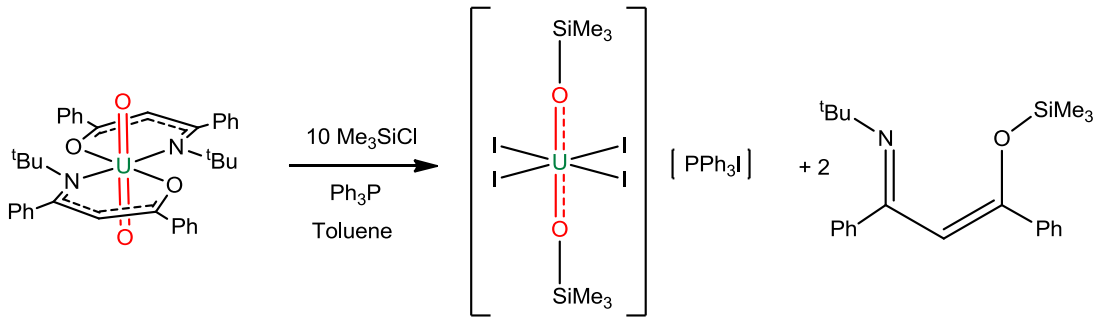

Scheme 14: Synthesis of $[Ph_3PI][U(OSiMe_3)_2I_4]$

It is clear from the different examples that the silylation can play an important role in the oxo functionalisation and in the immobilisation of the uranium species. Last year, Hayton and co-workers reported a mixed oxo functionalisation where the addition of $HSiPh_3$ to $UO_2(^{Ar}acnac)_2$ in the presence of borane $B(C_6F_5)_3$ leads to the formation of the complex$[UO(SiPh_3)(OB\{C_6F_5\}_3)(^{Ar}acnac)_2$ in the 5+ oxidation state (Scheme 15).[77] In the solid state structure, the uranium centre adopts an octahedral geometry. The two oxo groups are functionalised and elongated. Indeed, the U−O(silyloxide) bond length (2.034(9) Å) and the U−O(borane) bond length (1.941(8) Å) are elongated in comparison to the uranyl(VI) precursor. The NIR spectrum supports the formation of $5f^1$ ion

The borane, in this case, plays an important role in the reduction of the uranyl moiety. Indeed, the formation of an adduct between the borane molecule and one uranyl oxo group results in a shift of the U(VI)/U(V) couple to a more positive potential.[52]

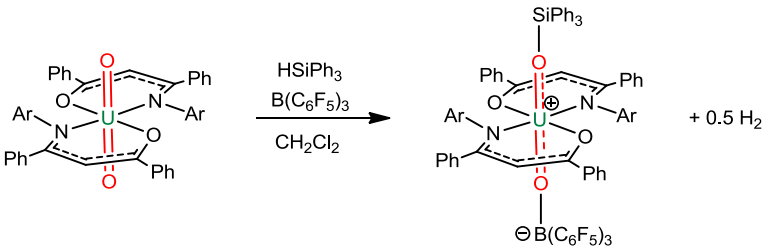

Scheme 15: Synthesis of a mixed oxo functionalisation

During the course of this thesis work, other members of our groups reported the first uranyl-4f metal interaction and demonstrated strong coupling between 4f and 5f electrons. The reaction between the uranyl Pacman and $[Sm(THF)_2\{N(SiMe_3)_2\}_2]$ or $[Y\{N(SiMe_3)_2\}_3]$ lead to the formation of a dimer $[UO_2M(py)_2(L)]_2$ (M = Sm, Y) (Scheme 16).[78] In the solid state structure, the uranium centre adopts pentagonal bipyramidal geometry. The fifth equatorial site of the uranium is occupied by the *exo*-oxo group of an adjacent molecule inducing a diamond-shaped $(UO_2)_2$ core. The UO bond lengths are elongated in comparison to the uranyl(VI) Pacman complex (1.890(5) Å and 1.941(5) Å for M = Sm; 1.919(4) Å and 1.965(4) Å for M = Y). The ^{1}H NMR spectra are consistent with the formation of a paramagnetic complex. In each FTIR spectrum, a broad band is observed at 724 cm^{-1} for the samarium complex and at 722 cm^{-1} for the yttrium complex and assigned to the U=O asymmetric stretch and supports reduction to U(V). The variable temperature magnetic behaviour of the two complexes shows a decrease in moment with decreasing temperature from 300 K to 5 K associated with the depopulation of excited crystal field states in the f-block cations and shows a system comprising two dimerized oxo-bridged 5f^1-4f^5 for the samarium complex, while for the yttrium complex this simplified to 5f^1-4f^0.

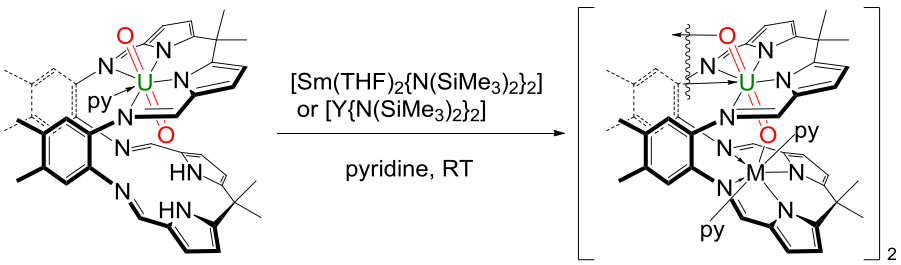

Scheme 16: Synthesis of uranyl-rare earth compounds

1.5. Outlook

In conclusion, the $[UO_2]^+$ can disproportionate to $[UO_2]^{2+}$ and U(IV) species. The use of appropriate ligand to complex the uranyl cation plays an important role in the stabilisation of the uranyl moiety in the 5+ oxidation state and can avoid the disproportionation.

As such, this thesis describes the synthesis and characterisations of a range of uranyl Pacman complexes in the 5+ oxidation state to understand the formation of these complexes. In this work, we try to probe the mechanism of the formation of the complex $[(Me_3SiO)UO(THF)Zn_2I_2(L)]$ and isolate the uranyl (VI) intermediate $[UO_2(THF)(K_2L)]$. Another way to probe this mechanism is the use of other alkali metal such as lithium, which can be easy to characterise by NMR spectroscopy. And finally the use of different reagents allows the functionalisation of the oxo groups.

1.6. References

(1) Allard, B.; Olofsson, U.; Torstenfelt, B. *Inorg. Chim. Acta* **1984**, *94*, 205.
(2) Vaughn, A. E.; Barnes, C. L.; Duval, P. B. *Angew. Chem., Int. Ed. Engl.* **2007**, *46*, 6622.
(3) Szabó, Z.; Toraishi, T.; Vallet, V.; Grenthe, I. *Coord. Chem. Rev.* **2006**, *250*, 784.
(4) King, R. B. *J. Coord. Chem.* **2005**, *58*, 47
(5) Denning, R. G. *J. Physic. Chem. A* **2007**, *111*, 4125.
(6) O'Grady, E.; Kaltsoyannis, N. *Journal of the Chemical Society, Dalton Transactions* **2002**, 1233.
(7) Sessler, J. L.; Melfi, P. J.; Pantos, G. D. *Coord. Chem. Rev.* **2006**, *250*, 816.
(8) Mayer, J. M. *Acc. Chem. Res.* **1998**, *31*, 441.
(9) Limberg, C. *Angew. Chem., Int. Ed. Engl.* **2003**, *42*, 5932.
(10) Amme, M.; Wiss, T.; Thiele, H.; Boulet, P.; Lang, H. *J. Nucl. Mater.* **2005**, *341*, 209.
(11) Lovley, D. R.; Phillips, E. J. P.; Gorby, Y. A.; Landa, E. R. *Nature* **1991**, *350*, 413.
(12) Suzuki, Y.; Kelly, S. D.; Kemner, K. M.; Banfield, J. F. *Nature* **2002**, *419*, 134.
(13) Renshaw, J. C.; Butchins, L. J. C.; Livens, F. R.; May, I.; Charnock, J. M.; Lloyd, J. R. *Environ. Sci. Technol.* **2005**, *39*, 5657.
(14) Charlet, L.; Silvester, E.; Liger, E. *Chem. Geol.* **1998**, *151*, 85.
(15) McCleskey, T. M.; Foreman, T. M.; Hallman, E. E.; Burns, C. J.; Sauer, N. N. *Environ. Sci. Technol.* **2000**, *35*, 547.
(16) Eliet, V.; Bidoglio, G. *Environ. Sci. Technol.* **1998**, *32*, 3155.
(17) Wang, W.-D.; Bakac, A.; Espenson, J. H. *Inorg. Chem.* **1995**, *34*, 6034.

(18) Takao, K.; Kato, M.; Takao, S.; Nagasawa, A.; Bernhard, G.; Hennig, C.; Ikeda, Y. *Inorg. Chem.* **2010**, *49*, 2349.
(19) Deshayes, L.; Keller, N.; Lance, M.; Navaza, A.; Nierlich, M.; Vigner, J. *Polyhedron* **1994**, *13*, 1725.
(20) Clark, D. L.; Keogh, D. W.; Palmer, P. D.; Scott, B. L.; Tait, C. D. *Angew. Chem., Int. Ed. Engl.* **1998**, *37*, 164.
(21) Thuery, P.; Nierlich, M.; Masci, B.; Asfari, Z.; Vicens, J. *J. Chem. Soc., Dalton Trans.* **1999**, 3151.
(22) Sessler, J. L.; Vivian, A. E.; Seidel, D.; Burrell, A. K.; Hoehner, M.; Mody, T. D.; Gebauer, A.; Weghorn, S. J.; Lynch, V. *Coord. Chem. Rev.* **2001**, *216–217*, 411.
(23) Day, V. W.; Marks, T. J.; Wachter, W. A. *J. Am. Chem. Soc.* **1975**, *97*, 4519.
(24) Burrell, A. K.; Hemmi, G.; Lynch, V.; Sessler, J. L. *J. Am. Chem. Soc.* **1991**, *113*, 4690.
(25) Burrell, A. K.; Cyr, M. J.; Lynch, V.; Sessler, J. L. *J. Chem. Soc., Chem. Commun.* **1991**, 1710.
(26) Sessler, J. L.; Seidel, D.; Vivian, A. E.; Lynch, V.; Scott, B. L.; Keogh, D. W. *Angew. Chem., Int. Ed. Engl.* **2001**, *40*, 591.
(27) Hobday, M. D.; Smith, T. D. *Coord. Chem. Rev.* **1973**, *9*, 311.
(28) Van Staveren, C. J.; Fenton, D. E.; Reinhoudt, D. N.; Van Eerden, J.; Harkema, S. *J. Am. Chem. Soc.* **1987**, *109*, 3456.
(29) Casellato, U.; Tamburini, S.; Tomasin, P.; Vigato, P. A. *Inorg. Chim. Acta* **2002**, *341*, 118.
(30) Sessler, J. L.; Mody, T. D.; Lynch, V. *Inorg. Chem.* **1992**, *31*, 529.
(31) Sessler, J. L.; Callaway, W. B.; Dudek, S. P.; Date, R. W.; Bruce, D. W. *Inorg. Chem.* **2004**, *43*, 6650.
(32) Veauthier, J. M.; Cho, W.-S.; Lynch, V. M.; Sessler, J. L. *Inorg. Chem.* **2004**, *43*, 1220.
(33) Givaja, G.; Blake, A. J.; Wilson, C.; Schroder, M.; Love, J. B. *Chem. Commun.* **2003**, 2508.
(34) Arnold, P. L.; Blake, A. J.; Wilson, C.; Love, J. B. *Inorg. Chem.* **2004**, *43*, 8206.
(35) Reilly, S. D.; Neu, M. P. *Inorg. Chem.* **2006**, *45*, 1839.
(36) Arnold, P. L.; Patel, D.; Blake, A. J.; Wilson, C.; Love, J. B. *J. Am. Chem. Soc.* **2006**, *128*, 9610.
(37) Sessler, J. L.; Gorden, A. E. V.; Seidel, D.; Hannah, S.; Lynch, V.; Gordon, P. L.; Donohoe, R. J.; Drew Tait, C.; Webster Keogh, D. *Inorg. Chim. Acta* **2002**, *341*, 54.
(38) Gorden, A. E. V.; Xu, J.; Raymond, K. N.; Durbin, P. *Chem. Rev.* **2003**, *103*, 4207.
(39) Nagasaki, S.; Kinoshita, K.; Enokida, Y.; Suzuki, A. *J. Nucl. Sci. Technol.* **1992**, *29*, 1100.
(40) Fortier, S.; Hayton, T. W. *Coord. Chem. Rev.* **2010**, *254*, 197.
(41) Sullivan, J. C.; Hindman, J. C.; Zielen, A. J. *J. Am. Chem. Soc.* **1961**, *83*, 3373.
(42) Sullivan, J. C. *J. Am. Chem. Soc.* **1962**, *84*, 4256.
(43) Sullivan, J. C. *Inorg. Chem.* **1964**, *3*, 315.

(44) Clark, D. L.; Conradson, S. D.; Donohoe, R. J.; Keogh, D. W.; Morris, D. E.; Palmer, P. D.; Rogers, R. D.; Tait, C. D. *Inorg. Chem.* **1999**, *38*, 1456.
(45) Wilkerson, M. P.; Burns, C. J.; Dewey, H. J.; Martin, J. M.; Morris, D. E.; Paine, R. T.; Scott, B. L. *Inorg. Chem.* **2000**, *39*, 5277.
(46) Sarsfield, M. J.; Helliwell, M.; Raftery, J. *Inorg. Chem.* **2004**, *43*, 3170.
(47) Burns, C. J.; Clark, D. L.; Donohoe, R. J.; Duval, P. B.; Scott, B. L.; Tait, C. D. *Inorg. Chem.* **2000**, *39*, 5464.
(48) Danis, J. A.; Lin, M. R.; Scott, B. L.; Eichhorn, B. W.; Runde, W. H. *Inorg. Chem.* **2001**, *40*, 3389.
(49) Arnold, P. L.; Love, J. B.; Patel, D. *Coord. Chem. Rev.* **2009**, *253*, 1973.
(50) Arnold, P. L.; Patel, D.; Pécharman, A.-F.; Wilson, C.; Love, J. B. *Dalton Trans.* **2010**, *39*, 3501.
(51) Sarsfield, M. J.; Helliwell, M. *J. Am. Chem. Soc.* **2004**, *126*, 1036.
(52) Hayton, T. W.; Wu, G. *Inorg. Chem.* **2009**, *48*, 3065.
(53) Morris, D. E. *Inorg. Chem.* **2002**, *41*, 3542.
(54) Hayton, T. W.; Wu, G. *Inorg. Chem.* **2008**, *47*, 7415.
(55) Mizuoka, K.; Tsushima, S.; Hasegawa, M.; Hoshi, T.; Ikeda, Y. *Inorg. Chem.* **2005**, *44*, 6211.
(56) Gritzner, G.; Selbin, J. *J. Inorg. Nucl. Chem.* **1968**, *30*, 1799.
(57) Mizuguchi, K.; Park, Y.-Y.; Tomiyasu, H.; Ikeda, Y. *J. Nucl. Sci. Technol.* **1993**, *30*, 542.
(58) Lee, S.-H.; Mizuguchi, K.; Tomiyasu, H.; Ikeda, Y. *J. Nucl. Sci. Technol.* **1996**, *33*, 190.
(59) Mizuoka, K.; Kim, S.-Y.; Hasegawa, M.; Hoshi, T.; Uchiyama, G.; Ikeda, Y. *Inorg. Chem.* **2003**, *42*, 1031.
(60) Kim, S.-Y.; Asakura, T.; Morita, Y.; Ikeda, Y. *J. Alloys Compd.* **2006**, *408–412*, 1291.
(61) Berthet, J.-C.; Siffredi, G.; Thuéry, P.; Ephritikhine, M. *Eur. J. Inorg. Chem.* **2007**, *2007*, 4017.
(62) Teruel, H.; Moret, Y. Y.; Perillo, B. *Polyhedron* **1998**, *18*, 419.
(63) Stavropoulos, P.; Bryson, N.; Youinou, M. T.; Osborn, J. A. *Inorg. Chem.* **1990**, *29*, 1807.
(64) Berthet, J.-C.; Thuery, P.; Ephritikhine, M. *Chem. Commun.* **2005**, 3415.
(65) Berthet, J.-C.; Nierlich, M.; Ephritikhine, M. *Angew. Chem., Int. Ed. Engl.* **2003**, *42*, 1952.
(66) Burdet, F.; Pécaut, J.; Mazzanti, M. *J. Am. Chem. Soc.* **2006**, *128*, 16512.
(67) Natrajan, L.; Burdet, F.; Pécaut, J.; Mazzanti, M. *J. Am. Chem. Soc.* **2006**, *128*, 7152.
(68) Berthet, J.-C.; Siffredi, G.; Thuery, P.; Ephritikhine, M. *Chem. Commun.* **2006**, 3184.
(69) Nocton, G.; Horeglad, P.; Pécaut, J.; Mazzanti, M. *J. Am. Chem. Soc.* **2008**, *130*, 16633.
(70) Mizuoka, K.; Ikeda, Y. *Radiochim. Acta* **2004**, *92*, 631.
(71) Arnold, P. L.; Patel, D.; Wilson, C.; Love, J. B. *Nature* **2008**, *451*, 315.
(72) Arnold, P. L.; Jones, G. M.; Odoh, S. O.; Schreckenbach, G.; Magnani, N.; Love, J. B. *Nat Chem* **2012**, *4*, 221.
(73) Pan, Q.-J.; Schreckenbach, G.; Arnold, P. L.; Love, J. B. *Chem. Commun.* **2011**.

(74) Brown, J. L.; Wu, G.; Hayton, T. W. *J. Am. Chem. Soc.* **2010**, *132*, 7248.
(75) Brown, J. L.; Mokhtarzadeh, C. C.; Lever, J. M.; Wu, G.; Hayton, T. W. *Inorg. Chem.* **2011**, *50*, 5105.
(76) Evans, D. F. *Journal of the Chemical Society (Resumed)* **1959**, 2003.
(77) Schnaars, D. D.; Wu, G.; Hayton, T. W. *Inorg. Chem.* **2011**, *50*, 4695.
(78) Arnold, P. L.; Hollis, E.; White, F. J.; Magnani, N.; Caciuffo, R.; Love, J. B. *Angew. Chem., Int. Ed. Engl.* **2011**, *50*, 887.

Chapter 2: Lithiation and reduction of the uranyl Pacman complex

2.1. Introduction

Reduction and oxo-functionalisation reactions of the uranyl dication are becoming important in understanding the chemical reactions and the mechanisms that occur during the immobilisation of uranium in the environment. The uranyl complexes of the Schiff-base pyrrole macrocycle H_4L adopt Pacman structures, placing the uranyl dication in a rigid and asymmetric coordination environment adjacent to the empty pocket, which can offer a place to other reagents such as transition metals to bind to the *endo* oxo group.[1,2] A new type of reaction for the uranyl ion was reported by Arnold, Love and co-workers in which the uranyl Pacman complex **[UO_2(THF)(H_2L)]** cleaved N-Si bonds to form the singly reduced and oxo-silylated complex **[(Me_3SiO)UO(THF)($ZnCl)_2$(L)]**, Equation (**1**).[3]

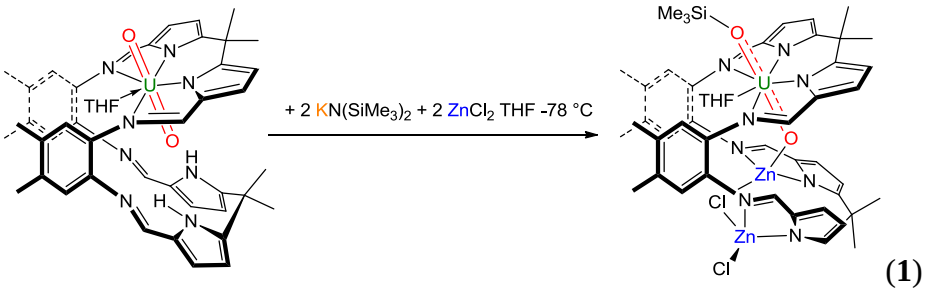

(**1**)

This reductive oxo-functionalisation was initiated by the reaction between **[UO_2(THF)(H_2L)]** and two equivalents of $KN(SiMe_3)_2$ forming a reactive intermediate that was thought to be the dipotassiated uranyl Pacman complex **[UO_2(THF)(K_2L)]** in the 6+ oxidation state, in accordance with the DFT calculations.[4] As this intermediate was not isolated, it was thought that the use of a lithium base such as $LiN(SiMe_3)_2$ to form the dilithiated complex **[UO_2(THF)(Li_2L)]** in the 6+ oxidation state may help characterisation, especially by $^7Li\{^1H\}$ NMR spectroscopy. Alkali metals have been shown previously to interact with the inert uranyl oxo groups, although this atypical Lewis base behaviour of the uranyl oxo is usually only demonstrated in the solid state.[5,6]

Dr Emmalina Hollis has contributed to this work with the synthesis and characterisation of the complex **[OUO(THF)Li(THF)(HL)]**; Prof Simon Parsons solved and refined the disorder components for the crystal structure of **[(py)$_3$LiOUO(py)Li(py)(HL)]**; Prof Laurent Maron and Dr Ahmed Yahia carried out the DFT calculations.

2.2. Synthesis of the monolithiated complex

2.2.1. Synthesis of [OUO(py)Li(py)(HL)]

The reaction between one equivalent of **[UO$_2$(py)(H$_2$L)]** and one equivalent of LiN(SiMe$_3$)$_2$ in pyridine at −40 °C in a Teflon-tapped NMR tube for 24 h results in a mixture of the four complexes **[UO$_2$(py)(H$_2$L)]**, **[OUO(py){Li(py)}(HL)]**, **[(py)$_3$LiOUO(py)Li(py)(HL)]** and **[(py)$_3$LiOUO(py){Li(py)}$_2$(L)]** in a ratio 0.5:0.25:0.13:0.12, Scheme **1**.

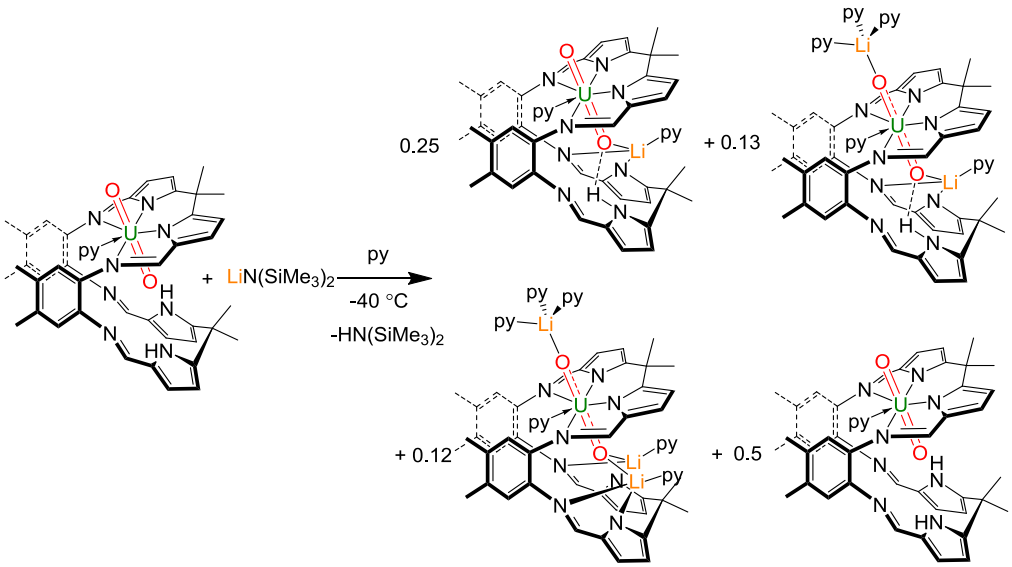

Scheme 1: Attempted synthesis of the complex **[OUO(py){Li(py)}(HL)]**

The mixture was characterised by ^{1}H NMR spectroscopy only due to the difficulties in isolating the separate components and only the resonances of the complex **[OUO(py){Li(py)}(HL)]** are described, as the remaining complexes and their syntheses are described below. In the ^{1}H NMR spectrum of **[OUO(py){Li(py)}(HL)]** the resonances are shifted in the diamagnetic part of the

spectrum and display an asymmetric ligand arrangement consistent with a wedged, Pacman structure in solution of C_1 symmetry. The most shifted resonance at 9.11 ppm corresponds to the single remaining pyrrole NH proton.

2.2.2. Synthesis of [OUO(THF)Li(THF)(HL)]

The reaction between one equivalent of **[UO_2(THF)(H_2L)]** and one equivalent of $LiN(SiMe_3)_2$ in THF at −78 ºC for 96 h leads to the formation of **[OUO(THF)Li(THF)(HL)]**, which was isolated after work-up from a concentrated solution of THF as a dark red solid in moderate yield (51%), Equation (**2**).

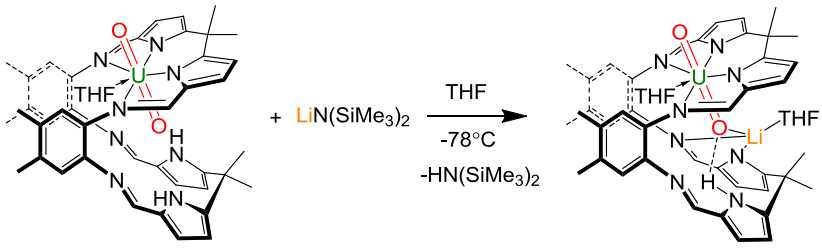

(**2**)

The complex was fully characterised, including by ^{1}H and ^{7}Li{^{1}H} NMR, FTIR spectroscopy, elemental analysis and X-ray diffraction studies. The ^{1}H NMR spectrum contains resonances for a new diamagnetic complex. The numbers of resonances and their integrations are consistent with a wedged, Pacman structure in solution of C_1 symmetry. The most diamagnetically shifted resonance at 9.11 ppm corresponds to the NH proton. Eight resonances, integrating for 3H each correspond to the methyl groups of the ligand. The four resonances at 5.05, 3.98, 1.11 and 0.89 ppm correspond to the coordinated THF molecule. The ^{7}Li{^{1}H} NMR spectrum shows only one resonance at 0.66 ppm. The elemental analysis supports the formulation of the complex **[OUO(THF)Li(THF)(HL)]**. The FTIR spectrum shows a broad band at 3350 cm^{-1} corresponding to the pyrrole NH, while the UO stretch is slightly shifted at 915 cm^{-1} but is in the range of the $[UO_2]^{2+}$.[7,8] Crystals of **[OUO(THF){Li(THF)}(HL)]** suitable for single crystal X-ray diffraction analysis were grown from a saturated THF solution (Figure 1).

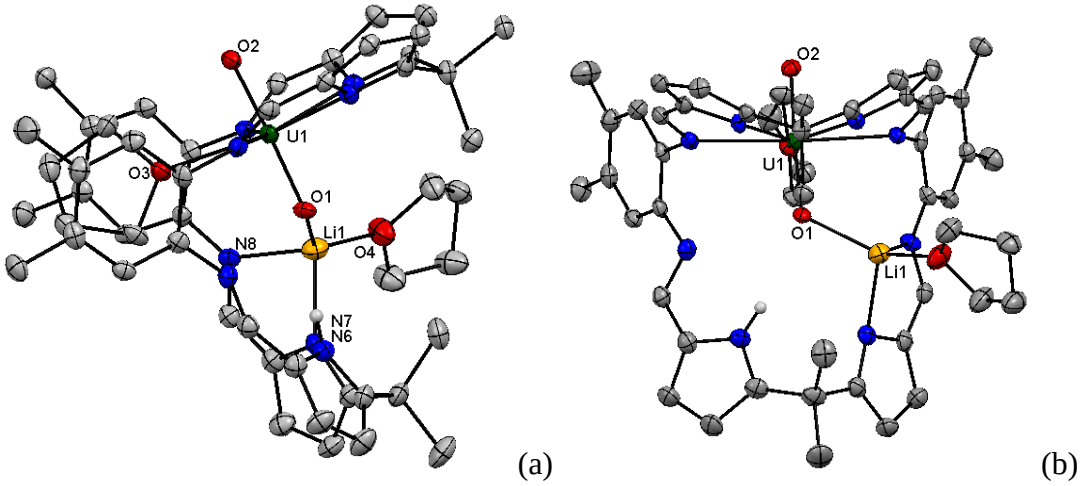

Figure 1: Solid state structure of **[OUO(THF){Li(THF)}(HL)]** showing side (a) and front view (b). For clarity all the hydrogen atoms and lattice molecules of solvent are omitted (except the pyrrole NH) (displacement ellipsoids drawn at 50% probability)

Table 1: Selected bond distances (Å) and angles (°) of **[OUO(THF){Li(THF)}(HL)]**

U1-O1	1.794(3)
U1-O2	1.767(3)
U1-O3	2.433(3)
O1-Li1	2.060(11)
O1···N6	3.288
O1-U1-O2	176.09(17)
Li1-O1-U1	120.7(3)

The Pacman structural motif of the uranyl macrocycle **[UO_2(THF)(H_2L)]** remains intact with one N_4 donor compartment occupied by the uranyl group and the other half occupied by one Li atom of approximately tetrahedral geometry, coordinated to the oxygen O4 from THF, the imine nitrogen N8, the pyrrole nitrogen N7 and the *endo*-oxo O1. The uranium centre is seven coordinate and displays a distorted pentagonal bipyramidal geometry with the oxo groups in a *trans* arrangement (O1-U1-O2 176.09(17)°); the equatorial sites are occupied by the nitrogen atoms of the macrocycle and an oxygen atom from a molecule of THF

which sits between the two macrocyclic aryl rings. From analysis of the uranium-oxygen bond lengths it is evident that the uranyl fragment is in the 6+ oxidation state. The *endo*- U1-O1 bond distance (1.794(3) Å) (Table 1) is slightly elongated in comparison with the precursor **[UO_2(THF)(H_2L)]** (U1-O1 1.770(3) Å) but in the range of the *endo*-oxo bond of the complexes [UO_2(THF)M(THF)(L)] (1.808(4) Å for M = Mn and 1.784(6) for M = Co) and typical of the $[UO_2]^{2+}$ dication.[1,2,9] The *exo*- U1-O2 bond distance is similar to that observed in **[UO_2(THF)(H_2L)]**. The U-O3 distance is slightly shorter in comparison to that observed in **[UO_2(THF)(H_2L)]** (2.433(3) Å / 2.457(3) Å respectively). The lower N4 compartment is oriented such that a hydrogen bond is evident between the pyrrole NH group and the *endo*-oxo group; the N···O separation is slightly elongated in comparison to **[UO_2(THF)(H_2L)]** (N···O 3.288 Å / 3.172 Å respectively).

2.3. Synthesis of the dilithiated complex

2.3.1. Synthesis of [(py)$_3$LiOUO(py)Li(py)(HL)]; reaction of [UO_2(py)(H_2L)] with two equivalents of LDA

The reaction between one equivalent of **[UO_2(py)(H_2L)]** and two equivalents of lithium diisopropylamide in pyridine at room temperature for 15 minutes leads to the formation of **[(py)$_3$LiOUO(py)Li(py)(HL)]** as a brown-yellow solid in a good yield (78 %), Scheme **2**.

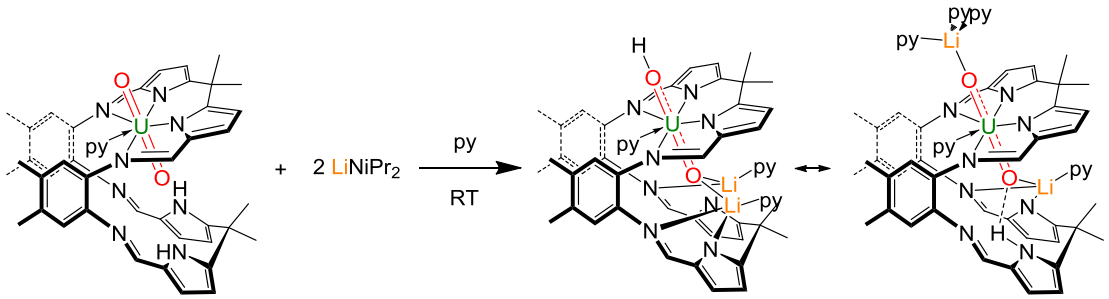

Scheme 2: Synthesis of **[(py)$_3$LiOUO(py)Li(py)(HL)]**

A similar reaction, in this case at −35 °C leads to the formation of a possible kinetic, symmetrical isomer **[HOUO(py){Li(py)}$_2$(L)]**. After work-up

[HOUO(py){Li(py)}$_2$(L)] is also obtained in moderate yield as a yellow solid (Scheme **2**).

The complex **[(py)$_3$LiOUO(py)Li(py)(HL)]** was fully characterised, including by ^{1}H and ^{7}Li{^{1}H} NMR spectroscopy, FTIR spectroscopy, SQUID, EPR and X-ray diffraction studies. The formation of a paramagnetic compound was observed in the ^{1}H NMR spectrum (Figure 2, lower spectrum), and although the individual resonances could not be assigned, the number and integrals of the paramagnetically shifted resonances are consistent with the retention of a wedged, Pacman structure in solution of C_1 symmetry. The most paramagnetic resonance at 60 ppm was assigned to the NH proton as it should be the closest to the paramagnetic UO_2 centre. The ^{7}Li{^{1}H} NMR spectrum at 25 °C contains only one broad resonance at 92 ppm. The ^{7}Li{^{1}H} NMR spectrum in pyridine at −35 °C shows decoalescence of the resonances but has not fully decoalesced to the low temperature limit because of the freezing point of the solvent. This decoalescence is due to a different environment of the two lithium atoms, so confirming the asymmetric ligand arrangement and Li occupancy (Figure 3).

The complex **[HOUO(py){Li(py)}$_2$(L)]** was only characterised by ^{1}H and ^{7}Li{^{1}H} NMR spectroscopy due to the difficulties in reproducing this reaction. The ^{7}Li{^{1}H} NMR spectrum contains only a broad resonance at 102 ppm, which is shifted in comparison to the other isomer **[(py)$_3$LiOUO(py)Li(py)(HL)]**. The ^{1}H NMR spectrum contains resonances that show a symmetric ligand arrangement and which is consistent with a wedged, Pacman structure of C_1 symmetry in solution (Figure 2, upper spectrum). The most paramagnetically shifted resonance at 86.6 ppm was assigned to the OH proton as it should be the closest to the paramagnetic uranyl centre. The two resonances integrating for 6H each at 0.41 and −2.48 ppm correspond to the methyl group on the aryl backbone.

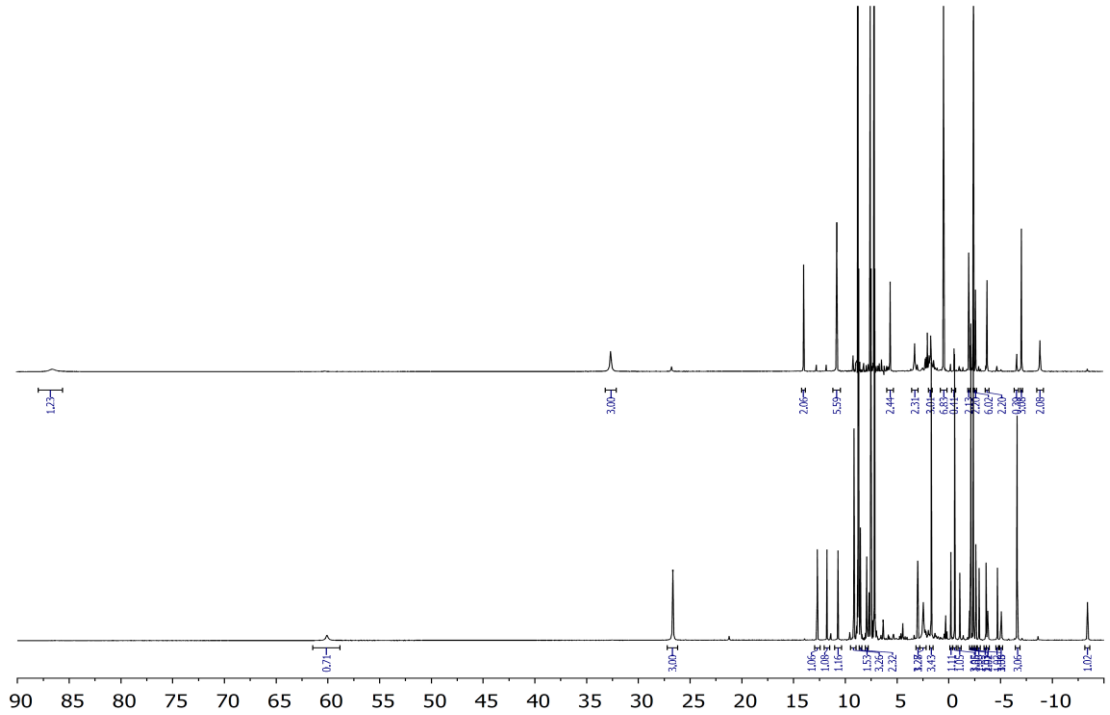

Figure 2: *In situ* ^{1}H NMR spectrum in d_5-pyridine of the reaction with LDA (2 eq.) to form dilithiated complex: upper = **[HOUO(py){Li(py)}$_2$L]**, formed at −35 °C; lower = **[(py)$_3$LiOUO(py)Li(py)(HL)]**, formed at room temperature (range 90 to −15 ppm).

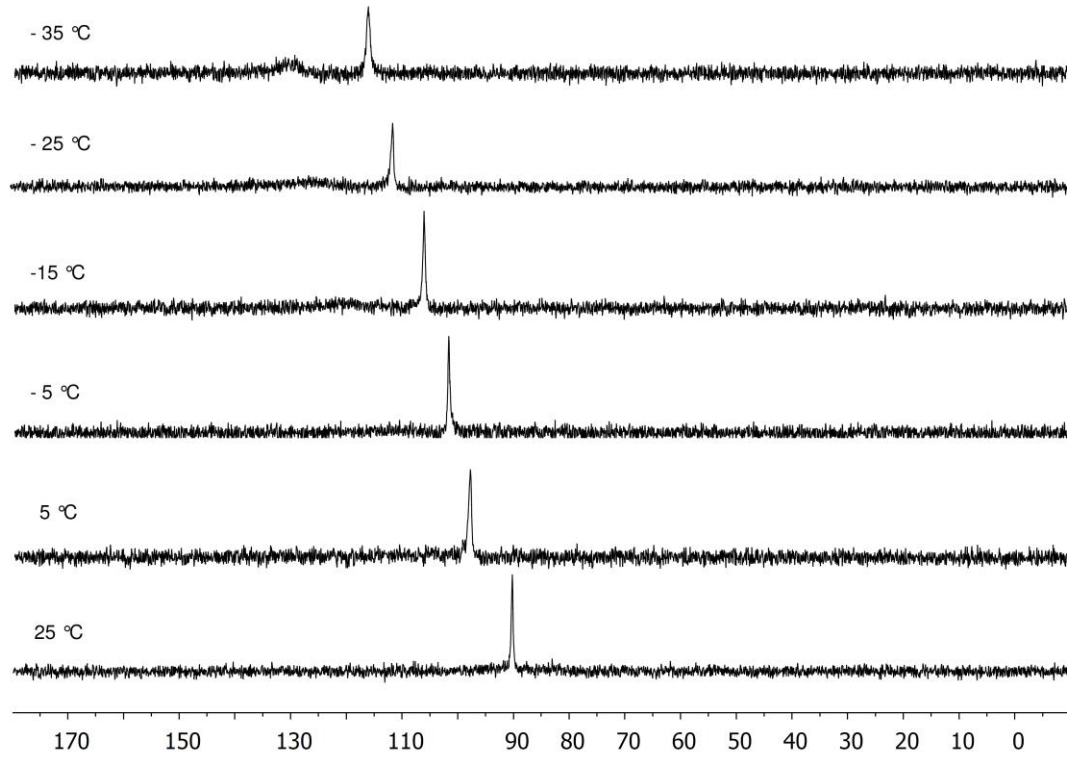

Figure 3: Variable temperature ^{7}Li{^{1}H} NMR spectrum of **[(py)$_3$LiOUO(py)Li(py)(HL)]** in d_5-pyridine between +25 °C and −35 °C.

The FTIR spectrum of **[(py)$_3$LiOUO(py)Li(py)(HL)]** contains a weak and very broad band at 3310 cm^{-1} which could derive from the pyrrole NH, and an absorption at 709 cm^{-1} assigned to the asymmetric $[UO_2]^+$ stretch, which is weakened substantially compared to that in the U^{VI} starting material **[UO$_2$(THF)(H$_2$L)]** (ν U=O 908 cm^{-1}) and in the range expected for $[UO_2]^+$.[10-12] Elemental analysis supports the formulation of **[(py)$_3$LiOUO(py)Li(py)(HL)]**.

A preliminary electron parmagnetic resonance study of **[(py)$_3$LiOUO(py)Li(py)(HL)]** at 22 K displays a strong, broad resonance at g = 3.85 that supports the presence of a single f electron.

The solid state structure of **[(py)$_3$LiOUO(py)Li(py)(HL)]** was determined by X-ray diffraction studies.

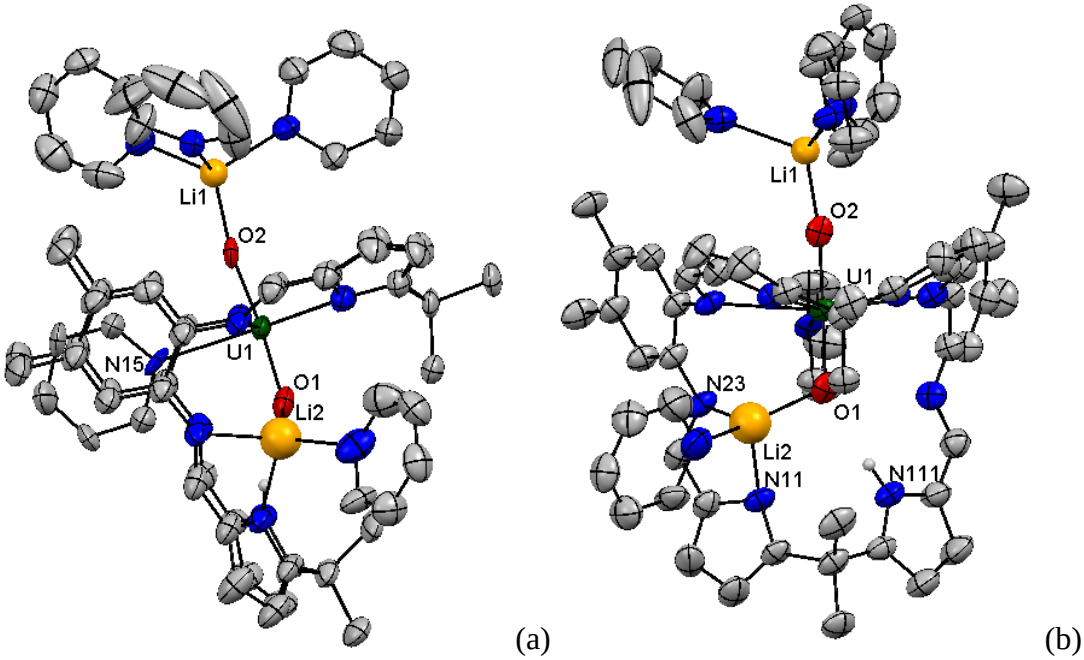

Figure 4: Solid state structure of **[(py)$_3$LiOUO{Li(py)}(HL)]**, showing side (a) and front view (b). For clarity all the hydrogen atoms (except the H from the NH) and lattice molecules of solvent are omitted (displacement ellipsoids drawn at 50% probability).

Table 2: Selected bond distances (Å) and angles (°) of **[(py)$_3$LiOUO{Li(py)}(HL)]**

U1-O1	1.834(4)
U1-O2	1.879(5)
U1-N15	2.564(11)
O1-Li2	1.94(2)
O2-Li1	1.927(13)
O1···N111	3.128
O1-U1-O2	174.82(15)
Li1-O2-U1	167.3(4)
Li2-O1-U1	113.6(7)

The Pacman structure of the uranyl macrocycle **[UO$_2$(py)(H$_2$L)]** remains intact; the uranyl fragment remains coordinated in one half of the macrocycle by four nitrogen atoms at standard distances and the other N4 donor compartment is occupied by one lithium (Li1), that functionalises the *endo*-oxo group. The *exo*-oxo group is also functionalised by one lithium cation that is coordinated by three pyridines (Figure 4). The uranium centre is seven coordinate and displays a distorted pentagonal bipyramidal geometry with the oxo groups *trans* (O1-U1-O2 174.82(15) °), the nitrogen atoms of the macrocycle occupy the equatorial sites of the uranium centre and the fifth site is occupied by the nitrogen atom N15 from a molecule of pyridine (Table 2). From analysis of the uranium-oxygen bond distances it is evident that the uranyl fragment is in the 5+ oxidation state. The *endo*-oxo bond distance (U1-O1 1.834(4) Å) is significantly elongated compared to that of $[UO_2]^{2+}$ in **[UO$_2$(py)(H$_2$L)]** (U1-O1 1.7779(18) Å) and is similar to experimental and calculated bond distances for $[UO_2]^{+}$ (range 1.811- 1.934 Å).[12-15] The *exo*-oxo bond distance (U1-O2 1.879(5) Å) is also longer than in **[UO$_2$(py)(H$_2$L)]** (U1-O2 1.7546(19) Å).[3,10] Both lithium atoms are four coordinate and display tetrahedral geometries. Li2 is sitting in half of the second pocket and coordinated by two nitrogen atoms of the macrocycle (imine N23 and pyrrole N11), the *endo*-oxo group O1 and the nitrogen of

a molecule of pyridine, the second lithium Li1 is coordinated by three molecules of pyridine and the *exo*-oxo group. The bond distance U1-N9 (2.564(11) Å) is in the range of the U1-N9 in the uranyl Pacman complex **[UO_2(py)(H_2L)]** (2.583(2) Å). The lower N4 compartment is oriented such that a hydrogen bond between the pyrrole NH group and the *endo*-oxo O1 is evident; the N···O separation is slightly shorter than in the precursor **[UO_2(py)(H_2L)]** (N···O 3.128 / 3.172 Å respectively).

2.3.2. Reaction with two equivalents of $LiN(SiMe_3)_2$

The reaction between one equivalent of **[UO_2(THF)(H_2L)]** and two equivalents of $LiN(SiMe_3)_2$ at −35 ºC in pyridine affords a mixture of paramagnetic and diamagnetic products similar to that seen above in Scheme 1. However, in the presence of dihydroanthracene, a substrate that contains a weak C-H bond, the reaction results in the clean formation of **[$(py)_3$LiOUO(py)Li(py)(HL)]** and the products of C-H bond homolysis, i.e. anthracene and 9,9',10,10'-tetrahydro-9,9'-bianthracene, Scheme (**3**).

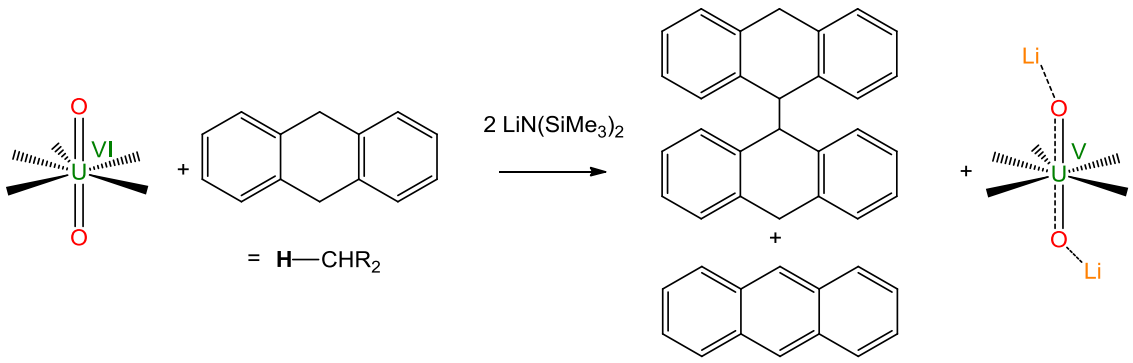

Scheme 3: Scheme of the CH atom-abstraction and formation of the dilithiated complex and by-products.

A similar reaction, in this case in the presence of one equivalent of xanthene leads to the formation of the coupled product resulting from C-H bond homolysis, 9,9'-dixanthene and a mixture of **[$(py)_3$LiOUO(py)Li(py)(HL)]**, **[$(py)_3$LiOUO(py){Li(py)}$_2$(L)]**, and some unreacted **[UO_2(THF)(H_2L)]** and xanthene. The reaction in the presence of toluene or cyclohexene did not lead to the formation of the desired product **[$(py)_3$LiOUO(py)Li(py)(HL)]** and no C-H activation products were observed.

2.3.3. Reaction with two equivalents of CpLi

The reaction between one equivalent of **[UO_2(THF)(H_2L)]** and two equivalents of C_5H_5Li in d_5-pyridine at room temperature shows the clean formation of the complex **[(py)$_3$LiOUO(py)Li(py)(HL)]** and cyclopentadiene (resonance at 2.79 ppm and integrating for 4H correspond to H-C_5H_5) in a ratio of 1:2, Equation (**3**) (Figure 5).

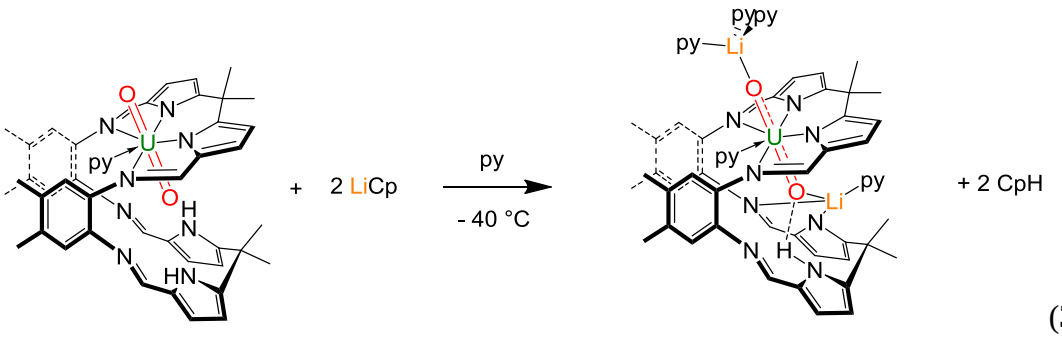

(**3**)

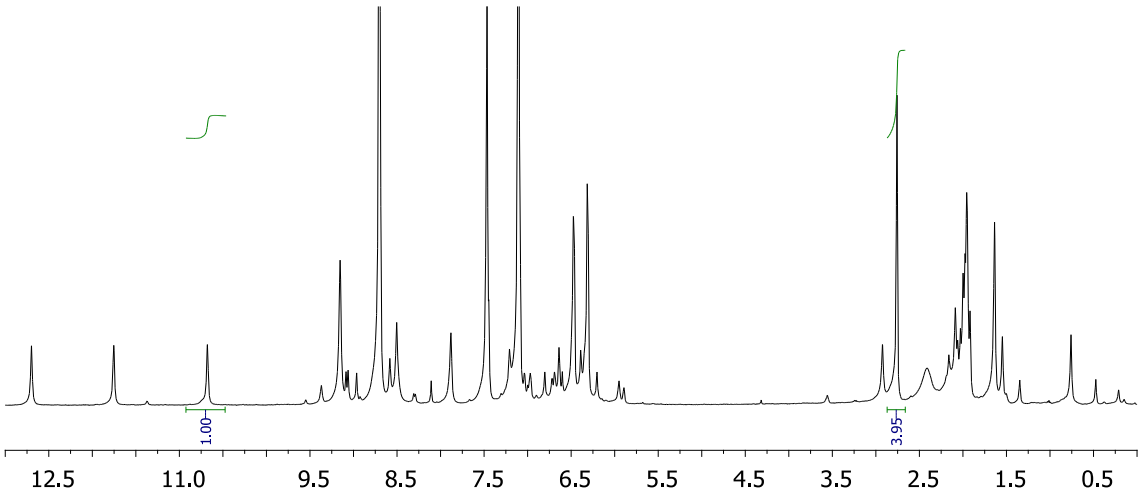

Figure 5: *In situ* ^{1}H NMR spectrum in d_5-pyridine of the reaction between **[UO_2(py)(H_2L)]** (1 eq.) and CpLi (2 eq.) (^{1}H NMR spectrum using pulse delays suitable for diamagnetic complexes between 13 and 0 ppm)

2.3.4. Reaction with two equivalents of $LiCPh_3$

The reaction between one equivalent of **[UO_2(THF)(H_2L)]** and two equivalents of trityl lithium in a mixture of pyridine, hexane and THF at −35 °C leads to the clean formation of **[(py)$_3$LiOUO(py)Li(py)(HL)]** and Ph_3CH, with no formation of Gomberg's dimer ($Ph_3CCH(C_6H_4)CPh_2$), Equation (**4**).

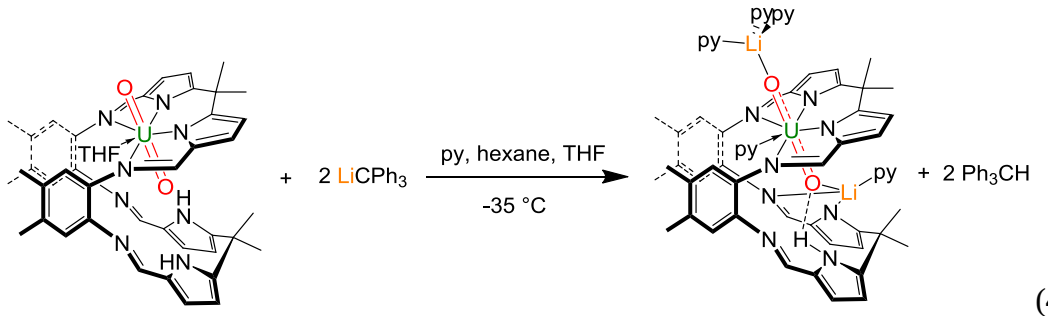

(**4**)

The comparison between the ^{1}H and $^{13}C\{^{1}H\}$ NMR spectra of this reaction with a genuine sample of Gomberg's dimer shows that the by-product formed is Ph_3CH, so in this case the reaction is not a radical reaction (Figures 6 and 7).[16]

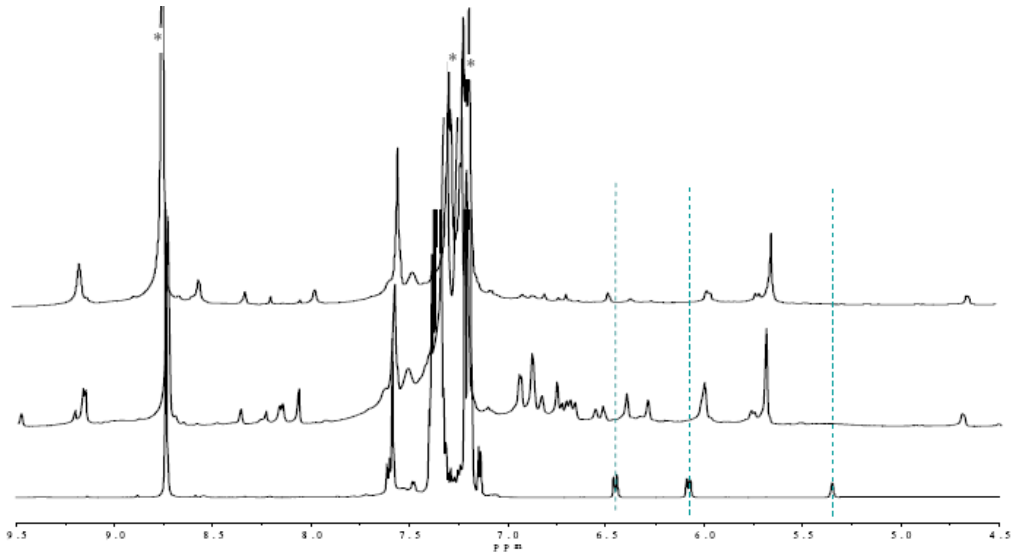

Figure 6: *In situ* ^{1}H NMR reaction in pyridine between one equivalent of **[UO_2(py)(H_2L)]** and two equivalents of Ph_3CLi to form **[(py)$_3$LiOUO(py)Li(py)(HL)]** and Ph_3CH. Stackplots of diamagnetic region, (top) before and (middle) after quenching to remove paramagnetic components; (bottom) a genuine sample of Gomberg's dimer made independently in pyridine. * = pyridine solvent; dotted vertical lines = characteristic diene CH resonances.

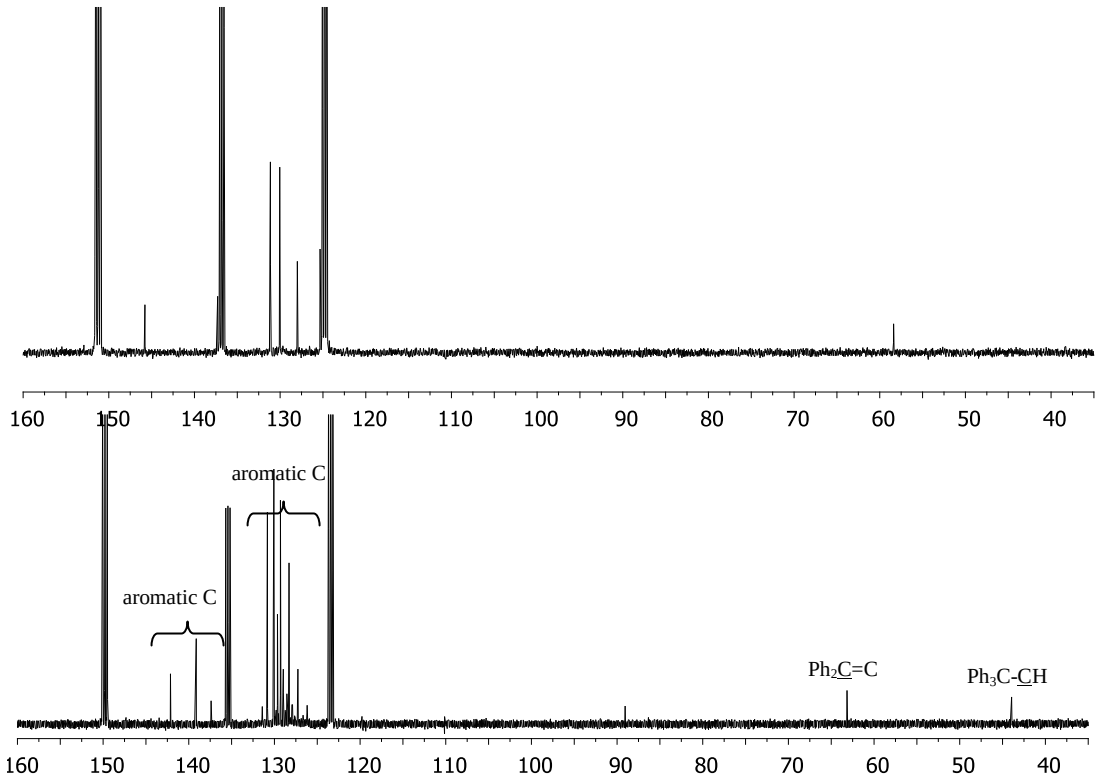

Figure 7: *In situ* $^{13}C\{^{1}H\}$ NMR reaction in pyridine between one equivalent of **[UO_2(py)(H_2L)]** and two equivalents of Ph_3CLi to form **[(py)$_3$LiOUO(py)Li(py)(HL)]** and Ph_3CH in d_5-pyridine (top); Gomberg's dimer made from chloride abstraction from $ClCPh_3$ in pyridine (bottom).

2.3.5. Reaction with two equivalents of lithium amide

The reaction between one equivalent of **[UO_2(THF)(H_2L)]** and two equivalents of $LiNH_2$ in pyridine at 120 °C for 48 h leads to the formation of the doubly lithiated compound **[(py)$_3$LiOUO(py)Li(py)(HL)],** Equation (**5**). Initially, the reaction affords a mixture of compounds which converts into the doubly lithiated compound after prolonged boiling in pyridine (by ^{1}H and $^{7}Li\{^{1}H\}$ NMR spectroscopy).

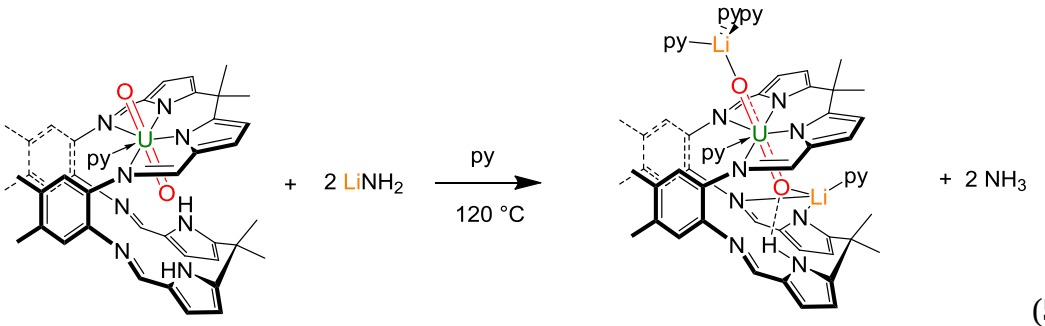

(**5**)

2.3.6. Reaction with two equivalents of lithium hydride

The reaction between one equivalent of **[UO_2(THF)(H_2L)]** and two equivalents of LiH in pyridine at 120 °C for 48 h leads to the formation of **[(py)$_3$LiOUO(py)Li(py)(HL)]**, Equation (**6**). As with the reaction with $LiNH_2$, a mixture of complexes is observed initially by NMR spectroscopy, but boiling at 120 ^{o}C converts these into the single, dilithiated complex.

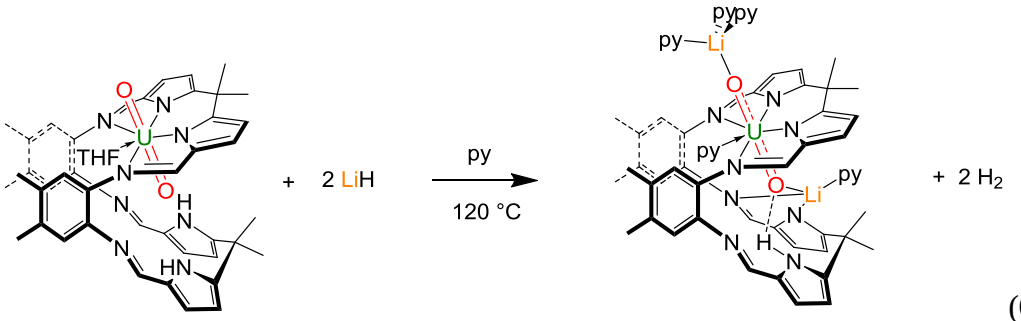

(**6**)

2.3.7. Reaction between Li_4L and UO_2Cl_2(THF)$_2$

The reaction between one equivalent of Li_4L and one equivalent of UO_2Cl_2(THF)$_2$ in pyridine at 120 °C for 48 h leads to the formation of **[(py)$_3$LiOUO(py)Li(py)(HL)]** in a good yield (67 %), Equation (**7**).

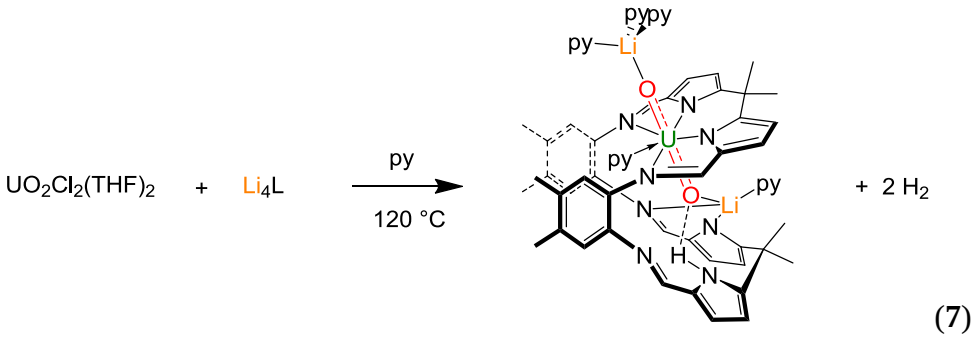

(**7**)

2.4. Synthesis of [(py)$_3$LiOUO(py){Li(py)}$_2$(L)]

The reaction between one equivalent of **[UO_2(THF)(H_2L)]** and three equivalents of LiN(SiMe$_3$)$_2$ in pyridine at room temperature for 16 h affords, after work-up, the complex **[(py)$_3$LiOUO(py){Li(py)}$_2$(L)]** as an orange-brown solid in a good yield (75%), Equation (**8**).

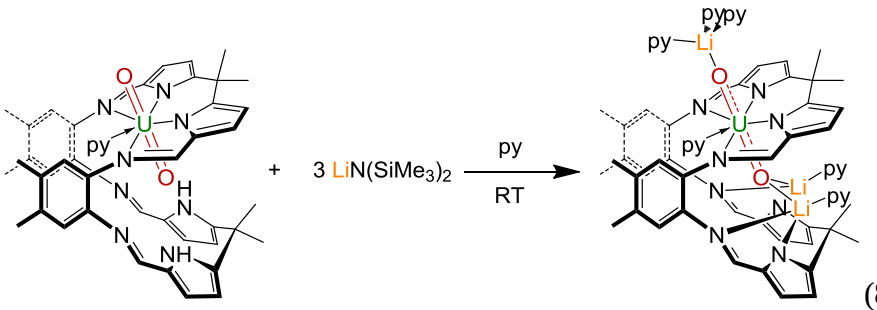

(**8**)

The complex was fully characterised; including by ^{1}H NMR and ^{7}Li{^{1}H} NMR spectroscopy, FTIR spectroscopy, elemental analysis and X-ray diffraction studies. The formation of a paramagnetic compound was observed in the ^{1}H NMR spectrum, with the numbers and integrals of the paramagnetically shifted resonances consistent with a wedged, Pacman structure of C_s symmetry in solution. The most paramagnetically shifted resonance, integrating for 3H corresponds to the *meso* methyl group pointing into the cleft of the ligand. Two resonances at 0.05 and −2.05 ppm, integrating for 6H each correspond to the methyl groups on the ligand backbone. The ^{7}Li{^{1}H} NMR spectrum contains only one resonance at 73 ppm, which implies that the three atoms of lithium are exchanging at room temperature. The FTIR spectrum does not contain a NH band, which agrees with the proposed formula, and the U=O stretch is shifted to 704 cm^{-1} and is in the range of the U=O stretch for U^{V} species and similar to that of the dilithiated complex **[(py)$_3$LiOUO(py)Li(py)(HL)]** (ν_{UO} 709 cm^{-1}).[10-12] The elemental analysis supports the formulation of **[(py)$_3$LiOUO(py){Li(py)}$_2$(L)]**. The solid state structure of **[(py)$_3$LiOUO(py){Li(py)}$_2$(L)]** was determined by X-ray diffraction (Figure 8). It was found that the Pacman structural motif of the uranyl macrocycle **[UO$_2$(THF)(H$_2$L)]** remains intact with one N4-donor compartment occupied by the uranyl and the other occupied by two lithium atoms Li2 and Li3 that functionalise the *endo*-oxo group. Li2 is sitting in half of the second pocket and coordinated by two nitrogen atoms of the macrocycle (imine N5 and pyrrole N6), the *endo*-oxo group and the nitrogen of a molecule of pyridine, as also Li3 (imine N9 and pyrrole N8). The *exo*-oxo group is also functionalised by a lithium atom Li1 with three coordinated pyridine molecules.

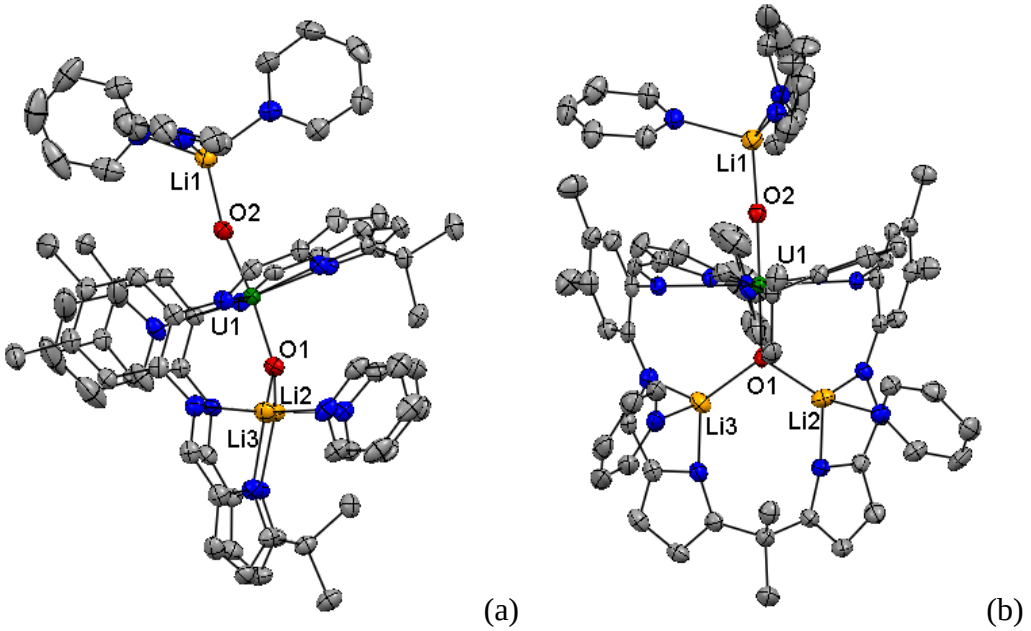

Figure 8: Solid state structure of **[(py)$_3$LiOUO(py){Li(py)}$_2$(L)]** showing side (a) and front view (b). For clarity all the hydrogen atoms and lattice molecules of solvent are omitted (displacement ellipsoids drawn at 50% probability).

Table 3: Selected bond distances (Å) and angles (°) of **[(py)$_3$LiOUO(py){Li(py)}$_2$(L)]**

U1-O1	1.894(2)
U1-O2	1.859(2)
U1-N9	2.617(3)
O1-Li2	1.979(7)
O1-Li3	1.976(7)
O2-Li1	1.914(7)
O1-U1-O2	174.21(10)
Li1-O2-U1	169.2(3)
Li2-O1-U1	123.1(2)

The uranium centre is seven coordinate and displays a distorted pentagonal bipyramidal geometry with the oxo groups *trans* (O1-U1-O2 174.21(10)°). From analysis of the uranium-oxygen bond lengths it is evident that the uranyl fragment is

in the 5+ oxidation state (Table 3). The *endo*- U1-O1 bond distance (1.894(2) Å) is significantly elongated compared to the bond distance of $[UO_2]^{2+}$ in the precursor **$[UO_2(py)(H_2L)]$** (U1-O1 1.7779(18) Å) and is similar to experimental and calculated bond distances for $[UO_2]^{+}$ (range 1.811- 1.934 Å).[3,10,12-15] The *exo*- U1-O2 bond (1.859(2) Å) distance is also longer than in **$[UO_2(py)(H_2L)]$** (U1-O2 1.7546(19) Å). The U1-O1 bond is longer than the U1-O2 bond. The UO bond lengths are in the same range to those of the dilithiated complex **$[(py)_3LiOUOLi(py)(HL)]$** (UO 1.834(4) and 1.879(5) Å). The three lithium atoms are four coordinate and display a tetrahedral geometry. The bond distance U1-N9 (2.617(3) Å) is slightly elongated in comparison to the U1-N9 bond distance (2.583(2) Å) in the uranyl complex **$[UO_2(py)(H_2L)]$** in the 6+ oxidation state.

2.5. Synthesis of $[Li(THF)][(THF)(Me_3Si)_2NLiOUO(THF)\{Li(THF)\}_2(L)]$

The reaction between one equivalent of **$[UO_2(THF)(H_2L)]$** and four equivalents of $LiN(SiMe_3)_2$ in THF at room temperature for 16 h leads to the formation of **$[Li(THF)][(THF)(Me_3Si)_2NLiOUO(THF)\{Li(THF)\}_2(L)]$** as a red-brown solid in a good yield (65%), Equation (**9**).

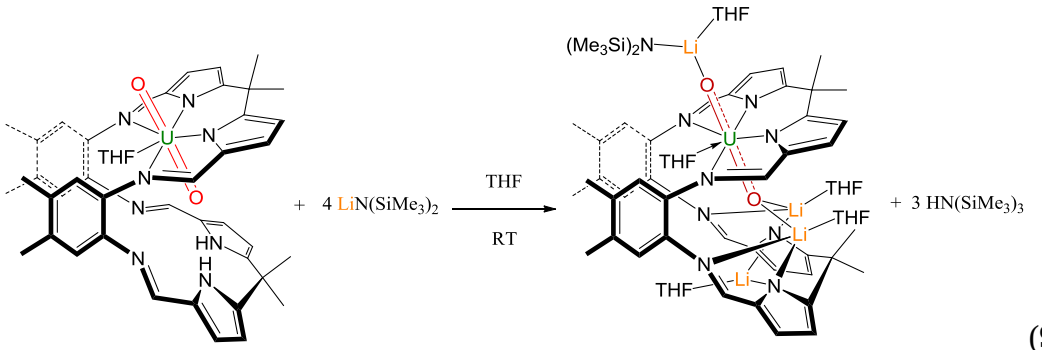

(**9**)

The complex was fully characterised, including by ^{1}H NMR and $^{7}Li\{^{1}H\}$ NMR spectroscopy, FTIR spectroscopy, SQUID, elemental analysis and X-ray diffraction studies. The formation of a paramagnetic compound was observed in the ^{1}H NMR spectrum in which the number and integrals of the paramagnetically-shifted resonances are concordant with a symmetric ligand arrangement, and consistent with a wedged, Pacman structure of C_s symmetry in solution (Figure 9). The most

paramagnetically shifted resonance corresponds to the *meso* methyl group within the cleft of the ligand and is the closest to the uranyl centre (see X-ray structure below). Two resonances at 0.41 and −0.95 ppm, integrating for 6H each correspond to the methyl groups on the aryl backbone. The $^{7}Li\{^{1}H\}$ NMR spectrum contains three resonances at 52.18, 38.52 and 20.45 ppm; these resonances are consistent with three different environments for the lithium atom (Figure 10). The resonance at around 1 ppm corresponds to free $LiN(SiMe_3)_2$.

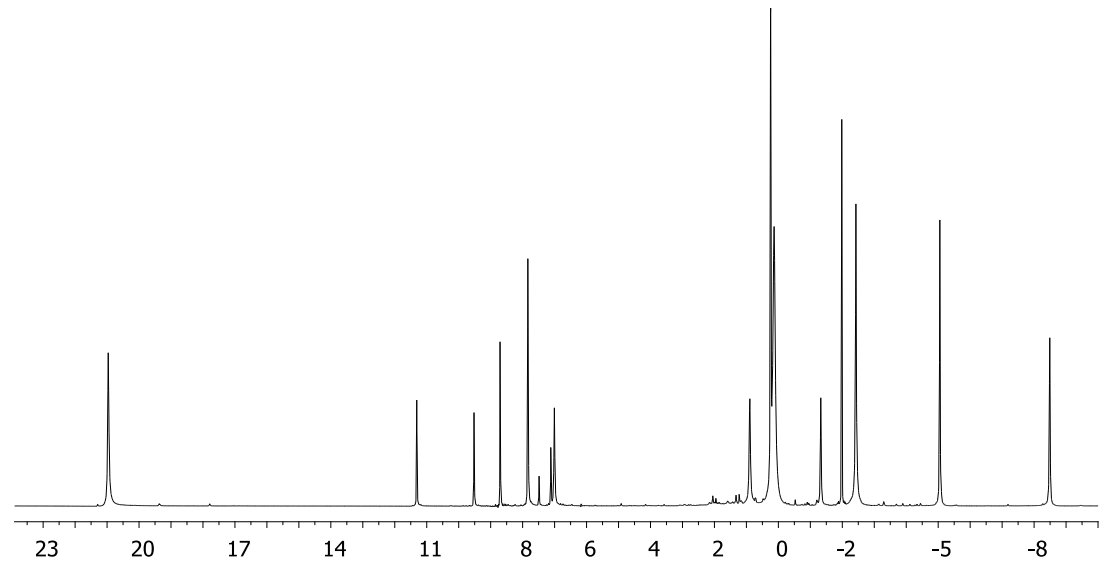

Figure 9: ^{1}H NMR spectrum (C_6D_6 + THF double presaturation) of **[Li(THF)][(THF)(Me$_3$Si)$_2$NLiOUO(THF){Li(THF)}$_2$(L)]**.

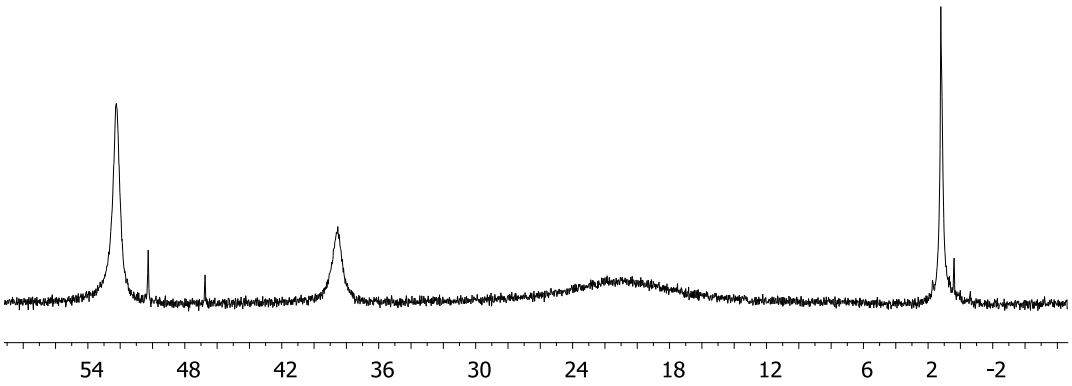

Figure 10: $^{7}Li\{^{1}H\}$ NMR spectrum C_6D_6 + THF double presaturation) of **[Li(THF)][(THF)(Me$_3$Si)$_2$NLiOUO(THF){Li(THF)}$_2$(L)]**

Temperature-dependent magnetic susceptibility data were collected for the isolated complex **[Li(THF)][(THF)(Me$_3$Si)$_2$NLiOUO(THF){Li(THF)}$_2$(L)]** from 2 to 300 K and is shown in Figure 11. The sample displays an effective magnetic moment that varies with the temperature, reaching an effective magnetic moment of 2.86 μ_B per uranium at 300 K. The study supports the presence of a single f-electron and no further reduction to U^{IV}.[17]

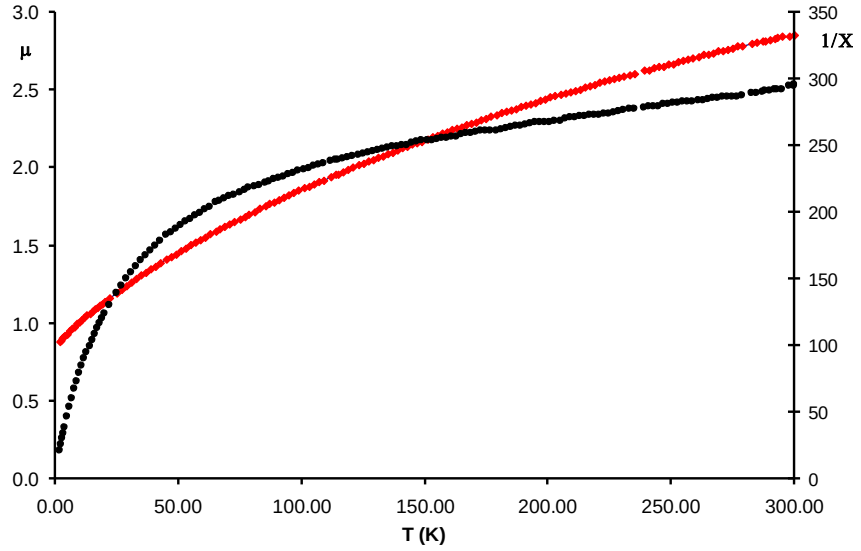

Figure 11: Solid state magnetic study of **[Li(THF)][(THF)(Me$_3$Si)$_2$NLiOUO(THF){Li(THF)}$_2$(L)]** from 2 to 300 K (red line μ; black line 1/χ)

In the FTIR spectrum, the absorption for the NH (at 3373 cm^{-1} in **[UO$_2$(THF)(H$_2$L)]** is absent, suggesting the loss of the pyrrole NH and the formation of **[Li(THF)][(THF)(Me$_3$Si)$_2$NLiOUO(THF){Li(THF)}$_2$(L)]**, and the characteristic absorption for the U=O bond at 908 cm^{-1} is not seen with two new absorptions appearing at 873 cm^{-1} and 704 cm^{-1}.[10-12] Elemental analysis supports the formulation of **[Li(THF)][(THF)(Me$_3$Si)$_2$NLiOUO(THF){Li(THF)}$_2$(L)]**. The complex was also characterised in the solid state by X-ray diffraction studies (Figure 12).

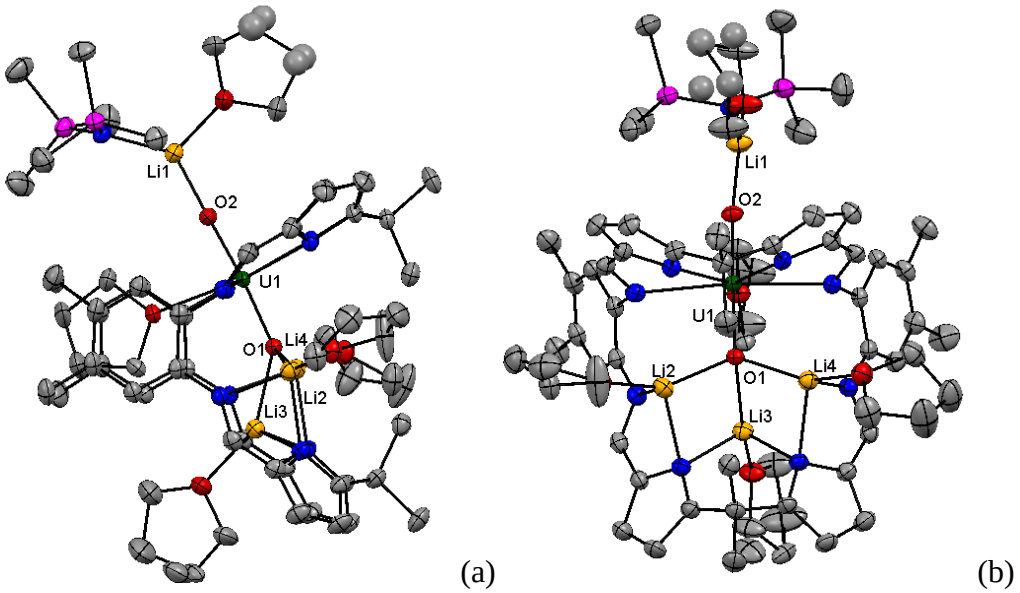

Figure 12: Solid state structure of **[Li(THF)][(THF)(Me$_3$Si)$_2$NLiOUO(THF){Li(THF)}$_2$(L)]**, showing side (a) and front view (b). For clarity all the hydrogen atom and the molecules of solvent are omitted (displacement ellipsoids drawn at 50% probability).

Table 4: Selected bond lengths (Å) and angles (°) of **[Li(THF)][(THF)(Me$_3$Si)$_2$NLiOUO(THF){Li(THF)}$_2$(L)]**

U1-O1	1.921(2)
U1-O2	1.850(2)
U1-O3	2.487(2)
O1-Li2	2.016(7)
O1-Li3	2.171(6)
O2-Li1	1.876(6)
O1-U1-O2	175.35(9)
Li1-O2-U1	174.0(3)
Li2-O1-U1	111.7(2)
Li3-O1-U1	142.8(2)

The Pacman structural motif of the uranyl macrocycle precursor remains intact with one N4 donor compartment occupied by the uranyl and the other by three lithium cations with a THF coordinated to each lithium atom. An interaction is observed between Li2, Li3, Li4 and the *endo*-oxo group, while the *exo*-oxo group O2 is coordinated to $Li\{N(SiMe_3)_2\}(THF)$. The uranium centre is seven coordinate and displays a distorted pentagonal bipyramidal geometry with the oxo group retaining a *trans* arrangement (O1-U1-O2 175.35(9)°) (Table 4). The equatorial sites are occupied by the nitrogen atoms of the macrocycle (U1-N1 2.599(3), U1-N2 2.465(3), U1-N3 2.467(3), U1-N4 2.577(3) Å) and the oxygen atom O3 from a THF molecule occupies the fifth site, sitting between the macrocyclic aryl rings. From analysis of the uranium-oxygen bond lengths it is evident that the uranyl fragment is in the 5+ oxidation state. The *exo*- U1-O2 bond distance (1.850(2) Å) is significantly elongated compared to that in the precursor complex **$[UO_2(THF)(H_2L)]$** (U1-O2 1.770(3) Å) and is similar to experimental and calculated bond distances for $[UO_2]^+$ (range 1.811- 1.934 Å).[3,10,12-15] The *endo*- U1-O1 bond distance (1.921(2) Å) is also longer than in **$[UO_2(THF)(H_2L)]$** (U1-O1 1.787(3) Å), but is within the range of distances reported for $[UO_2]^+$. The U1-O3 bond distance is elongated in comparison to the U1-O3 bond distance in the precursor uranyl Pacman complex **$[UO_2(THF)(H_2L)]$** (2.487(2) Å / 2.457(3) Å respectively). The UO bond lengths are similar to the UO bond lengths of the previous complexes **$[(py)_3LiOUOLi(py)(HL)]$** and **$[(py)_3LiOUO(py)\{Li(py)\}_2(L)]$**. Unusually, the *endo*-oxo bond is longer than the *exo*-oxo bond, and contrasts to those reported above and by us previously. The O1-Li2 and O1-Li3 bond lengths (2.016(7) and 2.171(6) Å) are elongated in comparison to the other lithiated complex in the 5+ oxidation state (1.94(2) Å for the dilithiated complex and 1.976(7) Å for the trilithiated complex).

2.6. Discussion

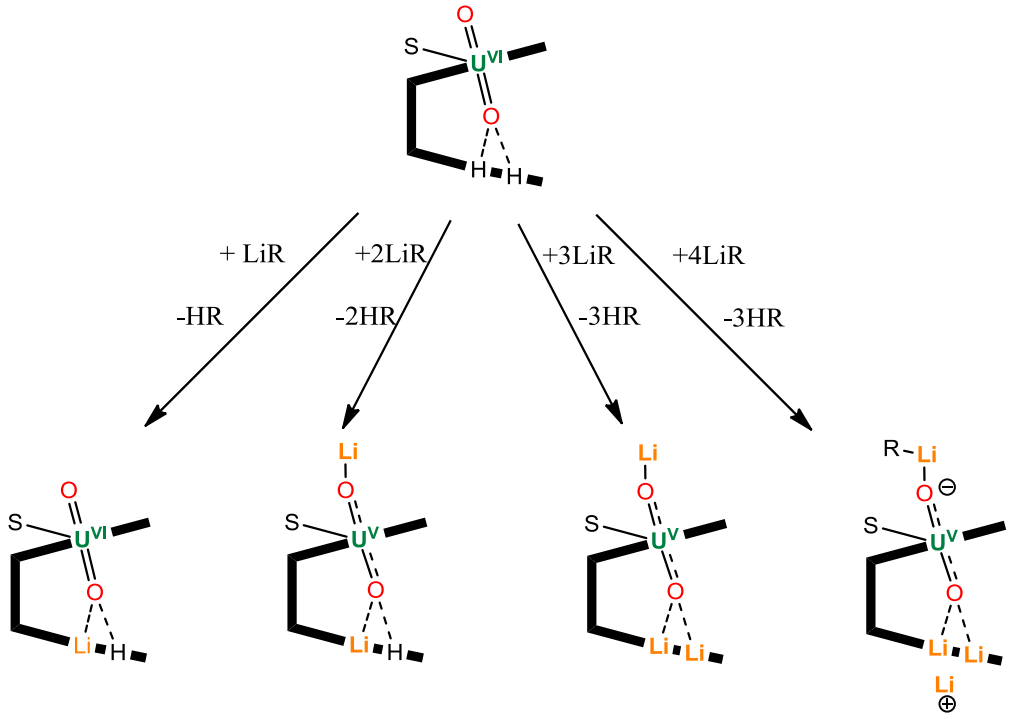

Scheme 4: Synthetic routes to lithiated diamagnetic and paramagnetic uranyl Pacman complexes

It has been thought that the reaction with a lithium base could provide structural and mechanistic information on the double deprotonation of the uranyl Pacman complex in the 6+ oxidation state $[UO_2(S)(H_2L)]$ (S = THF or py) by a potassium base.[3] In this chapter it has been shown that the use of different amounts of lithium reagent leads to the formation of the mono-, di-, tri- and tetra-lithiated complexes. To explain the reactivity of $[UO_2(S)(H_2L)]$ with the different amounts of lithium base and the formation of the singly reduced dilithiated complex **$[(py)_3LiOUO(py)Li(py)(HL)]$**, there are two possible mechanisms: direct reduction by the lithium reagent, C-H bond homolysis, either inter or intramolecularly. In each case, the first step of these reactions is the first deprotonation of one pyrrole NH by a lithium base and the formation of **[OUO(py)Li(py)(HL)]**. The most important step is the addition of the second equivalent of the lithium reagent, as it is the step during which the reduction of U(VI) to U(V) occurs (Figure 13).

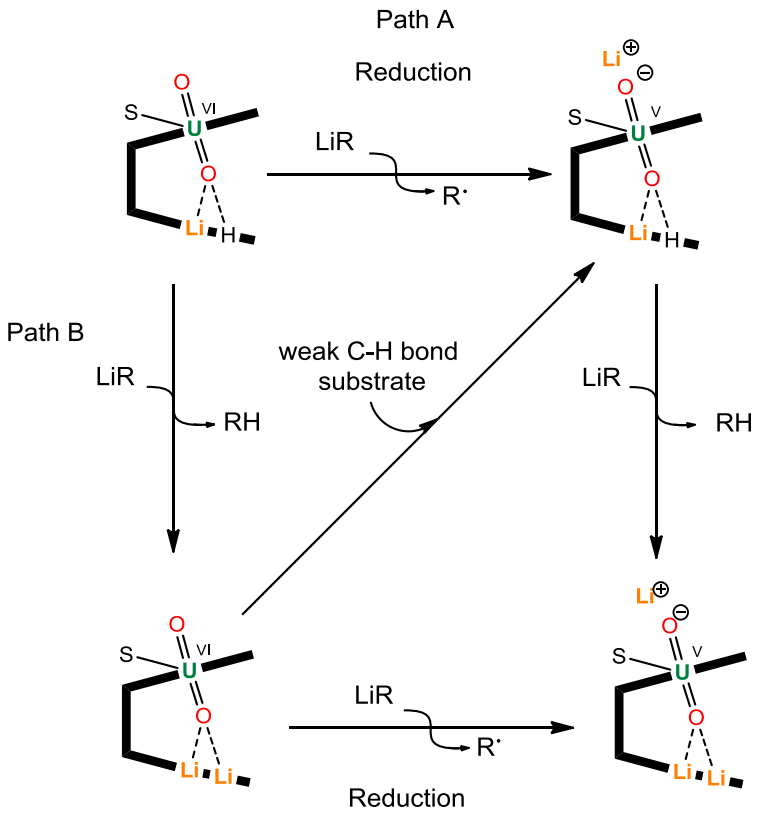

Figure 13: Possible mechanisms that generates uranyl $[UO_2]^+$ by reaction with a lithium reagent LiR. Two routes are proposed involving either Path A in which LiR (R = H, NH_2, N^iPr_2, $N(SiMe_3)_2$, CPh_3, C_5H_5) acts as a reducing agent or Path B in which LiR acts as a base.

2.6.1. Direct reduction: Path A.

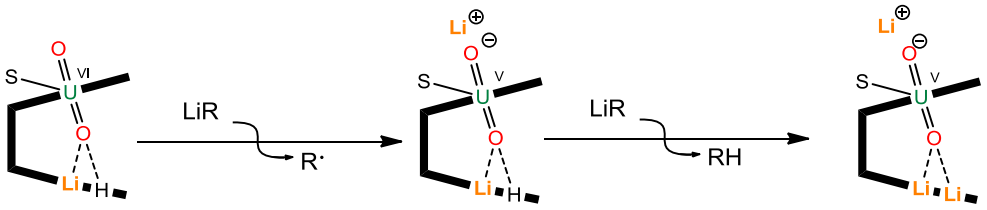

Scheme 5: Path A, lithium reagents acting as reductant

The addition of the first equivalent of lithium reagent acts as a base and deprotonates one pyrrole NH in the free pocket and leads to the formation of the

monolithiated complex **[OUO(THF){Li(THF)}(HL)]**. The addition of the second equivalent of lithium reagent such as LDA, LiH, and $LiNH_2$ can react as a direct reducing agent to lead to the formation of the dilithiated complex **[$(py)_3$LiOUO(py)Li(py)(HL)]**. According to the literature, the formation of an adduct between the Lewis acid $B(C_6F_5)_3$ and one of the uranyl oxo group in the complex $[UO_2(Acnac)_2]$ results in a shift of the U(VI)/U(V) couple from −1.35 V to −0.78 V (*vs.* Fc^+/Fc), i.e. a 0.57 V shift to a more positive potential.[18] The U(VI)/U(V) reduction potential of **[UO_2(THF)(H_2L)]** in THF is -0.54 V (versus standard hydrogen electrode (SHE)) but could have been shifted by the formation of the lithium adduct **[OUO(THF){Li(THF)}(HL)]** to a more positive potential (e.g. to + 0.03 V) and therefore could allow the reduction of this complex by addition of a second equivalent of lithium reagent such as LDA (oxidation potential E_{ox} = − 0.59 V versus SHE in THF/HMPA at −25 °C, HMPA = hexamethylphosphoramide).[19,20] Unfortunately we have been unable to measure the U(VI)/U(V) reduction potential of **[OUO(THF){Li(THF)}(HL)]** owing to a reaction with the electrolyte (Scheme **5**).

2.6.2. C-H bond homolysis: Path B

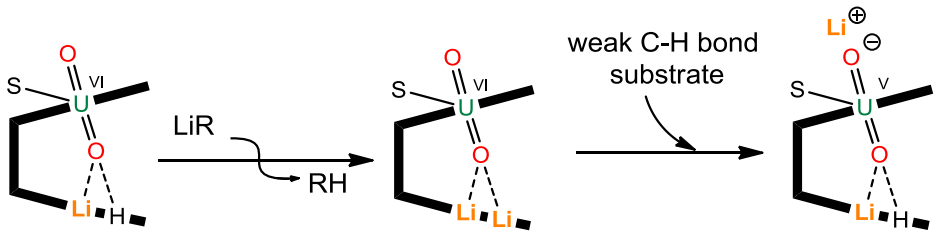

Scheme 6: Path B, lithium reagents acting as a base

In the case of $LiN(SiMe_3)_2$, the second equivalent can only react as a base. Indeed, its more positive oxidation potential (E_{ox} = +0.32 V versus SHE in THF at -25 °C) combined with the observation of the formation of two equivalents of $HN(SiMe_3)_2$ suggested that $LiN(SiMe_3)_2$ is acting only as a base and theoretically should form the uranyl Pacman complex $[UO_2(py)\{Li(py)\}_2(L)]$ in its 6+ oxidation state. The mixture observed from the reaction between one equivalent of **[UO_2(THF)(H_2L)]** and two equivalents of $LiN(SiMe_3)_2$ in the absence of a weak C-

H bond suggests that the reduction potential of $[UO_2(py)\{Li(py)\}_2(L)]$ is shifted to the positive such that a rapid reduction reaction occurs using $LiN(SiMe_3)_2$. However, in the presence of a weak C-H bond such as that in DHA, this complex can instead undergo H-abstraction followed by lithium rearrangement to form the dilithiated complex **$[(py)_3LiOUO(py)Li(py)(HL)]$** (Scheme 6). For this reduction and C-H abstraction reaction, two mechanisms are possible. The first possible mechanism is intermolecular C-H bond cleavage involving the uranyl oxo-group acting in a similar manner to a transition metal oxo complex to form initially the OH complex $[HOUO\{Li(py)_2\}(L)]$ (Figure 14). In this case, the oxo groups can undergo C-H bond cleavage and H-atom abstraction due to the formation of the Li_2 adduct that weakens the U=O bond, so the UO bond is more reactive.

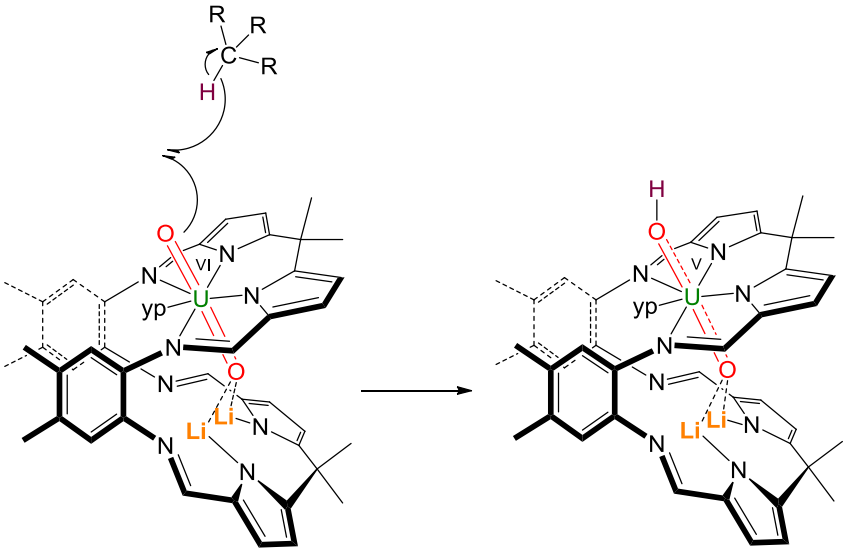

Figure 14: Reduction and C-H bond cleavage by the *exo*-oxo group

The second possible mechanism is an internal reduction and C-H bond cleavage by a pyrrolyl radical. Here, N-Li bond homolysis results in singly electron reduction of the uranyl and the formation of a pyrrolyl radical which is sufficiently reactive to abstract a hydrogen atom from some, but not all C-H substrates (Figure 15).[21]

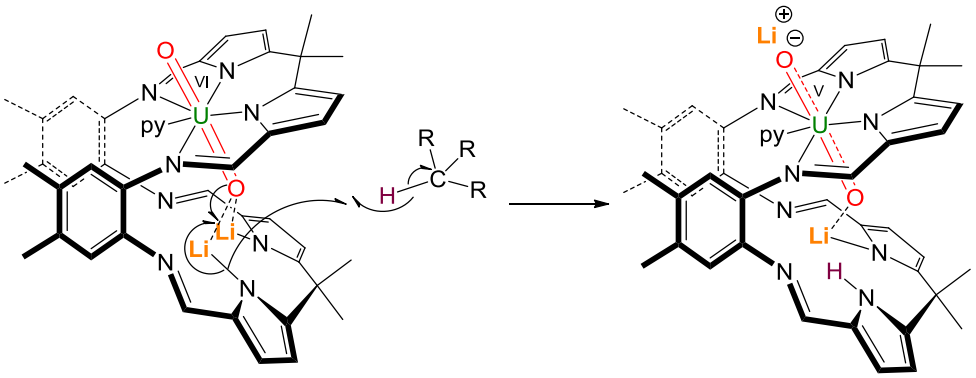

Figure 15: Reduction and C-H bond cleavage by the pyrrolyl radical

2.6.3. Reaction to probe the mechanisms

It is clear that the sequential addition of lithium reagent to the uranyl complex $[UO_2(S)(H_2L)]$ leads to the single-electron reduction and lithium functionalisation of the oxo groups. We know that the most important step is the addition of the second equivalent of lithium reagent because it is the point of the reduction, so to probe the mechanism, we carried out a few deuteration reactions.

The reaction between one equivalent of **$[UO_2(py)(H_2L)]$** and two equivalents of LDA in d_5-pyridine was monitored by ^{1}H NMR spectroscopy and showed, by comparison with the ^{1}H NMR spectrum of the same reaction in h_5-pyridine differences in integration at 60.1, 9.02, 7.74, 6.33, 5.49, 4.41, 2.49 and 1.58 ppm indicating incorporation of deuterium in several positions on the complex (Figure 16). The radical formed in this reaction is very reactive and will likely abstract H atom from the ligand as well as solvent and should deuterate the ligand or form $DN(^iPr)_2$.

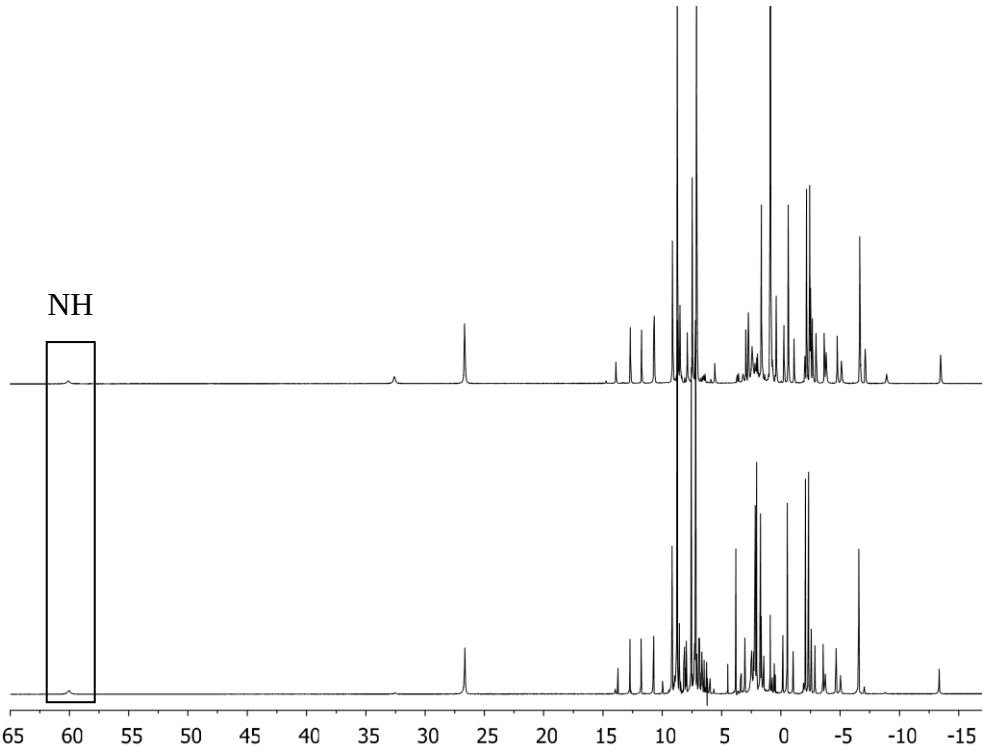

Figure 16: ^{1}H NMR spectra in pyridine of the reaction between one equivalent of **[UO_2(py)(H_2L)]** and two equivalents of LDA in d_5-pyridine (upper) or h_5-pyridine (lower)

The volatiles were removed from the reaction in d_5-pyridine and the residues redissolved in h_5-pyridine to allow the ^{2}H NMR spectrum to be obtained. Analysis of the NMR spectra shows deuterium incorporation in two places, at 60.1 ppm, which is assigned as the pyrrole NH and at 1.4 ppm assigned as a ligand *meso*-CH_3 group resonance (Figure 17). DN(^{i}Pr)$_2$ can not be observed in the ^{2}H NMR spectrum as it was removed from the reaction.

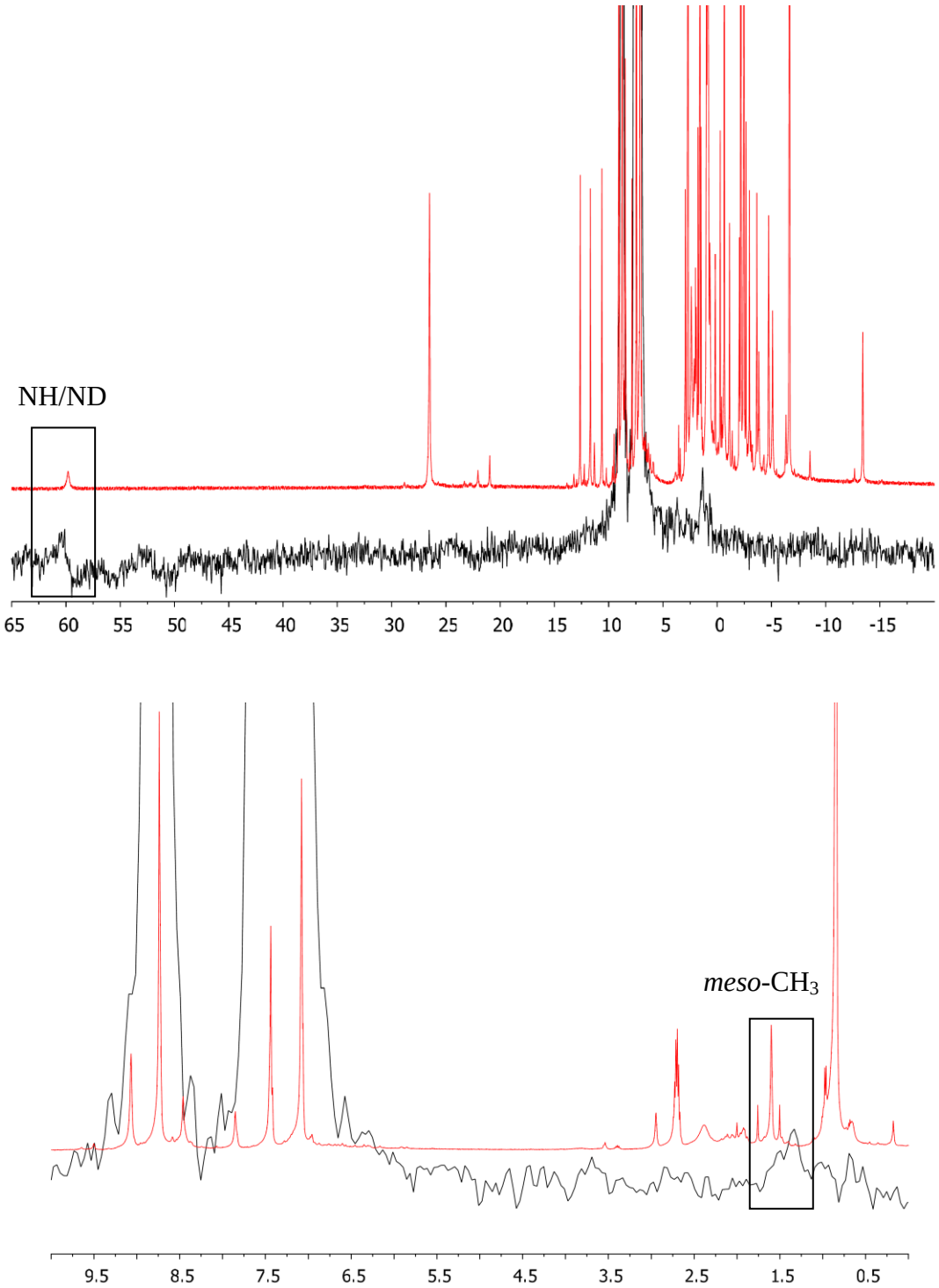

Figure 17: ^{1}H (red) and ^{2}H (black) NMR spectra overlaid (expansion underneath) of the reaction between one equivalent of **[UO_2(py)(H_2L)]** and two equivalents of LDA in d_5-pyridine. Two resonances are observed in the ^{2}H spectra that correspond to compound resonances; the high frequency singlet at 60.1 ppm assigned as the NH resonance, and a small resonance assigned as a ligand C*Me*$_2$ resonance.

The reaction between one equivalent of **[UO_2(THF)(H_2L)]** and two equivalents of LiC_5H_5 in d_5-pyridine leads cleanly to the formation of the dilithiated complex **[(py)$_3$LiOUO(py)Li(py)(HL)]** and two equivalents of HC_5H_5 as by-product identified by integration of the ^{1}H NMR spectrum (Figure 18). The ^{2}H NMR spectrum shows a resonance at 1.5 ppm assigned as a ligand meso-CH_3 resonance and indicating deuterium incorporation as seen in the preceding reaction (Figure 19). No radical-coupled products such as $C_{10}H_{10}$ or DC_5H_5 were present in the NMR spectra.

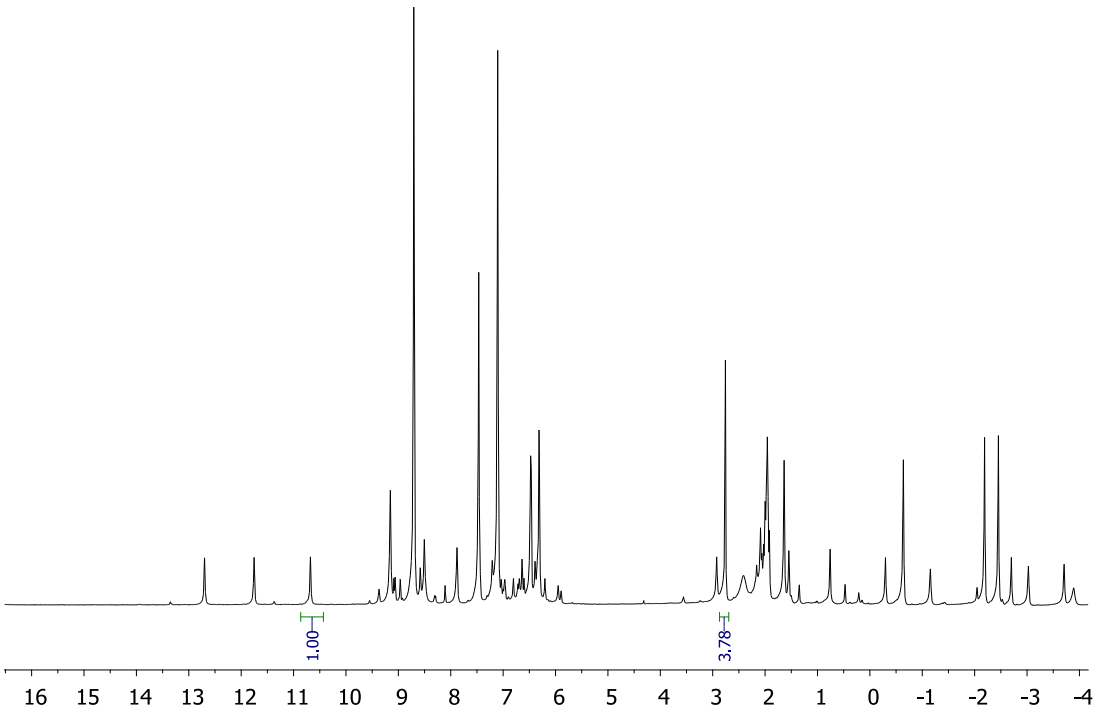

Figure 18: ^{1}H NMR spectrum using diamagnetic pulse sequences between 17 and −4 ppm of the reaction between one equivalent of **[UO_2(py)(H_2L)]** and two equivalents of LiC_5H_5 showing integration of the HC_5H_5 against one resonance of **[(py)$_3$LiOUO(py)Li(py)(HL)]** and a ratio of 2:1

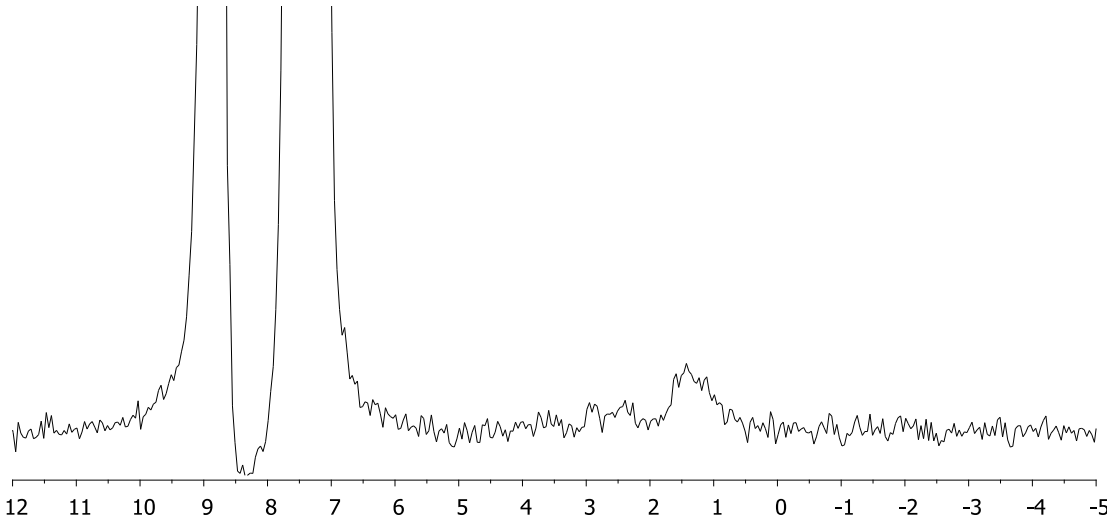

Figure 19: ^{2}H NMR spectrum of the reaction between one equivalent **[UO_2(py)(H_2L)]** and two equivalents of LiC_5H_5

Reactions were carried out in the presence of a weak C-H bonded substrate. The reaction between one equivalent of **[UO_2(py)(H_2L)]** and two equivalents of $LiN(SiMe_3)_2$ in the presence of five equivalents of H_4-DHA in d_5-pyridine leads to the rapid and clean formation of **[(py)$_3$LiOUO(py)Li(py)(HL)]**. Significantly, two equivalents of $HN(SiMe_3)_2$ were identified by integration of the N-H resonance at 1.46 ppm and the $SiMe_3$ resonance at 0.08 ppm, no $DN(SiMe_3)_2$ was observed in the ^{2}H NMR spectrum. Furthermore, a stoichiometric quantity of the coupled product 9,9',10,10'-tetrahydro-bianthracene is observed in the ^{1}H NMR spectrum and considered as the dominant H-abstraction along with a small amount of anthracene (Figure 20).[22,23] The reaction between one equivalent of **[UO_2(py)(H_2L)]** and two equivalents of $LiN(SiMe_3)_2$ in the presence of D_4-DHA in h_5-pyridine is less clean than the preceding reaction and leads to the formation of **[(py)$_3$LiOUO(py)Li(py)(HL)]** and a small quantity of **[(py)$_3$LiOUO(py){Li(py)}$_2$(L)]**; however, the formation of two equivalents of $HN(SiMe_3)_2$ is also observed. The ^{2}H NMR spectrum shows deuterium incorporation into **[(py)$_3$LiOUO(py)Li(py)(HL)]** at a few resonances corresponding to the deuteration of the ligand, and a broad band at 1.46 ppm suggesting that a small amount of $DN(SiMe_3)_2$ was formed during the reaction. The ^{2}H NMR spectrum shows as well the formation of the deuterated 9,9',10,10'-tetrahydro-bianthracene and the deuterated anthracene as by-products (Figure 21).

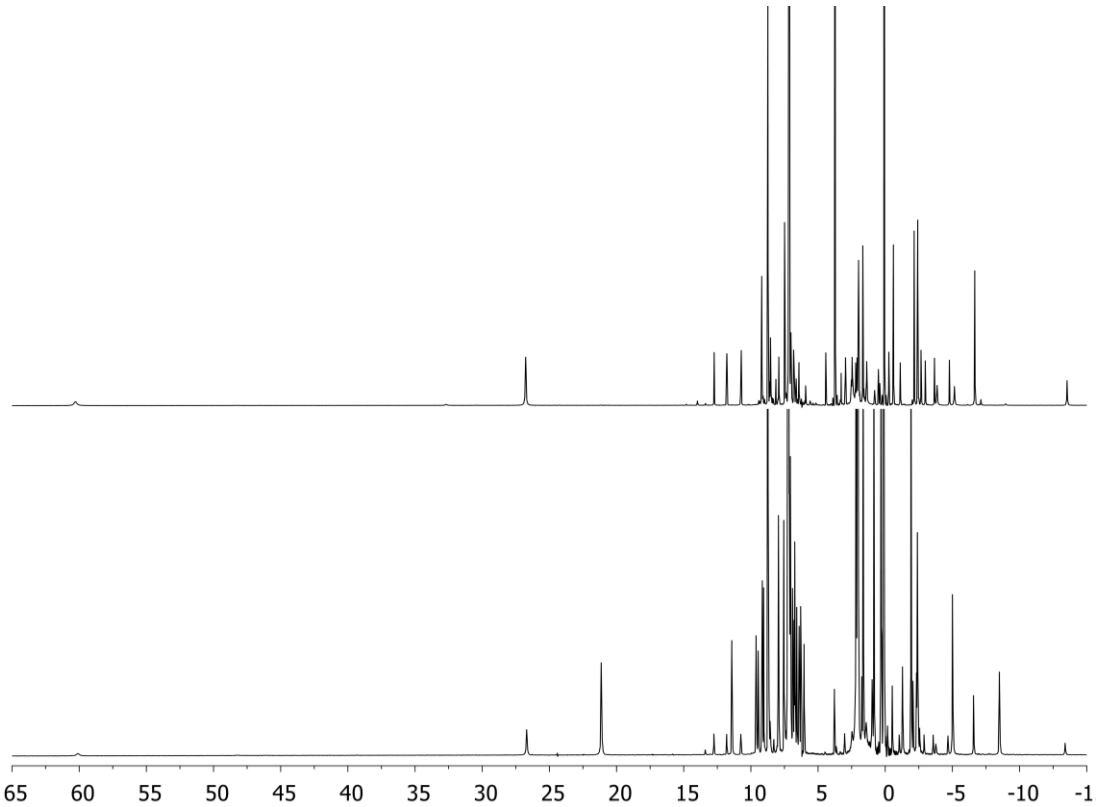

Figure 20: ^{1}H NMR spectra of the reaction between one equivalent of **[UO_2(py)(H_2L)]** and two equivalents of $LiN(SiMe_3)_2$ in the presence of H_4-DHA (upper) and D_4-DHA (lower)

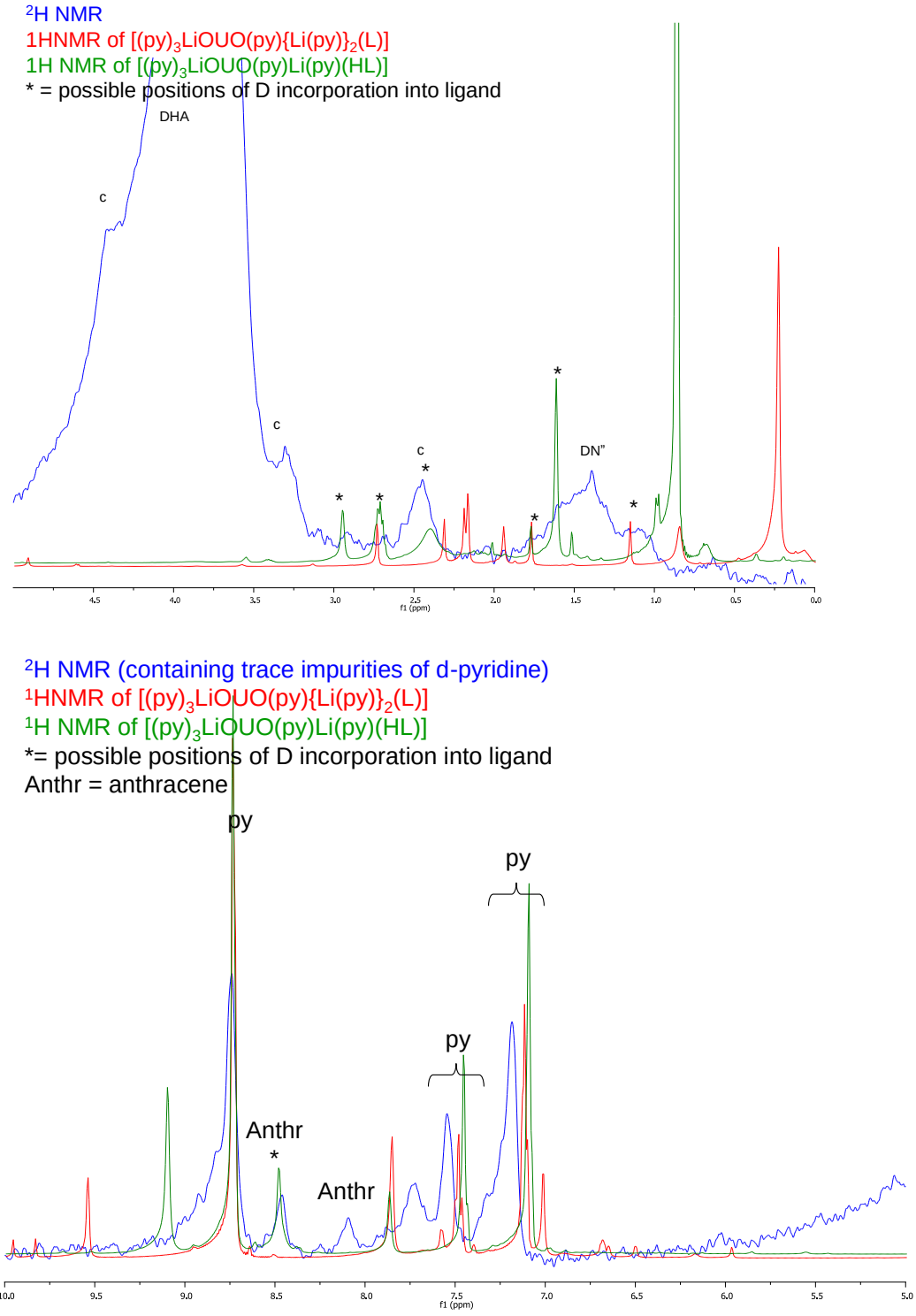

Figure 21: In situ ^{2}H NMR spectrum of the reaction between one equivalent of **$[UO_2(py)(H_2L)]$** and two equivalents of $LiN(SiMe_3)_2$ in the presence of D_4-DHA (blue) overlaid with ^{1}H NMR spectra of genuine samples of **$[(py)_3LiOUO(py)\{Li(py)\}_2(L)]$** (red) and **$[(py)_3LiOUO(py)Li(py)(HL)]$** (green) showing incorporation of deuterium into ligand

In this case, both C-H cleavage mechanisms are plausible; the ^{2}H NMR spectrum show deuterium incorporation into ligand CH and CH_3 bonds of the macrocycle but not clearly at the NH or (possible) OH resonances. As such, the direct interaction of an activated oxo group with the C-H bond appears unlikely. However, we know that the lithium cations exchange in the dilithiated complex **[(py)$_3$LiOUO(py)Li(py)(HL)]** at room temperature and that intermolecular reactions between uranyl species can occur as evidenced by the conversion of mixtures of **[(py)$_3$LiOUO(py){Li(py)}$_2$(L)]**, **[OUO(py)Li(py)(HL)]**, and **[UO$_2$(py)(H$_2$L)]** into **[(py)$_3$LiOUO(py)Li(py)(HL)]** at elevated temperature. So we cannot rule out the possibility of an oxo-based C-H bond cleavage mechanism.

The reaction between one equivalent of **[UO$_2$(py)(H$_2$L)]** with three equivalents of $LiN(SiMe_3)_2$ in d_5-pyridine produces only **[(py)$_3$LiOUO(py){Li(py)}$_2$(L)]** along with two equivalents of $HN(SiMe_3)_2$ and one equivalent of $DN(SiMe_3)_2$, identified by integration of N-H and $SiMe_3$ resonances in the ^{1}H NMR spectrum; $DN(SiMe_3)_2$ is supported by the presence of a resonance at 1.46 ppm in the ^{2}H NMR spectrum (Figure 22). As stated above, the generation of this complex can be explained if it is assumed that the reduction potential of the +VI intermediate dilithiated complex $[UO_2(py)(Li_2L)]$ has shifted to a more positive potential (+0.4 V versus SHE), upon the addition of the third equivalent of $LiN(SiMe_3)_2$ can effect the reduction. This implies the formation of two equivalents of $HN(SiMe_3)_2$ and one equivalent of the radical $\bullet N(SiMe_3)_2$ which in d_5-pyridine generates a mixture of $HN(SiMe_3)_2/DN(SiMe_3)_2$ in a ratio 2:1, as observed in the ^{1}H and ^{2}H NMR spectra (Figure 22).

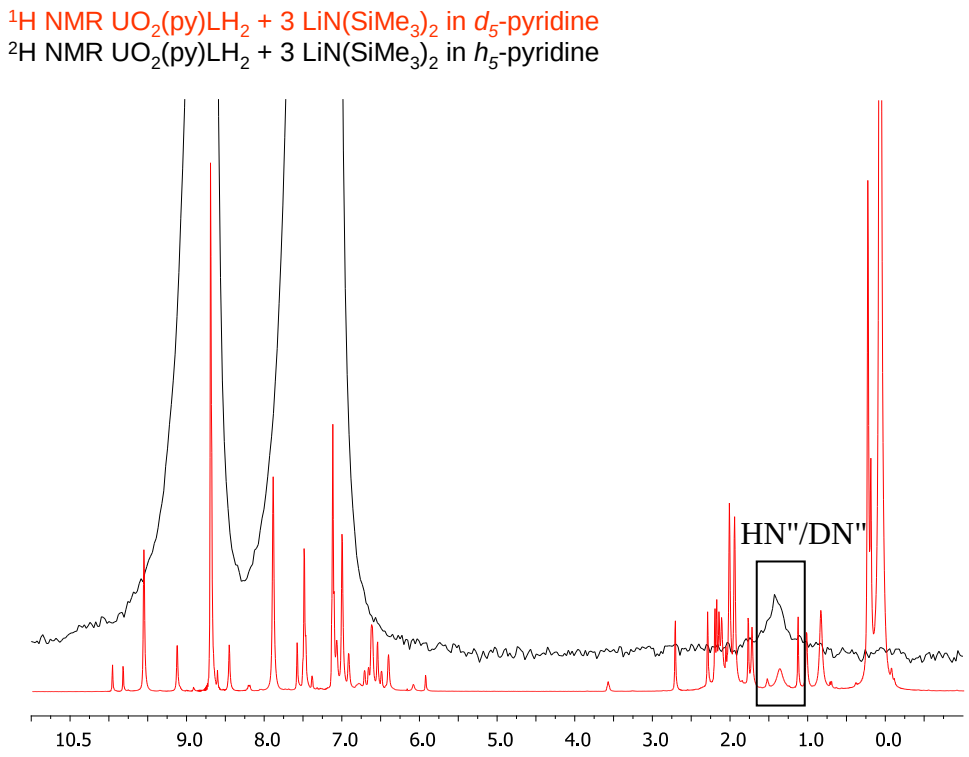

Figure 22: ^{1}H NMR spectrum of the reaction between one equivalent of **[UO_2(py)(H_2L)]** and three equivalents of $LiN(SiMe_3)_2$ in d_5-pyridine (red) overlaid with the ^{2}H NMR spectrum in h_5-pyridine of the same reaction in d_5-pyridine.

2.6.4. DFT calculations

To further investigate these mechanisms, DFT calculations were carried out by Prof. Laurent Maron and Dr Ahmed Yahia. The computed steps involved in the proposed paths A and B are found to be both kinetically and thermodynamically accessible at room temperature (Figure 23).

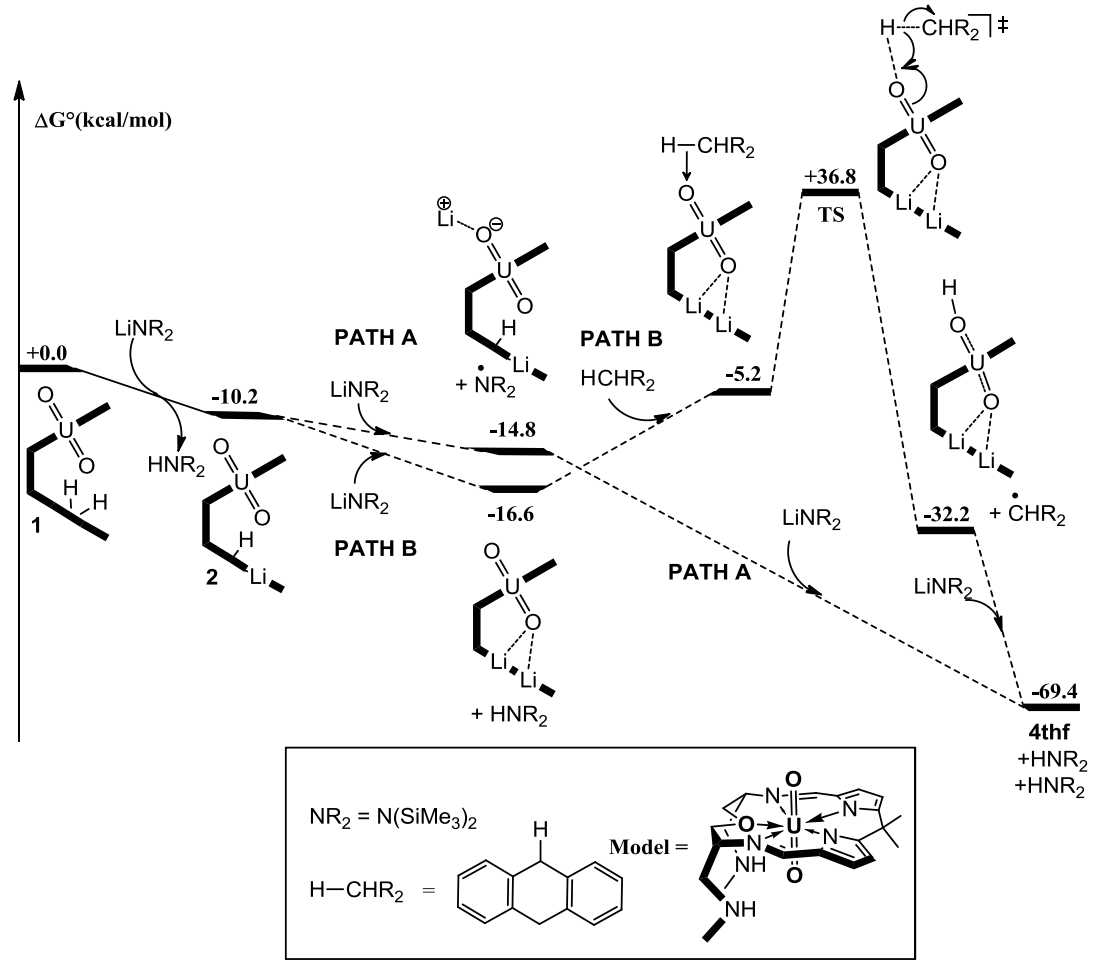

Figure 23: Computed energy profile for the reduction and oxo-group C-H activation by a model Pacman uranyl complex

The reduction of **[OUO(py)Li(py)(HL)]** by $LiN(SiMe_3)_2$ (Path A) is computed to be exergonic by −14.8 kcal mol^{-1}, while the deprotonation route (Path B), is −16.6 kcal mol^{-1}; the differences in these values are too small to show any preference from a computational perspective. Of the two possible C-H abstraction possibilities shown in Figure 23, the abstraction by the oxo-group from DHA has been computed and is found to be kinetically accessible with a barrier of 36.8 kcal mol^{-1} that is similar to that calculated for the analogous oxo silylation process.[4] Based on the geometry (the U-O bond is still short), the transition state is best described as a proton transfer between DHA and the exo-oxo group of $[UO_2]^{2+}$, with the reduction of the metal occurring immediately after the proton transfer, leading to **$[(py)_3LiOUO(py)Li(py)(HL)]$**. A DFT calculation for the energetics of the

alternative mechanism involving internal reduction and formation of a pyrrolyl radical (Path B) was not possible as it would not give the same product observed in the experiment and DFT cannot localise the electron. From **[(py)$_3$LiOUO(py)Li(py)(HL)]**, the formation of the triply-lithiated complex **[(py)$_3$LiOUO(py){Li(py)}$_2$(L)]** is computed to be highly favourable, and is exergonic by −69.4 kcal mol^{-1}.

2.7. Conclusions

We have shown reduction and oxo-functionalisation of the uranyl Pacman is induced by the endogenous bonding of lithium cations to the uranyl oxo group. The different results observed in this chapter suggest that more than one mechanism is possible and operates during the formation of the dilithiated complex. Lithium reagents such as LDA, $LiNH_2$, LiH, and LiC_5H_5 are likely to act as reductants and release a radical, which seems to be quenched by H-atom abstraction from the ligand or from the solvent. However, for $LiN(SiMe_3)_2$, we can state that the mechanism occurs by C-H bond homolysis by the doubly lithiated intermediate $[UO_2(py)(Li_2L)]$, but it is not possible to identify whether the U=O group or a pyrrolyl radical in the complex cleaves the C-H bond; unfortunately, DFT calculations have been unable to distinguish between the two mechanisms.

2.8. References

(1) Arnold, P. L.; Blake, A. J.; Wilson, C.; Love, J. B. *Inorg. Chem.* **2004**, *43*, 8206.
(2) Arnold, P. L.; Patel, D.; Blake, A. J.; Wilson, C.; Love, J. B. *J. Am. Chem. Soc.* **2006**, *128*, 9610.
(3) Arnold, P. L.; Patel, D.; Wilson, C.; Love, J. B. *Nature* **2008**, *451*, 315.
(4) Yahia, A.; Arnold, P. L.; Love, J. B.; Maron, L. *Chem. Commun.* **2009**, 2402.
(5) Burns, C. J.; Clark, D. L.; Donohoe, R. J.; Duval, P. B.; Scott, B. L.; Tait, C. D. *Inorg. Chem.* **2000**, *39*, 5464.
(6) Sarsfield, M. J.; Helliwell, M.; Raftery, J. *Inorg. Chem.* **2004**, *43*, 3170.
(7) Berthet, J.-C.; Nierlich, M.; Ephritikhine, M. *Dalton Trans.* **2004**, 2814.
(8) Berthet, J.-C.; Nierlich, M.; Ephritikhine, M. *Chem. Commun.* **2004**, 870.
(9) Hayton, T. W.; Wu, G. *Inorg. Chem.* **2008**, *47*, 7415.
(10) Arnold, P. L.; Love, J. B.; Patel, D. *Coord. Chem. Rev.* **2009**, *253*, 1973.
(11) Brown, J. L.; Wu, G.; Hayton, T. W. *J. Am. Chem. Soc.* **2010**, *132*, 7248.

(12) Berthet, J.-C.; Siffredi, G.; Thuery, P.; Ephritikhine, M. *Chem. Commun.* **2006**, 3184.
(13) Hay, P. J.; Martin, R. L.; Schreckenbach, G. *J. Physic. Chem. A* **2000**, *104*, 6259.
(14) Wander, M. C. F.; Kerisit, S.; Rosso, K. M.; Schoonen, M. A. A. *J. Physic. Chem. A* **2006**, *110*, 9691.
(15) Natrajan, L.; Burdet, F.; Pécaut, J.; Mazzanti, M. *J. Am. Chem. Soc.* **2006**, *128*, 7152.
(16) Lankamp, H.; Nauta, W. T.; MacLean, C. *Tetrahedron Lett.* **1968**, *9*, 249.
(17) Gamp, E.; Edelstein, N.; Malek, C. K.; Hubert, S.; Genet, M. *The Journal of Chemical Physics* **1983**, *79*, 2023.
(18) Hayton, T. W.; Wu, G. *Inorg. Chem.* **2009**, *48*, 3065.
(19) Bordwell, F. G.; Harrelson, J. A.; Satish, A. V. *The Journal of Organic Chemistry* **1989**, *54*, 3101.
(20) Bordwell, F. G.; Zhang, X.; Cheng, J. P. *The Journal of Organic Chemistry* **1991**, *56*, 3216.
(21) Kasai, P. H.; McLeod, D. *J. Am. Chem. Soc.* **1973**, *95*, 27.
(22) Lucas, R. L.; Powell, D. R.; Borovik, A. S. *J. Am. Chem. Soc.* **2005**, *127*, 11596.
(23) Zdilla, M. J.; Dexheimer, J. L.; Abu-Omar, M. M. *J. Am. Chem. Soc.* **2007**, *129*, 11505.

Chapter 3: Reactivity of the dilithiated complex

3.1. Introduction

As described in chapter two, new routes to form the singly-reduced uranyl have been developed and facilitate the understanding of the cation-cation interactions existing between the oxo group of the uranyl dication and alkali metals,[1,2] boranes,[3,4] transitions metals,[5] but only a few examples result in the formation of a covalent bond with the oxo group of the uranyl dication. These examples are limited to the formation of an O-Si bond as described. In 2008 it was shown by our groups that uranyl Pacman complexes can be reduced and oxo-functionalised via a treatment of the uranyl Pacman complex **[UO_2(THF)(H_2L)]** with two equivalents of potassium base and transition metal salts, forming the complex **[(Me_3SiO)UO(THF)($MX)_2$(L)]** (M = Fe, Zn; X = Cl, I), Equation (**1**).[6]

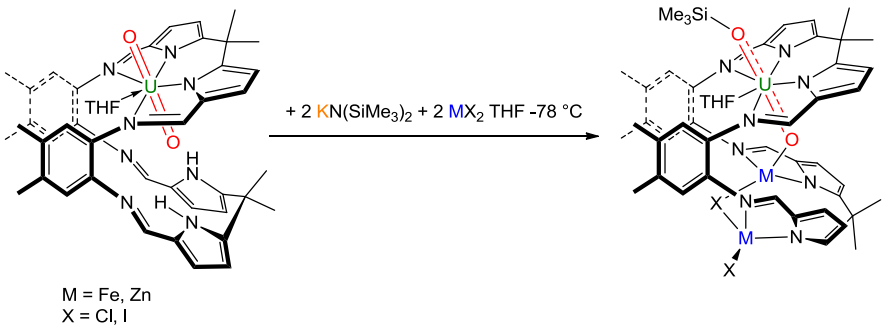

(**1**)

In 2010, Hayton and co-workers showed the direct reaction of the uranyl complexes with an excess of iodotrimethylsilane resulting in U^V oxo-silylation, Equation (**2**).[4,7,8]

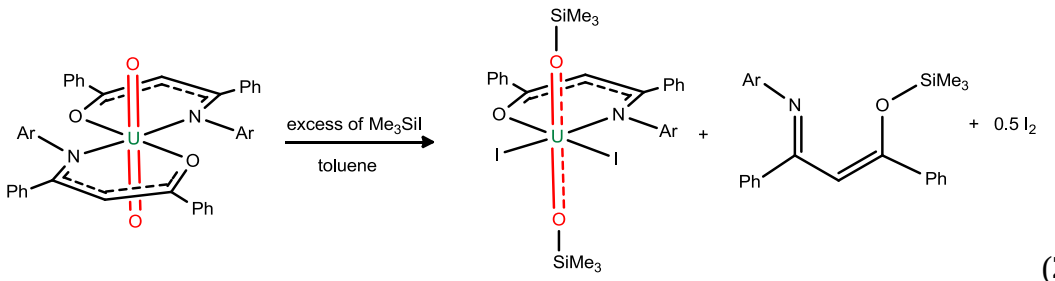

(**2**)

Berthet and co-workers reported that complete de-oxygenation of the uranyl can be realized by the addition of a large excess of trimethysilyl halides (Me_3SiX, X = Cl, Br, I) in acetonitrile forming U^{IV} halide complexes and $(Me_3Si)_2O$, Equation (**3**).[9]

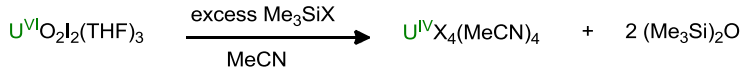

X = Cl, Br, or I (**3**)

3.2. Synthesis of [(R$_2$R'SiO)UO(py)Li(py)(HL)]

The complex described in Chapter 2, **[(py)$_3$LiOUO(py)Li(py)(HL)]**, is thermally stable, and its potential for further reactivity at the oxo group will be described in the following part.

3.2.1. Synthesis and characterisation of [(Me$_3$SiO)UO(py)Li(py)(HL)]

The one-pot reaction between one equivalent of **[(py)$_3$LiOUO(py)Li(py)(HL)]** and one equivalent of Me_3SiCl in pyridine at room temperature in a Teflon-tapped NMR tube results in a dark red solution and affords **[(Me$_3$SiO)UO(py)Li(py)(HL)]** as orange single crystals in moderate yield (45%), Equation (**4**).

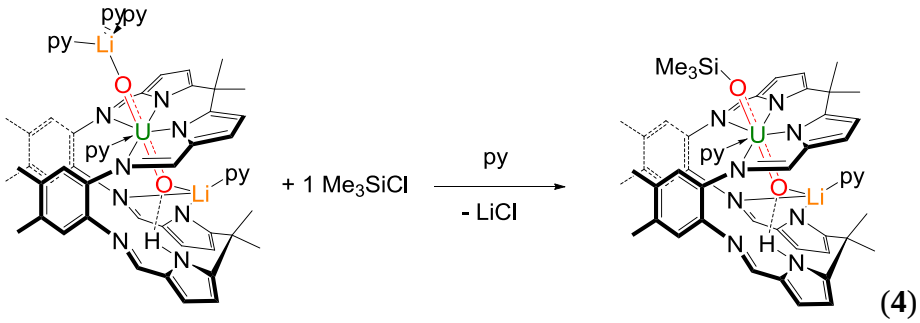

(**4**)

The complex has been fully characterised, including by ^1H and $^7Li\{^1H\}$ NMR spectroscopy and by FTIR spectroscopy. The complex crystallised from a saturated solution of pyridine at room temperature, unfortunately single crystals of sufficient quality were not obtained, precluding full X-ray analysis to confirm the connectivity of the complex as drawn in Equation 4. The formation of a new paramagnetic

compound is supported by the ^{1}H NMR spectrum, which contains the number of resonances with appropriate integral values consistent with the retention of a wedged, Pacman structure in solution of C_1 symmetry. Indeed the resonance integrals correspond to one or three protons, which are consistent with the asymmetric ligand; this is due to the lithium sitting in one side of the lower compartment. The resonance at 13.38 ppm, integrating for 9H, corresponds to the silyl group. The resonance at 39.26 ppm and integrating for 1 proton is assigned to the pyrrole NH. The ^{7}Li{^{1}H} NMR spectrum contains only one resonance at 74.83 ppm corresponding to the lithium coordinated to the pyrrole. The shift of this resonance is similar to the one observed in the di- and trilithiated complex **[(py)$_3$LiOUO(py){Li(py)}$_2$(L)]** (92 and 73 ppm respectively).

The FTIR spectrum displays a broad band at 3177 cm^{-1} corresponding to the pyrrole NH. Two stretches corresponding to the U=O at 861 and 705 cm^{-1}. These stretches are weakened substantially compared to that in the U^{VI} starting material **[UO$_2$(py)(H$_2$L)]** (ν U=O 908 cm^{-1}) but are in the range of the U=O stretches of the uranyl complexes in the 5+ oxidation state.[1,10]

3.2.2. Synthesis and characterisation of [(^{t}BuMe$_2$SiO)UO(py)Li(py)(HL)]

Similarly, the stoichiometric reaction between one equivalent of **[(py)$_3$LiOUO(py)Li(py)(HL)]** and ^{t}BuMe$_2$SiCl in pyridine in a Teflon-tapped NMR tube at room temperature results in the formation of a dark red solution which was characterised as containing the complex **[(^{t}BuMe$_2$SiO)UO(py)Li(py)(HL)]**, Equation (**5**).

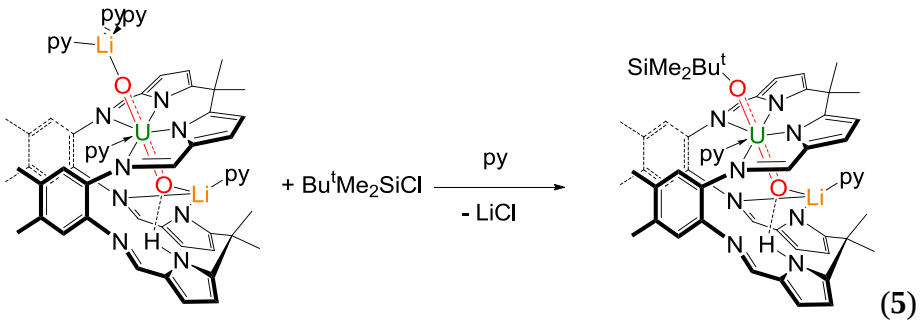

(**5**)

The compound was only characterised by ^{1}H NMR spectroscopy. The formation of a paramagnetic compound was observed in the ^{1}H NMR spectrum although all the resonances could not be assigned but the number and integrals of the paramagnetically shifted resonances are consistent with the retention of a wedged, Pacman structure in solution of C_1 symmetry. The most paramagnetically shifted resonance at 38.60 ppm is assigned to the pyrrole NH. The resonance at 8.36 ppm integrating for 9 protons can be assigned to the tert-butyl group of the silyl group on the *exo*-oxo group.

3.3. Synthesis and characterisation of [(HO)UO(py)(H$_2$L)]

The reaction between one equivalent of **[(py)$_3$LiOUO(py)Li(py)(HL)]** and 1.9 equivalents of HCl in Et_2O/pyridine (but this could vary according to the concentration of the solution of HCl in Et_2O and be 2 equivalents of HCl) at −40°C results in the formation of the protonated uranyl macrocycle **[(HO)UO(py)(H$_2$L)]** as a poorly soluble yellow-brown solid in good yield (70%), Equation (**6**).

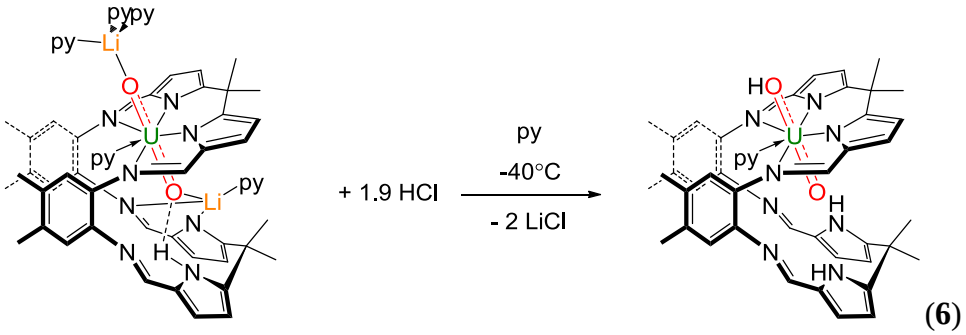

(**6**)

The complex was fully characterised, but unfortunately we have been unable to crystallise the complex and unequivocally confirm its structure in the solid state. The formation of a new paramagnetic compound was observed in the ^{1}H NMR spectrum although the individual resonances could not be assigned but the number and integrals of the paramagnetically shifted resonances suggest a symmetric ligand arrangement and are consistent with the retention of a wedged, Pacman structure in solution of C_s symmetry (Figure 1). The most paramagnetic resonance at 86.39 ppm, integrating for 1H, is assigned to the OH. The two resonances integrating for 6H each at 0.49 and −2.39 ppm correspond to the methyl group on the aryl backbone.

The pyridine in the fifth site is not observed in the spectrum due to the exchange with the deuterated pyridine. From the ^{1}H NMR spectrum we have been unable to determine if the complex was monomeric or dimeric. The $^{7}Li\{^{1}H\}$ NMR spectrum contains no resonance between 0 and 150 ppm supporting the absence of lithium in the N4-donor compartment.

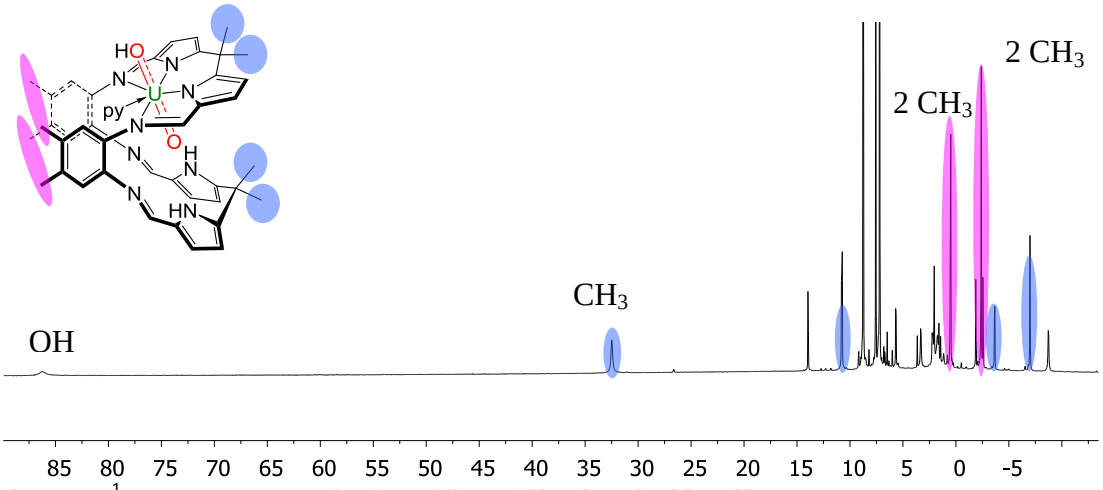

Figure 1: ^{1}H NMR spectrum in d_5-pyridine of **[(HO)UO(py)(H_2L)]**

The FTIR spectrum contains a weak and broad band at 3376 cm^{-1} which could derive from a pyrrole NH, a weak band at 3189 corresponding to the OH and an absorption at 765 cm^{-1} assigned to the asymmetric $[UO_2]^{+}$ stretch, which is weakened substantially compared to that in the U^{VI} starting material **[UO_2(THF)(H_2L)]** (ν U=O 908 cm^{-1}), and is in the same range of the $[UO_2]^{+}$ stretch observed in the complex $[U(OSiMe_3)_2(^{Ar}acnac)I_2]$ (Ar = 3,5-^{t}Bu2C_6H_3) reported by Hayton and co-workers (ν U=O 770 cm^{-1}). Elemental analysis supports the formulation of **[(HO)UO(py)(H_2L)]**.

To confirm the formation of the complex, the reaction between one equivalent of **[$(py)_3$LiOUO(py)Li(py)(HL)]** and 1.9 equivalents of DCl in Et_2O/pyridine has been followed by ^{1}H NMR and ^{2}H NMR spectroscopy (Figure 2). The ^{2}H NMR spectrum shows a resonance at 86.3 ppm corresponding to the OH resonance in the ^{1}H NMR spectrum and also a resonance at 7.30 ppm corresponding to one pyrrole NH. This resonance is obscured by the resonance of the pyridine in the ^{1}H NMR spectrum. The ^{1}H NMR spectrum of **[(DO)UO(py)(HDL)]** contains a

resonance at 86.39 ppm integrating for 0.5 proton indicating some exchange H/D between the OH and pyrrole NH.

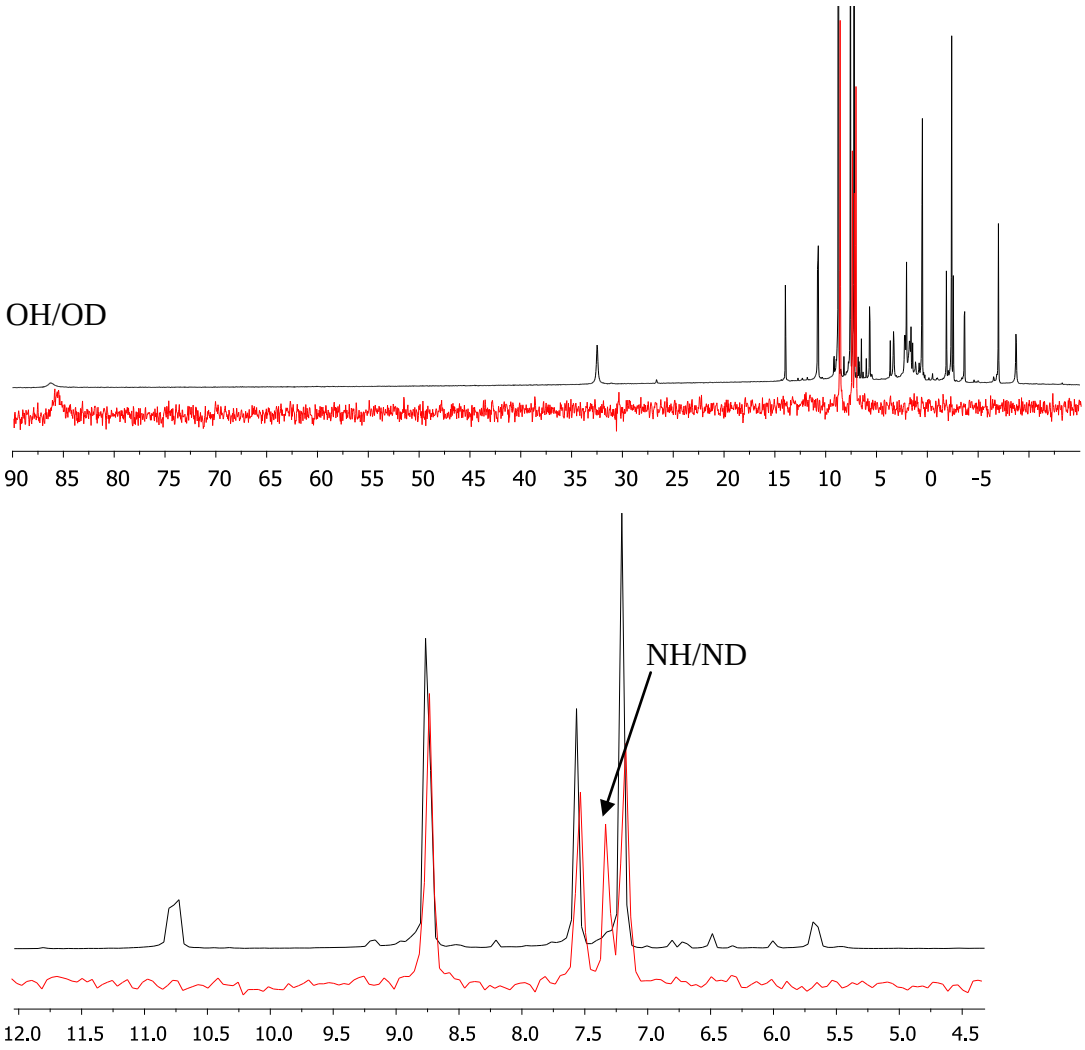

Figure 2: ^{1}H (black) and ^{2}H (red) NMR spectra overlaid (expansion underneath) of the reaction between one equivalent of **[(py)$_3$LiOUO(py)Li(py)(HL)]** and two equivalents of DCl.

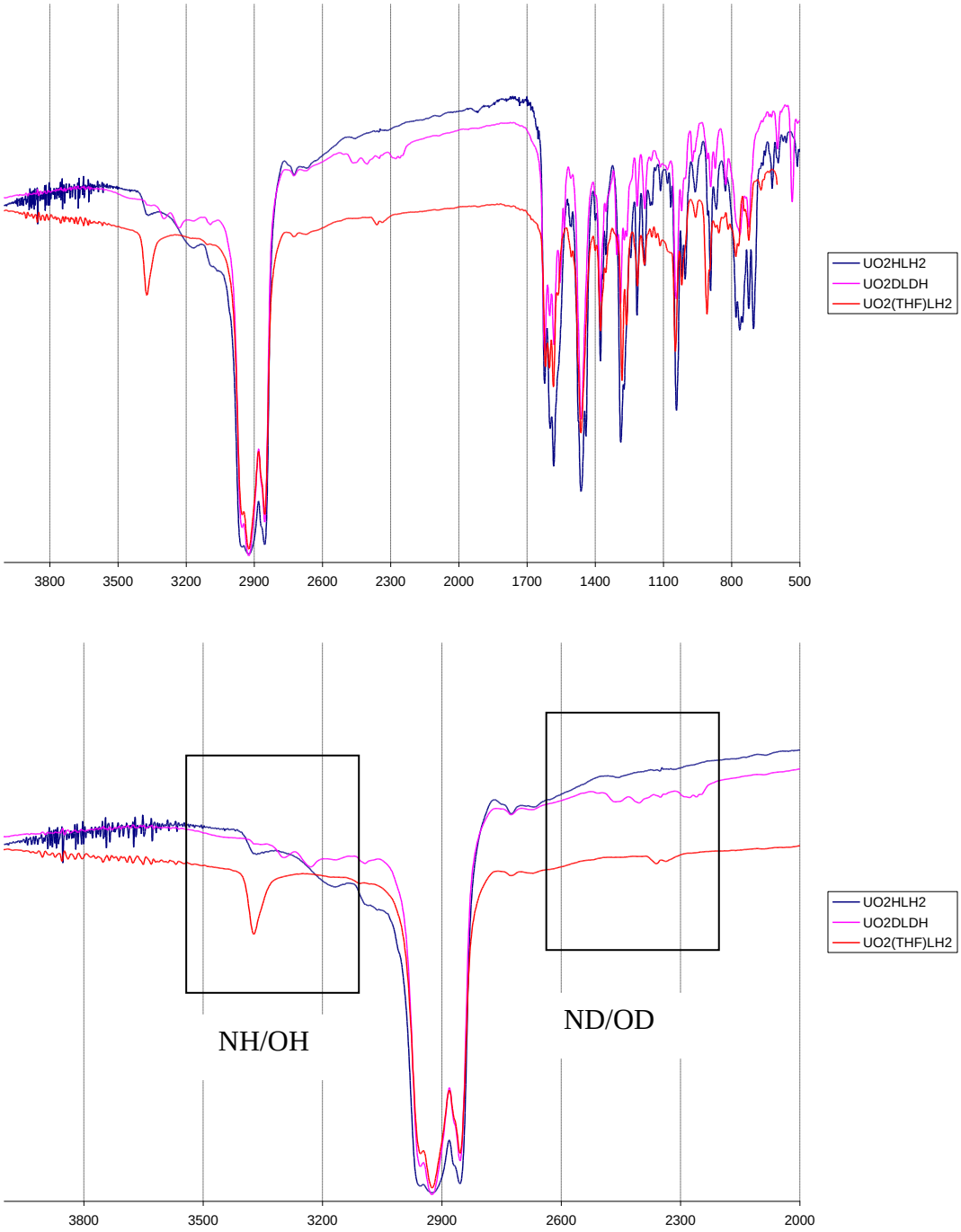

Figure 3: FTIR spectra overlaid of **[(HO)UO(py)(H_2L)]** (blue), **[(DO)UO(py)(DHL)]** (pink), and **[UO_2(THF)(H_2L)]** (red) (expansion underneath).

The FTIR spectrum of **[(DO)UO(py)(HDL)]** (Figure 3) shows the overlap of the OH and NH stretches between 3378 and 3108 cm^{-1}, the deuteration of the OH and NH is observed between 2478 and 2269 cm^{-1} and is in accordance with reduced mass calculated values between 2465 and 2259 cm^{-1} according to the empirical

equation $\nu_i/\nu = \sqrt{(\mu/\mu_i)}$, ($\nu_{ND} = \nu_{NH}$ x 0.730; $\nu_{OD} = \nu_{OH}$ x 0.727) (Figure 3 and Table 1).

	$\nu_{NH/OH}$	ν_i (calc)	ν_{obs}
NH/ND	3378	2465	2478
	3307	2414	2414
	3241	2365	2358
OH/OD	3178	2310	2298
	3108	2259	2269

Table 1: NH/ND and OH/OD stretches and calculated shifts for **[(HO)UO(py)(H_2L)]** and **[(DO)UO(py)(HDL)]**.

Unfortunately, we have been unable to crystallise **[(HO)UO(py)(H_2L)]**, but to confirm the 5+ oxidation state of **[(HO)UO(py)(H_2L)]**, the stoichiometric reaction between one equivalent of **[(HO)UO(py)(H_2L)]** and one equivalent of trityl chloride was carried out. The reaction was monitored by ^{1}H NMR spectroscopy and shows a 2:1 ratio of the single-electron oxidised product **[UO_2(py)(H_2L)]** and Gomberg's dimer, $Ph_3CCH(C_6H_4)CPh_2$, which is formed from single-electron abstraction and therefore the oxidation of **[(HO)UO(py)(H_2L)]**, Equation (**7**).[11] Also the stoichiometry of the reaction proves that the hydroxyl complex is monomeric; otherwise resonances of the complex **[(HO)UO(py)(H_2L)]** would be present in the ^{1}H NMR spectrum (Figure 4).

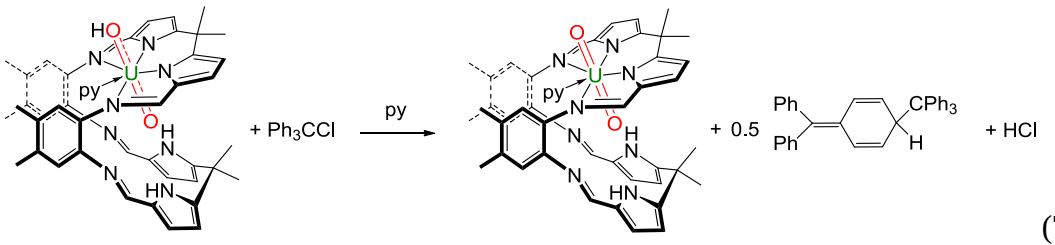

(**7**)

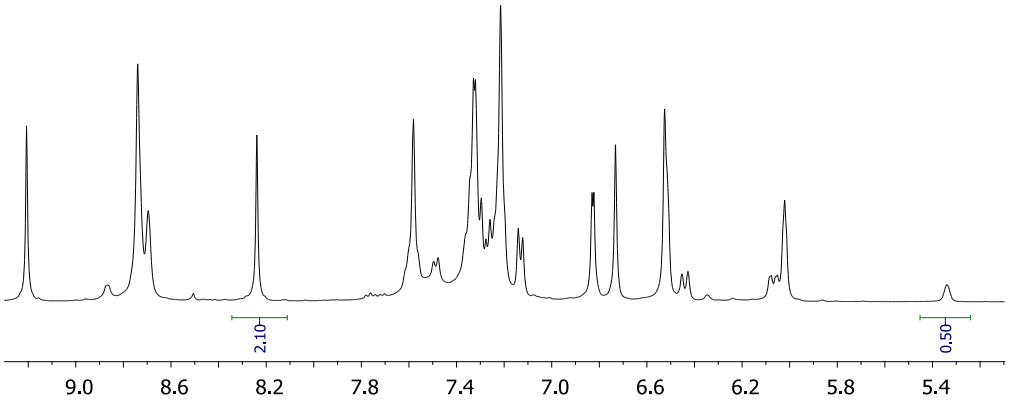

Figure 4: *In-situ* ^{1}H NMR spectrum of the reaction between **[(HO)UO(py)(H$_2$L)]** and Ph_3CCl

Another reaction to confirm the formation of **[(HO)UO(py)(H$_2$L)]** was the stoichiometric reaction between **[(HO)UO(py)(H$_2$L)]** and TEMPO ((2,2,6,6-tetramethylpiperidine-1-yl)oxyl) which regenerates cleanly **[UO$_2$(py)(H$_2$L)]** through H-abstraction, forming TEMPO-H (1-hydroxy-2,2,6,6-tetramethylpiperidine), Equation (**8**).

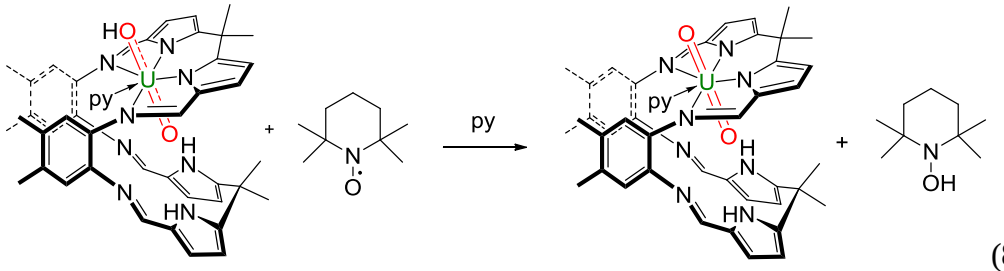

(**8**)

The reaction between one equivalent of **[(HO)UO(py)(H$_2$L)]** and two equivalents of $LiN(SiMe_3)_2$, monitored by ^{1}H NMR spectroscopy, regenerates **[(py)$_3$LiOUO(py)Li(py)(HL)]** and two equivalents of $HN(SiMe_3)_2$, Equation (**9**).

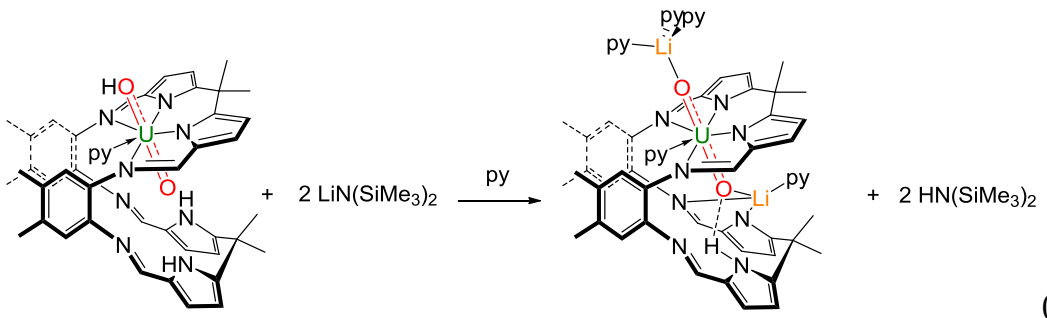

(**9**)

3.4. Silylation of reduced uranyl Pacman

The reactivity of **[(HO)UO(py)(H_2L)]** towards chlorosilanes has been monitored to prove the formation of **[(HO)UO(py)(H_2L)]** and to try to identify possible mechanisms for the silyl oxo functionalisation observed in the complexes **[(Me_3SiO)UO(THF)($MX)_2$(L)]** (M = Fe, Zn; X = Cl, I).[6] The DFT calculations of the reaction to form the complex [(Me_3SiO)UO(S)(Li_2L)] via the OH complex [(HO)UO(Li_2L)], suggest that the formation of the silylated product is not thermodynamically favourable from the OH intermediate. Indeed, the calculations show that the C-H abstraction from DHA by the oxo group of [OUO(S)(Li_2L)] leads to the formation of the intermediate [(HO)UO(S)(Li_2L)], which is computed to be exergonic by −32.2 kcal.mol^{-1} (Figure 5). From this intermediate the silylation reaction has been calculated and the product of the silylation [(Me_3SiO)UO(S)(Li_2L)] is computed to be exergonic by −32.3 kcal.mol^{-1}, which implies that [(HO)UO(S)(Li_2L)] and [(Me_3SiO)UO(S)(Li_2L)] (S= THF, pyridine) are at the same energetic level providing a reason why the dilithiated complex does not silylate in the presence of HN($SiMe_3$)$_2$.[2] In the case of the potassiation route, the silylation process is very favourable in comparison to the lithiation route.[12,13] Indeed, the double deprotonation of the uranyl Pacman **[UO_2(THF)(H_2L)]** by two equivalents of KH is very exergonic (−79.4 kcal.mol^{-1}), the reaction product of the silylation is exergonic (−134.1 kcal.mol^{-1}), which implies that the silylation is favourable.

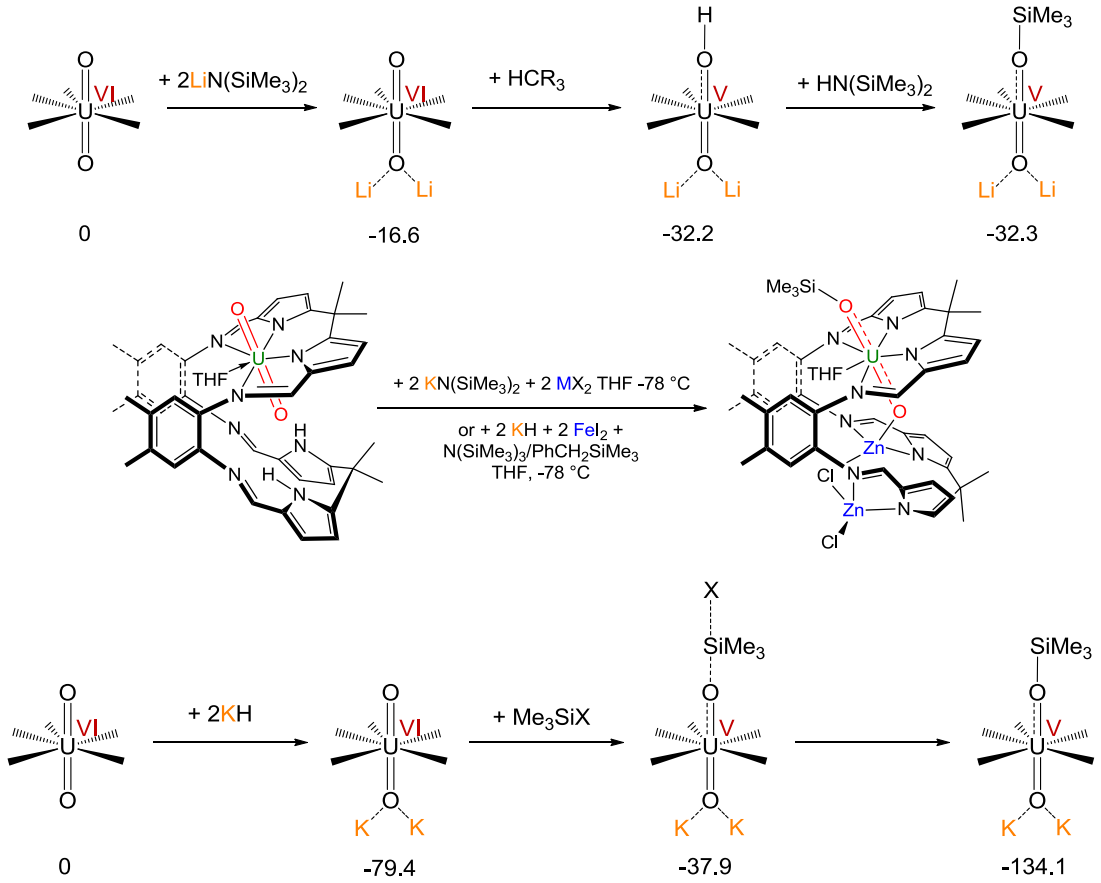

Figure 5: Proposed mechanisms for the oxo-functionalisation of the uranyl Pacman via the lithiation and the potassiation process.

However, in the case of the complex of **[(HO)UO(py)(H_2L)]** it has been thought that the silylation should be favourable, according to the calculated BDE (bond dissociation energy). Indeed the O-Si bond is stronger than the O-H bond, so the formation of the O-Si is more favourable than the formation of the O-H bond (BDE_{OSi} 128 kcal.mol^{-1}, BDE_{OH} 84.3 kcal.mol^{-1}) (Scheme 1).[14,15]

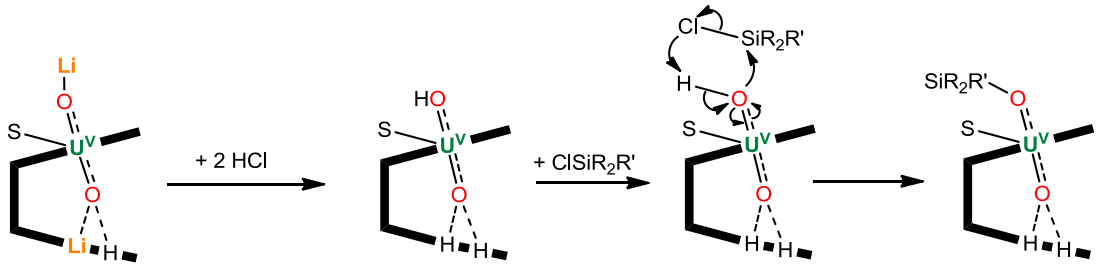

R = R' = Me
R = Me, R' = ^{t}Bu
R = Ph, R' = H

Scheme 1: Formation of the complex **[(HO)UO(py)(H_2L)]** then conversion into the silyl complexes **[(R'R_2SiO)UO(py)(H_2L)]**

3.4.1. Synthesis and characterisation of [(Me_3SiO)UO(py)(H_2L)]

The one-pot reaction between one equivalent of **[(HO)UO(py)(H_2L)]** and one equivalent of trimethylsilylchloride in pyridine at room temperature after 2 h results in the formation of **[(Me_3SiO)UO(py)(H_2L)]** as a brown-yellow solid in a good yield (78%), Equation (**10**).

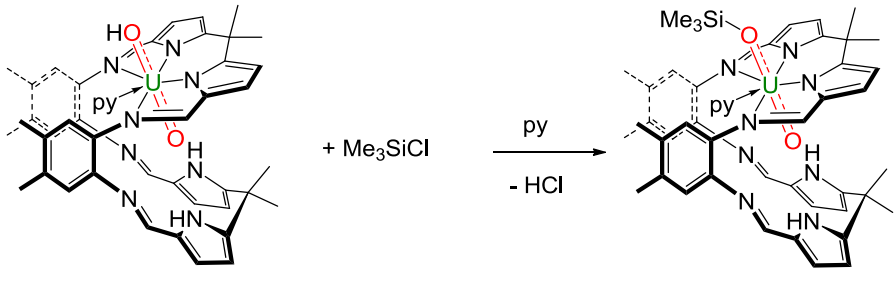

(**10**)

The complex was fully characterised. The formation of a new paramagnetic compound was observed in the ^{1}H NMR spectrum although the individual resonances could not be assigned but the number and integrals of the paramagnetically shifted resonances indicates a symmetric ligand arrangement and are consistent with the retention of a wedged, Pacman structure in solution of C_s symmetry (Figure 6). The most paramagnetically shifted resonance is assigned to the two pyrrole NH. The resonance at 15 ppm integrating for 9 protons is assigned to the silyl group on the *exo*-oxo group. The two resonances at 0.14 and −0.46 ppm integrating for 6H each correspond to the methyl group of the aryl backbone.

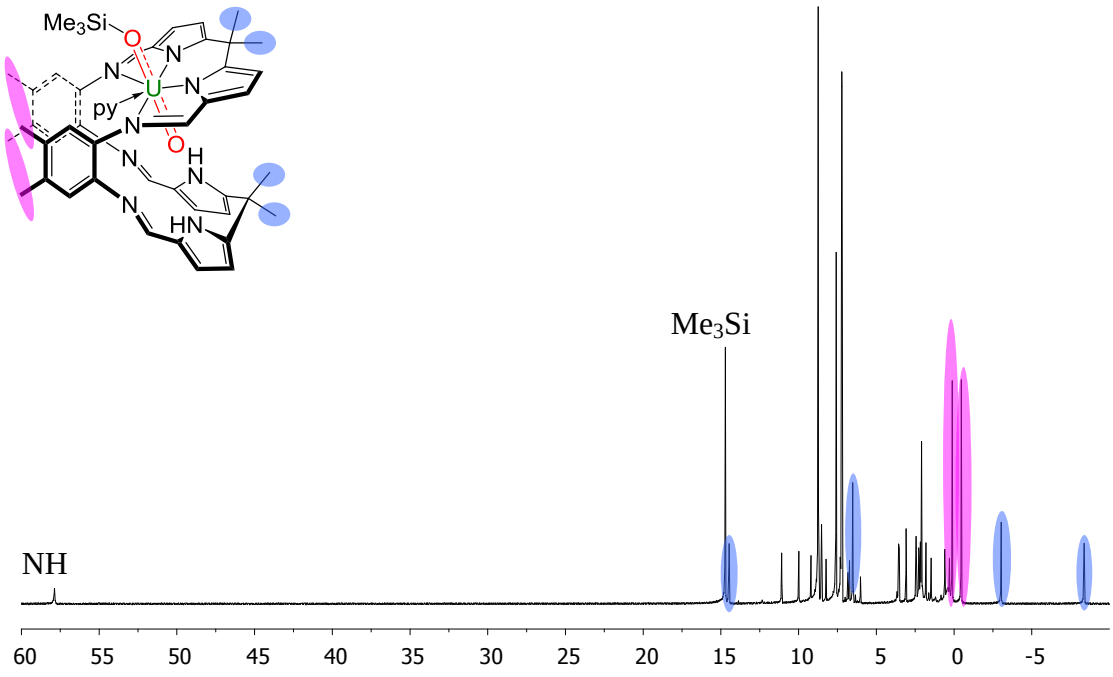

Figure 6: ^{1}H NMR spectrum of **[(Me$_3$SiO)UO(py)(H$_2$L)]**

To confirm the formation of the complex, the reaction between one equivalent of **[(DO)UO(py)(DHL)]** and one equivalent of Me_3SiCl has been monitored by ^{1}H and ^{2}H NMR spectroscopy (Figure 7). The ^{2}H NMR spectrum contains a resonance at 58.10 ppm corresponding to the pyrrole NH in the ^{1}H NMR spectrum. The resonance corresponding to the OD is not observed in the spectrum.

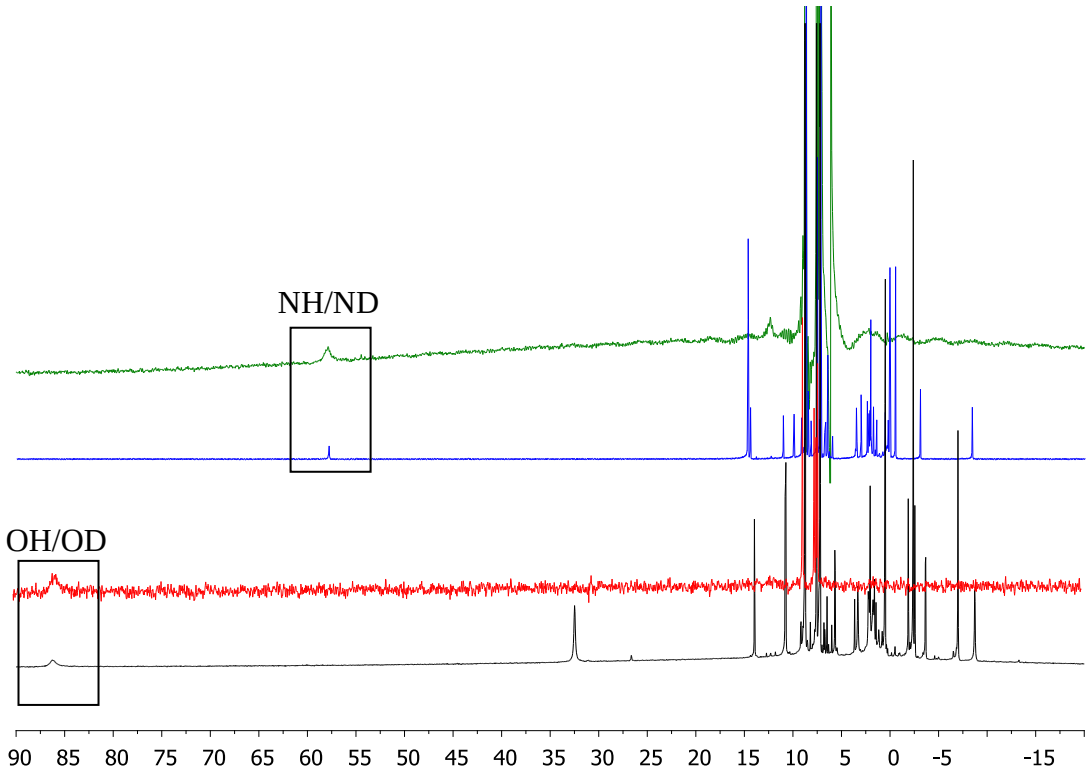

Figure 7: ^{1}H and ^{2}H NMR spectra of **[(Me$_3$SiO)UO(py)(H$_2$L)]** (blue) and **[(Me3SiO)UO(py)(HDL)]** (green), **[(HO)UO(py)(H$_2$L)]** (black), and **[(DO)UO(py)(HDL)]** (red) respectively showing NH/ND and OH/OD resonances

The FTIR spectrum contains a broad band at 3286 cm^{-1} which derives from the pyrrole NH and two stretches corresponding to the U=O at 860 cm^{-1} and 703 cm^{-1}. These stretches are weakened substantially compared to that in the U^{VI} starting material **[UO$_2$(THF)(H$_2$L)]** (ν U=O 908 cm^{-1}) and are in the range of the $[UO_2]^+$ and especially the $[UO_2]^+$ stretch observed in the complex $[U(OSiMe_3)_2(^{Ar}acnac)I_2]$ (Ar = 3,5-^{t}Bu2C$_6$H$_3$) presented by Hayton and co-workers (ν U=O 770 cm^{-1}). The SiMe$_3$ bands are also observed at 1255 cm^{-1}, 844 cm^{-1} and 757 cm^{-1} (Figure 8).

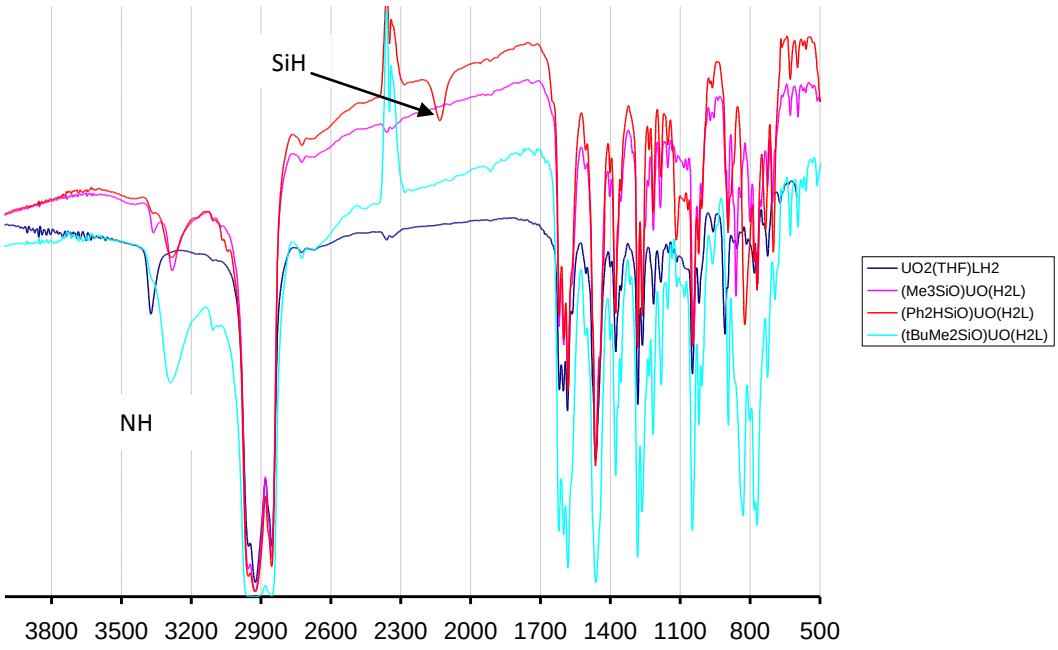

Figure 8: FTIR spectra of **[UO_2(THF)(H_2L)]** (blue), **[(Me_3SiO)UO(py)(H_2L)]** (pink), **[(^{t}BuMe_2SiO)UO(py)(H_2L)]** (cyan), and **[(Ph_2HSiO)UO(py)(H_2L)]** (red)

Crystals of **[(Me_3SiO)UO(py)(H_2L)]** suitable for single crystal X-ray diffraction analysis were grown from a saturated pyridine solution at −35 °C (Figure 9).

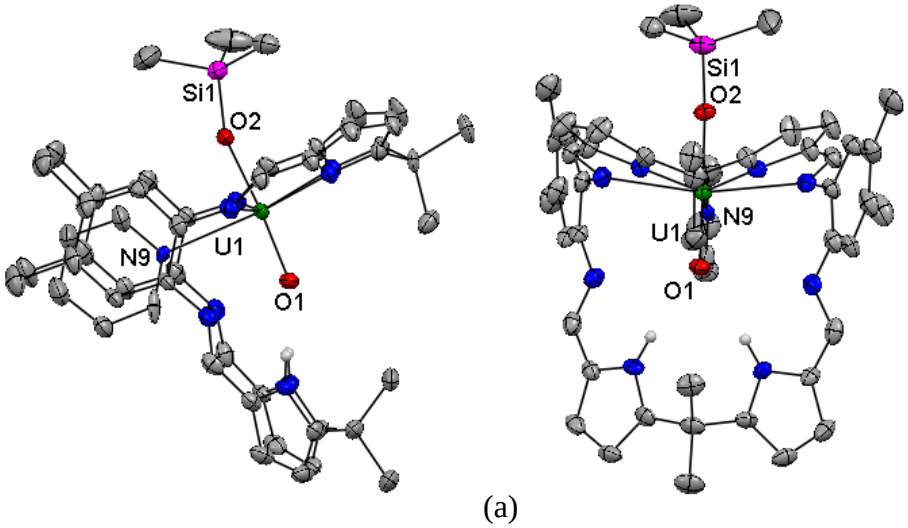

Figure 9: Solid state structure of **[(Me_3SiO)UO(py)(H_2L)]** showing side (a) and front (b) view. For clarity, hydrogen atoms, except the pyrrole NH, and lattice molecules of solvent are omitted.

Table 2: Selected bond distance (Å) and angles (°) of **[(Me_3SiO)UO(py)(H_2L)]**

U1-O1	1.854(4)
U1-O2	2.034(4)
U1-N9	2.649(5)
O2-Si1	1.667(5)
O1···N6	3.042
O1···N7	3.037
O1-U1-O2	176.03(19)
Si1-O2-U1	160.1(3)

The Pacman structural motif of the uranyl macrocycle **[UO_2(py)(H_2L)]** remains intact with one compartment occupied by the uranyl moiety and the other N_4 donor compartment remaining unoccupied. The uranium centre is seven coordinate and displays a distorted pentagonal bipyramidal geometry with the oxo groups retaining a *trans* arrangement (O1-U1-O2 176.15(9)°), and the equatorial site is occupied by the nitrogen atoms of the macrocycle and a nitrogen atom from a molecule of pyridine occupies the fifth equatorial site and sits between the two macrocyclic aryl rings. From analysis of the uranium-oxygen bond lengths it is evident that the uranyl fragment is in the 5+ oxidation state. The *endo*- U1-O1 distance (1.854(4) Å) distance is significantly elongated compared to the bond distance of $[UO_2]^{2+}$ in **[UO_2(py)(H_2L)]** (U1-O1 1.7779(18) Å) and is similar to experimental and calculated bond distances for $[UO_2]^{+}$ (range 1.811- 1.934 Å).[1,16-19] The *exo*- U1-O2 distance (2.034(4) Å) is also longer than in **[UO_2(py)(H_2L)]** (U1-O2 1.7546(19) Å). The Si1-O2 bond length (1.667(5) Å) is similar to others in the literature (range 1.631 to 1.655 Å) (Table 2).[20,21] The lower, vacant N4-donor compartment is oriented such that hydrogen bonds are evident between the *endo*-oxo group and the pyrrole NH groups; the N···O separations are shorter than in the precursor uranyl Pacman complex (N···O 3.037 Å / 3.172 Å respectively). On the other hand the U1-N9 distance is slightly elongated in comparison to the uranyl Pacman complex **[UO_2(py)(H_2L)]** (2.649(5) Å /2.583(2) Å respectively).

3.4.2. Synthesis and characterisation of [(^{t}BuMe$_2$SiO)UO(py)(H$_2$L)]

The reaction between one equivalent of **[(HO)UO(py)(H$_2$L)]** and one equivalent of *tert*-butyl(chloro)dimethylsilane in pyridine at room temperature over 2 h results in the formation of **[(^{t}BuMe$_2$SiO)UO(py)(H$_2$L)]**, which is isolated as a brown-yellow solid in a good yield (63%), Equation (**11**).

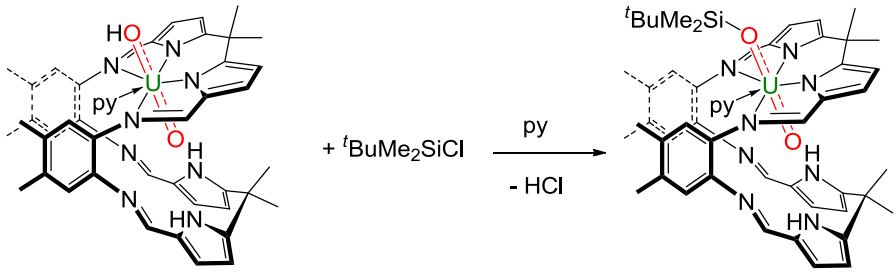

(**11**)

The complex was fully characterised. The formation of a new paramagnetic compound was observed in the ^{1}H NMR spectrum that the paramagnetically shifted resonances indicate a symmetric ligand arrangement and are consistent with the retention of a wedged, Pacman structure in solution of C_s symmetry (Figure 10). The ^{1}H NMR spectrum is similar to the ^{1}H NMR spectrum of **[(Me$_3$SiO)UO(py)(H$_2$L)],** with the most paramagnetic resonance at 54.13 ppm (56.56 ppm for **[(Me$_3$SiO)UO(py)(H$_2$L)]**) and is assigned to the two pyrrole NH. The resonance at 14.79 ppm integrating for 6H is assigned to the methyl groups of the silyl group on the *exo*-oxo group and the resonance at 9.23 ppm integrating for 9H is assigned to the ^{t}Butyl group. The two resonances at −0.16 and −0.38 ppm correspond to the methyl groups of the aryl backbone.

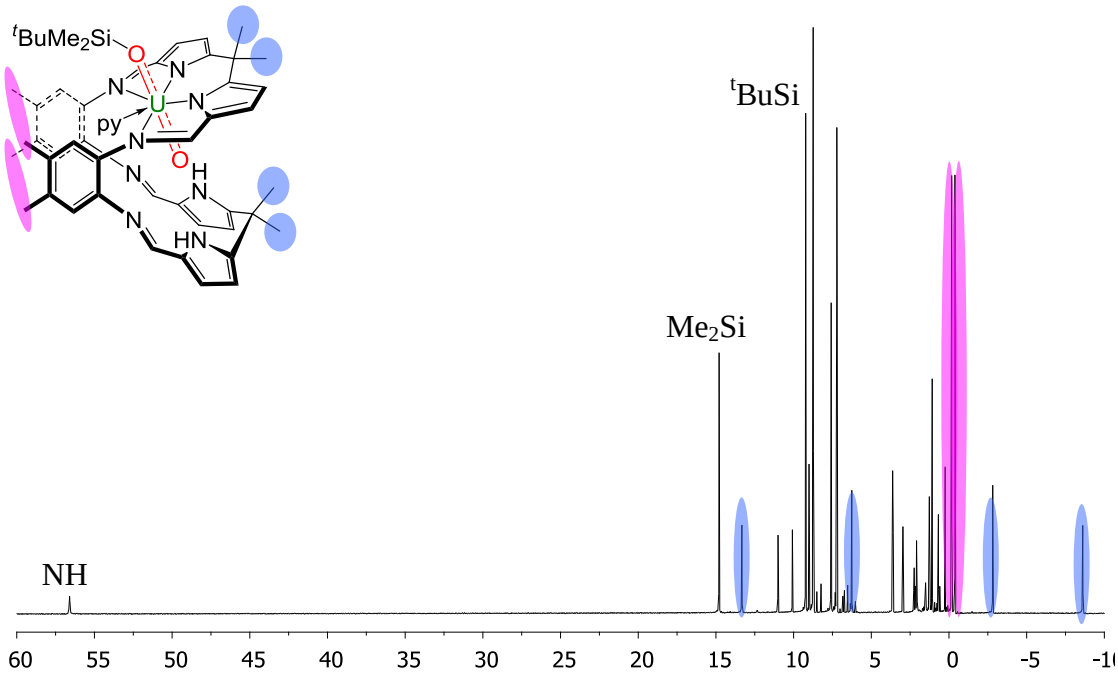

Figure 10: ^{1}H NMR spectrum of **[(^{t}BuMe$_2$SiO)UO(py)(H$_2$L)]**

The FTIR spectrum contains a broad band at 3290 cm^{-1} which derives from the NH pyrrole and two stretches corresponding to the U=O stretches at 831 cm^{-1} and 694 cm^{-1}. These stretches are weakened substantially compared to that in the U^{VI} starting material **[UO$_2$(THF)(H$_2$L)]** (ν U=O 908 cm^{-1}). The SiMe$_2$^{t}Bu bands are also observed at 1245 cm^{-1} (SiMe$_2$), 943 cm^{-1} (^{t}BuSi), 804 cm^{-1} (SiMe$_2$), 785 cm^{-1} (^{t}BuSi) and 684 cm^{-1} (^{t}BuSi) (Figure 8).

Crystals of **[(^{t}BuMe$_2$SiO)UO(py)(H$_2$L)]** suitable for single crystal X-ray diffraction analysis were grown from a saturated toluene solution at −35 °C (Figure 11).

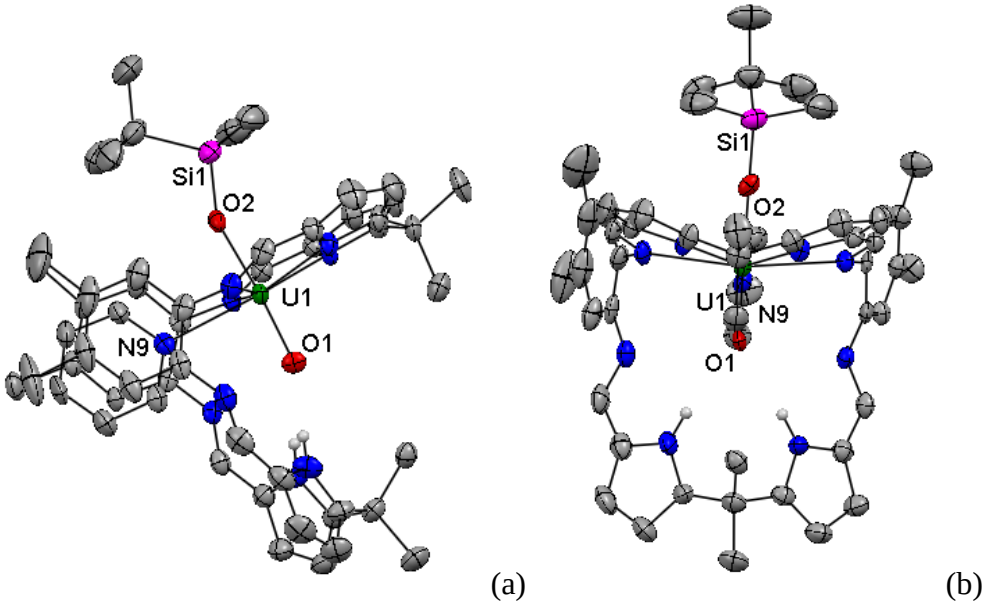

Figure 11: Solid state structure of **[(^{t}BuMe$_2$SiO)UO(py)(H$_2$L)]** showing side (a) and front (b) view. For clarity, hydrogen atoms, except the pyrrole NH, and lattice molecules of solvent are omitted.

The X-ray data showed problems consistent with multiple twinning. As such, only the connectivity was established. The Pacman structural motif of the uranyl macrocycle **[UO$_2$(THF)(H$_2$L)]** remains intact, the uranyl fragment is coordinated in one half of the macrocycle by four nitrogen atoms at standard distances and the other N_4 compartment remains unoccupied. The uranium centre is seven coordinate and displays a distorted pentagonal bipyramidal geometry with the oxo groups retaining a *trans*-arrangement, and the equatorial site is occupied by the nitrogen atoms of the macrocycle and a nitrogen atom from a molecule of pyridine occupies the fifth equatorial site and sits between the two macrocyclic aryl rings. The core structure of **[(^{t}BuMe$_2$SiO)UO(py)(H$_2$L)]** is similar to that of **[(Me$_3$SiO)UO(py)(H$_2$L)]**.

3.4.3. Synthesis and characterisation of [(Ph$_2$HSiO)UO(py)(H$_2$L)]

The one-pot reaction between one equivalent of **[(HO)UO(py)(H$_2$L)]** and one equivalent of Ph$_2$HSiCl in pyridine at room temperature after 2 h results, after work-up, in the formation of **[(Ph$_2$HSiO)UO(py)(H$_2$L)]** as a brown-yellow solid in good yield (67%), Equation (**12**).

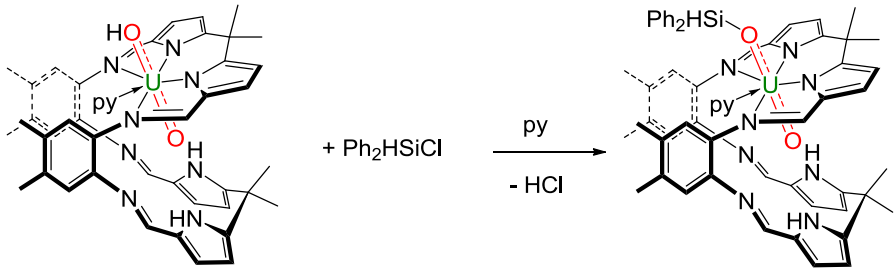

(**12**)

The complex has been characterised by ^{1}H NMR and FTIR spectroscopy. The ^{1}H NMR reveals the presence of paramagnetically shifted resonances between δ = 60 and –10 ppm, the number and integrals of which are consistent with a wedged Pacman structure in solution of C_s symmetry (Figure 12). The ^{1}H NMR spectrum is similar to the ^{1}H NMR spectra of **[(Me$_3$SiO)UO(py)(H$_2$L)]** and **[(^{t}BuMe$_2$SiO)UO(py)(H$_2$L)]**. The most paramagnetically shifted resonance at 54.13 ppm is assigned to the two pyrrole NH, the resonance at 37.21 ppm, integrating for 1H is assigned to the SiH. The aromatic protons of the phenyl rings of the silyl group are observed at 17.65, 9.87 and 9.15 ppm, integrating respectively for 4H, 4H and 2H. The two resonances at 0.10 and −0.25 ppm, each integrating for 6H, correspond to the methyl groups of the Pacman ligand aryl backbone.

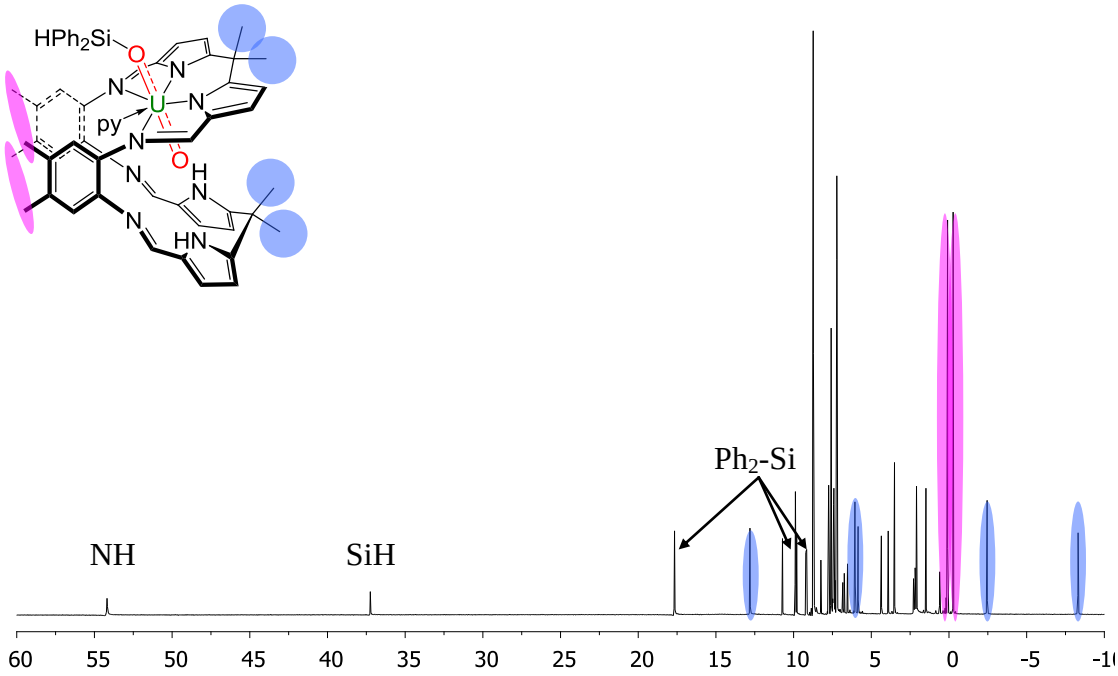

Figure 12: ^{1}H NMR spectrum of **[(Ph$_2$HSiO)UO(py)(H$_2$L)]**

The FTIR spectrum contains a broad band at 3291 cm^{-1} which derives from the pyrrole NH and two stretches corresponding to the U=O at 823 cm^{-1} and 700 cm^{-1}. These stretches are weakened substantially compared to that in the U^{VI} starting material **[UO$_2$(THF)(H$_2$L)]** (ν U=O 908 cm^{-1}) but are similar to the complexes **[(Me$_3$SiO)UO(py)(H$_2$L)]** and **[(t BuMe$_2$SiO)UO(py)(H$_2$L)]**. The broad band at 2142 cm^{-1} is assigned to the Si-H stretching mode. The bands corresponding to the Ph-Si are observed at 1650 cm^{-1}, 1430 cm^{-1} and 1118 cm^{-1} (Figure 8).

3.5. Reaction of [(HO)UO(py)(H$_2$L)] with chlorophosphine

3.5.1. Reaction of [(HO)UO(py)(H$_2$L)] with one equivalent of Ph$_2$PCl

The reaction between one equivalent of **[(HO)UO(py)(H$_2$L)]** and one equivalent of chlorodiphenylphosphine in pyridine at room temperature in a Teflon-tapped NMR tube, after 1 h, results in a colour change of the solution from brown to dark red and the formation of a pale red precipitate. The compound formed is proposed to be **[(Ph$_2$PO)UO(py)(H$_2$L)]**, with the precipitate proposed to be the pyridinium salt as a by-product, Equation (**13**).

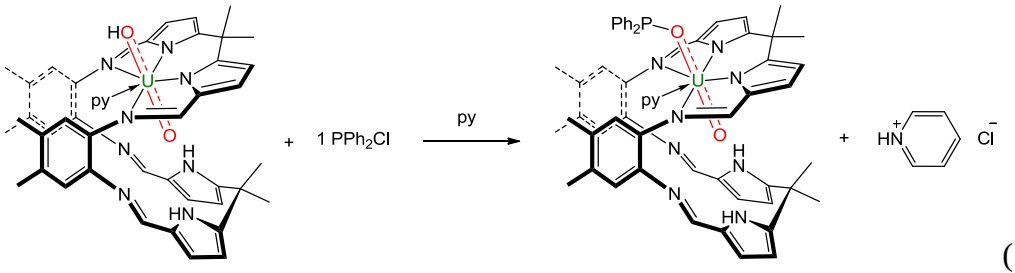

(**13**)

The formation of a new paramagnetic compound was observed in the ^{1}H NMR spectrum. If it is the proposed complex, the number and integrals of the paramagnetically shifted resonances suggest a symmetric ligand arrangement (Figure 13). The ^{1}H NMR spectrum is similar to those of the silyl complexes **[(R_2R'SiO)UO(py)(H_2L)],** with the most paramagnetic resonance at 53.92 ppm (56.56 ppm for **[(Me_3SiO)UO(py)(H_2L)]**) (Figure 14) tentatively assigned as the two pyrrole NH. The ^{1}H NMR spectrum contains three resonances for the phenyl groups on the phosphine at 19.8 ppm, 10.16 ppm, and 9.78 ppm, integrating for 4H, 4H, and 2H respectively. The two resonances at 0.09 and −0.24 ppm correspond to the methyl groups of the aryl backbone. The ^{31}P{^{1}H} NMR spectrum contains one resonance at 36 ppm and shifted in comparison with the chlorodiphenylphosphine (δ_P = 85 ppm) and with the triphenylphosphine oxide free ((δ_P = 130 ppm). Hayton and co-workers have observed the diamagnetic complex [UO_2(Ar_2nacnac)Cl(Ph_3PO)] and the ^{31}P{^{1}H} NMR spectrum shows only one singlet at 65.3 ppm.[22] In comparison to the other diamagnetic phosphine oxide complexes of uranyl, the phosphorus resonance of the proposed complex **[(Ph_2PO)UO(py)(H_2L)]** is shifted highfield.[23]

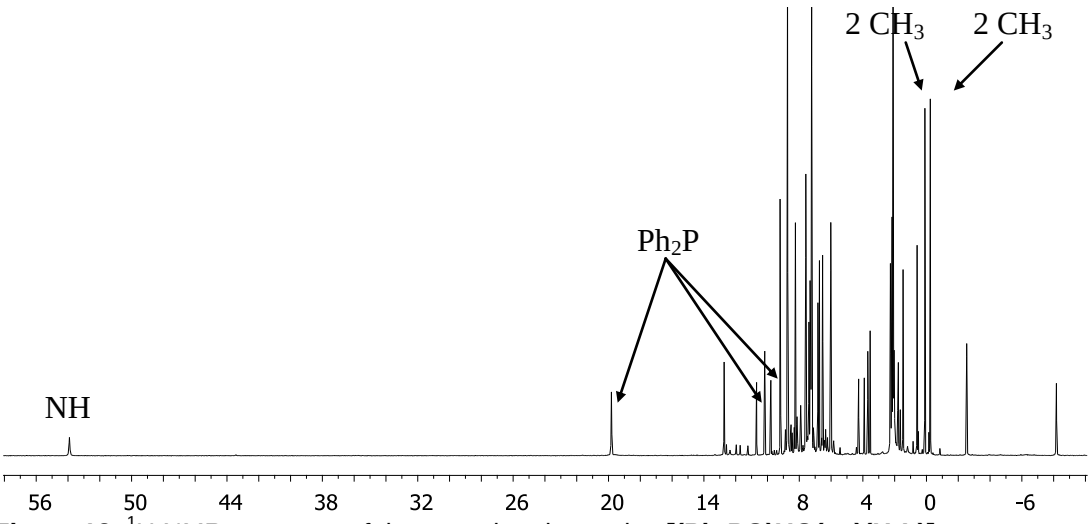

Figure 13: ^{1}H NMR spectrum of the speculated complex **[(Ph_2PO)UO(py)(H_2L)]**

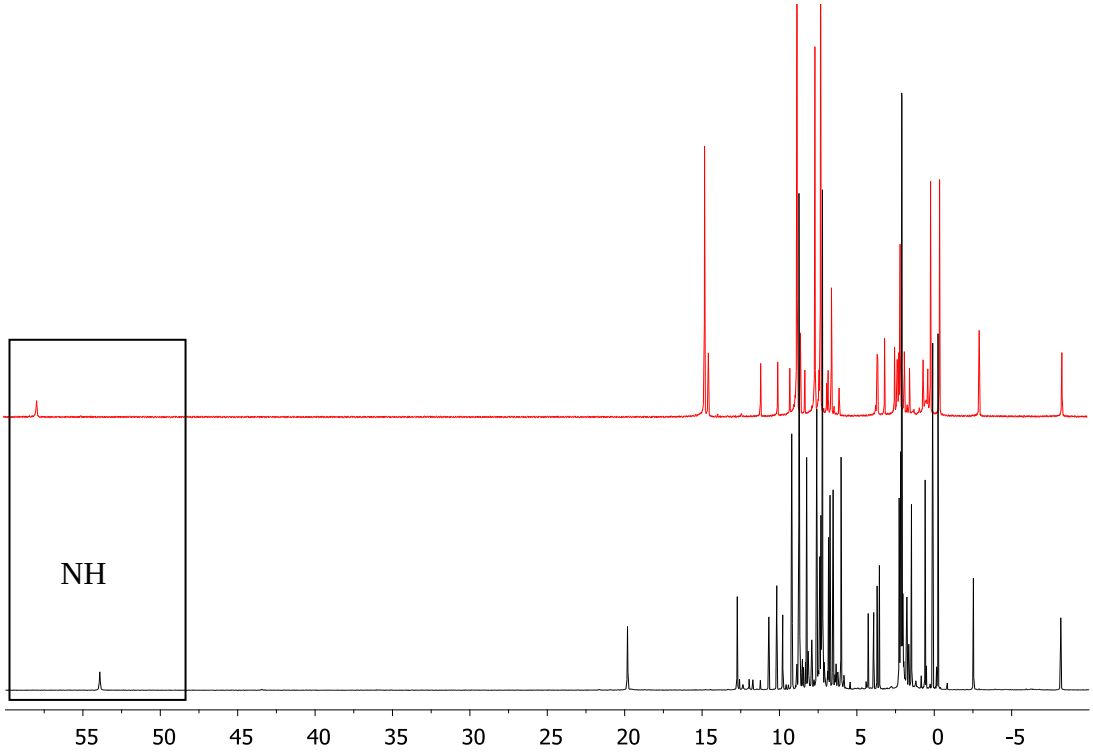

Figure 14: ^{1}H NMR spectra of the proposed product **[(Ph_2PO)UO(py)(H_2L)]** (black) and **[(Me_3SiO)UO(py)(H_2L)]** (red)

The FTIR spectrum contains a broad band at 3343 cm^{-1} which is assigned as the NH pyrrole and two stretches corresponding to the U=O at 802 cm^{-1} and 696 cm^{-1}. These stretches are weakened substantially compared to that in the U^{VI} starting material **[UO_2(py)(H_2L)]** (ν U=O 908 cm^{-1}) and are similar to the other silylated

complex presented below (860 and 703 cm^{-1} for **[(Me$_3$SiO)UO(py)(H$_2$L)]** for example) and in the range of the $[UO_2]^+$ stretches.[1,10] A band is observed at 1097cm^{-1} and corresponds to the PO stretch and is in the similar than the PO stretch in other complexes.[24]

3.5.2. Reaction of [(HO)UO(py)(H$_2$L)] with two equivalents of Ph$_2$PCl

The one-pot reaction between one equivalent of **[(HO)UO(py)(H$_2$L)]** and two equivalents of chlorodiphenylphosphine results in the formation of a new complex that we propose to be **[ClUO(py)(H$_2$L)]** (Scheme **2**).

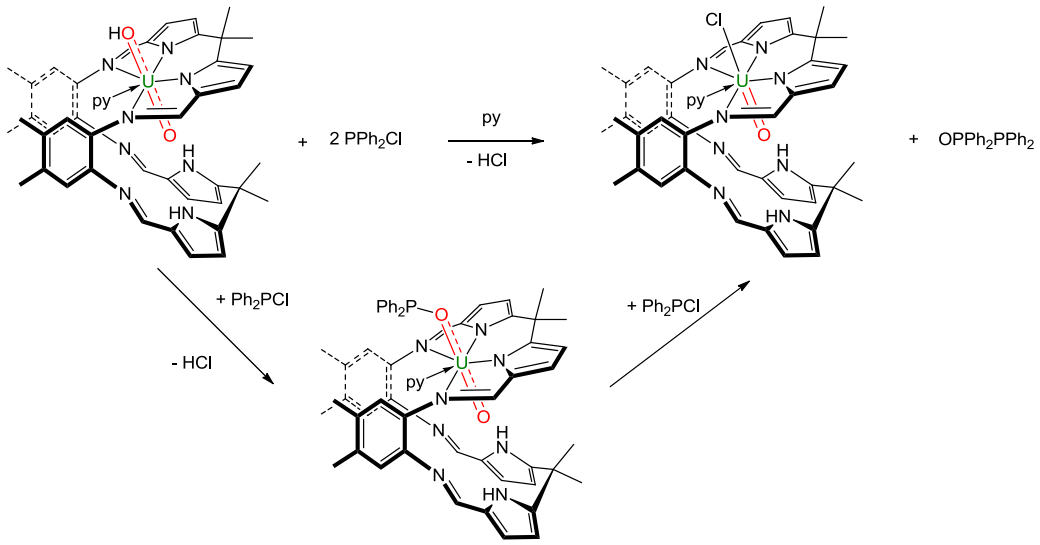

Scheme 2: Synthesis of the proposed complex **[ClUO(py)(H$_2$L)]**

The ^{1}H NMR spectrum shows the formation of a new paramagnetical compound. All the resonances could not be assigned but if it is the proposed complex the number and integrals are consistent with a wedged, Pacman structure (Figure 15). The most paramagnetically shifted resonance at 44.54 ppm, integrating for 2H, is assigned to the pyrrole NH. The two resonances at 0.50 and −0.15 ppm, each integrating for 6H, can be assigned to the methyl groups of the aryl backbone. Three resonances at 8.14, 7.92 and 7.39 ppm integrating respectively for 5H, 5H, and 10H, correspond to the resonances of the by-product O=PPh$_2$PPh$_2$. The ^{31}P{^{1}H} NMR spectrum contains two doublets at 36.76 and −21.91 ppm corresponding to the free O=PPh$_2$PPh$_2$.[25] When the reaction is monitored by ^{1}H NMR spectroscopy, the

formation of an intermediate which has the same resonances as **[(Ph$_2$PO)UO(py)(H$_2$L)]** is observed to appear, and then be consumed as the reaction proceeds. The ^{1}H NMR spectrum has some similarities in the shift of different resonances with the ^{1}H NMR spectra of **[(Me$_3$SiO)UO(py)(H$_2$L)]** and the proposed complex **[(Ph$_2$PO)UO(py)(H$_2$L)]** such as the shift for the methyl group on the backbone of the ligand and the shift of the resonance of one methyl in the same zone than the two other complexes (Figure 16).

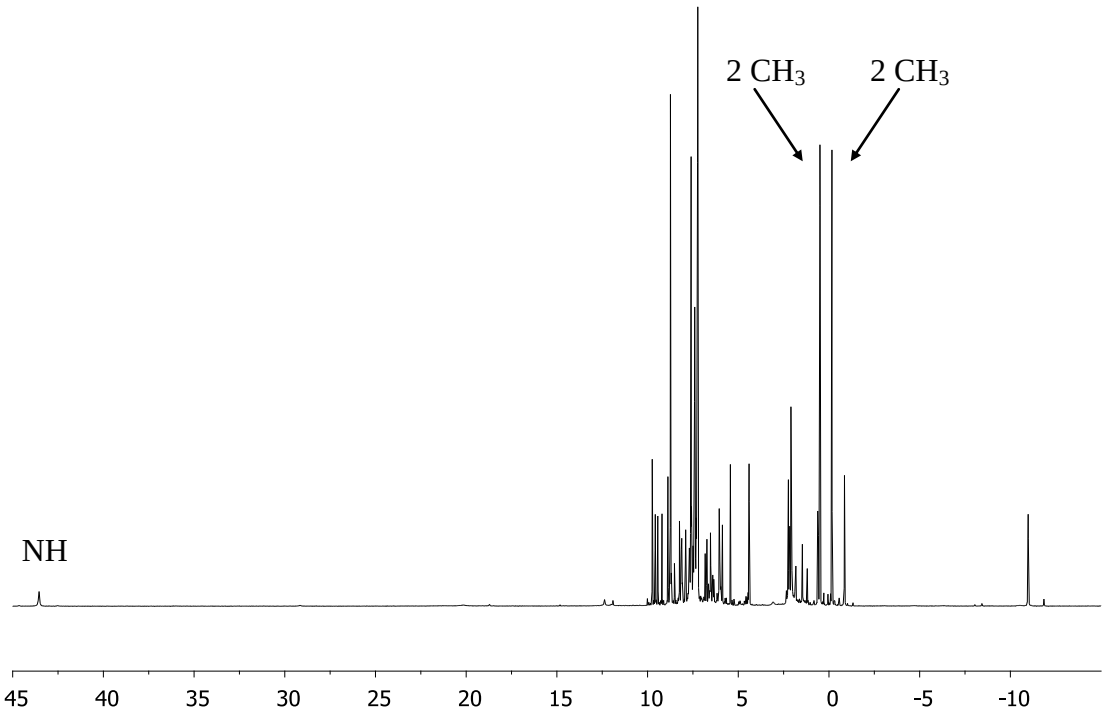

Figure 15: ^{1}H NMR spectrum of the speculative complex **[ClUO(py)(H$_2$L)]**

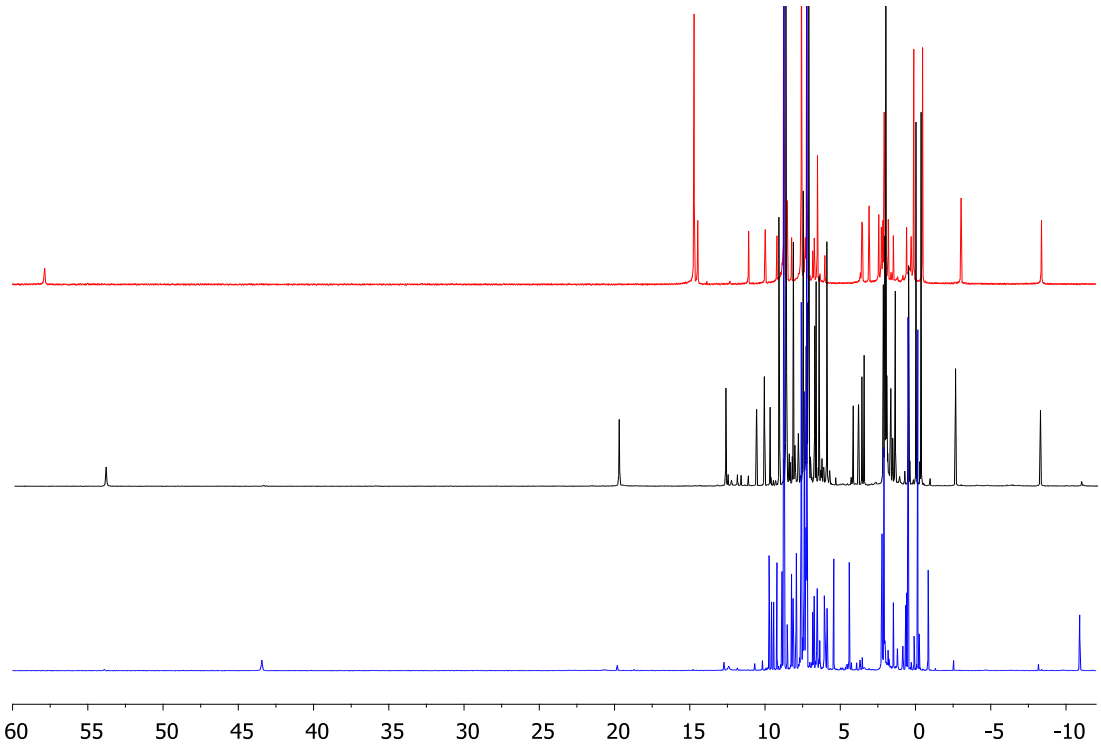

Figure 16: ^{1}H NMR spectra of **[(Me$_3$SiO)UO(py)(H$_2$L)]** (red), and the speculative complexes **[(Ph$_2$PO)UO(py)(H$_2$L)]** (black) and **[ClUO(py)(H$_2$L)]** (blue)

The complex is not stable and decomposes over time. Attempts to crystallise the complex were unsuccessful.

3.5.3. Attempted synthesis of [MeOUO(py)(H$_2$L)]

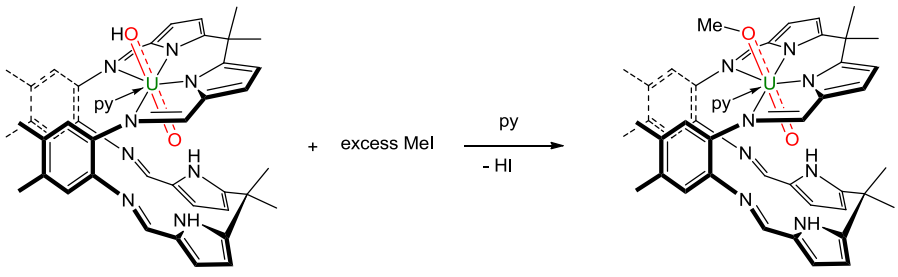

(**14**)

With the successful synthesis of **[(R'R$_2$SiO)UO(py)(H$_2$L)]**, it was considered possible that the complex **[MeOUO(py)(H$_2$L)]** could be synthesised from the one-pot reaction between **[(HO)UO(py)(H$_2$L)]** and an excess of MeI in pyridine at room temperature. However, the ^{1}H NMR spectrum of the reaction mixture remains unchanged after a few days storage at room temperature, Equation (**14**).

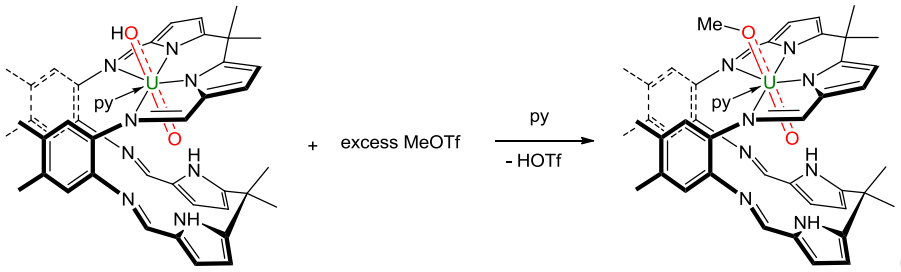

(**15**)

Another attempt to form this complex via the reaction between **[(HO)UO(py)(H$_2$L)]** and one equivalent of trifluoromethanesulfonate (methyltriflate) in pyridine in a Teflon-tapped NMR tube at room temperature for a few days did not form the expected product **[MeOUO(py)(H$_2$L)]**. The ^{1}H NMR spectrum shows no change, Equation (**15**).

3.5.4. Attempted synthesis of [(PhCH$_2$O)UO(py)(H$_2$L)]

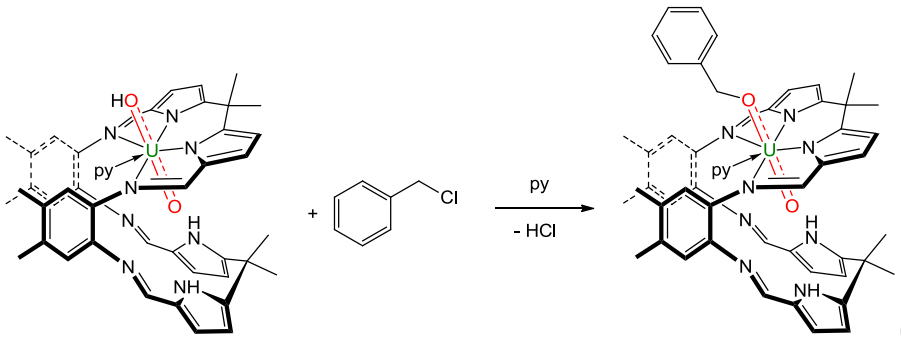

(**16**)

Another reaction to target a complex containing a C-O covalent bond was the reaction of one equivalent of **[(HO)UO(py)(H$_2$L)]** with one equivalent of benzyl chloride in pyridine at room temperature to synthesise the complex **[(PhCH$_2$O)UO(py)(H$_2$L)]**. This reaction was monitored by ^{1}H NMR spectroscopy. The ^{1}H NMR spectrum is unchanged and contains only the resonances of **[(HO)UO(py)(H$_2$L)]** and benzyl chloride after a week at room temperature, Equation (**16**).

3.6. Discussion

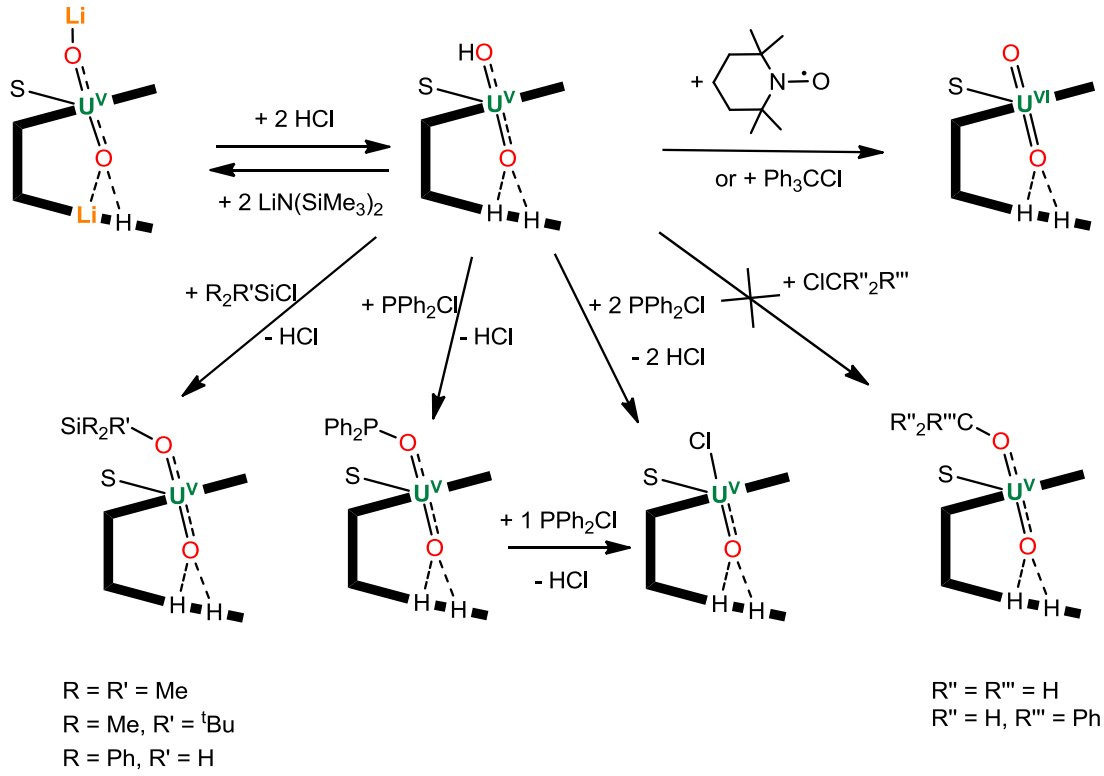

Scheme 3: Synthetic procedures to produce paramagnetic uranyl Pacman complexes

We have shown that the formation of a protonated uranyl complex via the reaction of the dilithiated uranyl complex and two equivalents of HCl is possible. The ^{1}H NMR spectrum of **[(HO)UO(py)(H$_2$L)]** shows the formation of a paramagnetic complex between +90 and −10 ppm, the most paramagnetically shifted resonance corresponds to the OH. The deuteration of **[(HO)UO(py)(H$_2$L)]** confirms the presence of OD and ND bonds which is observed in the ^{2}H NMR spectrum and in the FTIR spectrum. It is also observed that complete deuteration is not occurring and that an H/D exchange operates between the NH/ND and OH/OD protons. No lithium resonance is observed in the ^{7}Li{^{1}H} NMR spectrum suggesting that the complex is not lithiated. Unfortunately, we have been unable to crystallise the complex and unequivocally determine its structure but to confirm the oxidation state, the stoichiometric reaction between **[(HO)UO(py)(H$_2$L)]** and trityl chloride was carried out. The reaction was monitored by ^{1}H NMR spectroscopy and shows the formation

of the Gomberg's dimer and **[UO_2(py)(H_2L)]** in a ratio 1:2. Another reaction to confirm the oxidation state has been carried out. The reaction of **[(HO)UO(py)(H_2L)]** and TEMPO was monitored by ^{1}H NMR spectroscopy. The reaction cleanly regenerates the uranyl Pacman complex through an H-abstraction and forms TEMPO-H, proving the presence of labile proton via a radical reaction. Furthermore, the reaction between one equivalent of **[(HO)UO(py)(H_2L)]** and two equivalents of $LiN(SiMe_3)_2$ regenerates the dilithiated uranyl complex **[$(py)_3$LiOUO(py)Li(py)(HL)]**.

The H-atom functionalisation of the uranyl oxo group is important to aqueous uranyl chemistry. A few experimental works have been performed on the exchange of the uranyl oxo ligands under basic conditions and show that the uranyl dication $[UO_2]^{2+}$ in aqueous solutions has 5 water molecules coordinated, which at high pH formed hydroxide ligands around the uranyl dication which can exchange with the oxo group.[26] The study of Clark and co-workers used $[NEt_4][OH]$ as the hydroxide source. Under these conditions the uranyl species present in solution was thought to be $[UO_2(OH)_5]^{3-}$, but the isolated product in the solid state was $[UO_2(OH)_4]^{2-}$. They speculated that the UO bonds were weakened by the strongly donating hydroxide ligand; they proposed a water assisted proton transfer (Path A) or a direct proton transfer (Path B) (Scheme 4).[27]

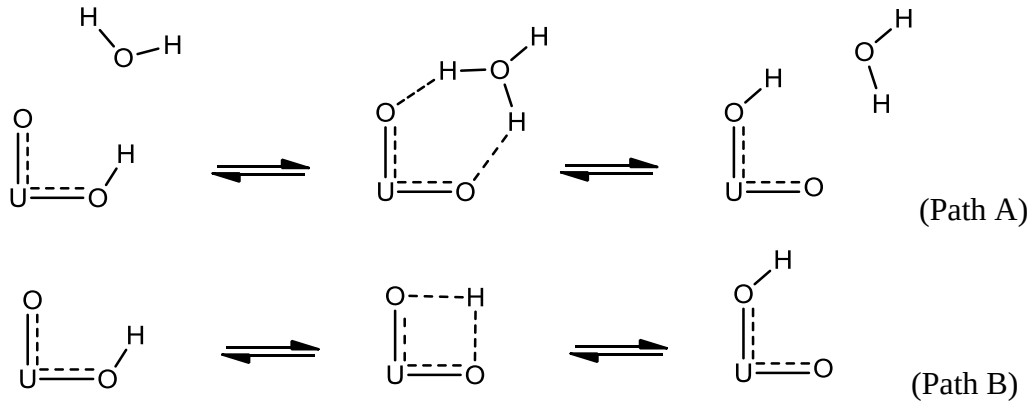

Scheme 4: Two possible pathways for the hydroxide ligand exchange

From this study Schreckenbach and co-workers have studied possible mechanisms for the yl exchange by DFT calculations. A possible mechanism could involve a *cis*-uranyl species, but seems unlikely due to the high energy computed for

this species. Shamov and Schreckenbach have recently proposed an alternative route via a tris(oxo) species $[UO_3(OH)_3]^{3-}$ as an intermediate. The tris(oxo) species is accessible through water elimination from the pentakis(hydroxyl)species $[UO_2(OH)_5]^{3-}$ (this intermediate has been suggested by the experiments of Clark and co-workers) (Scheme 5).

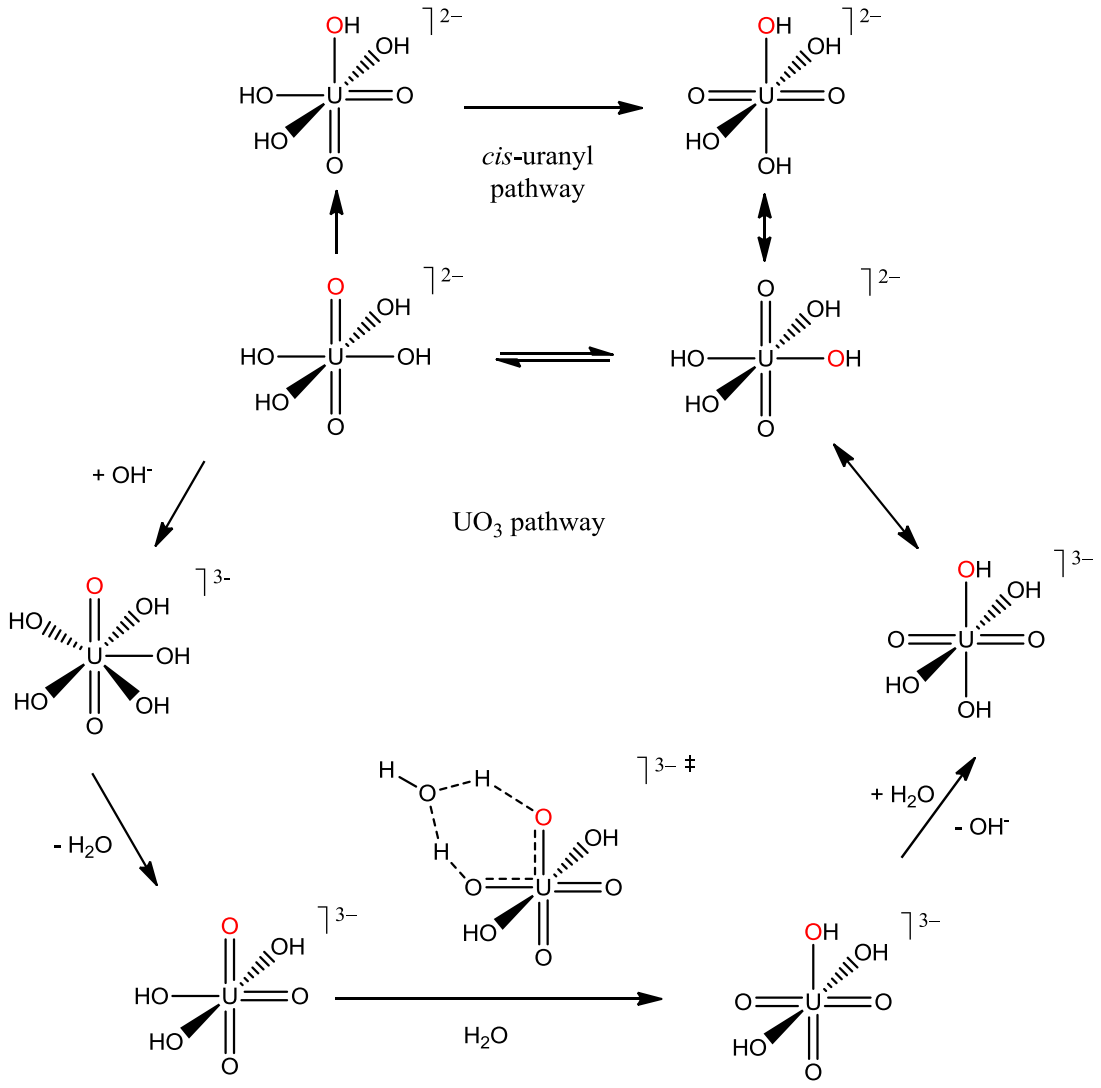

Scheme 5: *cis*-uranyl and UO_3 pathways for the yl exchange

DFT calculations suggest that the deprotonation of one equatorial hydroxyl group and proton-shuttling to an axial oxo group is the key in the exchange of the ligand and interesting geometries such as T shaped and cis uranyl cations.[28-30]

Reactions between **[(HO)UO(py)(H_2L)]** and chlorosilanes (Me_3SiCl, $^tBuMe_2SiCl$ and Ph_2HSiCl) in pyridine result in the formation of new silylation of the oxo group of uranyl Pacman complexes. The ^{1}H NMR spectra of the new silyl complexes are similar with the resonances shifted between δ= +60 and −10 ppm and the NH resonances around 60 ppm confirming the retention of the oxidation state of the uranium. To confirm the assignment of the NH, the reaction between **[(DO)UO(py)(DHL)]** and Me_3SiCl was monitored by ^{1}H NMR and ^{2}H NMR spectroscopy, the ^{1}H NMR and ^{2}H NMR spectra contain a resonance at *ca*. 58 ppm corresponding to the NH and ND. The silyl groups in all the ^{1}H NMR spectra contain the resonance for alkyl group around the same shift (*ca.* 15 ppm). The resonance for the alkyl group on the silicon is also observed in the ^{1}H NMR spectra of **[(Me_3SiO)UO(py)Li(py)(HL)]** and **[(^{t}BuMe$_2$SiO)UO(py)Li(py)(HL)]** at *ca.* 15 ppm, the resonance the most shifted for these complexes is at ca. 38 ppm, integrating for 1H and corresponds to the NH. Due to the presence of HCl in the chlorosilane, **[(Me_3SiO)UO(py)(H_2L)]** or **[(^{t}BuMe$_2$SiO)UO(py)(H_2L)]** are forming as a contaminant during the reaction to form **[(Me_3SiO)UO(py)Li(py)(HL)]** or **[(^{t}BuMe$_2$SiO)UO(py)Li(py)(HL)]**.

The FTIR spectra of **[(R_2R'O)UO(py)(H_2L)]** show the stretches corresponding to the NH around 3300cm^{-1} and two UO stretches for each complex are displayed in the same range around 860-823 and 700 cm^{-1} (Table 3 and Figure 17). In the case of **[(Me_3SiO)UO(py)Li(py)(HL)]**, the stretch corresponding to the NH is at 3177 cm^{-1} which is shifted in comparison to the **[(R_2R'O)UO(py)(H_2L)]** complexes. This is possibly due to the presence of one lithium cation in the N4-donor pocket. The U=O stretches are in the same range around 861 cm^{-1}.

		ν_{NH} (cm^{-1})	ν_{UO} (cm^{-1})
$[UO_2(THF)(H_2L)]$	$O{=}U^{VI}{=}O$	3373	908
$[(Me_3SiO)UO(py)(H_2L)]$	$Me_3Si{-}O{-}U^{V}{=}O$	3286	860 and 703
$[(^tBuMe_2SiO)UO(py)(H_2L)]$	$^tBuMe_2Si{-}O{-}U^{V}{=}O$	3290	831 and 694
$[(Ph_2HSiO)UO(py)(H_2L)]$	$Ph_2HSi{-}O{-}U^{V}{=}O$	3291	823 and 700

Table 3: FTIR selected bands v (cm^{-1}) for the complexes **$[UO_2(THF)(H_2L)]$**, **$[(Me_3SiO)UO(py)(H_2L)]$**, **$[(^tBuMe_2SiO)UO(py)(H_2L)]$**, and **$[(Ph_2HSiO)UO(py)(H_2L)]$**

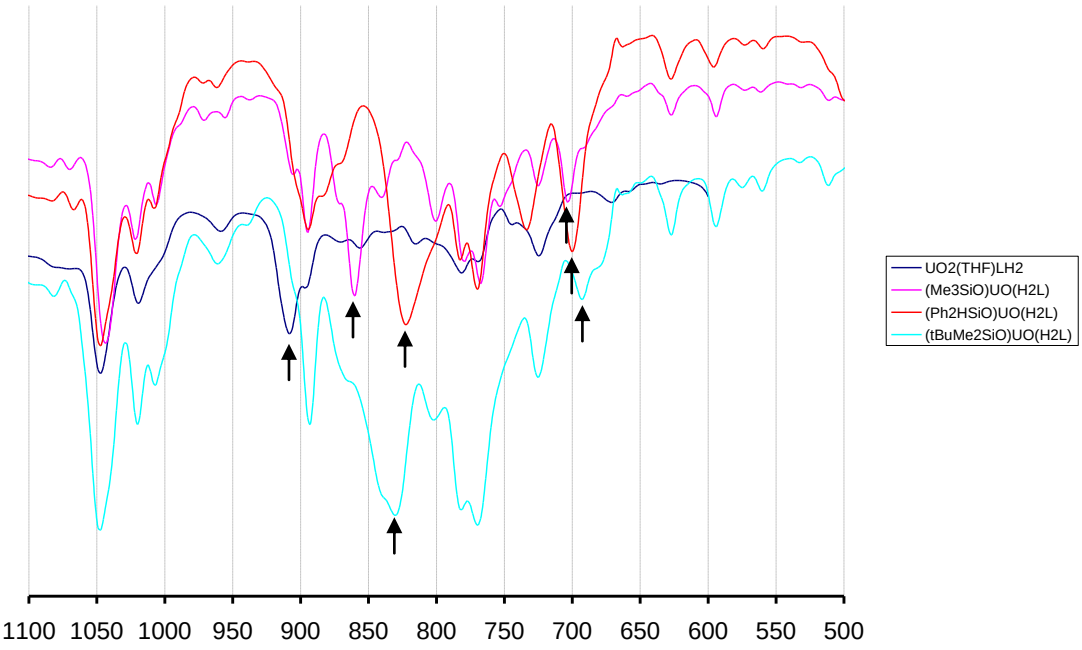

Figure 17: FTIR spectra of **$[UO_2(THF)(H_2L)]$** (blue), **$[(Me_3SiO)UO(py)(H_2L)]$** (pink), **$[(^tBuMe_2SiO)UO(py)(H_2L)]$** (cyan), and **$[(Ph_2HSiO)UO(py)(H_2L)]$** (red). Arrows indicate v(U=O).

Single crystals X-ray structures of the complexes **$[(Me_3SiO)UO(py)(H_2L)]$** and **$[(^tBuMe_2SiO)UO(py)(H_2L)]$** confirm the gross structure and the formation of a O-Si bond between the *exo*-oxo group of the uranyl Pacman complexes and the silyl group. The structures show that N4-donor compartment is vacant and the evidence of an interaction between the NH pyrrole and the *endo* oxo group by the orientation of the NH and the distance N···O.[31] The UO bonds are elongated in comparison to the uranyl Pacman complex **$[UO_2(py)(H_2L)]$** but are similar to those seen in related

uranyl siloxide and uranyl complexes in 5+ oxidation state; in contrast U^{IV} and U^{III} siloxide bonds are significantly longer.[16,32,33] The Si-O bonds are similar to those observed in uranyl complexes and oxo-derived siloxides.[20,21]

This is the first observation of metathesis of a functional group that is covalently bound to the uranyl oxo group.

The reaction of **[(R_2R'SiO)UO(py)Li(py)(HL)]** with an excess of chlorosilanes (2 or more equivalents) or the reaction of **[(R_2R'SiO)UO(py)(H_2L)]** with an excess of chlorosilanes does not afford new complexes such as silylation of one of the pyrrole N of the N4-donor compartment, or silylation of the *endo*-oxo group or a change in the oxidation state of the uranium as described by Hayton and co-workers.[7,8] They have shown that the reaction of the uranyl(VI) complex $[UO_2(^{Ar}acnac)_2]$ with an excess of Me_3SiI results in the formation of the uranyl complex $[U(OSiMe_3)_2(^{Ar}acnac)I_2]$ and the loss of one ligand. In our case, it is possible that the silylation on the *endo* oxo group is not occurring due to a lack of space in the N4-donor compartment.

On the same principle, the stoichiometric reaction between chlorodiphenylphosphine and **[(HO)UO(py)(H_2L)]** suggest the formation of the complex **[(Ph_2PO)UO(py)(H_2L)]**. The ^{1}H NMR spectrum shows similarities with the **[(R_2R'O)UO(py)(H_2L)]** complexes (Figure 14). The resonance for the NH is shifted in the same range as the NH of the silyl complexes as well as the methyl groups on the aryl backbone and the resonance for the methyl groups of the dipyrromethane part of the ligand. The FTIR spectrum displays stretches for the NH at 3343 cm^{-1} and the UO stretches are in the same range as those observed in the silyl complexes, so, by analogy, we can speculate that the **[(Ph_2PO)UO(py)(H_2L)]** complex could possess the same structure as the silyl complexes, but further investigations have to be done to confirm this suggestion.

The reaction between one equivalent of **[(HO)UO(py)(H_2L)]** and two equivalents of chlorodiphenylphosphine produces a new complex. The ^{1}H NMR spectrum shows some similarities with the silyl complexes and the speculated complex **[ClUO(py)(H_2L)]** in the number of resonances and their shifts, but the resonance we suppose to be attributed to the pyrrole NH is shifted as well as one resonance for one of the methyl groups on the dipyrromethane part of the ligand

(Figure 16). The ^{1}H NMR spectrum as well as the $^{31}P\{^{1}H\}$ NMR spectrum contains resonances indicating the formation of free $O{=}PPh_2PPh_2$.[25] Unfortunately, until now we have been unable to crystallise the complex, but we can suggest a mechanism for the reaction. The first step of the reaction is the reaction of the protonated uranyl complex with one equivalent of chlorodiphenylphosphine forming the complex **[(Ph$_2$PO)UO(py)(H$_2$L)]**. The formation of this complex can be seen when the reaction is monitored by ^{1}H NMR spectroscopy and also the formation of one equivalent of HCl which is reacting with a molecule of pyridine forming the pyridinium salt and precipitating out. The second step of the reaction is the introduction of the second equivalent of chlorodiphenylphosphine, which reacts with the *exo*-oxo group forming the de-oxygenated complex **[ClUO(py)(H$_2$L)]** and the by-product Ph_2POPPh_2, which is expected to exist in solution as the isomer $O{=}PPh_2PPh_2$ (Scheme 6).[25]

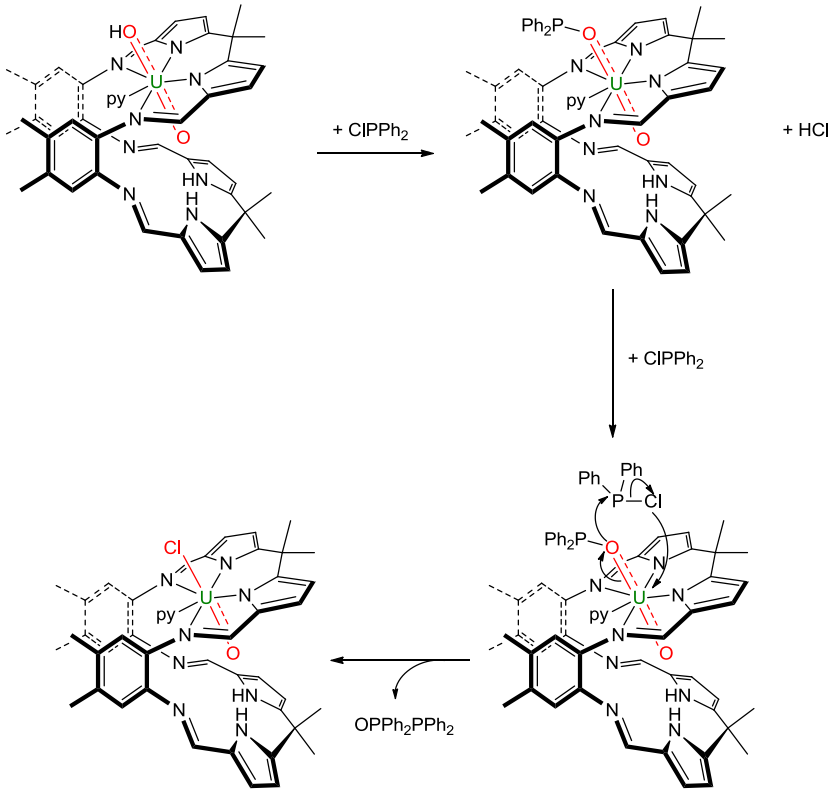

Scheme 6: Proposed mechanism for the formation of the speculated complexes **[(Ph$_2$PO)UO(py)(H$_2$L)]** and **[ClUO(py)(H$_2$L)]**.

3.7. Conclusions

In conclusion, we have shown that it is possible to form new O-H and O-Si covalent bonds with the oxo group of the uranyl complex without a change in the oxidation state of the uranyl by the addition of acid to the dilithiated complex **[(py)$_3$LiOUO(py)Li(py)(HL)]**. Further investigation to identify whether modification of the fifth equatorial, solvent, site in **[(HO)UO(py)(H$_2$L)]** will enable us to identify possible adducts that can help better define uranyl oxo-ion exchange processes.

This chapter also describes the possible formation of an O-P covalent bond between the uranyl and a phosphine. The addition of two equivalents of chlorodiphenylphosphine is proposed to extract the *exo* oxygen of the $[UO_2]^+$ and replaces it with a chloride forming the complex **[ClUO(py)(H$_2$L)]**. Further investigations are needed to confirm the formation of these complexes. The new complexes possess a vacant N4-donor compartment where further reactions with the *endo* oxo group could occur. Unfortunately, we have been unable to observed any O-C bond formation from the addition of MeX (X = I or OTf) to the **[(HO)UO(py)(H$_2$L)]**.

3.8. References

(1) Arnold, P. L.; Love, J. B.; Patel, D. *Coord. Chem. Rev.* **2009**, *253*, 1973.
(2) Arnold, P. L.; Pécharman, A.-F.; Hollis, E.; Yahia, A.; Maron, L.; Parsons, S.; Love, J. B. *Nat Chem* **2010**, *2*, 1056.
(3) Hayton, T. W.; Wu, G. *Inorg. Chem.* **2009**, *48*, 3065.
(4) Schnaars, D. D.; Wu, G.; Hayton, T. W. *Inorg. Chem.* **2011**, *50*, 4695.
(5) Arnold, P. L.; Patel, D.; Blake, A. J.; Wilson, C.; Love, J. B. *J. Am. Chem. Soc.* **2006**, *128*, 9610.
(6) Arnold, P. L.; Patel, D.; Wilson, C.; Love, J. B. *Nature* **2008**, *451*, 315.
(7) Brown, J. L.; Wu, G.; Hayton, T. W. *J. Am. Chem. Soc.* **2010**, *132*, 7248.
(8) Brown, J. L.; Mokhtarzadeh, C. C.; Lever, J. M.; Wu, G.; Hayton, T. W. *Inorg. Chem.* **2011**, null.
(9) Berthet, J.-C.; Siffredi, G.; Thuéry, P.; Ephritikhine, M. *Eur. J. Inorg. Chem.* **2007**, *2007*, 4017.
(10) Berthet, J.-C.; Siffredi, G.; Thuery, P.; Ephritikhine, M. *Chem. Commun.* **2006**, 3184.
(11) Arnold, P. L.; Turner, Z. R.; Kaltsoyannis, N.; Pelekanaki, P.; Bellabarba, R. M.; Tooze, R. P. *Chem. Eur. J.* **2010**, *16*, 9623.

(12) Yahia, A.; Arnold, P. L.; Love, J. B.; Maron, L. *Chem. Commun.* **2009**, 2402.
(13) Yahia, A.; Arnold, P. L.; Love, J. B.; Maron, L. *Chemistry – A European Journal* **2010**, *16*, 4881.
(14) Drago, R. S. *J. Phys. Chem.* **1991**, *95*, 9800.
(15) Yin, G.; Danby, A. M.; Kitko, D.; Carter, J. D.; Scheper, W. M.; Busch, D. H. *J. Am. Chem. Soc.* **2008**, *130*, 16245.
(16) Zi, G.; Jia, L.; Werkema, E. L.; Walter, M. D.; Gottfriedsen, J. P.; Andersen, R. A. *Organometallics* **2005**, *24*, 4251.
(17) Hay, P. J.; Martin, R. L.; Schreckenbach, G. *J. Physic. Chem. A* **2000**, *104*, 6259.
(18) Wander, M. C. F.; Kerisit, S.; Rosso, K. M.; Schoonen, M. A. A. *J. Physic. Chem. A* **2006**, *110*, 9691.
(19) Cotton, F. A.; Marler, D. O.; Schwotzer, W. *Inorg. Chem.* **1984**, *23*, 4211.
(20) Money, J. K.; Folting, K.; Huffman, J. C.; Collison, D.; Temperley, J.; Mabbs, F. E.; Christou, G. *Inorg. Chem.* **1986**, *25*, 4583.
(21) Do, Y.; Simhon, E. D.; Holm, R. H. *Inorg. Chem.* **1985**, *24*, 1831.
(22) Hayton, T. W.; Wu, G. *J. Am. Chem. Soc.* **2008**, *130*, 2005.
(23) Kannan, S.; Moody, M. A.; Barnes, C. L.; Duval, P. B. *Inorg. Chem.* **2006**, *45*, 9206.
(24) John, G. H.; May, I.; Sarsfield, M. J.; Collison, D.; Helliwell, M. *Dalton Trans.* **2007**, 1603.
(25) Fei, Z.; Scopelliti, R.; Dyson, Paul J. *Eur. J. Inorg. Chem.* **2004**, *2004*, 530.
(26) Fortier, S.; Hayton, T. W. *Coord. Chem. Rev.* **2010**, *254*, 197.
(27) Clark, D. L.; Conradson, S. D.; Donohoe, R. J.; Keogh, D. W.; Morris, D. E.; Palmer, P. D.; Rogers, R. D.; Tait, C. D. *Inorg. Chem.* **1999**, *38*, 1456.
(28) Bühl, M.; Schreckenbach, G. *Inorg. Chem.* **2010**, *49*, 3821.
(29) Shamov, G. A.; Schreckenbach, G. *J. Am. Chem. Soc.* **2008**, *130*, 13735.
(30) Hratchian, H. P.; Sonnenberg, J. L.; Hay, P. J.; Martin, R. L.; Bursten, B. E.; Schlegel, H. B. *J. Physic. Chem. A* **2005**, *109*, 8579.
(31) Arnold, P. L.; Blake, A. J.; Wilson, C.; Love, J. B. *Inorg. Chem.* **2004**, *43*, 8206.
(32) Porchia, M.; Brianese, N.; Casellato, U.; Ossola, F.; Rossetto, G.; Zanella, P.; Graziani, R. *J. Chem. Soc., Dalton Transactions* **1989**, 677.
(33) Korobkov, I.; Gambarotta, S.; Yap, G. P. A. *Angew. Chem., Int. Ed. Engl.* **2002**, *41*, 3433.

Chapter 4: Reduction and oxo group functionalisation of the uranyl dication

4.1. Introduction

The uranyl dication $[UO_2]^{2+}$ is kinetically inert and thermodynamically stable, so reaction at the oxo groups are difficult, and only a few example are known. This is in contrast with transition metal oxo complexes from the same group as uranium in the Periodic Table. Indeed, reactions such as oxygenation of hydrocarbons or oxygen-atom transfers have been seen with $[CrO_2]^{2+}$, $[MoO_2]^{2+}$ and other transition metal analogues, Equation (**1**).[1-4]

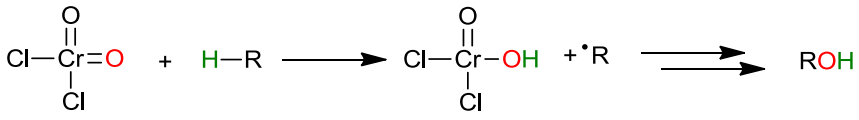

(1)

In this chapter, we will concentrate on the synthesis of the complexes **$[(Me_3SiO)UO(THF)(MX)_2(L)]$** (M = Fe, Zn; X = I, Cl), described previously by Arnold, Love and co-workers, in order to understand the possible mechanism of the reaction between **$[UO_2(THF)(H_2L)]$**, $KN(SiMe_3)_2$ and transition metal halides MX_2, Equation (**2**).[5]

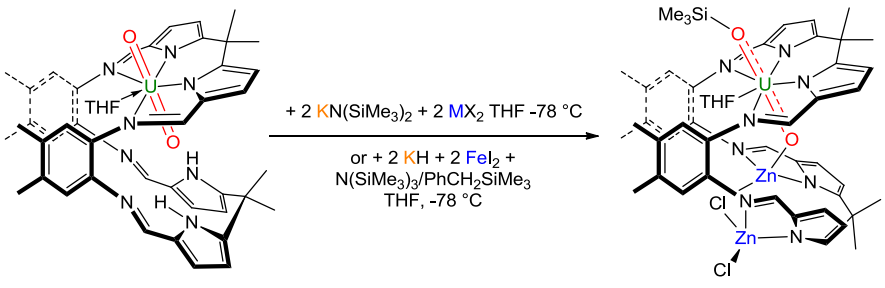

(2)

4.2. Synthesis of $[(Me_3SiO)UO(THF)(MX)_2(L)]$

4.2.1. Synthesis of $[(Me_3SiO)UO(THF)(ZnCl)_2(L)]$

To understand and explain the mechanism of the silyl oxo functionalisation observed in the complexes **$[(Me_3SiO)UO(MX)_2(L)]$** (M = Fe, Zn; X = Cl, I) by treatment of the precursor uranyl Pacman complex **$[UO_2(THF)(H_2L)]$** with two equivalents of potassium base and two equivalents of transition metal salts, several reactions have been attempted. There were some difficulties repeating these reactions under the conditions described previously, so for these reasons other routes were evaluated.[5]

The stoichiometric reaction between $Zn[N(SiMe_3)_2]_2$ and $ZnCl_2$ in toluene at room temperature for 2 h results in the formation of a gel which is dried under reduced pressure to afford **$[Zn\{N(SiMe_3)_2\}Cl]$** in good yield, Equation (**3**).

$$Zn[N(SiMe_3)_2]_2 + ZnCl_2 \xrightarrow{\text{Toluene}} 2\ Zn\{N(SiMe_3)_2\}Cl \qquad \textbf{(3)}$$

The compound **$[Zn\{N(SiMe_3)_2\}Cl]$** is only characterised by ^{1}H NMR spectroscopy, and the ^{1}H NMR spectrum in C_6D_6 contains one resonance at 0.20 ppm for the silylamide protons.

The one pot reaction between one equivalent of **$[UO_2(THF)(H_2L)]$** and two equivalents of **$[Zn\{N(SiMe_3)_2\}Cl]$** in toluene at 110 °C for 24 h results in a suspension. The filtrate is isolated and dried to afford the known complex **$[(Me_3SiO)UO(THF)(ZnCl)_2(L)]$** as a brown solid in good yield (62%). Furthermore, the solids are dried to afford a mixture of **$[UO_2(THF)(ZnCl)(HL)]$, $[UO_2(THF)(H_2L)]$**, and **$[(THF)Cl_2ZnOUO(THF)Zn(THF)(HL)]$** in a ratio 1:0.13:0.32, Equation (**4**).

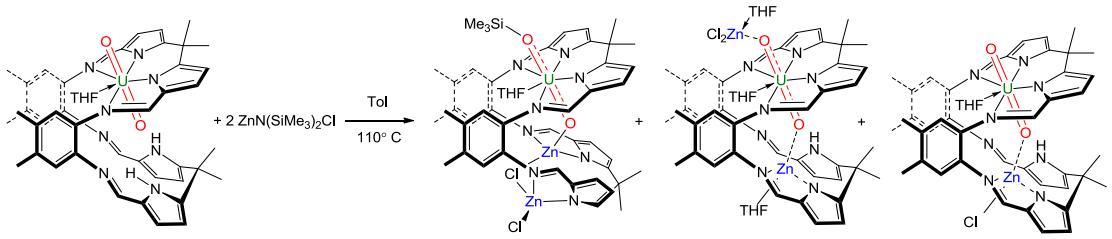

(4)

The oxo-silylated U^{V} complex **[(Me$_3$SiO)UO(THF)(ZnCl)$_2$(L)]** was fully characterised, including by ^{1}H NMR and FTIR spectroscopy, elemental analysis, and X-ray diffraction studies. In the ^{1}H NMR spectrum of **[(Me$_3$SiO)UO(THF)(ZnCl)$_2$(L)]** resonances between 13 and −5 ppm are seen and are consistent with the formation of a paramagnetic compound. Although the individual resonances could not be assigned, the number and their integrals are consistent with the retention of a wedged, Pacman structure in solution of C_1 symmetry (Figure 1). The resonance at 7.32 ppm integrating for 9H corresponds to the silyl group bound to the *exo*-oxo group, and eight resonances integrating for 3H each correspond to the methyl groups on the ligand at 6.78, 6.05, 1.64, 0.84, 0.62, 0.07, −0.04, −0.07, and −3.91 ppm.

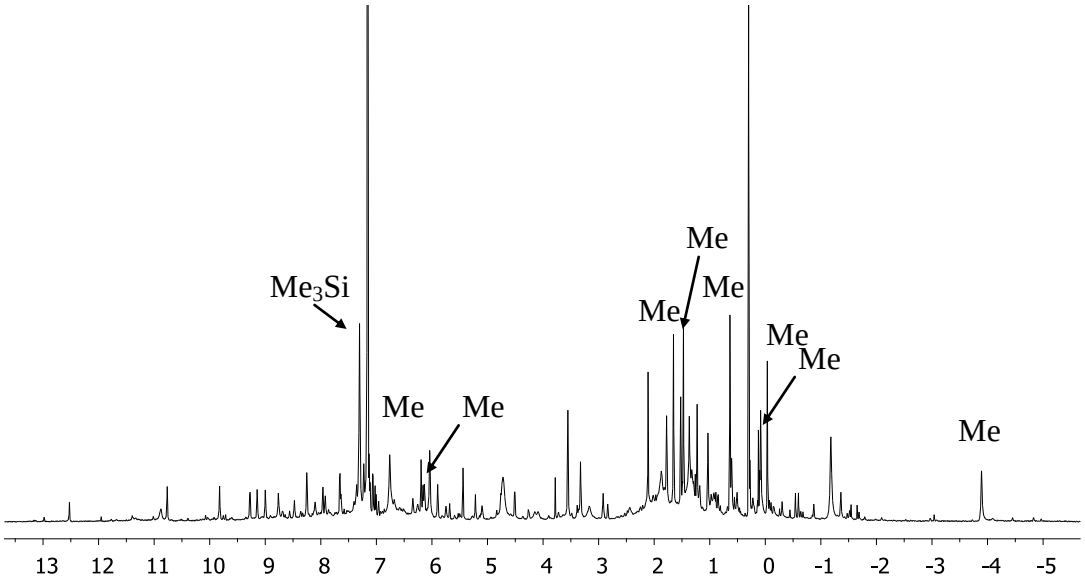

Figure 1: ^{1}H NMR spectrum of **[(Me$_3$SiO)UO(THF)(ZnCl)$_2$(L)]** in d_6-benzene

Elemental analysis supports the formulation of **[(Me$_3$SiO)UO(THF)(ZnCl)$_2$(L)]**. The FTIR spectrum contains no broad band corresponding to the pyrrole NH (at 3373 cm^{-1} in the precursor complex **[UO$_2$(THF)(H$_2$L)]**). Two stretches corresponding to the U=O are observed at 841 cm^{-1} and 770 cm^{-1}, and are weakened substantially compared to that in the U^{VI} starting material **[UO$_2$(THF)(H$_2$L)]** (ν U=O 908 cm^{-1}), but are in the range of the [UO$_2$]$^+$ stretches in the literature.[6-8] Absorptions associated with SiMe$_3$ vibrations are also observed at 1248 cm^{-1}, 844 cm^{-1} and 758 cm^{-1}.

Crystals of **[(Me$_3$SiO)UO(THF)(ZnCl)$_2$(L)]** suitable for analysis by single crystal X-ray diffraction were grown from a saturated d_6-benzene solution (Figure 2).

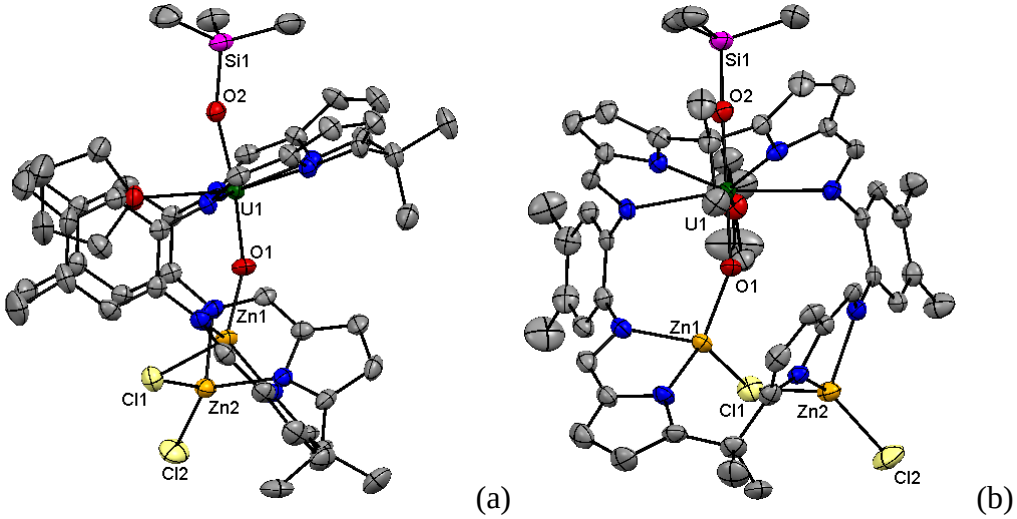

Figure 2: Solid state structure of **[(Me$_3$SiO)UO(THF)(ZnCl)$_2$(L)]** showing side (a) and front view (b). For clarity, all the hydrogen atoms and lattice molecules of solvent are omitted (displacement ellipsoids drawn at 50% probability).

Table 1: Selected bond distances (Å) and angles (°) of **[(Me$_3$SiO)UO(THF)(ZnCl)$_2$(L)]**

U1-O1	1.872(3)
U1-O2	1.991(4)
U1-O3	2.467(4)
O2-Si1	1.694(4)
O1-Zn1	1.958(4)
Zn1-Cl1	2.3055(16)
Zn2-Cl1	2.3332(16)
Zn2-Cl2	2.1939(16)
O1-U1-O2	172.99(19)
Si1-O2-U1	162.0(2)
U1-O1-Zn1	148.6(2)
Zn1-Cl1-Zn2	89.12(6)

The Pacman structural motif seen in the uranyl macrocycle **[UO$_2$(THF)(H$_2$L)]** remains intact with one compartment occupied by the uranyl moiety and the other N_4 compartment now occupied by two tetrahedral Zn atoms, each coordinated to a pyrrole-imine nitrogen chelate and which results in a distortion of the compartment by the flipping of one of the pyrrole-imine chelates out of the usual N_4-donor plane; overall, this results in a desymmetrisation of the ligand. One Zn atom (Zn1) is coordinated to the *endo*-oxo group (Zn1-O1 1.958(4) Å) and one Cl atom (Zn1-Cl1 2.3055(16) Å), the second Zn atom (Zn2) is coordinated to two Cl atoms (Zn2-Cl1 2.3332(16) and Zn2-Cl2 2.1939(16) Å). The uranium centre is seven coordinate and displays a distorted pentagonal bipyramidal geometry with the oxo groups retaining a *trans* arrangement (O1-U1-O2 172.99(19)°). The equatorial sites are occupied by the four nitrogen atoms of the macrocyclic compartment and an oxygen atom from a molecule of THF in the fifth equatorial site that sits between the two macrocyclic aryl rings. From analysis of the uranium-oxygen bond lengths it is

evident that the uranyl fragment is in the 5+ oxidation state. The *endo*-oxo group bond distance (U1-O1 1.872(3) Å) is significantly elongated compared to the bond distance of $[UO_2]^{2+}$ in **$[UO_2(THF)(H_2L)]$** (U1-O1 1.787(3) Å) and is similar to experimental and calculated bond distances for $[UO_2]^{+}$ (range 1.811- 1.934 Å).[9-13] The *exo*-oxo bond distance (U1-O2 1.991(4) Å) is also longer than in **$[UO_2(THF)(H_2L)]$** (U1-O2 1.770(3) Å).[9] The Si1-O2 bond length (1.694(5) Å) is similar to the known Si-O bond in the literature (range 1.631 to 1.655 Å) (Table 1).[7,14-16] Hayton and co-workers observed the same range of UO and OSi bond lengths in the doubly silylated complex $[U(OSiMe_3)_2I_2(^{Ar}acnac)]$.[7] The U-O3 distance is in the same range to the one observed in the precursor uranyl Pacman complex (2.467(4) Å / 2.457(3) Å respectively). This crystal structure is similar to the one published in Nature in 2008, the bond lengths are identical but the difference are the halide atoms and the I/Cl disorder component observed in the published structure, which is due to the incorporation of a chloride atom from the presence of KCl in the starting material **$[UO_2(THF)(H_2L)]$**.

The ^{1}H NMR spectrum of the residual solids isolated after filtration of **$[(Me_3SiO)UO(THF)(ZnCl)_2(L)]$** in d_5-pyridine displays sets of resonances for three complexes, one for a paramagnetic compound, and the others for two diamagnetic compounds. One diamagnetic set corresponds to the starting material **$[UO_2(THF)(H_2L)]$** (Figure 3). The resonances of the paramagnetic compound are consistent, by their number and their integration, with the retention of a wedged, Pacman motif in solution of C_1 symmetry. The second diamagnetic complex has also an asymmetric ligand arrangement by the number of resonances and their integrations. From this spectrum it has been deduced that the by-products of this reaction are **$[(THF)Cl_2ZnOUO(THF)Zn(THF)(HL)]$** and **$[UO_2(THF)(ZnCl)(HL)]$** (these two complexes are identified later in this chapter) and unreacted uranyl Pacman complex **$[UO_2(THF)(H_2L)]$**.

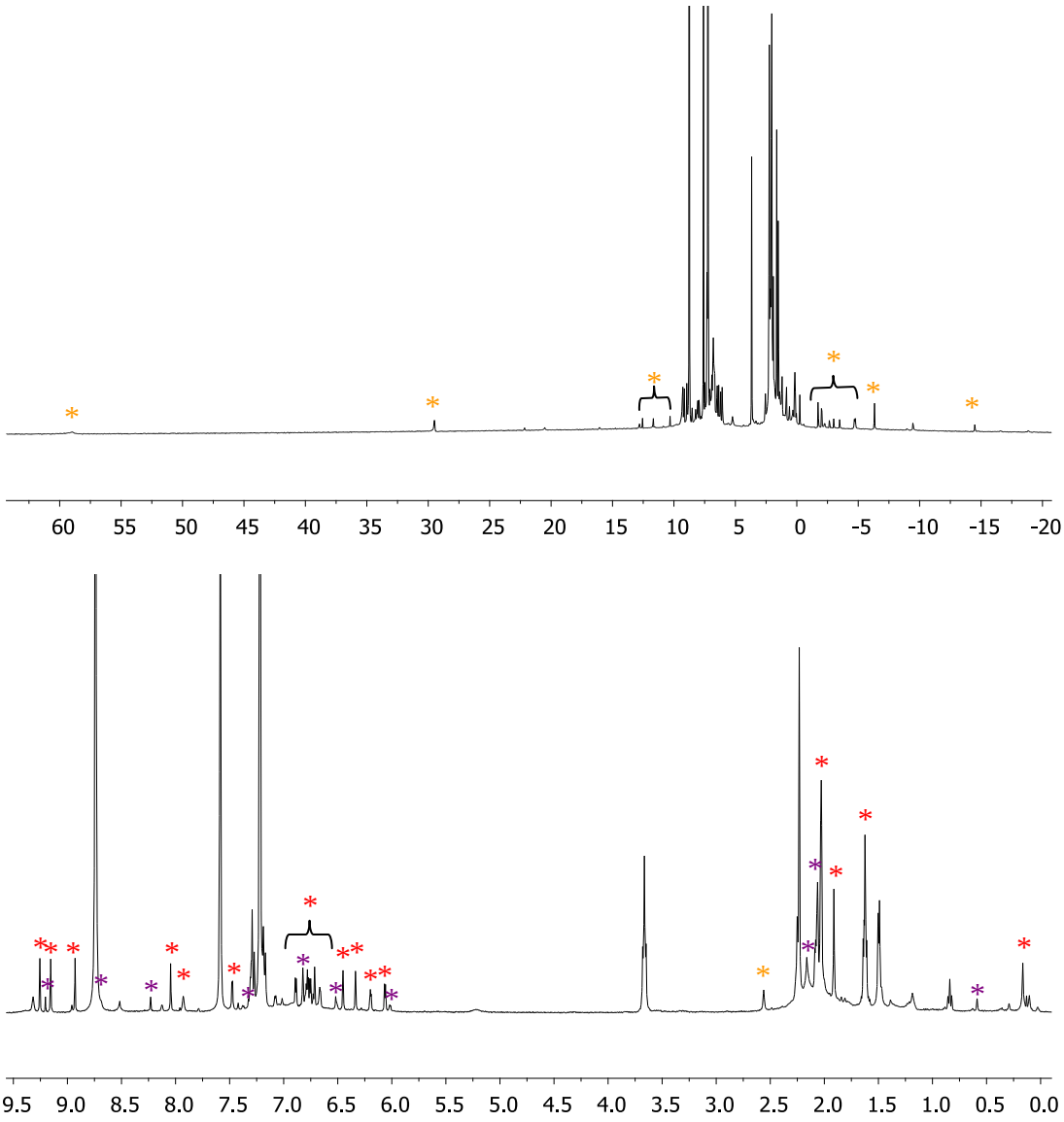

Figure 3: ^{1}H NMR spectra of the residual solids showing the mixture of **[UO_2(THF)(H_2L)]** (purple star), **[UO_2(THF)(ZnCl)(HL)]** (red star), and **[(THF)Cl_2ZnOUO(THF)Zn(THF)(HL)]** (orange star) (top: full spectrum, bottom: expansion).

4.2.2. Synthesis of [(Me_3SiO)UO(py)($ZnCl)_2$(L)]

In a similar manner to that described above, the reaction between one equivalent of the pyridine adduct **[UO_2(py)(H_2L)]** and two equivalents of **[Zn{N($SiMe_3)_2$}Cl]** in benzene in a Teflon-tapped NMR tube at 80 °C resulted in a suspension with a dark brown solution. As before, the reaction was monitored by ^{1}H NMR spectroscopy and formation of a paramagnetic compound was observed (Figure 5). The resonance at 8.06 ppm, integrating for 9H, corresponds to the silyl

group bound to the *exo*-oxo group and eight resonances integrating for 3H each correspond to the methyl groups on the ligand at 4.52, 4.13, 1.06, 0.88, 0.44, 0.28, −0.24, and −3.95 ppm. The spectrum is similar to the ^{1}H NMR spectrum of **[(Me$_3$SiO)UO(THF)(ZnCl)$_2$(L)].**

4.2.3. Alternative method to synthesise [(Me$_3$SiO)UO(py)(ZnCl)$_2$(L)]

The reaction between one equivalent of **[(Me$_3$SiO)UO(py)(H$_2$L)]** and two equivalents of KN(SiMe$_3$)$_2$ in d_6-benzene in a Teflon-tapped NMR tube at room temperature for 24 h results in a darker-coloured solution and the formation of a new complex that is, judging by the loss of the resonances due to the N-H protons, probably **[(Me$_3$SiO)UO(py)(K$_2$L)]**. The subsequent addition of $ZnCl_2$ results in the precipitation of KCl and the formation of the complex **[(Me$_3$SiO)UO(py)(ZnCl)$_2$(L)]** (Scheme 1).

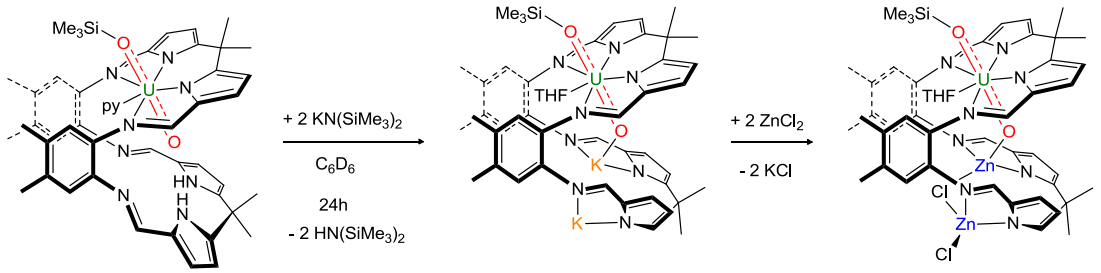

Scheme 1: Synthesis of **[(Me$_3$SiO)UO(py)(ZnCl)$_2$(L)]**

The ^{1}H NMR spectrum of the first step displays a new paramagnetic compound (Figure 4). The resonances are paramagnetically shifted and are consistent with the retention of a wedged, Pacman structure in solution of C_1 symmetry. The most paramagnetically shifted resonance at 13.72 ppm, integrating for 9H, corresponds to the silyl group. Eight resonances integrating for 3H each correspond to the methyl group on the ligand.

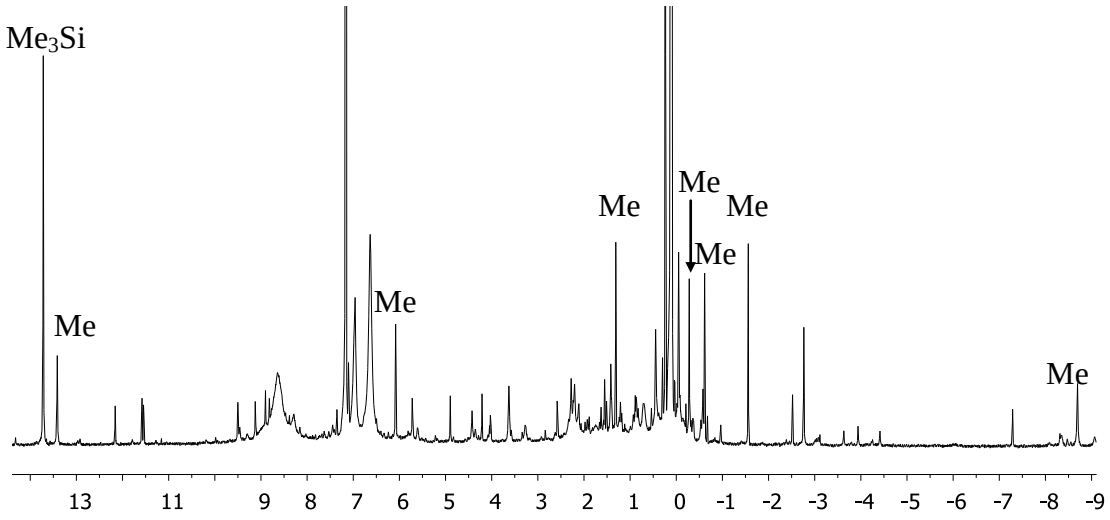

Figure 4: ^{1}H NMR spectrum of **[(Me$_3$SiO)UO(py)(K$_2$L)]** in d_6-benzene

The ^{1}H NMR spectrum of the second step is identical to the ^{1}H NMR spectrum that results from the reaction of one equivalents of **[UO$_2$(py)(H$_2$L)]** and two equivalents of **[Zn{N(SiMe$_3$)$_2$}Cl]** affording the complex **[(Me$_3$SiO)UO(py)(ZnCl)$_2$(L)]** (Figure 5).

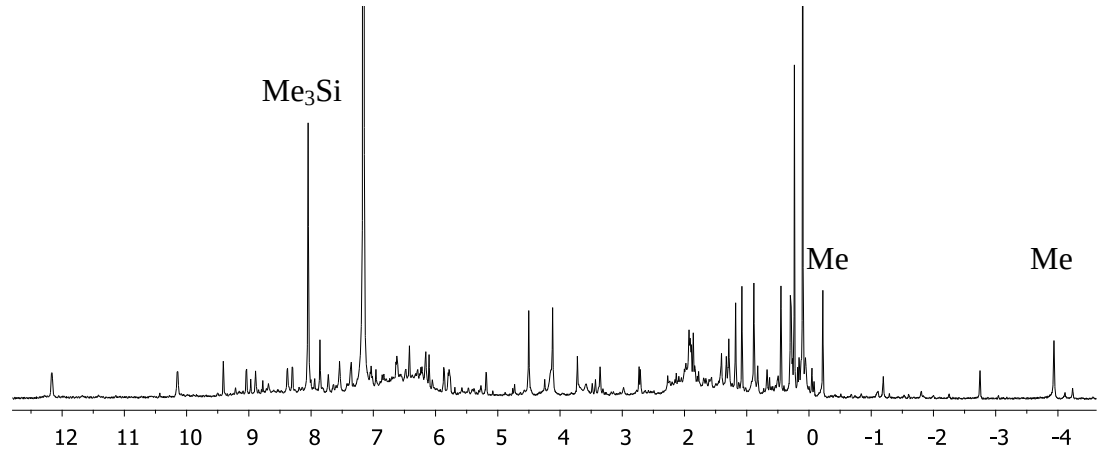

Figure 5: ^{1}H NMR spectrum of **[(Me$_3$SiO)UO(py)(ZnCl)$_2$(L)]** in d_6-benzene

Single crystals of **[Cl$_2$Zn(py)OUO(py)Zn(py)(HL)]** were grown from a saturated solution of benzene. The crystals are from the reaction between a trace of dilithiated complex **[(py)$_3$LiOUO(py)Li(py)(HL)]** (from the reaction to make **[(HO)UO(py)(H$_2$L)]** by the addition of HCl to **[(py)$_3$LiOUO(py)Li(py)(HL)]** then the addition of Me$_3$SiCl to this mixture to obtain **[(Me$_3$SiO)UO(py)(H$_2$L)]**) and two equivalents of $ZnCl_2$ (Figure 6).

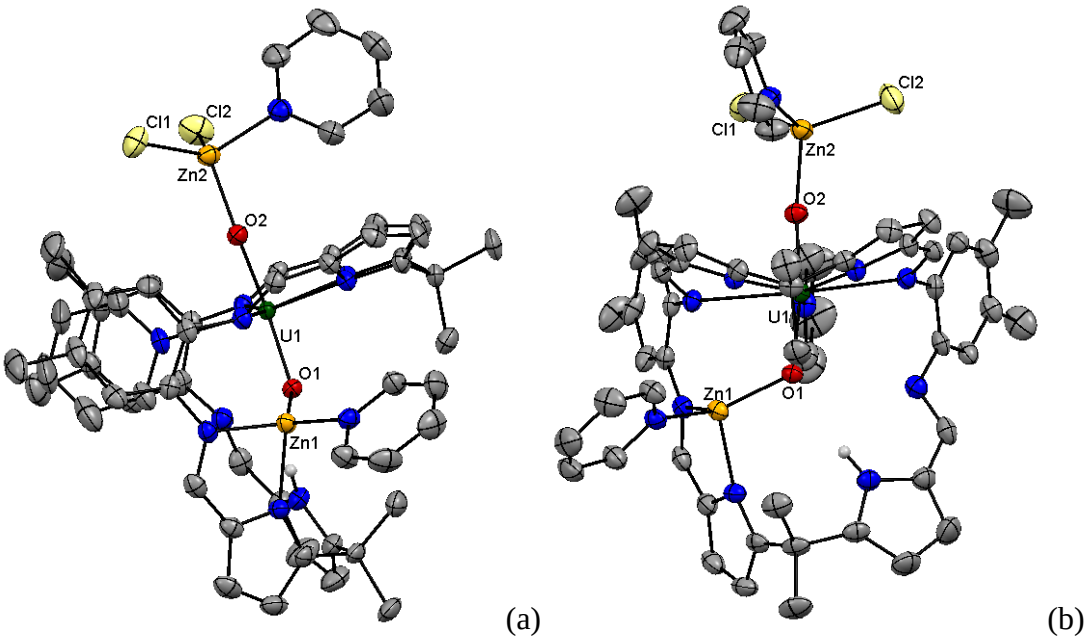

Figure 6: Solid state structure of **[(py)Cl_2ZnOUO(py)Zn(py)(HL)]** showing side (a) and front view (b). For clarity, the hydrogen atoms, except the pyrrole NH, and lattice molecules of solvent are omitted (displacement ellipsoids drawn at 50% probability).

Table 2: Selected bond distances (Å) and angles (°) of **[Cl_2Zn(py)OUO(py)Zn(py)(HL)]**

U1-O1	1.934(2)
U1-O2	1.887(3)
U1-N9	2.586(3)
O1-Zn1	1.962(2)
O2-Zn2	1.989(3)
O1···N7	3.068
O1-U1-O2	170.47(13)
Zn1-O1-U1	119.51(13)
Zn2-O2-U1	172.99(15)

The uranium centre is seven coordinate and displays a distorted pentagonal bipyramidal geometry with the oxo groups *trans* (O1-U1-O2 170.47(11)°), and the equatorial sites occupied by the nitrogen atoms of the macrocycle and the nitrogen atom from a molecule of pyridine that sits between the two macrocyclic aryl rings. From analysis of the uranium-oxygen bond lengths it is evident that the uranyl fragment is in the 5+ oxidation state. The *endo*-oxo bond distance (U1-O1 1.934(2) Å) is significantly elongated compared to the bond distance of $[UO_2]^{2+}$ in **$[UO_2(py)(H_2L)]$** (U1-O1 1.7779(18) Å) and is similar to experimental and calculated bond distances for $[UO_2]^{+}$ (range 1.811- 1.934 Å).[11,12] The *exo*-oxo bond distance (U1-O2 1.887(3) is also longer than in **$[UO_2(py)(H_2L)]$** (U1-O2 1.7546(19) Å). In comparison to bond distance in the dilithiated complex **$[(py)_3LiOUO(py)Li(py)(HL)]$** (U1-O1 1.834(4) Å and U1-O2 1.879(5) Å), the U1-O1 bond distance is slightly elongated and the U1-O2 bond distance is similar. Both zinc atoms are four coordinate and display tetrahedral geometries. One zinc atom is sitting in half of the second pocket and coordinated to two nitrogen atoms (pyrrole N8 and imine N9) of the macrocycle, the *endo*-oxo group of $[UO_2]^{+}$ and the nitrogen of a molecule of pyridine, while the second is coordinated to one molecule of pyridine, two chlorine atoms, and the *exo*-oxo group (Table 2). The bond distance U1-N9 (2.586(3) Å) is similar to that seen in the analogues in the 6+ oxidation state. The lower N4 compartment is oriented such that hydrogen bond is evident between the remaining pyrrole NH group and the *endo*-oxo O1; the N···O separation is slightly shorter than in the precursor uranyl Pacman (N···O 3.068 / 3.172 Å respectively). The core structure is similar to the dilithiated complex **$[(py)_3LiOUO(py)Li(py)(HL)]$**.[17]

4.3. Synthesis and characterisation of $[(py)X_2ZnOUO(S)Zn(py)(HL)]$ (S = THF or py)

4.3.1. Reaction of $[(py)_3LiOUO(py)Li(py)(HL)]$ and two equivalents of ZnI_2

The one-pot reaction between one equivalent of **$[(py)_3LiOUO(py)Li(py)(HL)]$** and two equivalents of ZnI_2 in pyridine at room temperature for 16 h results in a colour change from brown-yellow to dark red and, on removal of the volatiles

affords **[(py)I$_2$ZnOUO(py)Zn(py)(HL)]** as a brown solid in good yield (76% with 2LiI incorporated), Equation (**5**).

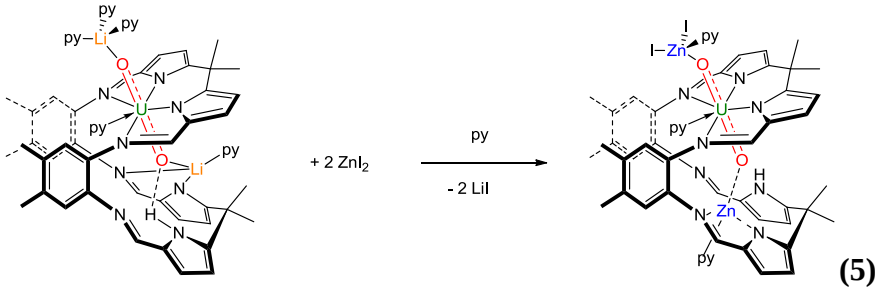

(5)

The compound was fully characterised. It is clear from the ^{1}H NMR spectrum that this compound is paramagnetic, adopts a Pacman structure, and is of C_1 symmetry (Figure 7). The most contact-shifted paramagnetic resonance at 58.43 ppm is assigned to the pyrrole NH. The eight resonances integrating for 3H each at 29.29, 10.31, 5.04, 2.50, −0.35, −1.75, −2.05, and −6.32 ppm are assigned to the methyl group of the ligand.

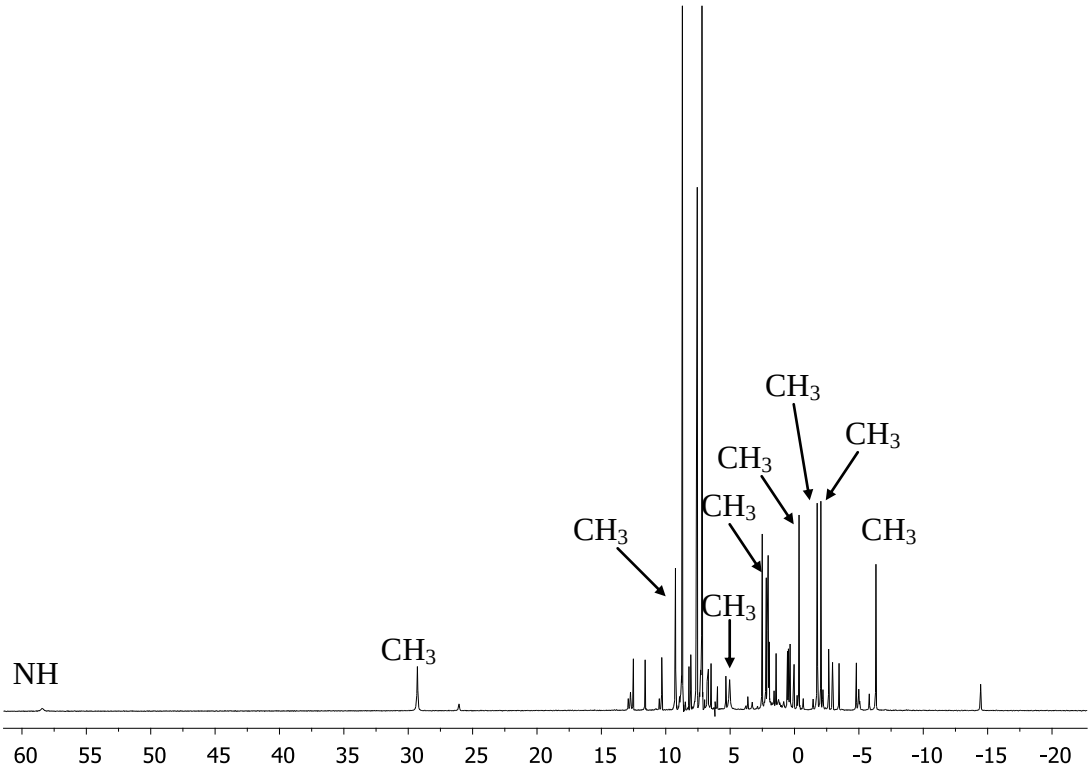

Figure 7: ^{1}H NMR spectrum of **[(py)I$_2$ZnOUO(py)Zn(py)(HL)]** in d_5-pyridine

The FTIR spectrum contains one broad band at 3329 cm^{-1} corresponding to the presence of a pyrrole NH (3373 cm^{-1} in the starting material **[UO_2(THF)(H_2L)]**) and two U-O stretches at 877 and 699 cm^{-1}. These latter stretches are weakened in comparison to the starting material **[UO_2(THF)(H_2L)]** (ν_{UO} = 908 cm^{-1}) and in the range of those found in literature.[6-8] Elemental analysis supports the formulation of **[(py)I_2ZnOUO(py)Zn(py)(HL)][LiI]$_2$** so suggesting that two equivalents of LiI are incoporated

4.3.2. Reaction of [(py)$_3$LiOUO(py)Li(py)(HL)] and two equivalents of $ZnCl_2$

Similarly, the reaction between one equivalent of **[(py)$_3$LiOUO(py)Li(py)(HL)]** and two equivalents of $ZnCl_2$ in a Teflon-tapped NMR tube in pyridine results in a dark red solution of the complex **[(py)Cl_2ZnOUO(py)Zn(py)(HL)]**, Equation (**6**).

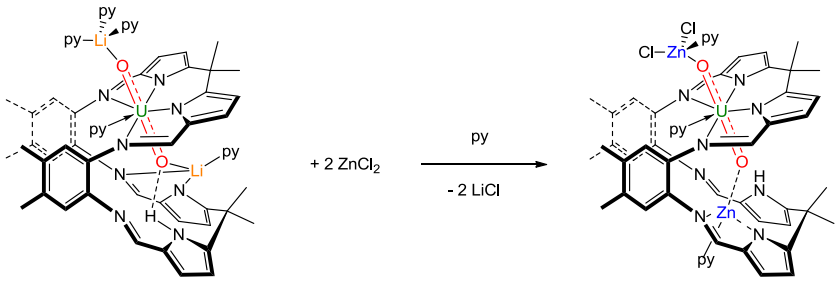

(6)

The complex was only characterised by ^{1}H NMR spectroscopy, which displays resonances due to the formation of a paramagnetic complex and is identical to that seen for **[(py)I_2ZnOUO(py)Zn(py)(HL)]** (Figure 7).

4.3.3. Reaction of [(THF)$_3$KOUO(THF)K(THF)(HL)] and two equivalents of ZnI_2

4.3.3.1. Synthesis and characterisation of [(THF)$_3$KOUO(THF)K(THF)(HL)]

The reaction between one equivalent of **[UO_2(THF)(H_2L)]** and two equivalents of KH in THF at +78 °C for 2 h results in the formation of a red solution, which on removal of the volatiles affords **[(THF)$_3$KOUO(THF)K(THF)(HL)]** as a dark red solid in good yield (94%), Equation (**7**).

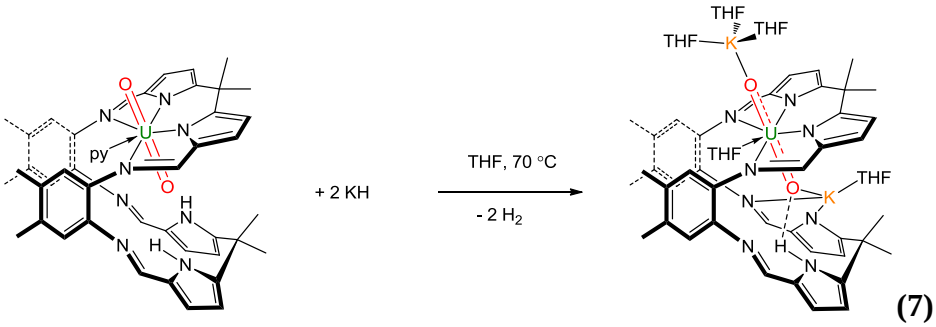

(7)

The complex was fully characterised, including by ^{1}H NMR spectroscopy, FTIR spectroscopy, and elemental analysis. The ^{1}H NMR spectrum displays a new paramagnetic compound of C_s symmetry and not the expected C_1 symmetry seen in the Li and Zn analogues (Figure 8). This is probably because the radius of the potassium cation is considerably bigger than that of Zn^{2+} or Li^{+} (138, 74, 78 pm respectively) and could sit in the middle of the second compartment, so resulting in a symmetric ligand arrangement. The most contact-shifted paramagnetic resonance at 90.05 ppm is assigned to the pyrrole NH, and suggests a close hydrogen-bonding interaction between this hydrogen and the uranyl cation. The four resonances integrating for 3H each at 30.08, 10.62, −1.94, −7.29 ppm and two resonances integrating for 6H each at 0.41, and −2.07 ppm are assigned to the *meso*- and aryl-methyl groups of the ligand, respectively.

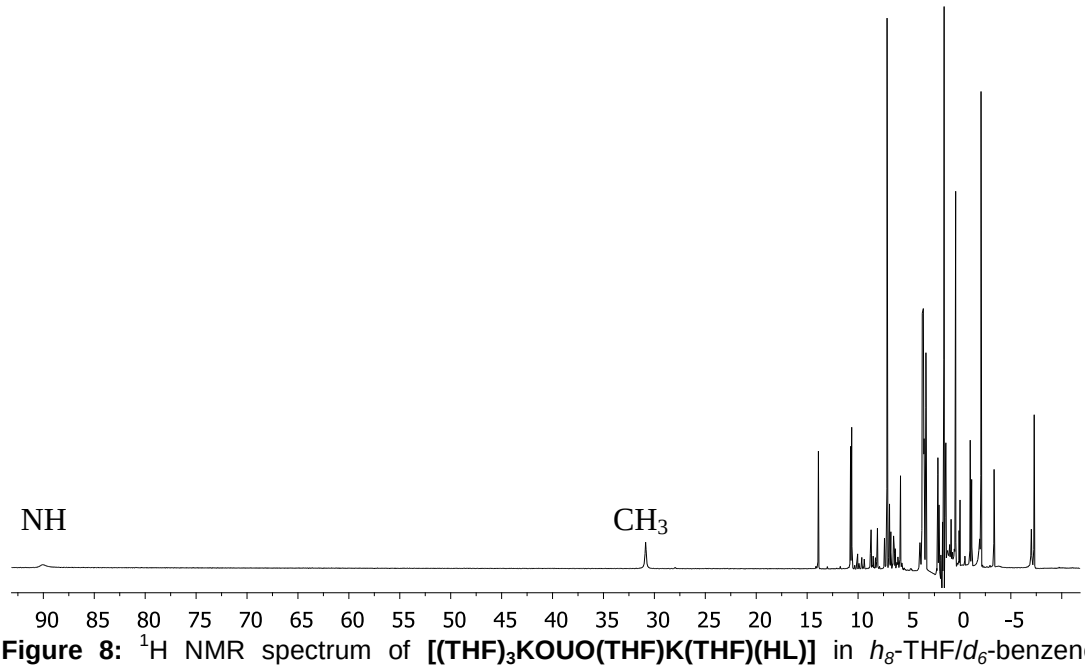

Figure 8: ^{1}H NMR spectrum of **[(THF)$_3$KOUO(THF)K(THF)(HL)]** in h_8-THF/d_6-benzene (double pre-saturation of the protio solvent)

The FTIR spectrum contains a broad band at 3417 cm^{-1} which corresponds to the pyrrole NH. Two bands for the UO stretches are observed at 808 and 736 cm^{-1} and are weakened in comparison to the UO stretches in the starting material but are in the range for $[UO_2]^+$.[6-8]

4.3.3.2.Synthesis and characterisation of [(THF)I_2ZnOUO(THF)Zn(THF)(HL)]

In a similar manner to the reaction between the dilithiated complex **[(py)$_3$LiOUO(py)Li(py)(HL)]** and two equivalents of ZnX_2 (X = Cl, I), the reaction between one equivalent of **[(THF)$_3$KOUO(THF)K(THF)(HL)]** and two equivalents of ZnI_2 in THF for 16 h results in a suspension. The suspension was filtered and the volatiles were removed to afford **[(THF)I_2ZnOUO(THF)Zn(THF)(HL)]** in good yield (85 %), Equation (**8**).

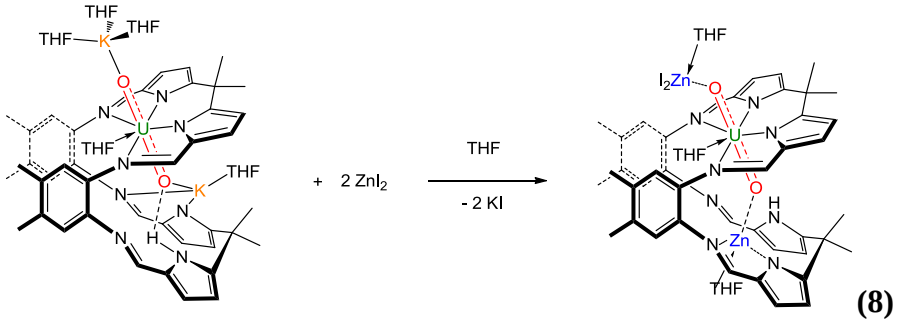

(8)

This complex was characterised by ^{1}H NMR spectroscopy and X-ray diffraction studies. The ^{1}H NMR spectrum displays a different paramagnetic compound in comparison to the ^{1}H NMR spectrum of the complex **[(THF)$_3$KOUO(THF)K(THF)(HL)]**. The number and integrals of the paramagnetically shifted resonances are consistent with the retention of a wedged, Pacman structure in solution of C_1 symmetry (Figure 9). The spectrum is similar to the ^{1}H NMR spectra of the pyridine-solvated complexes **[(py)X$_2$ZnOUO(py)Zn(py)(HL)]**. The most shifted resonance at 65.80 ppm corresponds to the pyrrole NH. Eight resonances integrating for 3H each correspond to the methyl groups of the ligand.

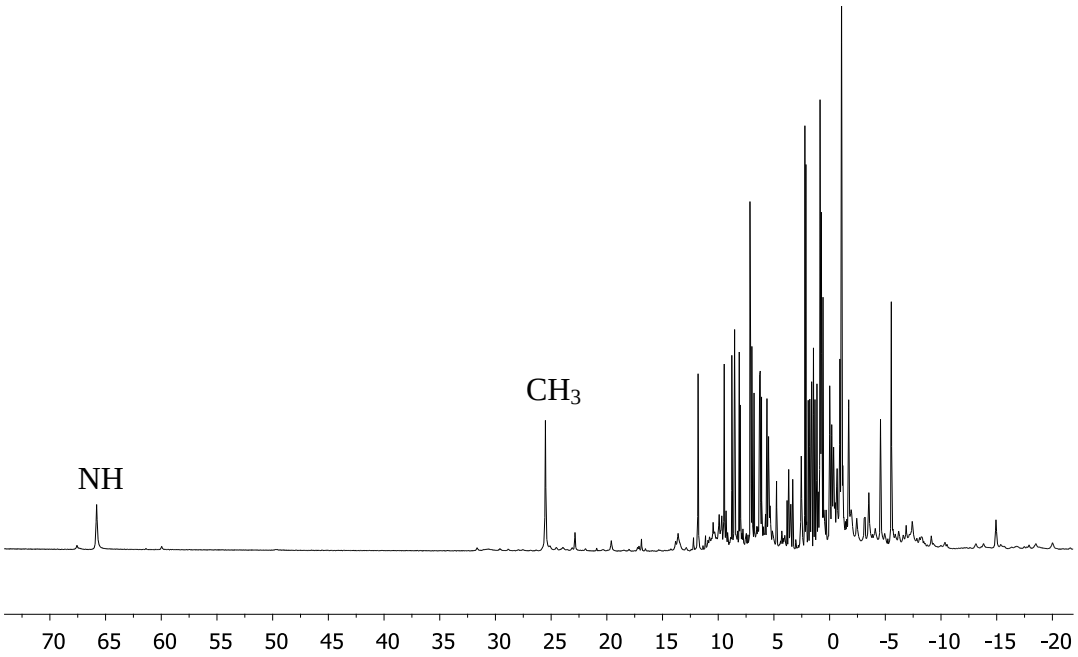

Figure 9: ^{1}H NMR spectrum of **[(THF)I$_2$ZnOUO(THF)Zn(THF)(HL)]** h_8-THF/d_6-benzene (double pre-saturation of the protio solvent)

Single crystals of **[I$_2$Zn(py)OUO(THF)Zn(py)(HL)]** were grown from a saturated solution of THF that contained a few drops of d_6-benzene and which resulted from an *in-situ* reaction between one equivalent of **[UO$_2$(py)(H$_2$L)]** and two equivalents of KH in THF with subsequent addition of ZnI_2 (Figure 10).

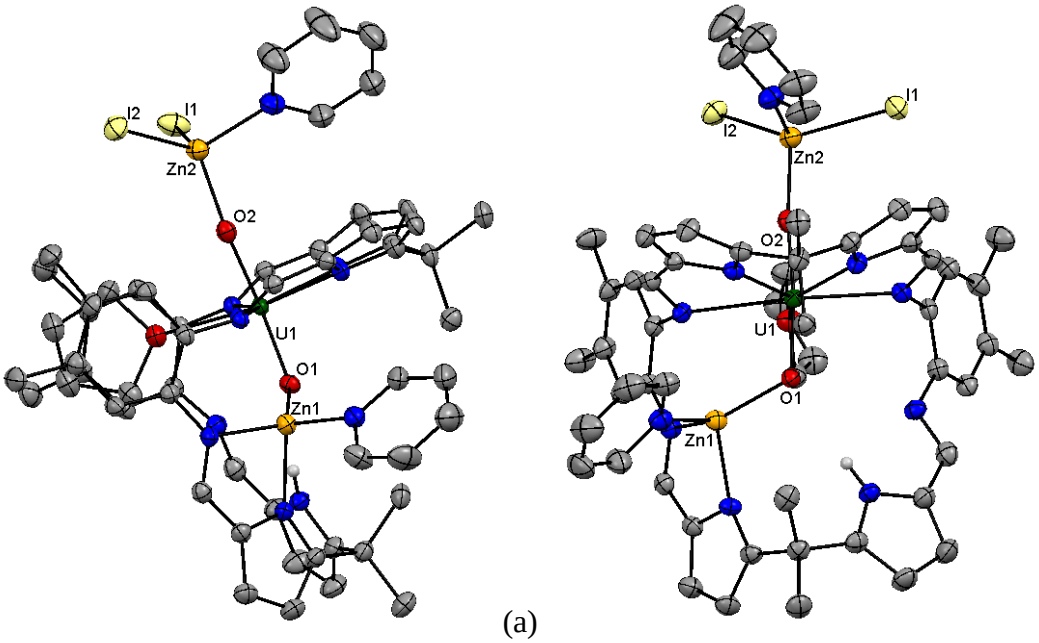

Figure 10: Solid state structure of **[I_2Zn(py)OUO(THF)Zn(py)(HL)]** showing side (a) and front views (b). For clarity the hydrogen atoms, except the pyrrole NH, and lattice molecules of solvent are omitted (displacement ellipsoids drawn at 50% probability).

Table 3: Selected bond distances (Å) and angles (°) of **[I_2Zn(py)OUO(THF)Zn(py)(HL)]**

U1-O1	1.908(3)
U1-O2	1.879(3)
U1-O3	2.473(3)
O1-Zn1	1.965(3)
O2-Zn2	1.988(3)
O1···N6	3.178
O1-U1-O2	173.03(13)
Zn1-O1-U1	118.92(15)
Zn2-O2-U1	172.27(19)

The crystal structure is similar to **[Cl_2Zn(py)OUO(py)Zn(py)(HL)]**. The uranium centre is seven coordinate and displays a distorted pentagonal bipyramidal

geometry with the oxo groups *trans* (O1-U1-O2 173.03(13)°), and the equatorial sites are occupied by four nitrogen atoms of the macrocycle and nitrogen atom from a molecule of pyridine that sits between the two macrocyclic aryl rings. From analysis of the uranium-oxygen bond lengths it is evident that the uranyl fragment is in the 5+ oxidation state. The *endo*- U1-O1 distance (1.908(3) Å) is significantly elongated compared to the bond distance of $[UO_2]^{2+}$ in **$[UO_2(THF)(H_2L)]$** (U1-O1 1.787(3) Å) and is similar to experimental and calculated bond distances for $[UO_2]^{+}$ (range 1.811- 1.934 Å) (Table 3).[11,12] The *exo*- U1-O2 distance (1.879(3) Å) is also longer than in **$[UO_2(THF)(H_2L)]$** (U1-O2 1.770(3) Å). Both zinc atoms (Zn1 and Zn2) are four coordinate and display a tetrahedral geometry, Zn1 is sitting in half of the second pocket and coordinated to two nitrogen (pyrrole and imine) atoms of the macrocycle, the *endo*-oxo group (Zn1-O1 1.965(3) Å) and the nitrogen of a molecule of pyridine, Zn2 is coordinated to one molecule of pyridine, two iodide atoms (I1 and I2), and the *exo*-oxo group (Zn2-O2 1.988(3) Å). The U1-O3 bond distance is elongated of 0.016 Å in comparison to the U1-O3 bond length in the uranyl Pacman complex **$[UO_2(THF)(H_2L)]$** (2.473(3) Å / 2.457(3) Å respectively). The lower N4 donor compartment is oriented such that hydrogen bond is evident between the pyrrole NH and the *endo*-oxo group (3.178 Å / 3.098 Å respectively).

4.4. Attempted synthesis of $[(Me_3SiO)UO(THF)(ZnI)_2(L)]$: *in-situ* reaction between $[UO_2(THF)(H_2L)]$, two equivalents of $KN(SiMe_3)_2$, and two equivalents of ZnI_2.

The synthesis of **$[(Me_3SiO)UO(THF)(ZnI)_2(L)]$** by the route described previously by Arnold, Love and co-workers was of limited success. The reaction between one equivalent of **$[UO_2(THF)(H_2L)]$** and two equivalents of $KN(SiMe_3)_2$ in THF at −78 °C was allowed to warm to room temperature over 15 min, then cooled down to −78°C. This solution was added to a suspension of ZnI_2 in toluene at −78 °C and stirred for 72 h. The suspension was filtered and the filtrate was dried under reduced pressure to afford a brown solid. The ^1H NMR spectrum of this material contained the resonances of the starting material **$[UO_2(THF)(H_2L)]$**, an unknown diamagnetic compound, and a trace of the desired complex

[(Me$_3$SiO)UO(THF)(ZnI)$_2$(L)]. This reaction was repeated several times and in some cases the ^{1}H NMR spectrum displayed resonances corresponding to the complex **[(THF)I$_2$ZnOUO(THF)Zn(THF)(HL)]** and other resonances of an unknown complex (Scheme 2).

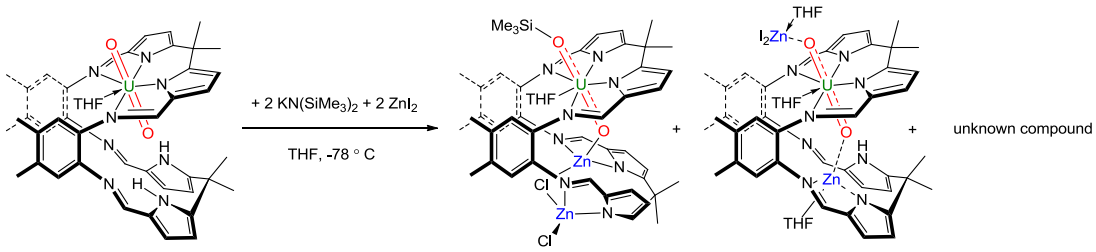

Scheme 2: Attempted synthesis of **[(Me$_3$SiO)UO(THF)(ZnCl)$_2$(L)]**

4.5. Attempted synthesis of [UO$_2$(S)(K$_2$L)] (s = THF or pyridine): reaction between [UO$_2$(S)(H$_2$L)] and two equivalents of KN(SiMe$_3$)$_2$

The reaction between one equivalent of **[UO$_2$(py)(H$_2$L)]** and two equivalents of KN(SiMe$_3$)$_2$ in pyridine at −40 °C is allowed to warm to room temperature over 24 h, and results in a dark red solution that affords the diamagnetic uranyl hydroxide **[UO$_2$(OHK)(KHL)]** as a brown solid after work-up, Scheme (**3**).

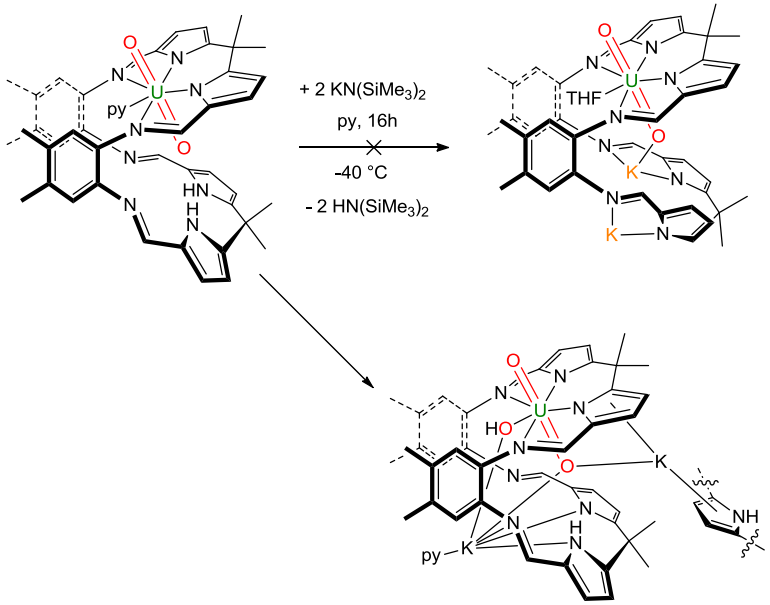

Scheme 3: Synthesis of **[UO$_2$(OHK)(KHL)]**

The compound was characterised by ^{1}H NMR spectroscopy and X-ray diffraction studies. The ^{1}H NMR spectrum displays resonances between 13 and 0 ppm corresponding to a diamagnetic compound. The number of resonances and their integrations indicates a symmetric ligand arrangement of C_s symmetry. The resonance that at highest frequency 12.57 ppm could correspond to the OH and another resonance at 9.22 ppm integrating only for 1H which is likely to correspond to the single pyrrole NH.

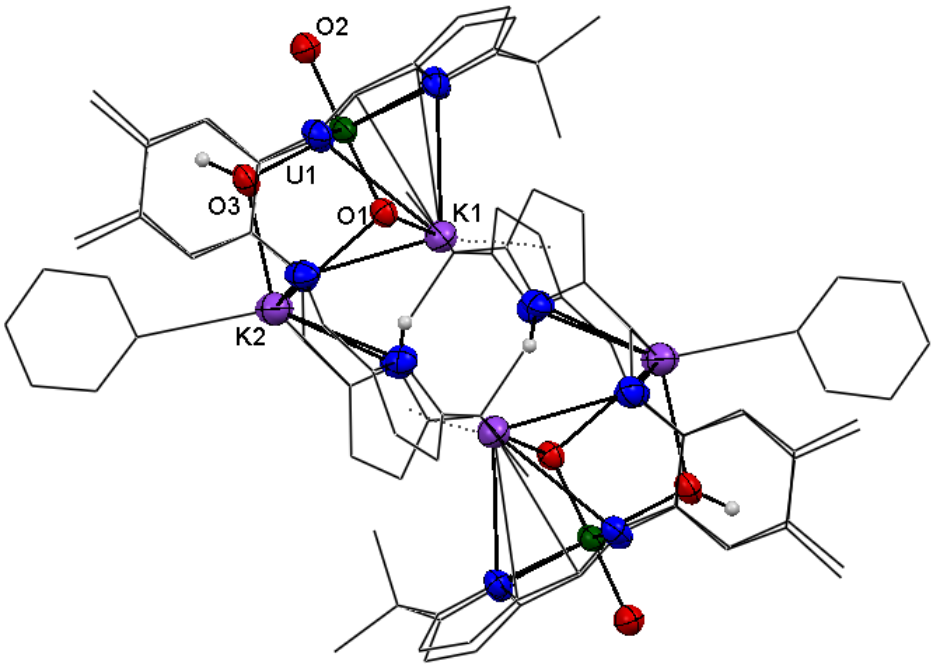

(a)

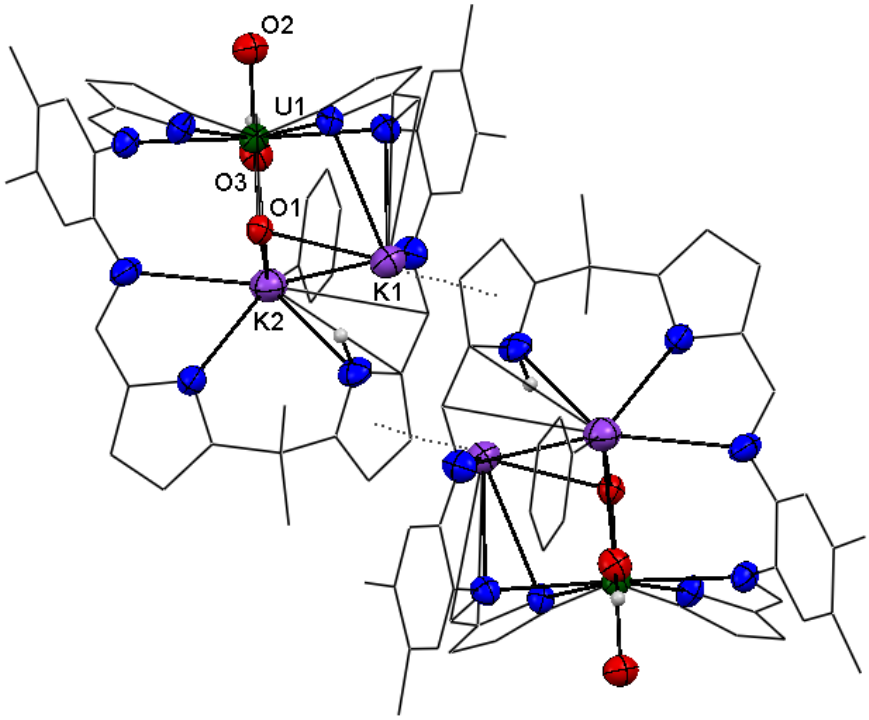

(b)

Figure 11: Solid state structure of **[UO_2(OHK)(KHL)]** showing side (a) and front view (b). For clarity, all hydrogen atoms except on the hydroxide oxygen and pyrrole nitrogen and lattice molecules of solvent are omitted (displacement ellipsoids drawn at 50% probability).

Table 4: Selected bond distances (Å) and angles (°) of **[UO_2(OHK)(KHL)]**

U1-O1	1.818(3)
U1-O2	1.773(3)
U1-O3	2.157(3)
N7···O1	3.447
O1-K1	2.743(3)
O3-K2	2.601(3)
O1-U1-O2	178.40(14)
U1-O1-K1	108.90(13)
U1-O3-K2	104.88(13)

Single crystals of **[UO_2(OHK)(KHL)]** suitable for X-ray diffraction studies were grown from a saturated by slow diffusion of hexane into pyridine. The uranium centre is seven coordinate and displays a distorted pentagonal bipyramidal geometry with the oxo groups *trans* (O1-U1-O2 178.40(14)°), and the equatorial sites occupied by four nitrogen atoms of the macrocycle and an oxygen atom from KOH that sits between the two macrocyclic aryl rings. From analysis of the uranium-oxygen bond lengths it appears that the uranium is in the 6+ oxidation state (Figure 11). The oxo group (U1-O1 1.818(3) Å and U1-O2 1.773(3) Å) bond distances are similar to the UO bond distances in the uranyl Pacman complex **[UO_2(THF)(H_2L)]** (U1-O1 1.787(3) and U1-O2 1.770(3) Å) and in the range of the $[UO_2]^{2+}$ (Table 4).[6,9,18]

4.6. Synthesis and characterisation of [{UO_2(OH)K(C_6H_6)(H_2L)}$_2$]

The reaction between one equivalent of **[UO_2(THF)(H_2L)]** and one equivalent of dry KOH (from the reaction between one equivalent of potassium and 0.99 equivalent of water in toluene) at room temperature for 16 h in THF results in a colour change of the solution from dark brown to red. The volatiles were removed and the resulting solid was recrystallised from benzene to obtain the uranyl

hydroxide **[{UO_2(OH)K(C_6H_6)(H_2L)}$_2$]** as orange block crystals in moderate yield (25 %), Equation (**9**).

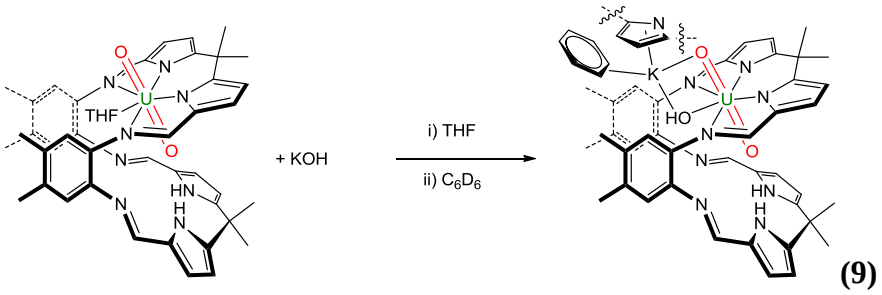

(9)

The complex was fully characterised, including by ^{1}H NMR and FTIR spectroscopy, elemental analysis, and X-ray diffraction studies.

The ^{1}H NMR spectrum supports the presence of a diamagnetic compound; the resonances are assignable and are consistent with the retention of a wedged, Pacman structure in solution of C_s symmetry. The spectrum displays a resonance at 9.96 ppm integrating for 1H and corresponds to the OH group, and the resonances for the core of the macrocycle are shifted in the same area than the resonances in the starting material **[UO_2(THF)(H_2L)]**. Elemental analysis supports its formulation.

The FTIR spectrum shows two broad bands at 3626 cm^{-1} and 3329 cm^{-1} corresponding to the OH and the pyrrole NH stretches respectively. The U=O stretch is slightly shifted from that of the precursor to 895 cm^{-1} (ν_{UO} = 908 cm^{-1} in **[UO_2(THF)(H_2L)]**).

Single crystals were grown form a C_6D_6 saturated solution and were suitable for X-ray diffraction studies.

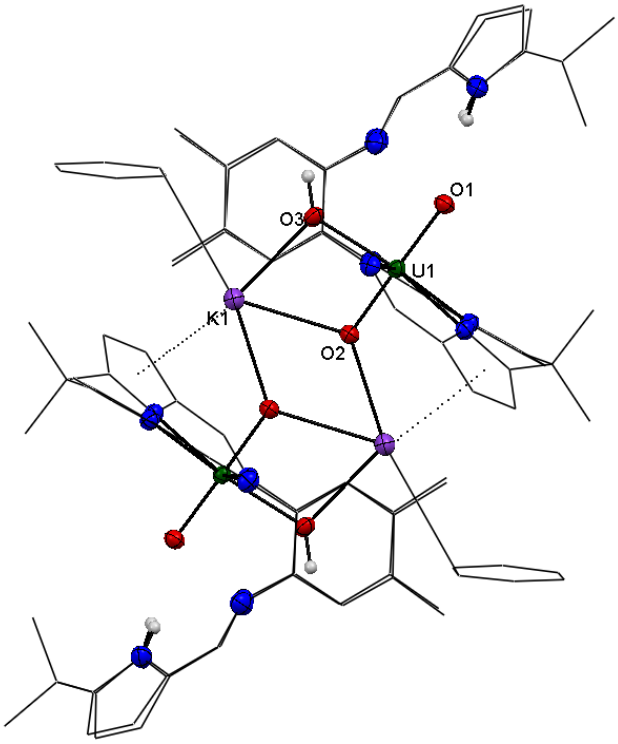

(a)

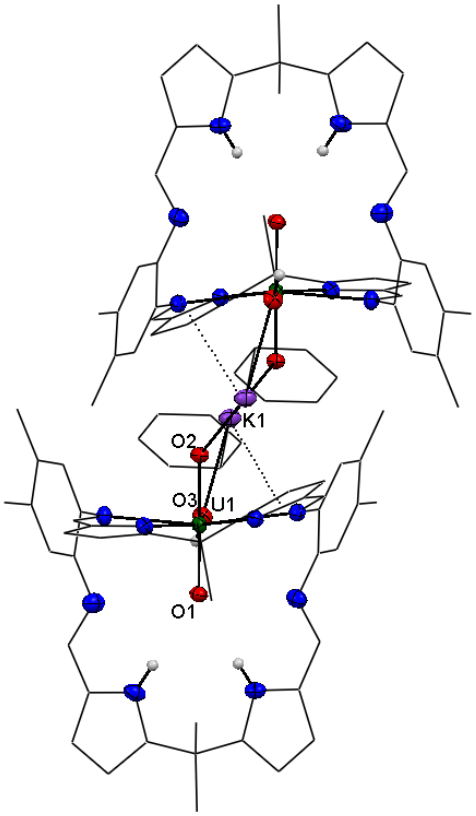

(b)

Figure 12: Solid state of **[{UO_2(OH)K(C_6H_6)(H_2L)}$_2$]**. For clarity the hydrogen atoms, except the pyrrole hydrogen atom and the hydroxyl hydrogen, and lattice molecules of solvent are omitted (displacement ellipsoids drawn at 50% probability).

The solid state X-ray diffraction structure shows a dimeric potassium oxide adduct. The presence of KOH in **[{UO_2(OH)K(η^2-C_6H_6)(H_2L)}$_2$]** does not disrupt the general Pacman structural motif, and the uranyl fragment remains coordinated in one half of the macrocycle by four nitrogen atoms (U1-N1 2.532(2), U1-N2 2.476(2), U1-N3 2.505(2), U1-N4 2.604(2) Å) at standard distances (Figure 12). The uranium-oxo bond distances (U1-O1 1.7956(16) and U1-O2 1.8027(16) Å) are longer than those reported for **[UO_2(THF)(H_2L)]** although they still support a 6+ oxidation state of the uranyl dication. The pentagonal bipyramidal coordination sphere of the uranium metal centre is completed in the equatorial plane by a hydroxo ligand (U1-O3 2.1862(18) Å), which resides in the fifth equatorial site usually occupied by a molecule of solvent (THF or pyridine), in-between the macrocyclic aryl rings. The potassium is sitting outside of the macrocycle and interacts with the *exo*-oxo group and one pyrrole of another Pacman core. The structure is different to the structure of the complex **[UO_2(OHK)(KHL)]** by the number and the position of the potassium cation, indeed the potassium is coordinated to the hydroxyl ligand in the fifth equatorial site but in the case of the complex **[UO_2(OHK)(KHL)]** the potassium is sitting in the cleft of the Pacman core. These two complexes have similarity by the UO bond distances which are in the same range (1.818(3) and 1.773(3) Å) as well as the U1-O3 bond distance (2.157(3) Å).

4.7. Metallation reactions of di- and tri-lithiated complexes

4.7.1. Reaction between [(py)$_3$LiOUO(py)Li(py)(HL)] and one equivalent of ZnI_2; synthesis and characterisation of [IZn(py)$_2$OUO(py)(H_2L)]

The one pot reaction between one equivalent of **[(py)$_3$LiOUO(py)Li(py)(HL)]** and one equivalent of ZnI_2 at room temperature for 2 h in pyridine results in the formation of the complex **[IZn(py)$_2$OUO(py)(H_2L)]** as a yellow brown solid in good yield (75%), Equation (**10**).

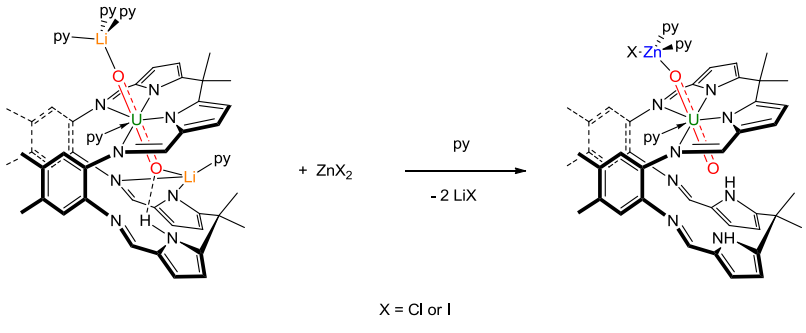

(10)

The compound was fully characterised, including by ^{1}H NMR spectroscopy, FTIR spectroscopy and by X-ray diffraction studies. The ^{1}H NMR displays a new paramagnetic compound between 76 and −6 ppm. The number of resonances and their integrations are consistent with the retention of a wedged, Pacman structure in solution of C_s symmetry (Figure 13). The most paramagnetically shifted resonance at 75.11 ppm integrates for 2H and corresponds to the two pyrrole NH. Two resonances at 0.43, and 1.83 ppm, integrating for 6H each correspond to the methyl group on the aryl backbone.

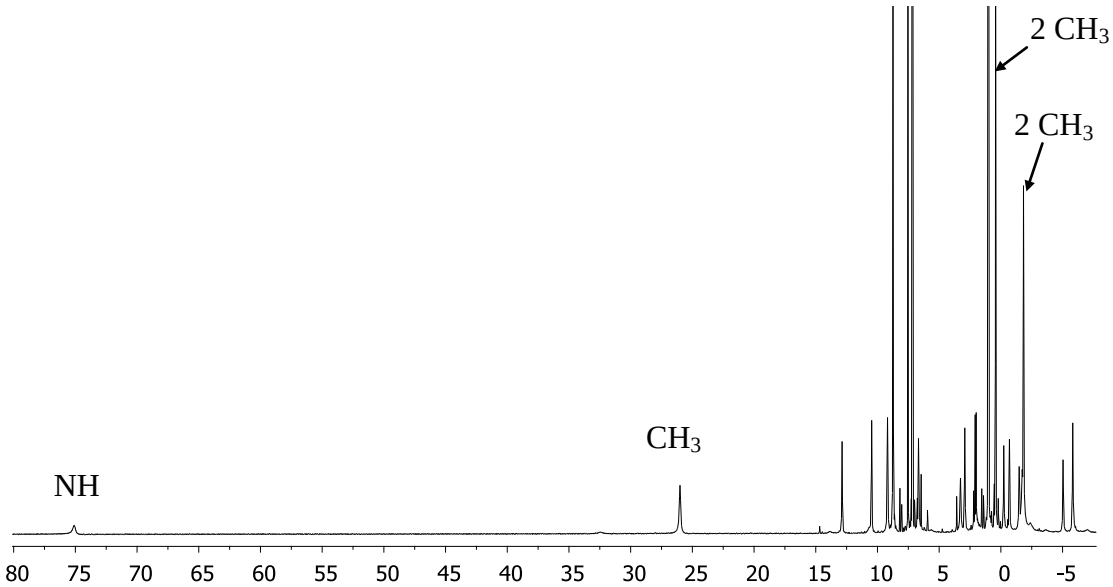

Figure 13: ^{1}H NMR spectrum of **[IZn(py)$_2$OUO(py)(H$_2$L)]** in d_5-pyridine

The FTIR spectrum contains a broad absorption at 3366 cm^{-1} corresponding to the pyrrole NH stretch. Two bands at 872 and 702 cm^{-1} correspond to the UO stretches which are weakened in comparison to the UO band in the starting material

[UO_2(THF)(H_2L)] (ν_{UO} = 908 cm^{-1}) and are in the same range than those observed in the different singly reduced $[UO_2]^+$ complexes.[6,8,17]

Single crystals of **[IZn(py)$_2$OUO(py)(H_2L)]** suitable for X-ray diffraction studies were grown from a saturated solution of pyridine (Figure 14).

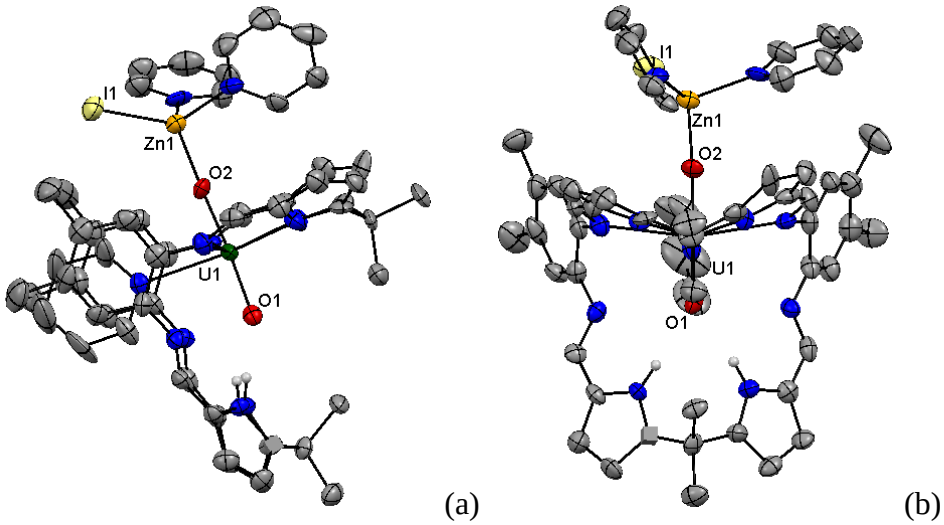

Figure 14: Solid state structure of **[IZn(py)$_2$OUO(py)(H_2L)]** showing side (a) and front view (b). For clarity the hydrogen atoms, except the pyrrole hydrogen atoms, and lattice molecules of solvent are omitted (displacement ellipsoids drawn at 50% probability).

Table 5: Selected bond distances (Å) and angles (°) of **[IZn(py)$_2$OUO(py)(H_2L)]**

U1-O1	1.847(10)
U1-O2	1.905(9)
U1-N9	2.607(12)
O2-Zn1	1.919(10)
O1···N6	2.995
O1···N7	2.909
O1-U1-O2	176.5(4)
Zn1-O2-U1	176.4(7)

The uranium centre is seven coordinate and displays a distorted pentagonal bipyramidal geometry with the oxo groups in a *trans*-arrangement (O1-U1-O2 176.5(4)°). The equatorial uranium sites are occupied by the nitrogen atoms of the macrocycle and nitrogen atom from a molecule of pyridine occupies the fifth equatorial site and sits between the two macrocyclic aryl rings. From analysis of the uranium-oxygen bond lengths it is evident that the uranyl fragment is in the 5+ oxidation state. The *endo*-oxo group bond distance (U1-O1 1.847(10) Å) is significantly elongated compared to the bond distance of $[UO_2]^{2+}$ in **$[UO_2(py)(H_2L)]$** (U1-O1 1.7779(18) Å) and is similar to experimental and calculated bond distances for $[UO_2]^{+}$ (range 1.811- 1.934 Å) (Table 5).[11,12] The *exo*-oxo bond distance is also longer than in **$[UO_2(py)(H_2L)]$** (U1-O2 1.905(9) Å / U1-O2 1.7546(19) Å respectively). The zinc atom is four coordinate and displays a tetrahedral geometry, and is coordinated to two molecules of pyridine, one iodide atom, and the *exo*-oxo group (Zn1-O2 1.919(10) Å). The other N4-donor compartment stays vacant and is oriented such that hydrogen bonds are evident between the pyrrole NH and the *endo*-oxo group; the N···O separations are shorter than in the analogous U^{VI} complex (N···O 2.995 / 3.172 Å respectively). The distance U1-N9 is slightly elongated than in the analogous U^{VI} complex (2.607(12) / 2.583(2) Å).

4.7.2. Reaction of $[(py)_3LiOUO(py)\{Li(py)\}_2(L)]$ with three equivalents of ZnI_2

The one-pot reaction between one equivalent of **$[(py)_3LiOUO(py)\{Li(py)\}_2(L)]$** and three equivalents of ZnI_2 in pyridine at room temperature in a Teflon-tapped NMR tube for 16 h results in a red solution. A few days later red block single crystals were grown from a saturated solution of d_5-pyridine at −35 °C, Equation (**11**).

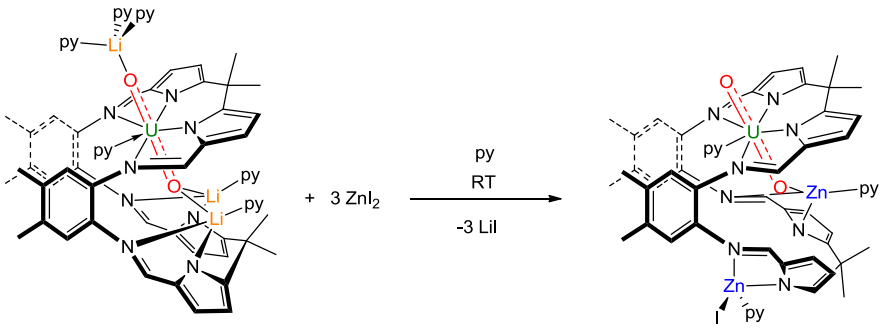

(11)

The complex was characterised by ^{1}H NMR, FTIR spectroscopy and an X-ray diffraction study. The formation of a new paramagnetic compound was observed in the ^{1}H NMR spectrum with a series of resonances between 30 and −7 ppm. These resonances were not assignable to specific proton environments but the number of resonances and their integrals are consistent with the retention of a wedged, Pacman structure in solution of C_1 symmetry.

The FTIR spectrum contains no broad band corresponding to the pyrrole NH (at 3373 cm^{-1} in the starting material **[UO$_2$(THF)(H$_2$L)]**). Two stretches corresponding to the U=O are observed at 876 cm^{-1} and 803 cm^{-1} and these stretches are weakened substantially compared to that in the U^{VI} starting material **[UO$_2$(THF)(H$_2$L)]** (ν U=O 908 cm^{-1}) and in the range of U=O stretches for [UO$_2$]$^{+}$.[6,8]

Crystals of **[UO$_2$(py)Zn(py)ZnI(py)(L)]** suitable for single crystal X-ray diffraction analysis were grown from a saturated pyridine solution (Figure 15).

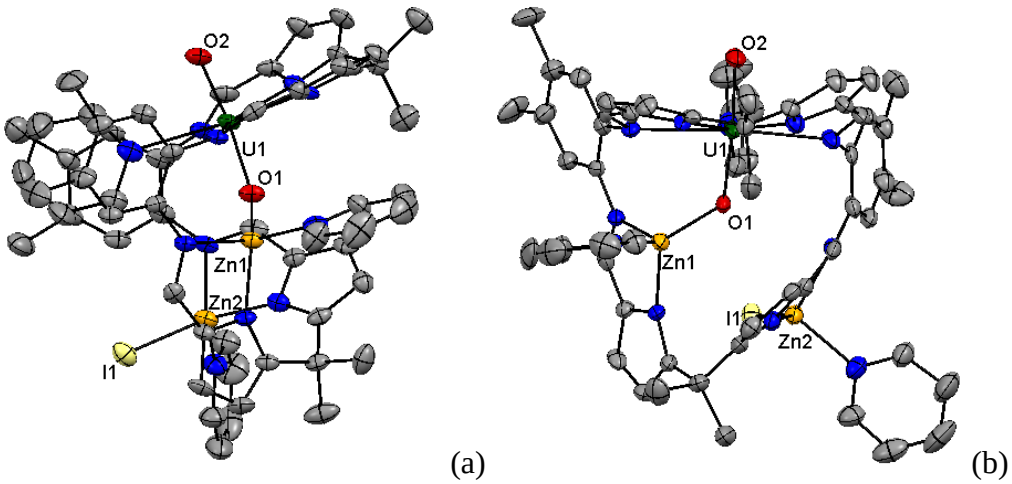

Figure 15: Solid state structure of **[UO_2(py)Zn(py)ZnI(py)(L)]** showing side (a) and front (b) view. For clarity, all the hydrogen atoms and lattice molecules of solvent are omitted (displacement ellipsoids drawn at 50% probability).

Table 6: Selected bond distances (Å) and angles (°) of **[UO_2(py)Zn(py)ZnI(py)(L)]**

U1-O1	1.919(4)
U1-O2	1.840(4)
U1-N9	2.629(5)
O1-Zn1	1.913(3)
O1-U1-O2	171.85(16)
Zn1-O1-U1	102.65(13)

The Pacman structural motif seen in the complex **[UO_2(py)(H_2L)]** remains intact with one compartment occupied by the uranyl moiety and the other N_4 compartment is occupied by two tetrahedral Zn atoms, each coordinated to one N atom from the pyrrole, which causes a distortion of the compartment by the flip of one of the pyrrole-imine units, desymmetrising the ligand. One Zn atom (Zn1) is coordinated to the *endo*-oxo group, the imine nitrogen, the pyrrole nitrogen and the nitrogen of a molecule of pyridine; the second Zn atom (Zn2) is coordinated to an iodide atom, the pyrrole nitrogen, the imine nitrogen and the nitrogen of a molecule of pyridine. The uranium centre is seven coordinate and displays a distorted pentagonal bipyramidal geometry with the oxo groups retaining a *trans* arrangement

(O1-U1-O2 171.85(16)°), the equatorial sites occupied by the nitrogen atoms of the macrocycle, and an nitrogen atom from a molecule of pyridine in the fifth equatorial site, sitting between the two macrocyclic aryl rings (Table 6). From analysis of the uranium-oxygen bond lengths it is evident that the uranyl fragment is in the 5+ oxidation state. The *endo*-oxo group bond distance (U1-O1 1.919(4) Å) is elongated significantly compared to the bond distance of $[UO_2]^{2+}$ in **$[UO_2(py)(H_2L)]$** (U1-O1 1.7779(18) Å) and is similar to experimental and calculated bond distances for $[UO_2]^{+}$ (range 1.811- 1.934 Å).[11,12] The *exo*-oxo bond distance is also longer than in **$[UO_2(py)(H_2L)]$** (U1-O2 1.840(4) Å / 1.7546(9) Å respectively). The UO bond distances are in the same range of these in the complex **$[(Me_3SiO)UO(THF)(ZnCl)_2(L)]$**, the Zn1-O1 bond distance are also very similar (1.913(3) Å / 1.958(4) Å respectively).

4.8. Discussion

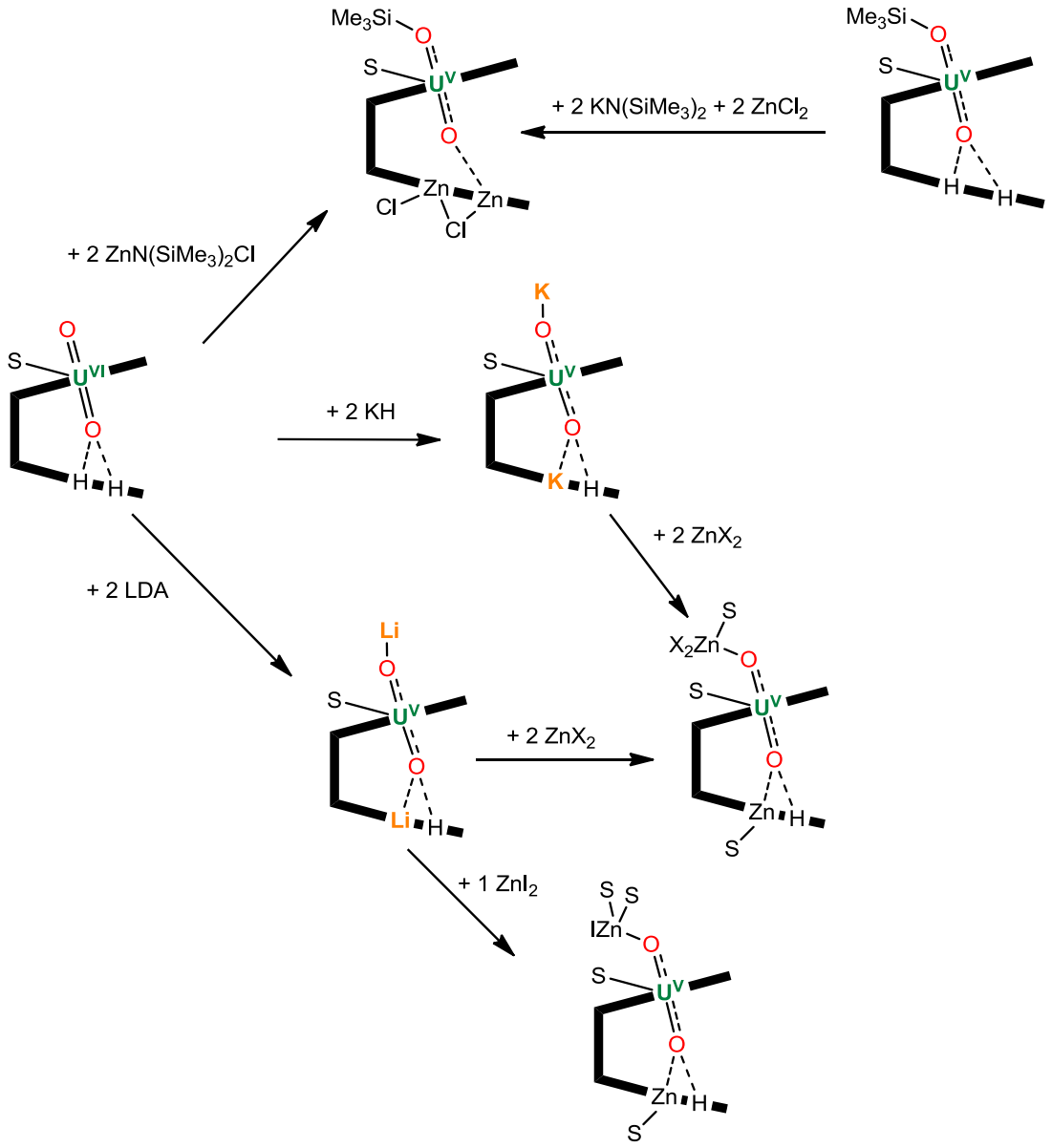

Scheme 4: Synthetic procedures to produce paramagnetic uranyl Pacman complexes

It has been shown by Arnold, Love and co-workers in Nature in 2008, that the formation of the complex **[(Me$_3$SiO)UO(py)(ZnCl)$_2$(L)]** can be carried out using the reaction between one equivalent of **[UO$_2$(THF)(H$_2$L)]**, two equivalents of KN(SiMe$_3$)$_2$ and two equivalents of ZnCl$_2$, where the proposed mechanism is the double deprotonation of the uranyl Pacman complex **[UO$_2$(THF)(H$_2$L)]** by two equivalents of KN(SiMe$_3$)$_2$ then addition of two equivalents of ZnCl$_2$ to form the complex **[(Me$_3$SiO)UO(py)(ZnCl)$_2$(L)]**.[5] This route has some difficulties to be

reproduced; the attempted synthesis of this complex via the route described earlier is not conclusive. Indeed, the reaction between the uranyl Pacman complex with two equivalents of $KN(SiMe_3)_2$ then addition of two equivalents of $ZnCl_2$ was monitored by ^1H NMR spectroscopy. The ^1H NMR spectrum was seen to contain a small amount of paramagnetically shifted resonances corresponding to the complex **[(Me$_3$SiO)UO(THF)(ZnCl)$_2$(L)]** and another unknown diamagnetic complex. Because of this small amount of the complex **[(Me$_3$SiO)UO(THF)(ZnCl)$_2$(L)]** it was decided to try the reaction between one equivalent of $ZnCl_2$ and one equivalent of $[Zn\{N(SiMe_3)_2\}_2]$ to form an equilibrium and afford the compound mixed ligand **[Zn{N(SiMe$_3$)$_2$}Cl]**. In the route described earlier in this chapter, the ^1H NMR spectrum, the FTIR spectrum, and the X-ray studies confirm the formation of the complex **[(Me$_3$SiO)UO(py)(ZnCl)$_2$(L)]** by the reaction of one equivalent of the uranyl Pacman complex **[UO$_2$(THF)(H$_2$L)]** and two equivalents of **[Zn{N(SiMe$_3$)$_2$}Cl]**. The different ^1H NMR spectra seen using these different routes could explain the possible mechanism of this reaction. The first step is probably the deprotonation of one pyrrole NH in the vacant compartment by one equivalent of **[Zn{N(SiMe$_3$)$_2$}Cl]** (Figure 2) forming the uranyl Pacman complex **[UO$_2$(THF)(ZnCl)(HL)]** in the 6+ oxidation state that is insoluble in toluene and one equivalent of $HN(SiMe_3)_2$ (Scheme 5). It is therefore likely that an adduct between the zinc cation and the uranyl *endo*-oxo group is formed and that this results in a shift of the reduction potential of the uranyl, as seen by Hayton and co-workers and in the lithium chemistry described in Chapter 2.[17,19] The enhanced Lewis basicity of the exo-oxo group should enable the second molecule of **[Zn{N(SiMe$_3$)$_2$}Cl]** to coordinate, resulting in the second step involving reductive silylation, forming the uranyl(V) Pacman complex **[(Me$_3$SiO)UO(THF)(ZnCl)(HL)]** and a radical $[Zn\{N(SiMe_3)\}Cl]^{\bullet}$. This radical can react with the other pyrrole NH forming the desired complex and the radical $[HNSiMe_3]^{\bullet}$, which can then react with a molecule of solvent to give $[H_2NSiMe_3]$, this compound is very instable and is not isolable.[20]

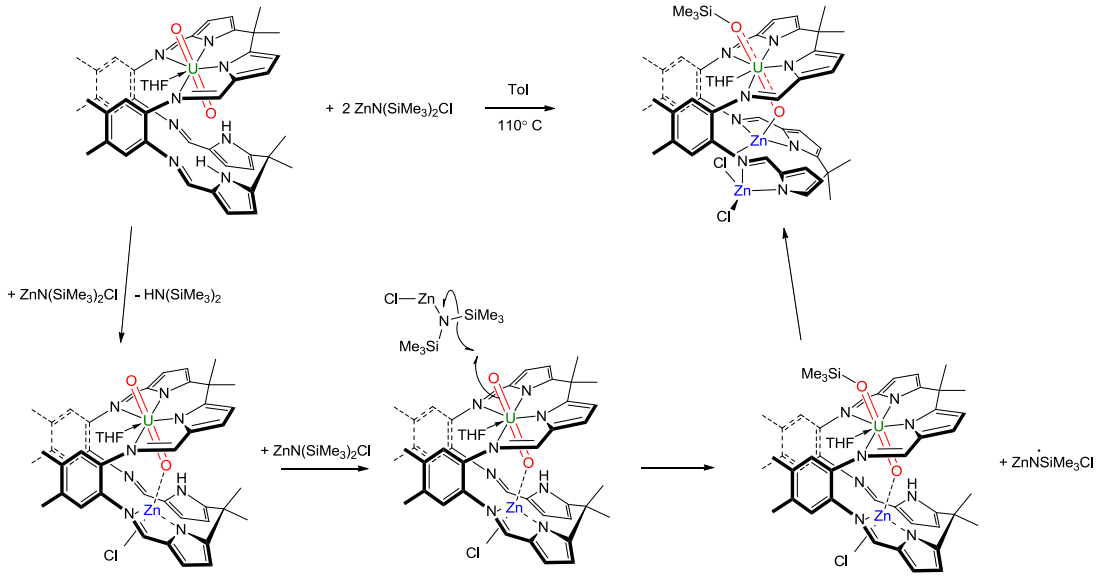

Scheme 5: Proposed mechanism for the synthesis of the complex **[(Me$_3$SiO)UO(THF)(ZnCl)$_2$(L)].**

The FTIR spectrum of **[(Me$_3$SiO)UO(THF)(ZnCl)$_2$(L)]** shows no broad band corresponding to the pyrrole NH at 3373 cm^{-1} in the starting material **[UO$_2$(THF)(H$_2$L)]**. This absence proves that the two pyrrole NH have been deprotonated. The shift of the UO stretch was seen and are displayed at 841 and 770 cm^{-1} which are in the range of the $[UO_2]^+$ stretches of the doubly silylated complex [U(OSiMe$_3$)$_2$I$_2$(^{Ar}acnac)] presented by Hayton and co-workers (ν_{UO} 847 and 770 cm^{-1}) (Figure 16).[7]

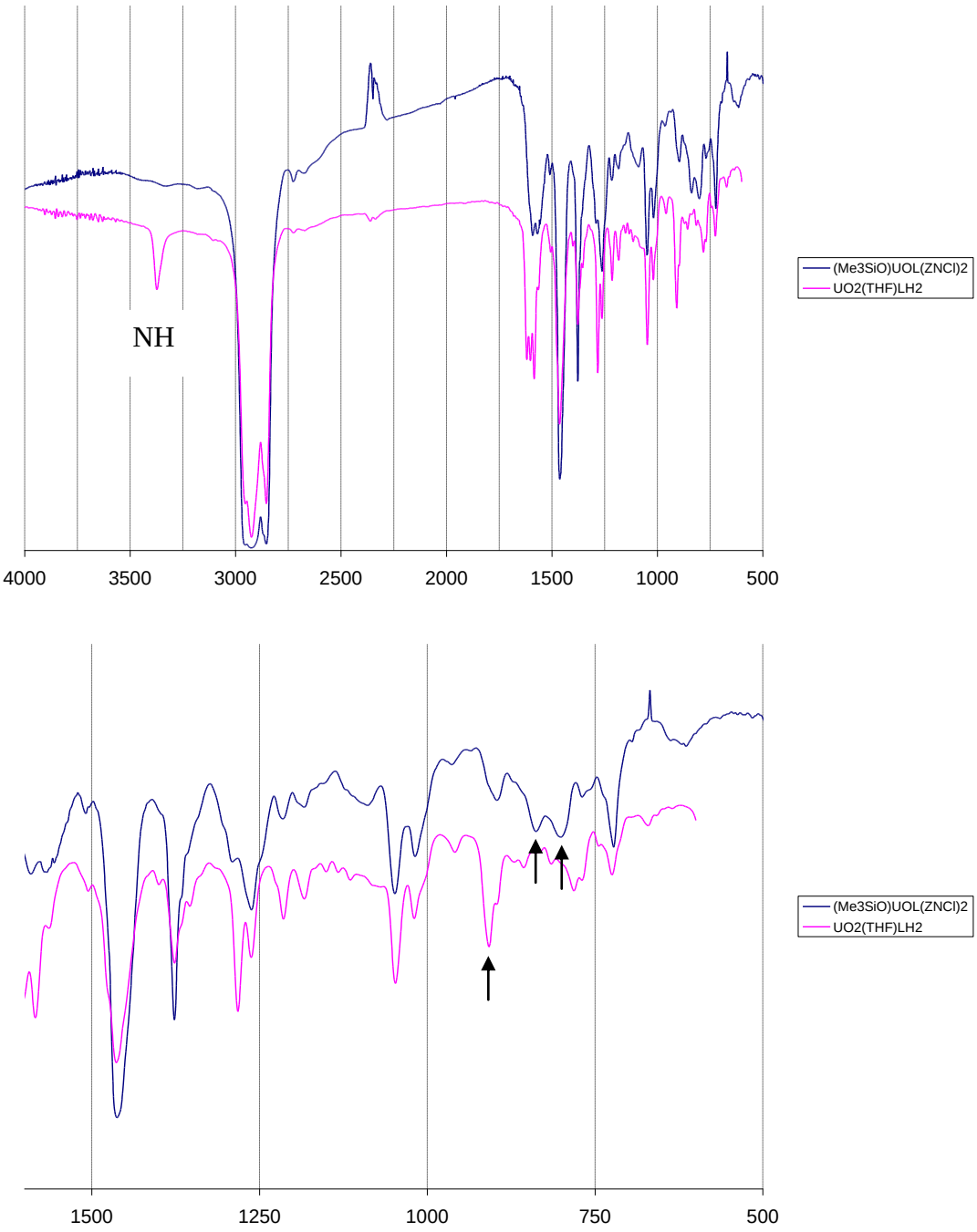

Figure 16: FTIR spectra of **$[UO_2(THF)(H_2L)]$** (pink), **$[(Me_3SiO)UO(py)(ZnCl)_2(L)]$** (blue). Arrows indicate v(U=O).

We could suggest that the presence of the chloride in the complex **$[Zn\{N(SiMe_3)_2\}Cl]$** can play a determinant role in this chemistry. We know that the reaction between one equivalent of **$[UO_2(THF)(H_2L)]$** and one equivalent of $M\{N(SiMe_3)_2\}_2$ results in the double deprotonation of the pyrrole NH and leads to

the formation of the uranyl (VI) Pacman complex **[UO_2(THF)M(L)]**. Unpublished work shows that the reaction between one equivalent of **[UO_2(THF)(H_2L)]** and two equivalents of M{$N(SiMe_3)_2$}$_2$ (M = Zn, Mn) results in the formation of a uranyl complex in the 5+ oxidation state without silylation of the oxo group.[18] The first step is the double deprotonation of the vacant compartment by the one equivalent of M{$N(SiMe_3)_2$}$_2$ as described above (Scheme 6).

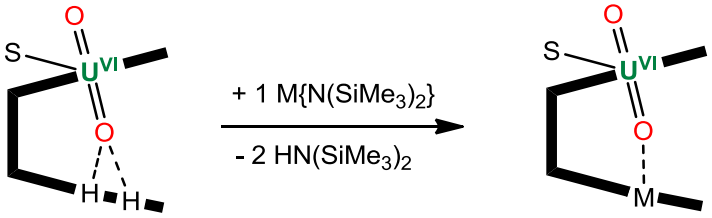

Scheme 6: Metallation and formation of the M-OU adduct

The metal atom is sitting in the middle of the pocket and the uranium centre is in the same oxidation state. As above, the disruption in the uranyl bonding caused by the presence of this Zn-yl interaction allows the second molecule of M{$N(SiMe_3)_2$}$_2$ to react with the *exo*-oxo group via reduction so leading to the formation of [({Me_3Si}$_2$NZnO)UO(S)(ZnL)] and the radical [$N(SiMe_3)_2$]$^{\bullet}$ which can react with a molecule of solvent to give [$HN(SiMe_3)_2$] (Scheme 7).

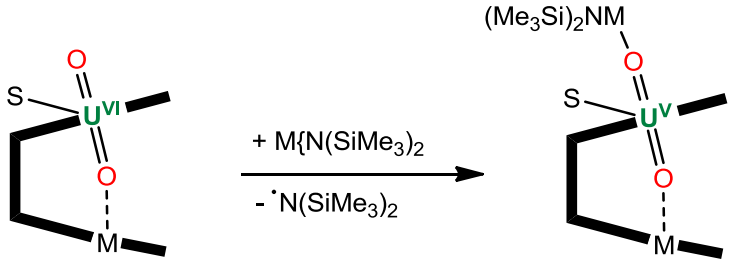

Scheme 7: Second metallation and reduction

We have also found that the reaction of **[UO_2(THF)(H_2L)]** with an excess of **[Zn{$N(SiMe_3)_2$}Cl]** (more than two equivalents) leads to the formation of free ligand and the butterfly compound **[(Me_3SiOUO)$_2$(L)]** described by Arnold, Love and co-

workers (Figure 17). In our discussion, the butterfly complex is only characterised by ^{1}H NMR spectroscopy and this reaction needs further experiments to determine the possible mechanism.[21]

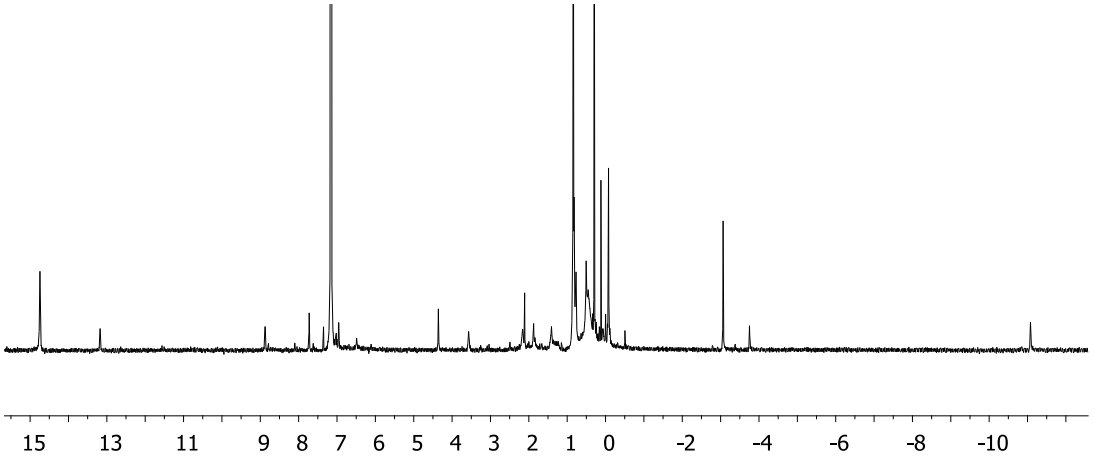

Figure 17: ^{1}H NMR of the butterfly complex **[(Me$_3$SiOUO)$_2$(L)]**

Alternatively, the complex **[(Me$_3$SiO)UO(py)(ZnCl)$_2$(L)]** can also be made by the reaction between one equivalent of **[(Me$_3$SiO)UO(py)(H$_2$L)]** and two equivalents of KN(SiMe$_3$)$_2$ followed by, after 24 h, the addition of two equivalents of ZnCl$_2$. In this case, the uranyl moiety is already silylated and at the reduced, 5+ oxidation state, and the reaction is only a deprotonation of the pyrrole NH by the base KN(SiMe$_3$)$_2$ and the exchange between the K cation and ZnCl$_2$. The oxidation state is retained.

These reactions to form the complex **[(Me$_3$SiO)UO(S)(ZnCl)$_2$(L)]** are in contrast with chemical analogues from the same group as uranium. Indeed, treatment of the molybdenum and the tungsten *cis*-dioxo complexes [M^{VI}O$_2$(1,2-S$_2$C$_6$H$_4$)$_2$] with chlorosilane affords [M^{VI}O(OSiR$_3$)(1,2-S$_2$C$_6$H$_4$)$_2$] in which the silylation of one of the oxo groups occurs without redox reactions, Equation (**12**).[22]

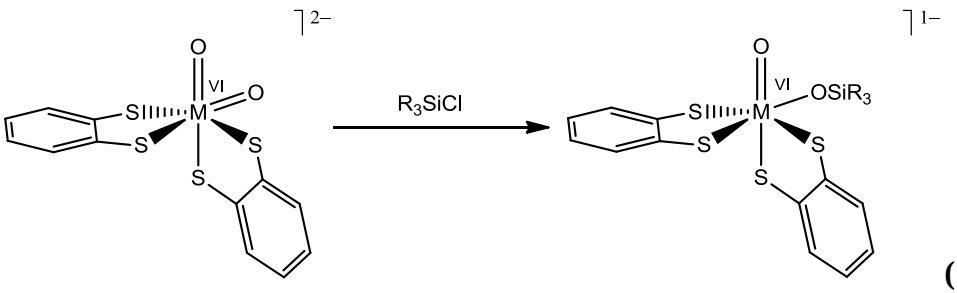

(12)

In the case of the uranyl dication, the silylation seems to occur with redox reaction as seen before in this discussion. Reductive silylation of the uranyl has been described by Arnold, Love and co-workers, and also by Hayton and co-workers.[5,23] Hayton and co-workers have shown that the silylation of the uranyl oxo ligands is concomitant with the reduction of the uranium centre to uranium (V) and requires Lewis acid activation, in this case borane-mediated silylation of $[UO_2(^{Ar}acnac)_2]$. They showed that the reaction between $[UO_2(^{Ar}acnac)_2]$ with only silane did not afford the expected complex, which demonstrated the need for borane to silylate the complex and implies that the silane alone is not reducing enough to effect silylation, Equation (**13**).

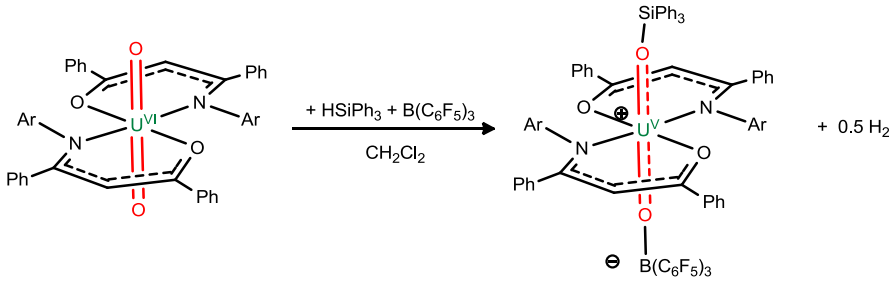

(13)

We have attempted to discover the intermediate step to the formation of **$[(Me_3SiO)UO(py)(ZnCl)_2(L)]$** in the reaction with the potassium base and metal halide. So, the reaction between **$[UO_2(THF)(H_2L)]$** and two equivalents of $KN(SiMe_3)_2$ was carried out and does not lead to the formation of the dipotassiated uranyl Pacman complex **$[UO_2(THF)(K_2L)]$** in the 6+ oxidation state but instead forms the uranyl complex **$[UO_2(OHK)(KHL)]$** (Scheme 8). The formation of this complex is supported by ^1H NMR spectroscopy, IR spectroscopy and X-ray diffraction studies. This complex could be a decomposition product of the proposed

complex because of its instability. We also described different reactivity when using KH. Indeed the reaction between one equivalent of **[UO_2(THF)(H_2L)]** and two equivalents of KH at −78 °C, after being allowed to warm to room temperature leads, after work-up to the formation of the hydroxyl complex **[{UO_2(OH)K(C_6H_6)(H_2L)}$_2$]**. In contrast, the same reaction at + 78 °C for 2 h leads to the uranyl Pacman complex **[(THF)$_3$KOUO(THF)K(THF)(HL)]**, a complex similar to the dilithiated uranyl Pacman complex **[(py)$_3$LiOUO(py)Li(py)(HL)]**.[9] The complex **[{UO_2(OH)K(C_6H_6)(H_2L)}$_2$]** can also be obtained by addition of dry KOH to the precursor uranyl Pacman complex.

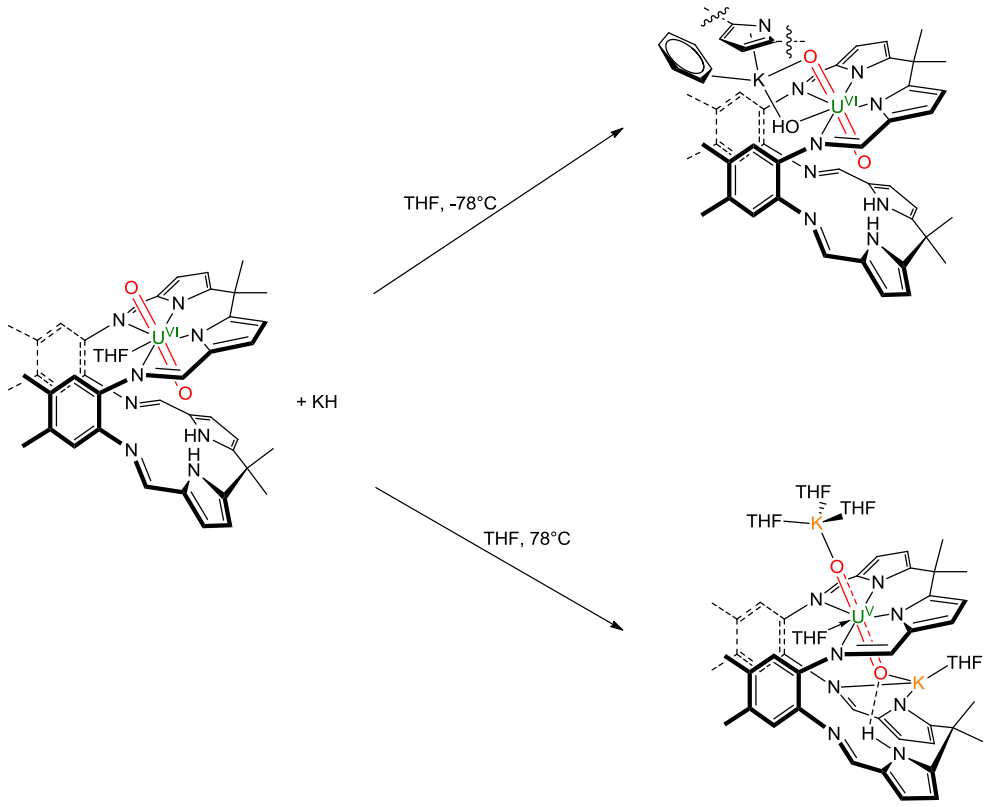

Scheme 8: Different reactivity of KH

Other routes have been tried to silylate the oxo group. The reaction between the dilithiated complex **[(py)$_3$LiOUO(py)Li(py)(HL)]** and two equivalents of ZnX_2 (X = Cl, I) in the presence of a source of silyl group such as $N(SiMe_3)_3$ and $HN(SiMe_3)_2$ leads only to the formation of the paramagnetic uranyl Pacman complexes **[(py)X_2ZnOUO(py)Zn(py)(HL)]**. The same reaction has been attempted in absence of silyl source and leads to the same complex showing that the silyl

source does not play a role in this reaction. The complexes are similar to the dilithiated complex **[(py)$_3$LiOUO(py)Li(py)(HL)]** by their ^{1}H NMR and IR spectra, and their X-ray structure are similar with the UO bond lengths in the same range.[17] The reaction between the dipotassiated complex **[(THF)$_3$KOUO(THF)K(THF)(HL)]** and two equivalents of ZnI_2 leads to the formation of the same complex **[(S)X$_2$ZnOUO(S)Zn(S)(HL)]** (S = THF, pyridine).

The reaction between the dilithiated complex and one equivalent of ZnI_2 leads to the formation of **[IZn(py)$_2$OUO(py)(H$_2$L)]** which has been characterised by ^{1}H NMR spectroscopy and X-ray diffraction studies. In this complex, the functionalisation is only at the *exo*-oxo group and the lower N4 compartment of the Pacman ligand is free, this structure is similar to the complexes **[(R$_2$R'SiO)UO(py)(H$_2$L)]**, so reaction could occur in the empty compartment.[16] Another reaction between the trilithiated complex **[(py)$_3$LiOUO(py){Li(py)}$_2$(L)]** and three equivalents of ZnI_2 leads to the formation of **[UO$_2$(py)Zn(py)ZnI(py)(L)]**. The complex is fully characterised; the *endo*-oxo group is functionalised and because of the presence of two zinc atoms in the lower compartment, a flipping of one of the pyrrole-imine chelates out of the usual N_4-donor plane is observed as seen in the complex **[(Me$_3$SiO)UO(py)(ZnCl)$_2$(L)]**.[5]

4.9. Conclusions

In conclusion, we have shown different ways to reduce and functionalise the oxo groups. On one hand we have found two routes to synthesise the oxo-silylated complexes **[(Me$_3$SiO)UO(S)(MX)$_2$(L)]** in good yield. On another hand, we have attempted to silylate the uranyl Pacman complex **[(py)$_3$LiOUO(py)Li(py)(HL)]** by addition of a silane source and in presence of transition metal without any success. We also show that the proposed intermediate step in the synthesis of **[(Me$_3$SiO)UO(S)(MX)$_2$(L)]**, published in Nature, is maybe not the dipotassiated uranyl Pacman complex due to the difficulties to reproduce the reaction and to isolate the complex. In this chapter, it is possible that a different mechanism operates and involves uranyl oxo group activation by metallation and U-OM bond formation make the oxo-bond more Lewis basic, allowing coordination of the second **[ZnCl{N(SiMe$_3$)$_2$}]**. The reduction potential is probably shifted to a more positive

potential and facilitates the homolytic N-Si bond cleavage and reductive silylation. Alternatively, homolytic M-N bond cleavage can occur to form reduced and metallated uranyl.

4.10. References

(1) Mayer, J. M. *Acc. Chem. Res.* **1998**, *31*, 441.
(2) Kühn, F. E.; Santos, A. M.; Abrantes, M. *Chem. Rev.* **2006**, *106*, 2455.
(3) Nam, W. *Acc. Chem. Res.* **2007**, *40*, 522.
(4) Jin, N.; Ibrahim, M.; Spiro, T. G.; Groves, J. T. *J. Am. Chem. Soc.* **2007**, *129*, 12416.
(5) Arnold, P. L.; Patel, D.; Wilson, C.; Love, J. B. *Nature* **2008**, *451*, 315.
(6) Arnold, P. L.; Love, J. B.; Patel, D. *Coord. Chem. Rev.* **2009**, *253*, 1973.
(7) Brown, J. L.; Wu, G.; Hayton, T. W. *J. Am. Chem. Soc.* **2010**, *132*, 7248.
(8) Berthet, J.-C.; Siffredi, G.; Thuery, P.; Ephritikhine, M. *Chem. Commun.* **2006**, 3184.
(9) Arnold, P. L.; Patel, D.; Pécharman, A.-F.; Wilson, C.; Love, J. B. *Dalton Trans.* **2010**, *39*, 3501.
(10) Zi, G.; Jia, L.; Werkema, E. L.; Walter, M. D.; Gottfriedsen, J. P.; Andersen, R. A. *Organometallics* **2005**, *24*, 4251.
(11) Hay, P. J.; Martin, R. L.; Schreckenbach, G. *J. Physic. Chem. A* **2000**, *104*, 6259.
(12) Wander, M. C. F.; Kerisit, S.; Rosso, K. M.; Schoonen, M. A. A. *J. Physic. Chem. A* **2006**, *110*, 9691.
(13) Cotton, F. A.; Marler, D. O.; Schwotzer, W. *Inorg. Chem.* **1984**, *23*, 4211.
(14) Money, J. K.; Folting, K.; Huffman, J. C.; Collison, D.; Temperley, J.; Mabbs, F. E.; Christou, G. *Inorg. Chem.* **1986**, *25*, 4583.
(15) Do, Y.; Simhon, E. D.; Holm, R. H. *Inorg. Chem.* **1985**, *24*, 1831.
(16) Arnold, P. L.; Pécharman, A.-F.; Love, J. B. *Angew. Chem., Int. Ed. Engl.* **2011**, *50*, 9456.
(17) Arnold, P. L.; Pécharman, A.-F.; Hollis, E.; Yahia, A.; Maron, L.; Parsons, S.; Love, J. B. *Nat Chem* **2010**, *2*, 1056.
(18) Arnold, P. L.; Patel, D.; Blake, A. J.; Wilson, C.; Love, J. B. *J. Am. Chem. Soc.* **2006**, *128*, 9610.
(19) Hayton, T. W.; Wu, G. *Inorg. Chem.* **2009**, *48*, 3065.
(20) Bordeau, M.; Frainnet, E.; Clement, C. *J. Organomet. Chem.* **1982**, *229*, 119.
(21) Arnold, P. L.; Jones, G. M.; Odoh, S. O.; Schreckenbach, G.; Magnani, N.; Love, J. B. *Nat Chem* **2012**, *4*, 221.
(22) Lorber, C.; Donahue, J. P.; Goddard, C. A.; Nordlander, E.; Holm, R. H. *J. Am. Chem. Soc.* **1998**, *120*, 8102.
(23) Schnaars, D. D.; Wu, G.; Hayton, T. W. *Inorg. Chem.* **2011**, *50*, 4695.

Chapter 5: General conclusions

The use of the polypyrrolic Schiff base ligand to complex the uranyl dication leads to the formation of the uranyl(VI) Pacman complex **$[UO_2(S)(H_2L)]$** in the 6+ oxidation state (S = THF, pyridine), in which the ligand promotes a hinged Pacman topology. These compounds and their distinct structures have been used to study the chemistry of the uranyl ion. Indeed, the uranyl ion is desymmetrised with one oxo group outside the macrocycle and one inside the cleft. It was observed that H bonding between the *endo* oxo group and the pyrrole NH occurred, causing an elongation in one U=O bond distance.

We have shown that the use of varying amounts of lithium reagents leads to the single-electron reduction and oxo functionalisation of the uranyl Pacman complex forming di-, tri- or tetralithiated complexes. This reduction is dependant on the lithium reagent and can proceed through two different mechanisms. The lithium reagents LDA, $LiNH_2$, $LiCPh_3$, LiH or LiC_5H_5 appear to act as reductants with the radical that is released being quenched by the ligand. For $LiN(SiMe_3)_2$, we can invoke hydrogen-atom abstraction by the uranyl Pacman complex, either directly at the oxo group, or indirectly by a pyrrolyl radical. Both of these mechanisms are reliant on the formation of Li adducts of $[UO_2]^{2+}$ which, in a similar manner to that described in the literature, causes a positive shift in the U^{VI}/U^{V} reduction couple. The formation of the dilithiated complex **$[(py)_3LiOUO(py)Li(py)(HL)]$** is in contrast with the silylation chemistry observed for the doubly potassiated uranyl macrocyclic analogue $[UO_2(S)(K_2L)]$ and suggests that the nature of the metals incorporated into the bottom pocket of the macrocycle are an important variable. These complexes should offer access to a wide range of new covalent bond-forming reactions of the uranyl oxo groups.

The dilithiated complex **$[(py)_3LiOUO(py)Li(py)(HL)]$** reacts with a Brønsted acid to form the unique uranyl(V) hydroxide **$[(HO)UO(py)(H_2L)]$** and could help to define uranyl ion exchange process. This complex can undergo silylation and leads to the formation of the silylated complex without the presence of transition metal in the second Pacman compartment, in contrast to that seen previously. We have shown that it is possible to carry out new OH and OSi bond

forming reactions from a uranyl complex in 5+ oxidation state without disproportionation, the reaction that would be expected for $[UO_2]^+$ complexes.

The **[(HO)UO(py)(H_2L)]** complex also reacts with chlorophosphine to lead to new complexes that, while needing further characterisation, suggest that O-atom abstraction is occurring. No reactions between the uranyl hydroxide and a carbon source such as methyltriflate, methyl iodide or benzylchloride were observed.

We have also tried to investigate the mechanism of formation of the complexes **[(Me_3SiO)UO(THF)(MX)$_2$(L)]** (M = Zn, Fe; X = Cl, I), but because of some difficulties in reproducing this chemistry, alternative routes were sought. Thus the reaction between the uranyl Pacman complex **[UO_2(THF)(H_2L)]** and two equivalents of **[Zn{N($SiMe_3$)$_2$}Cl]** led to the formation of the expected oxo-silylated complex. Another route was to exploit singly reduced silylated complex **[(Me_3SiO)UO(py)(H_2L)]** and react it with two equivalents of KN($SiMe_3$)$_2$ followed by the addition of two equivalents of $ZnCl_2$; this also led to the formation of the desired complex. We have also shown that the reaction between zinc halides and the dilithated complex **[(py)$_3$LiOUO(py)Li(py)(HL)]** form the new uranyl-zinc complexes **[(py)X_2ZnOUO(py)Zn(py)(HL)]** (X = Cl, I). Interestingly, a similar reaction in the presence of silyl source such as N($SiMe_3$)$_3$ does not lead to the formation of the desired silylated **[(Me_3SiO)UO(THF)(MX)$_2$(L)]**. Finally, we tried to isolate the intermediate $[UO_2(S)(K_2L)]$ (S = THF, pyridine) by the reaction between the uranyl(VI) Pacman complex and two equivalents of potassium base, but without any success. Indeed, the reactions between **[UO_2(THF)(H_2L)]** with two equivalents of KN($SiMe_3$)$_2$ or KH do not lead to the expected product. These reactive uranyl complexes may provide interesting functional chemical model for the highly radioactive plutonium and neptunium dioxo complexes.

Chapter 6: Experimental details

6.1. Experimental details

All manipulations were carried out under a dry, oxygen-free dinitrogen atmosphere using standard Schlenk techniques, in an Mbraun Unilab unless otherwise stated (except for the syntheses of LH_4 and $[UO_2\{N(SiMe_3)_2\}(THF)_2]$). The solvents used were degassed and purified by passage through activated alumina towers prior to use. All deuterated solvents were refluxed over potassium, vacuum transferred and freeze-pump-thaw degassed three times prior to use.

All elemental analysis samples were sealed in glass ampoules under vacuum and were determined by Mr. Stephen Boyer at London Metropolitan University, Analytische Laboratorien Germany and Medac Ltd UK.

^{1}H NMR spectra were recorded at 298 K on a Bruker ARX250, Bruker DPX360, Bruker AVA400, Bruker DMX500 and Bruker Avance 600 MHz spectrometers operating at 250.13, 360.13, 400.25, 500.13 and 599.92 MHz respectively. ^{2}H NMR spectra were recorded at 298 K on a Bruker AVA400 and Bruker Avance 600 MHz spectrometers operating at 76.77 and 92.07 MHz respectively. $^{13}C\{^{1}H\}$ on a Bruker AVA 400 spectrometer at 100.57 MHz at 298 K. $^{7}Li\{^{1}H\}$ NMR spectra were recorded at 298 K on a Bruker AVA400 spectrometer operating at 155.42 MHz. $^{31}P\{^{1}H\}$ NMR spectra were recorded on a Bruker AVA400 spectrometer operating at 161.89 MHz. Chemical shifts are reported in parts per million and referenced to residual proton resonances calibrated against external TMS. When the solvent is THF, the ^{1}H NMR experiment was recorded with double-presaturation of THF with a small quantity of d_6-benzene added as a deuterium lock.

Infrared spectra were recorded on a JASCO 410 spectrophotometer.

Surface Enhanced Raman Spectroscopy (SERS) spectra were recorded by Prof. Duncan Graham and Dr Iain Lamour at the University of Strathclyde using a Renishaw inverted inVia Raman microscope and an excitation wavelength of 785 nm (50% level laser power from 3.39 mW unfocused laser) between 100 and 3200 cm^{-1}. Samples were deposited as a thin layer by evaporation of two drops of a solution of compound. The substrate was Klarite on a microscope slide. For air and moisture

sensitive samples the Klarite chip was covered by a microscope cover slip, sealed with silicone grease, to protect the sample. Blank spectra for each of the slides were recorded prior to use. All spectra were baseline corrected using GRAMS software and normalised.

X-ray diffraction data on single crystal were collected at 150 K on a Bruker SMART 1000 diffractometer equipped with a CCD area detector using graphite monochromated using Mo Kα radiation (λ = 0.71073 Å) or at 170K using an Oxford Cryosystems low temperature device attached to an Oxford Diffraction Xcalibur Eos diffractometer equipped with an Eos detector and operating graphite monochromated Mo*K*α radiation (λ = 0.71073 Å) or at 100 K on an Oxford Diffraction Supernova diffractometer using mirror monochromated Cu-Kα radiation (λ = 1.54178 Ǻ).

Variable temperature magnetic susceptibilities were measured using a Quantum Design MPMS-XL SQUID spectrometer operating at 1000 Oe in the temperature range 2 to 300 K. The sample was loaded in a gel capsule in a dinitrogen glovebox and suspended in a plastic straw. Diamagnetic contributions of the ligand were calculated using Pascal's constants and the effective magnetic moment (μ_{eff}) were calculated using the expression $\mu_{eff} = 2.828\ (\chi T)^{½}$.

EPR spectra were recorded by Prof Kartsen Meyer and Dr Oanh Lam at Friedrich-Alexander-Universität Germany, using a JEOL continuous wave spectrometer JES-FA200 equipped with an X-band high-power low-noise Dual-Gunn oscillator bridge (microwave source) and a high sensitivity cylindrical mode cavity. The system carries a Hall field controller as well as an X-band digital frequency counter. For low-temperature experiments the spectrometer is equipped with a helium cryostat system to record spectra down to as low as 4 K.

DFT calculations were carried out by Dr Ahmed Yahia and Prof Laurent Maron at Université Paul Sabatier, Toulouse III, France. Calculations were carried out at the DFT level of theory using the hybrid functional B3PW91.[1] Geometry optimisations were carried out without any symmetry restrictions and the nature of the *extrema* (*minima*) was verified with analytical frequency calculations. For all transition states, the intrinsic reaction coordinate was followed to verify the direct connection between the transition state and adducts. All these computations were performed with the Gaussian 03 suite of programs. Gibbs free energies were obtained

at 298.15 K within the harmonic approximation. The electronic density was analyzed using the Natural Bonding Analysis (NBO) technique.[2]

Pyrrole was distilled under reduced pressure prior to use. $KN(SiMe_3)_2$ was synthesised according to literature procedures. $LiN(SiMe_3)_2$ was purchased from Aldrich, recrystallised from hexane and sublimed at 110 °C at 1 x 10^{-4} Torr. Dihydroanthracene was sublimed at 80-90 °C at 1 x 10^{-4} Torr before use. The silyl chlorides Ph_2HSiCl, $^tBuMe_2SiCl$ and Me_3SiCl were distilled from Mg turnings under N_2. The metal halide $ZnCl_2$, ZnI_2 and $FeBr_2$ were dried with Me_3SiCl under N_2. Dry KOH was prepared by addition of degassed water to potassium in toluene. All other reagents were used as purchased from Sigma Aldrich without further purification.

6.2. Syntheses and characterisations

Synthesis of dimethyldipyrromethane [3]

To a mixture of pyrrole (88 mL, 1.268 mol) and acetone (7.8 mL, 0.105 mol) was added slowly TFA (1.5 mL) *via* a pipette. The yellow-green solution turned green-brown. After 10 min, a solution of NaOH (0.2 M, 100 mL) was added to make a basic solution. The product was extracted with ethyl acetate and the organic layer was washed with de-ionised water (3 × 30 mL). The organic layer was dried with Na_2SO_4. The solvent and any excess of pyrrole were removed under reduced pressure. A green-brown solution was obtained, then distilled to leave a white crystal solid in 53% yield.

^1H NMR ($CDCl_3$): δ_H 7.41 (s, 2H, NH), 6.38 (m, 4H, pyrrole), 1.43 (s, 6H, CH_3) ppm.

Synthesis of diformylmethyldipyrromethane [4]

$POCl_3$ was added drop wise to a stirred solution of **dimethyldipyrromethane** (9.72 g, 0.056 mol) in cold (0°C) DMF (100mL). The resulting solution was stirred for 1 h. De-ionised water (100 mL) was added slowly to quench the reaction. A solution of KOH (2.5 M, 400 mL) was added slowly until to obtain a strong basic solution was

obtained. A precipitate was formed and filtered, washed with water and diethyl ether. A pale pink solid was obtained and dried under reduced pressure. (11.57g, 77%)

^{1}H NMR ($CDCl_3$): δ_H 10.81 (s, 2H, NH), 9.31 (s, 2H, CHO), 6.90 (d, 2H, *J* = 3.9 Hz, pyr), 6.26 (d, 2H, *J* = 3.9 Hz, pyr), 1.80 (s, 6H, CH_3) ppm.

Synthesis of [H_4L] [5]

To a stirred solution of **diformylmethyldipyrromethane** (14.88 g, 0.06 mol) and 4,5-dimethyl-1,2-phenylenediamine (8.17 g, 0.06 mol) in hot (40 °C) methanol (50 mL) was added slowly the para-toluenesulfonic acid (22.8 g, 0.108 mol). After a few minutes an orange precipitate was obtained, filtered then washed with methanol. This salt was redissolved in methanol, heated at 50 °C and then an excess of triethylamine was added, causing the immediately loss of the orange colour. The yellow precipitate was filtered washed with methanol and ether and then dried under reduced pressure (heated at 120 °C overnight) to afford [**H_4L]** as a yellow solid (18 g, 84 %).

^{1}H NMR (C_6D_6): δ_H 9.71 (s, 4H, NH), 8.49 (s, 4H, imine), 7.47 (s, 4H, ar), 6.63 (d, 4H, *J* = 2.8 Hz, pyr), 6.27 (d, 4H, *J* = 2.8 Hz, pyr), 2.37 (s, 12H, CH_3ar), 1.38 (s, 12H, CH_3) ppm.

Synthesis of [$UO_2Cl_2(THF)_2$] [6]

Concentrated hydrochloric acid in water (20 ml) was added to uranium trioxide (10 g, 0.03 mol) until a yellow solution was formed. The solution was heated at 110 °C to drive off the water and the excess of HCl under a constant stream of N_2. Once a yellow solid was formed, the heating continued for 30 min to 1 h then the product was dried under reduced pressure. Dry THF (100 mL) was added to the product to form a suspension. Trimethylsilylchloride (22.83 mL, 0.209 mol) was added portion wise, and stirred for 16 h. The solution was concentrated to half volume, dry hexane was added (100mL) and stirred for 1 h. A yellow solid and a mostly colourless solution were obtained, filtered. The solid was washed with hexane (2 × 50mL) and dried under reduced pressure. A bright yellow solid was obtained with 88% yield (15.02 g).

Synthesis of $[UO_2\{N(SiMe_3)_2\}(THF)_2]$ [7]

A solution of $KN(SiMe_3)_2$ (2.46 g, 12.36 mmol)in THF (30mL) was added to a solution of **$[UO_2Cl_2(THF)_2]$** (3 g, 6.18 mmol) in THF (30 mL), the suspension was stirred for 24 h, then hexane was added and the suspension was filtered over celite. The solvent was removed, then was added a mixture of hexane/THF (10:1), and the solution was crystallised at −30 °C. Red-orange crystals were obtained in 35% yield (1.56 g).

^{1}H NMR (C_6D_6): δ_H 4.05 (br, 8H, THF), 1.40 (br, 8H, THF), 0.48 (s, 36H, Me) ppm.

Synthesis of $[UO_2\{N(SiMe_3)_2\}(py)_2]$

A solution of $KN(SiMe_3)_2$ (3.858 g, 7.95 mmol) in pyridine was added slowly to a solution of $[UO_2Cl_2(THF)_2]$ (4.691g, 7.95 mmol) in pyridine, the suspension was stirred for 24 h, then filtered over celite. The solvent was removed then the solid was redissolved in pyridine. The solution was crystallised at −30 °C. Orange crystals were obtained in 70 % yield (5 g).

Synthesis of $[UO_2(THF)(H_2L)]$ [8]

A solution of $[H_4L]$ (3.2 g, 4.8 mmol) in cold (−78 °C) THF (20 mL) was added slowly to a stirred solution of **$[UO_2\{N(SiMe_3)_2\}_2(THF)_2]$** (3.6 g, 4.8 mmol) in THF (20ml) cooled to −78 °C. The resulting solution was allowed to warm to room temperature over 16 h, after which the volatiles were removed under reduced pressure and the residual solid redissolved in THF (15 mL). Addition of hexane (20 mL) to this solution resulted in a precipitate that was isolated by filtration, washed with hexane (2 × 10 mL), and dried under vacuum. A brown solid was obtained in 60% yield (3 g).

^{1}H NMR (C_6D_6): δ_H 8.74 (s, 2H, imine), 8.49 (s, 2H, NH), 7.99 (s, 2H, imine), 7.18 (s, 2H, aryl), 6.81 (s, 2H, aryl), 6.78 (d, 2H, *J* = 3 Hz, pyrrole), 6.72 (d, 2H, *J* = 3 Hz, pyrrole), 6.27 (d, 2H, *J* = 3Hz, pyrrole), 5.86 (d, 2H, pyrrole), 4.83 (m, 2H, THF), 3.94 (m, 2H, THF), 2.23 (s, 3H, methyl), 2.13 (s, 3H, methyl), 2.08 (s, 3H,

methyl), 2.00 (s, 6H, 2 × 3 methyl), 1.31 (s, 3H, methyl), 0.86 (m, 2H, THF), 0.71 (m, 2H, THF), 0.52 (s, 3H, methyl) ppm.

IR (Nujol mull, cm^{-1}): ν 3373 (br, NH), 1619 (s), 1601 (s), 1583 (s), 1281(s), 1263 (m), 1214 (m), 1181 (m), 1049 (s), 1019 (m), 959 (w), 908 (s), 895 (sh), 780 (m), 766 (m).

Synthesis of $[UO_2(py)(H_2L)]$

A solution of [**H_4L]** (3.52 g, 5.3 mmol) in cold (−35 °C) pyridine (20 mL) was added slowly to a stirred solution of [**$UO_2\{N(SiMe_3)_2\}(py)_2$]** (4 g, 5.3 mmol) in pyridine (20 mL) cooled to −35 °C. The resulting solution was allowed to warm to room temperature over 16 h, after which the volatiles were removed under reduced pressure and the residual solid redissolved in pyridine (15 mL). Addition of hexane (20 mL) to this solution resulted in a precipitate that was isolated by filtration, washed with hexane (2 × 10 mL), and dried under vacuum. A brown solid was obtained in 80 % yield (4.3 g).

^{1}H NMR (d_5-pyridine): δ_H 9.20 (s, 2H, imine), 8.69 (s, 2H, NH), 8.23 (s, 2H, imine), 7.32 (s, 2H, aryl), 6.82 (s, 2H, aryl), 6.72 (s, 2H, pyrrole), 6.51 (s, 4H, pyrrole), 6.02 (s, 2H, pyrrole), 2.26 (s, 3H, methyl), 2.16 (s, 3H, methyl), 2.07 (s, 12H, 4 × methyl), 1.47 (s, 3H, methyl), 0.58 (s, 3H, methyl).

6.3. Synthetic procedures for Chapter 2

Synthesis of [OUO(py){Li(py)}(HL)]

To a solution of **$[UO_2(py)(H_2L)]$** (24.7 mg, 0.024 mmol) in pyridine (0.5 mL) at −40 ºC was added slowly a solution of $LiN(SiMe_3)_2$ (4 mg, 0.024 mmol) in pyridine at −40 ºC in a Teflon-tapped NMR tube. The resulting solution is a mixture between **$[UO_2(py)(H_2L)]$**, **[OUO(py){Li(py)}(HL)]**, **$[(py)_3LiOUO(py)Li(py)(HL)]$** and **$[(py)_3LiOUO(py)\{Li(py)\}_2(L)]$** in a ratio 1:0.5:0.26:0.24. Here are listed only the resonances for **[OUO(py){Li(py)}(HL)]**.

^{1}H NMR (*d*$_5$-pyridine): δ_H 9.11 (s, 1H), 7.31 (s, 1H), 7.28 (s, 1H), 7.15(s, 1H), 7.08 (s, 1H), 6.97 (s, 1H), 6.92 (s, 1H), 6.86 (s, 1H), 6.72 (s, 1H), 6.61 (s, 1H), 6.43 (s, 1H), 6.32 (s, 1H), 6.24 (s, 1H), 6.06 (s, 1H), 2.23 (s, 3H), 2.19 (s, 3H), 2.12 (s, 3H), 2.09, (s, 3H), 1.65, (s, 6H), 0.86 (s, 6H) ppm

Synthesis of [(py)$_3$LiOUO(py)Li(py)(HL)]

To a solution of **[UO$_2$(py)(H$_2$L)]** (150 mg, 0.135mmol) in pyridine (20 mL) was added slowly a solution of two equivalents of LDA (28.9 mg, 0.270 mmol) in pyridine (10 mL). After 1h the volatiles were removed under reduced pressure to afford **[(py)$_3$LiOUO(py)Li(py)(HL)]** (150 mg, 78 %). Orange single crystals suitable for X-ray diffraction studies were grown from a saturated pyridine solution of **[(py)$_3$LiOUO(py)Li(py)(HL)]** at −35 °C.

Analysis. Found: C, 55.39; H, 4.62; N, 12.26 %. $C_{47}H_{46}N_9O_2Li_2U$ requires C, 55.30; H, 4.54; N, 12.35 %.

IR (Nujol mull, cm^{-1}): ν 3310 (br, w), 1580, 1282, 1215, 1185, 1040, 960, 893(s), 880(sh), 772(s), 724(s), 709(s), 620.

^{1}H NMR (*d*$_5$-pyridine): δ_H 60.09 (s, 1H), 26.67 (s, 3H), 12.71 (s, 1H), 11.77 (s, 1H), 10.70 (s, 1H), 9.16 (s, 3H), 8.54 (s, 2 x 1H), 7.93 (s, 1H), 3.00 (s, 1H), 2.46 (s, 3H), 1.69 (s, 3H), −0.21 (s, 1H), −0.56 (s, 1H), −1.06 (s, 1H), −2.11 (s, 3H), −2.60 (s, 1H), −2.92 (s, 1H), −3.60 (s, 1H), −3.75 (s, 1H), −4.69 (s, 1H), −5.06 (s, 1H), −6.60 (s, 3H), −13.40 (s, 1H) ppm.

^{7}Li{^{1}H} NMR (*d*$_5$-pyridine): δ_{Li} 92 (br s) ppm.

Magnetic moment (SQUID, powdered sample, ITU) μ_{eff} 1.76 μ_B

EPR, solid sample (22 K, 0.998 mW, 8955.768 MHz) g = 1.98 and g = 3.85

2nd method: reaction with two equivalents of LiN(SiMe$_3$)$_2$ in the presence of DHA

To a solution of **[UO$_2$(py)(H$_2$L)]** (100 mg, 0.094 mmol) and DHA (17.15 mg, 0.095 mmol) in pyridine (20 mL) at −40 °C was added a solution of two equivalents of LiN(SiMe$_3$)$_2$ (31.5 mg, 0.188 mmol) in pyridine (20 mL) at −40 °C. The resulting solution was allowed to warm to room temperature over 2 h, after which the volatiles

were removed under reduced pressure. A red-brown solid was obtained, which was found to be a mixture of **[(py)$_3$LiOUO(py)Li(py)(HL)]**, anthracene, and 9,9',10,10'-tetrahydro-9,9'-bianthracene.

In an NMR tube-scale repeat of this reaction, using five equivalents of DHA, the ratio of **[(py)$_3$LiOUO(py)Li(py)(HL)]**: anthracene: 9,9',10,10'-tetrahydro-9,9'-bianthracene : DHA = 1: 0.10 : 0.45 : 4.

3rd method: reaction with LiCp

Pyridine (0.5 mL) was added to a mixture of **[UO$_2$(py)(H$_2$L)]** (25 mg, 0.02mmol) and CpLi (3.04 mg, 0.04mmol) in pyridine at room temperature. The ^{1}H NMR spectrum shows the formation of **[(py)$_3$LiOUO(py)Li(py)(HL)]** and CpH in a ratio 1:2.

4th method: reaction with LiCPh$_3$

To a colourless solution of triphenylmethane (0.650 g, 2.66 mmol) in THF (20 mL) at −78 ºC was added a solution of *tert*-butyllithium in hexanes (1.7 molar, 1.5 mL, 0.9 eq.). The resulting red solution of LiCPh$_3$ was stirred at −78 ºC for 2 h. To a solution of **[UO$_2$(THF)(H$_2$L)]** (0.20 g, 0.185 mmol) in pyridine (20 mL) at −40 ºC was added dropwise this solution of trityllithium in a hexane/THF mixture (1.5 mL). The suspension was allowed to warm to room temperature and stirred for 16 h, after which the product had partially precipitated. The suspension was filtered and the volatiles were removed from the filtrate under reduced pressure to afford **[(py)$_3$LiOUO(py)Li(py)(HL)]** and HCPh$_3$ as a brown solid (0.150 g, 68 %) characterised by comparison with the ^{1}H NMR spectra of a genuine sample prepared as above. The ^{1}H and ^{13}C{^{1}H} NMR spectra of the *in situ* reaction products are shown below, including the spectrum of an independently made sample of Gomberg's dimer.

5th method: reaction with $LiNH_2$

To a solution of **[UO_2(THF)(H_2L)]** (50 mg, 0.046 mmol) in pyridine (20 mL) at −40 ºC was added a suspension of $LiNH_2$ (2.1 mg, 0.092 mmol) in pyridine (5 mL) at −40 ºC. The solution was allowed to warm to room temperature over 16 h with stirring, then heated at 110 °C for 16 h. The volatiles were removed to afford a brown yellow solid characterised as **[$(py)_3$LiOUO(py)Li(py)(HL)]** (35 mg, 62 %).

6th method: reaction with LiH

To a suspension of LiH (1.5 mg, 0.19 mmol) in pyridine (5 mL) at −40 °C was added a solution of **[UO_2(THF)(H_2L)]** (100 mg, 0.095 mmol) in pyridine (20 mL) at −40 °C. The suspension was stirred at room temperature for 24 h then was heated at 110 °C for 16 h. The volatiles were removed under reduced pressure to afford a brown-yellow solid characterised as **[$(py)_3$LiOUO(py)Li(py)(HL)]** (80 mg, 72 %).

7th method: reaction between Li_4L and $UO_2Cl_2(THF)_2$:

Pyridine (0.5 mL) was added to a mixture of **Li_4L** (20 mg, 0.03 mmol) and **$UO_2Cl_2(THF)_2$** (14.5 mg, 0.03 mmol) in a Teflon-tapped NMR tube at room temperature. After 24 h the solution was heated at 110 °C for 16 h to afford a greenish yellow solution which was dried to a brown-yellow solid, characterised as **[$(py)_3$LiOUO(py)Li(py)(HL)]** (24 mg, 67 %).

Synthesis of the kinetic isomer

To a solution of **[UO_2(py)(H_2L)]** (150 mg, 0.135 mmol) in pyridine (20 mL) at −35 °C was added slowly a solution of 2 equivalents of LDA (28.9 mg, 270 mmol) in pyridine (10 mL). The suspension was allowed to warm to room temperature and stirred for 16 h, after which the product had partially precipitated. The suspension was filtered and the volatiles were removed from the filtrate under reduced pressure to afford the kinetic isomer of **[$(py)_3$LiOUO(py)Li(py)(HL)]** (60.6 mg, 38 %).

^{1}H NMR (d_5-pyridine): δ_H 86.61 (s, 1H), 32.58 (s, 3H), 13.93 (s, 2H), 10.73 (s, 3H + 2H), 5.59 (s, 2H), 3.21 (s, 2H), 1.66 (s, 3H), 0.41 (s, 6H), −2.00 (s, 2H), −2.48 (s, 6H), −2.66 (s, 2H), −3.77 (s, 2H), −7.11 (s, 3H), −8.89(s, 2H) ppm.

^{7}Li{^{1}H} NMR (d_5-pyridine): δ_{Li} 102 (br, s) ppm.

Conversion of the kinetic isomer to the thermodynamic isomer

A solution containing predominantly kinetic isomer (and approx 15 % thermodynamic isomer) was heated to reflux in pyridine for three days. The conversion to the thermodynamic isomer was monitored by ^{1}H NMR spectroscopy, with 32 % conversion achieved after 3 days.

Synthesis of [(py)$_3$LiOUO(py){Li(py)}$_2$(L)]

To a solution of **[UO$_2$(py)(H$_2$L)]** (162 mg, 0.15 mmol) in pyridine (40 mL) was added a solution of LiN(SiMe$_3$)$_2$ (75 mg, 0.45 mmol) in pyridine (40 mL). The solution was stirred for 16 h, and volatiles removed under reduced pressure to afford [(py)$_3$LiOUO(py){Li(py)}$_2$(L)] as a brown solid (160 mg, 75 %). Orange single crystals suitable for X-ray diffraction studies were grown from a saturated pyridine solution of [(py)$_3$LiOUO(py){Li(py)}$_2$(L)].

Analysis. Found: C, 60.47; H, 4.81; N, 13.86 % $C_{71}H_{68}Li_3N_{14}O_2U$ requires C, 60.55; H, 4.87; N, 13.92 %.

IR (nujol mull, cm^{-1}): ν 1593, 1564, 1512, 1440, 1351, 1277, 1210, 1186, 1147, 1111, 1037, 1017, 897, 792 (s), 751, 704 (s), 663, 620.

^{1}H NMR (*d*$_5$-pyridine): δ_H 21.36 (s, 3H), 11.42 (s, 2H), 9.58 (s, 3H), 7.97 (s, 4H), 6.99 (s, 2H) 0.84 (s, 2H), 0.05 (s, 6H), −1.46 (s, 2H), −2.05 (s, 6H), −2.57 (s, 3H), −5.19 (s, 3H), −8.78 (s, 2H) ppm.

^{7}Li{^{1}H} NMR : δ_{Li} 73 ppm.

Synthesis of [Li(THF)][(THF)$_2$(Me$_3$Si)$_2$NLiOUO(THF){Li(THF)}$_2$(L)]

To a solution of **[UO$_2$(THF)(H$_2$L)]** (150 mg, 0.15 mmol) in THF (40 mL) was added a solution of lithium *bis*(trimethylsilyl)amine (100 mg, 0.6 mmol) in THF (40 mL). The solution was stirred for 16 h, the volatiles were removed to leave a red-brown solid in 65 % yield (143 mg). Orange single crystals suitable for X-ray diffraction studies were grown from a saturated pyridine solution of **[Li(THF)][(THF)$_2$(Me$_3$Si)$_2$NLiOUO(THF){Li(THF)}$_2$(L)]**.

Analysis. Found: C, 55.54, H, 6.37, N, 8.57% $C_{68}H_{93}N_9O_7Si_2Li_4U$ requires C, 55.37, H, 6.34, N, 8.62%

IR (Nujol mull, cm^{-1}): ν 1591, 1275, 1185, 1045, 1018, 873, 826, 764, 695.

^{1}H NMR (THF + C_6D_6 capillary, double presaturation): δ_H 20.37 (s, 3H), 10.90 (s, 2H), 9.31 (s, 2H), 7.51 (s, 2H), 7.32 (s, 3H), 1.89 (s, 2H), 0.41 (s, 6H, CH3 aryl), −0.95 (s, 6H, CH3 aryl), −1.56 (s, 2H), −4.99 (s, 3H), −7.1 (s, 3H) ppm.

$^{7}Li\{^{1}H\}$ NMR: δ_{Li} 52.18, 38.52, 20.45 ppm.

Magnetic moment (SQUID, powdered sample, gelatine capsule, 300 K): μ_{eff} 2.86

6.4. Synthetic procedures for Chapter 3

Reaction of [(py)$_3$LiOUO(py)Li(py)(HL)] and one equivalent of Me_3SiCl

To a solution of **[(py)$_3$LiOUO(py)Li(py)(HL)]** (25 mg, 0.02 mmol) in d_5-pyridine (0.5 mL) was added one equivalent of Me_3SiCl (2.5 μL, 0.02mmol) in a Teflon-tapped NMR tube at room temperature. After 15 min the reaction is finished.

^{1}H NMR (d_5-pyridine): δ_H 39.26 (s, 1H), 13.38 (s, 9H), 11.99 (s, 1H), 11.25 (s, 1H), 11.21 (s, 1H), 9.79 (s, 1H), 9.05 (s, 1H), 8.89 (s, 1H), 6.99 9s, 1H), 5.94 (s, 3H), 5.52 (s, 1H), 5.05 (s, 1H), 4.49 (s, 1H), 2.81 (s, 1H), 2.69 (s, 1H), 1.75 (s, 1H), 1.44 (s, 1H), 0.32 (s, 1H), −0.173 (s, 3H), −0.42 (s, 3H), −1.29 (s, 3H), −1.87 (s, 3H), −2.71 (s, 3H), −6.54 (s, 1H), −7.74 (s, 3H) ppm.

IR (Nujol mull, cm^{-1}): ν 3177, 1649, 1554, 1307, 1278, 1242, 1215, 1156, 1063, 1047, 991, 903, 887, 874, 861, 807, 795, 778, 721.

Reaction of [(py)$_3$LiOUO(py)Li(py)(HL)] and one equivalent of $^{t}BuMe_2SiCl$

To a solution of **[(py)$_3$LiOUO(py)Li(py)(HL)]** (25 mg, 0.02 mmol) in d_5-pyridine (0.5 mL) was added one equivalent of $^{t}BuMe_2SiCl$ (3.19 mg, 0.02 mmol) in a Teflon-tapped NMR tube at room temperature. After 15 min the reaction is finished.

^{1}H NMR (d_5-pyridine): δ_H 38.60 (s, 1H), 16.03 (s, 3H), 12.32 (s, 3H), 12.26 (s, 1H), 11.24 (s, 1H), 11.19 (s, 1H), 10.93 (s, 3H), 8.34 (s, 9H), 6.81 (s, 1H), 5.84 (s, 1H), 5.79 (s, 3H), 5.47 (s, 1H), 5.39 (s, 1H), 5.33 (s, 1H), 3.08 (s, 1H), 2.47 (s, 1H) 1.63

(s, H), 1.04 (s, 3H), 0.94 (s, 1H), 0.58 (s, 1H), 0.34 (s, 1H), −0.07 (s, 3H), −0.21 (s, 3H), −0.219 (s, 3H), −1.23 (s, 3H), −1.37 (s, 1H), −2.33 (s, 3H), −6.15 (s, 1H), −7.64 (s, 3H) ppm.

Synthesis of [(HO)UO(py)(H_2L)]

To a solution of **[$(py)_3$LiOUO(py)Li(py)(HL)]** (250 mg, 0.21 mmol) in pyridine (10 mL) was added 1.9 equivalents of HCl in Et_2O (2 mL, 0.4 mmol). The resulting suspension was stirred for 2 h, after which the precipitate isolated and dried under vacuum, to afford 151.6 mg, 71% of **[(HO)UO(py)(H_2L)]** as a brown-yellow solid.

Analysis. Found: C, 56.19; H, 4.93; N, 12.56 %. $C_{47}H_{48}N_9O_2U$ requires C, 55.95; H, 4.80; N, 12.49 %

IR (Nujol mull, cm^{-1}): ν 3376, 3189, 1623, 1600, 1583, 1288, 1265, 1218, 1103, 1045, 1020, 892, 800 (UO strecth), 782, 765, 725, 709.

^{1}H NMR (d_5-pyridine): δ_H 86.39 (s, 1H), 32.47 (s, 3H), 13.94 (s, 2H), 10.73 (s, 3H + 2H), 5.66 (s, 2H), 3.30 (s, 3H), 2.05 (s, 2H), 1.74 (s, 2H), 0.49 (s, 6H), −1.89 (s, 2H), −2.39 (s, 6H), −2.56 (s, 2H), −3.67 (s, 2H), −7.01 (s, 3H), −8.75 (s, 2H) ppm.

Synthesis of [(DO)UO(py)(DHL)]

To a solution of **[$(py)_3$LiOUO(py)Li(py)(HL)]** (200 mg, 0.17mmol) in pyridine (10mL) was added 1.9 equivalents of DCL in Et2O (3.39 mL, 0.024 mmol). The resulting suspension was stirred for 2 h, after which the precipitate was isolated and dried under vacuum, to afford 120 mg, 70 % of **[(DO)UO(py)(DHL)]** as a brown-yellow solid.

IR (Nujol mull, cm^{-1}): ν 3374, 3305, 3237, 3172, 3106, 2476, 2414, 2364, 1623, 1602, 1583, 1552, 1305, 1290, 1272, 1216, 1184, 1045, 1020, 973, 892, 873, 827, 765, 725.

^{1}H NMR (d_5-pyridine): δ_H 86.39 (s, 0.5H), 32.47 (s, 3H), 13.94 (s, 2H), 10.73 (s, 3H + 2H), 5.66 (s, 2H), 3.30 (s, 3H), 2.05 (s, 2H), 1.74 (s, 2H), 0.49 (s, 6H), −1.89 (s, 2H), −2.39 (s, 6H), −2.56 (s, 2H), −3.67 (s, 2H), −7.01 (s, 3H), −8.75 (s, 2H) ppm.

^{2}H NMR (h_5-pyridine): δ_H 86.3 (s, OH), 7.30 (s, NH) ppm.

Synthesis of [(Me_3SiO)UO(py)(H_2L)]

To a solution of **[(HO)UO(py)(H_2L)]** (75 mg, 0.074 mmol) in pyridine (10 mL) was added neat Me_3SiCl (9.4 μL, 0.074 mmol). The solution was stirred for 2h after which the suspension was filtered and the volatiles evaporated from the filtrate to afford 63 mg, 78% of **[(Me_3SiO)UO(py)(H_2L)]** as a brown-yellow solid. Red single crystals suitable for X-ray diffraction studies were grown from a saturated pyridine solution of **[(Me_3SiO)UO(py)(H_2L)]** at −35 °C.

Analysis.Found: C, 53.28; H, 4.79; N, 11.93 %. $C_{50}H_{56}N_9O_2SiU$ requires C, 55.55; H, 5.22; N, 11.66 %.

IR (Nujol mull, cm^{-1}): ν 3286 (NH), 1621, 1602, 1583, 1284, 1263, 1216, 1186, 1045, 1033, 1016, 894, 860 (UO stretch), 802, 781, 767, 744, 703 (UO stretch).

^{1}H NMR (d_5-pyridine): δ_H 58.10 (s, 2H), 15.02 (s, 9H), 14.58 (s, 3H), 11.13 (s, 2H), 10.04 (s, 2H), 8.63 (s, 2H), 6.65 (s, 3H), 3.60 (s, 2x2H), 3.19 (s, 2H), 2.48 (s, 2H), 1.87(s, 2H), 0.14 (s, 6H), −0.46, (s, 6H), −2.95 (s, 3H), −8.40 (s, 3H) ppm.

Synthesis of [(Me_3SiO)UO(py)(DHL)]

To a solution of **[(DO)UO(py)(DHL)]** (25mg, 0.02 mmol) in d_5-pyridine (0.5 mL) in a Teflon-tapped NMR tube at room temperature was added Me_3SiCl (excess 5μL, 0.04 mmol). The reaction was monitored by ^{1}H and ^{2}H NMR spectroscopy.

^{1}H NMR (d_5-pyridine): δ_H 58.10 (s, 1H), 15.02 (s, 9H), 14.58 (s, 3H), 11.13 (s, 2H), 10.04 (s, 2H), 8.63 (s, 2H), 6.65 (s, 3H), 3.60 (s, 2x2H), 3.19 (s, 2H), 2.48 (s, 2H), 1.87(s, 2H), 0.14 (s, 6H), −0.46, (s, 6H), −2.95 (s, 3H), −8.40 (s, 3H) ppm.

^{2}H NMR (h_5-pyridine): δ_H 58.10 (s, 1 NH) ppm.

Synthesis of [(^{t}BuMe$_2$SiO)UO(py)(H_2L)]

To a solution of **[(HO)UO(py)(H_2L)]** (100 mg, 0.09 mmol) in pyridine (10 mL) was added solid ^{t}BuMe$_2$SiCl (14.9 mg, 0.09 mmol). The solution was stirred for 2 h after which the suspension was filtered and the volatiles evaporated from the filtrate to afford 70 mg, 63 % of **[(^{t}BuMe$_2$SiO)UO(py)(H_2L)]** as a brown-yellow solid. Red single crystals suitable for X-ray diffraction studies were grown from a saturated toluene solution of **[(^{t}BuMe$_2$SiO)UO(py)(H_2L)]** at −35 °C.

Analysis. Found: C, 56.06; H, 5.69; N, 9.90 %. $C_{53}H_{62}N_9O_2SiU$ requires C, 56.67; H, 5.56; N, 11.22 %.

IR (Nujol mull, cm^{-1}): ν 3290 (NH), 1622, 1583, 1282, 1263, 1217, 1182, 1047, 1020, 893, 831 (UO stretch), 769, 725, 694 (UO stretch).

^1H NMR (d_5-pyridine): δ_H 56.56 (s, 2H), 14.79 (s, 6H), 13.33 (s, 3H), 11.00 (s, 2H), 10.09 (s, 2H), 9.23 (s, 9H), 9.01 (s, 2H), 6.26 (s, 3H), 3.60 (s, 2 x 2H), 2.98 (s, 2H), 1.28 (s, 2H), 1.09 (s, 2H), −0.16 (s, 6H), −0.38 (s, 6H), −2.80 (s, 3H), −8.59 (s, 3H) ppm.

Synthesis of [(Ph_2HSiO)UO(py)(H_2L)]

To a solution of **[(HO)UO(py)(H_2L)]** (75 mg, 0.074 mmol) in pyridine (10 mL) was added neat Ph_2HSiCl (14.6 μL, 0.074 mmol). The solution was stirred for 2 h after which the suspension was filtered and the volatiles evaporated from the filtrate to afford 60 mg, 67 % of **[(Ph_2HSiO)UO(py)(H_2L)]** as a brown-yellow solid.

IR (Nujol mull, cm^{-1}): ν 3291, 2142 (Si-H), 1619, 1600, 1583, 1282, 1261, 1218, 1184, 1118 (Si-Ph), 1047, 1022, 894, 823 (UO stretch), 771, 734, 700 (UO stretch).

^1H NMR (d_5-pyridine): δ_H 54.13 (s, 2H, NH), 37.21 (s, 1H, SiH), 17.65 (m, 4H, PhSi), 12.79 (s, 3H), 10.70 (s, 2H), 9.87 (m, 4H, SiPh), 9.79 (s, 2H), 9.15 (m, 2H, SiPh), 8.67 (s, 2H), 6.04 (s, 3H), 4.35 (s, 2H), 3.91 (s, 2H), 3.51 (s, 4H), 1.49 (s, 2H), 0.10 (s, 6H), −0.25 (s, 6H), −2.44 (s, 3H), −8.28 (s, 3H) ppm.

Synthesis of [(Ph_2PO)UO(py)(H_2L)]

To a solution of **[(HO)UO(py)(H_2L)]** (25mg, 0.02 mmol) in d_5-pyridine (0.5 mL) in a Teflon-tapped NMR tube at room temperature was added Ph_2PCl (5.9mg, 0.02 mmol). The solution became dark red and a precipitate was formed. The reaction was monitored by ^1H and $^{31}P\{^1H\}$ NMR spectroscopy.

^1H NMR (d_5-pyridine): δ_H 53.90 (s, 2H), 19.8 (s, 4H), 12.71 (s, 3H), 10.68 (d, 2H), 10.16 (t, 4H), 9.78 (d, 2H), 9.16 (t, 2H), 6.51 (s, 2H), 6.01 (s, 3H), 4.25 (s, 2H), 3.90 (s, 2H), 3.68 (s, 2H), 3.53 (s, 2H), 1.75 (s, 2H), 0.09 (s, 6H), −0.24 (s, 6H), −2.53 (s, 3H), −8.18 (s, 3H) ppm.

$^{31}P\{^1H\}$ NMR (d_5-pyridine): δ_P 36.73 ppm.

Reaction of [(HO)UO(py)(H_2L)] with two equivalents of Ph_2PCl

To a solution of **[(HO)UO(py)(H_2L)]** (25 mg, 0.02 mmol) in d_5-pyridine (0.5 mL) in a Teflon-tapped NMR tube at room temperature was added two equivalents of Ph_2PCl (10.9mg, 0.04 mmol). The solution became dark red and a precipitate was formed. The reaction was monitored by ^1H and $^{31}P\{^1H\}$ NMR spectroscopy.

^1H NMR (d_5-pyridine): δ_H 44.54 (s, 2H), 9.73 (s, 2H), 9.58 (d, 2H), 9.42 (d, 2H), 8.87 (s, 2H), 6.06 (s, 2H), 5.88 (d, 2H), 5.43 (s, 2H), 4.40 (s, 3H), 2.23 (s, 3H), 0.65 (s, 2H), 0.50 (s, 6H), −0.15 (s, 6H), −0.84 (s, 3H), −10.91 (s, 3H) ppm. (O=PPh2-PPh2 free 8.14 (m, 5H), 7.92 (m, 5H), 7.39 (m, 10H) ppm.)

$^{31}P\{^1H\}$ NMR (d_5-pyridine): δ_P 36.76 (d, $J_{P\text{-}P}$ 225.9 Hz), -21.91 (d, $J_{P\text{-}P}$ 225.9 Hz) ppm. (O=PPh_2-PPh_2 free)

Reaction of [(HO)UO(py)(H_2L)] and MeI, attempted synthesis of [MeOUO(py)(H_2L)]

To a solution of **[(HO)UO(py)(H_2L)]** (25 mg, 0.02 mmol) in d_5-pyridine (0.5 mL) in a Teflon-tapped NMR tube at room temperature was added an excess(0.1 mL) of MeI. The reaction was monitored by ^1H NMR spectroscopy. The ^1H NMR spectrum shows no change after a week.

Reaction of [(HO)UO(py)(H_2L)] and $PhCH_2Cl$, attempted synthesis of [$C_6H_5CH_2$OUO(py)(H_2L)]

To a solution of **[(HO)UO(py)(H_2L)]** (25mg, 0.02 mmol) in d_5-pyridine (0.5 mL) in a Teflon-tapped NMR tube at room temperature was added an excess (0.1 mL) of $PhCH_2Cl$. The reaction was monitored by ^1H NMR spectroscopy. The ^1H NMR spectrum shows no change.

Reaction of [(HO)UO(py)(H_2L)] with $(Me_3Si)_2$; attempted synthesis of [(Me_3SiO)UO(py)(H_2L)]

To a solution of **[(HO)UO(py)(H_2L)]** (25mg, 0.02 mmol) in d_5-pyridine (0.5 mL) in a Teflon-tapped NMR tube at room temperature was added one equivalent of $(Me_3Si)_2$ (2.9 mg, 0.02 mmol). The reaction was monitored by ^1H NMR spectroscopy. The ^1H NMR spectrum presents no change after a week.

Reaction of [(HO)UO(py)(H_2L)] with N($SiMe_3$)$_3$; attempted synthesis of [(Me_3SiO)UO(py)(H_2L)]

To a solution of **[(HO)UO(py)(H_2L)]** (25mg, 0.02 mmol) in d_5-pyridine (0.5 mL) in a Teflon-tapped NMR tube at room temperature was added one equivalent of N($SiMe_3$)$_3$ (4.7 mg, 0.02 mmol). The reaction was monitored by ^{1}H NMR spectroscopy. The ^{1}H NMR spectrum presents no change after a week.

6.5. Synthetic procedures for Chapter 4

Synthesis of [Zn{N($SiMe_3$)$_2$}Cl]

To a mixture of $ZnCl_2$ (105.8 mg, 0.77 mmol) and [Zn(N($SiMe_3$)$_2$)$_2$] (300 mg, 0.77 mmol) was added toluene (10mL) The suspension was stirred until formation of a gel. The volatiles were removed under reduced pressure to afford a colourless solid (400 mg).

^{1}H NMR (C_6D_6): δ_H 0.2 ppm.

Synthesis of [(Me_3SiO)UO(THF)($ZnCl)_2$L]

To a mixture of **[UO_2(THF)(H_2L)]** (50 mg, 0.048mmol) and **[Zn{N($SiMe_3$)$_2$}Cl]** (25.5 mg, 0.097 mmol) was added toluene (5 mL) and the solution was heated at 110 °C for 24 h. The suspension was filtered and the filtrate was dried under vacuum to afford a brown solid in 62% yield (38.4 mg). Red block crystal suitable for X-ray diffraction studies were grown from a saturated C_6D_6 solution of **[(Me_3SiO)UO(THF)($ZnCl)_2$L]** at room temperature.

Analysis. Found: C, 46.30; H, 4.50; N, 8.72 %. $C_{49}H_{57}Cl_2N8O_3SiZn_2U$ requires C, 46.19; H, 4.52; N, 8.80 %.

^{1}H NMR (C_6D_6): δ_H 12.56 (s, 1H), 10.74 (s, 1H), 9.84 (s, 1H), 9.27 (s, 1H), 9.14 (s, 1H), 9.01 (s, 1H), 8.25 (s, 1H), 7.98 (s, 1H), 7.65 (s, 1H), 7.32 (s, 9H), 6.78 (s, 3H), 6.19 (s, 1H), 6.05 (s, 1H), 5.88 (s, 1H), 5.43 (s, 1H), 4.50 (s, 1H), 2.89 (s, 1H), 1.64 (s, 3H), 0.845 (s, 3H), 0.62 (S, 3H), 0.07 (s, 3H), −0.04 (s, 3H), −0.07 (s, 1H), −1.19 (s, 1H), −1.38 (s, 1H), −3.91 (s, 3H) ppm.

IR (Nujol mull, cm^{-1}): ν 1591, 1568, 1509, 1291, 1262, 1215, 1182, 1089, 1048, 1018, 960, 897, 836, 801, 768, 722, 637.

Synthesis of [$(Me_3SiO)UO(py)(ZnCl)_2L$]

To a mixture of **[$UO_2(py)(H_2L)$]** (25 mg, 0.02 mmol) and **[$Zn\{N(SiMe_3)_2\}Cl$]** (11.2 mg, 0.05 mmol) was added C_6D_6 (0.5 mL) in a Teflon-tapped NMR tube at room temperature. The solution was heated at 80 °C for 24 h.

^{1}H NMR (C_6D_6): δ_H 12.18 (d, 2H), 10.15 (d, 2H), 9.42 (s, 1H), 9.05 (s, 1H), 8.90 (s, 1H), 8.54 (s, 1H), 8.39 (s, 1H), 8.32 (s, 1H), 8.06 (s, 9H), 7.88 (s, 1H), 7.54 (s, 1H), 7.41 (s, 1H), 6.63 (s, 1H), 6.42 (s, 1H), 6.17 (s, 1H), 6.11 (s, 1H), 5.87 (s, 1H), 5.78 (s, 1H), 5.34 (s, 1H), 5.18 (s, 1H), 4.52 (s, 3H), 4.13 (s, 3H), 2.72 (s, 1H), 2.71 (s, 1H), 1.06 (s, 3H), 0.88 (s, 3H), 0.44 (s, 3H), 0.28 (s, 3H), −0.24 (s, 3H), −2.78 (s, 1H), −3.95 (s, 3H) ppm.

2nd method to synthesise [$(Me_3SiO)UO(py)(ZnCl)_2L$]

C_6D_6 (0.5 mL) was added to a mixture of **[$(Me_3SiO)UO(py)(H_2L)$]** (12.2 mg, 0.011 mmol) and $KN(SiMe_3)_2$ (4.5 mg, 0.022 mmol) in a Teflon-tapped NMR tube at room temperature. After 24h, two equivalents of $ZnCl_2$ (2.98 mg, 0.022 mmol) were added. The reaction was monitored by ^{1}H NMR spectroscopy.

^{1}H NMR (C_6D_6): δ_H 12.18 (d, 2H), 10.15 (d, 2H), 9.42 (s, 1H), 9.05 (s, 1H), 8.90 (s, 1H), 8.54 (s, 1H), 8.39 (s, 1H), 8.32 (s, 1H), 8.06 (s, 9H), 7.88 (s, 1H), 7.54 (s, 1H), 7.41 (s, 1H), 6.63 (s, 1H), 6.42 (s, 1H), 6.17 (s, 1H), 6.11 (s, 1H), 5.87 (s, 1H), 5.78 (s, 1H), 5.34 (s, 1H), 5.18 (s, 1H), 4.52 (s, 3H), 4.13 (s, 3H), 2.72 (s, 1H), 2.71 (s, 1H), 1.06 (s, 3H), 0.88 (s, 3H), 0.44 (s, 3H), 0.28 (s, 3H), −0.24 (s, 3H), −2.78 (s, 1H), −3.95 (s, 3H) ppm.

Synthesis of [$(py)I_2ZnOUO(py)Zn(py)(HL)$]

To a mixture of **[$(py)_3LiOUO(py)Li(py)(HL)$]** (207 mg, 0.17 mmol) and ZnI_2 (112.51 mg, 0.35 mmol) was added pyridine (10 mL). The solution was stirred for 16 h, the volatiles were removed then the solid was washed with toluene (3 x 5 mL) to afford **[$(py)I_2ZnOUO(py)Zn(py)(HL)$]** with 2 LiI incorporated as a brown solid in 76%.

Analysis. Found: C, 39.44; H, 3.86; N, 8.92 %. $C_{62}H_{61}I_4Li_2N_{12}O_2UZn_2$ requires C, 39.26; H, 3.24; N, 8.86 %.

^{1}H NMR (d_5-pyridine): δ_H 58.43 (s, 1H), 29.29 (s, 3H), 12.52 (s, 1H), 11.60 (s, 1H), 10.31 (s, 3H), 8.06 (s, 1H), 5.33 (s, 1H), 5.04 (s, 3H), 2.50 (s, 3H), 1.43 (s, 1H), 0.47 (s, 1H), 0.34 (s, 1H), 0.03 (s, 1H), −0.35 (s, 3H), −1.75 (s, 3H), −2.05 (s, 3H), −2.21 (s, 1H), −2.65 (s, 1H), −2.96 (s, 1H), −2.96 (s, 1H), −3.46 (s, 1H), −4.80 (s, 1H), −6.32 (s, 1H), −4.99 (s, 1H), −5.81 (s, 1H), −6.32 (s, 3H), −14.45 (s, 1H) ppm.

^{7}Li{^{1}H} NMR (d_5-pyridine): δ_{Li} 5.0 ppm

IR (Nujol mull, cm^{-1}): ν 3329(NH), 1580, 1512, 1377, 1278, 1215, 1184, 1151, 1067, 1043, 1003, 979, 893, 873, 778, 754, 728, 697.

Synthesis of [(py)Cl$_2$ZnOUO(py)Zn(py)(HL)]

To a mixture of **[(py)$_3$LiOUO(py)Li(py)(HL)]** (50 mg, 0.04 mmol) and $ZnCl_2$ (11.56 mg, 0.08 mmol) was added pyridine (10 mL). The solution was stirred for 16 h, the volatiles were removed then the solid was washed with toluene (3 x 5 mL) to afford **[(py)Cl$_2$ZnOUO(py)Zn(py)(HL)]**.

^{1}H NMR (d_5-pyridine): δ_H 58.43 (s, 1H), 29.29 (s, 3H), 12.52 (s, 1H), 11.60 (s, 1H), 10.31 (s, 3H), 8.06 (s, 1H), 5.33 (s, 1H), 5.04 (s, 3H), 2.50 (s, 3H), 1.43 (s, 1H), 0.47 (s, 1H), 0.34 (s, 1H), 0.03 (s, 1H), −0.35 (s, 3H), −1.75 (s, 3H), −2.05 (s, 3H), −2.21 (s, 1H), −2.65 (s, 1H), −2.96 (s, 1H), −2.96 (s, 1H), −3.46 (s, 1H), −4.80 (s, 1H), −6.32 (s, 1H), −4.99 (s, 1H), −5.81 (s, 1H), −6.32 (s, 3H), −14.45 (s, 1H) ppm.

Reaction of [UO$_2$(THF)(H$_2$L)] with two equivalents of KH to afford [(THF)$_3$KOUO(THF)K(THF)(HL)]

To a solution of **[UO$_2$(THF)(H$_2$L)]** (200 mg, 0.17 mmol) in THF (10 mL) was added two equivalents of KH (13.57 mg, 0.24 mmol). The suspension was heated at 78°C for 2 h. The volatiles were removed to afford **[(THF)$_3$KOUO(THF)K(THF)(HL)]** as a dark red solid in 94 % yield (160 mg).

Analysis. Found: C, 48.40; H, 4.40; N, 10.18 %. $C_{46}H_{49}K_2N_8O_3U$ requires C, 51.24; H, 4.58; N, 10.39 %.

IR (Nujol mull, cm^{-1}): ν 3417, 1589 1565, 1286, 1211, 1186, 1114, 1085, 1037, 1014, 964, 892, 808 (U=O), 794, 767, 736 (U=O), 725.

^{1}H NMR (C_6D_6 + THF double presaturation): δ_H 90.05 (s, 1H), 30.08 (s, 3H), 13.89 (s, 2H), 10.73 (s, 2H), 10.62 (s, 3H), 5.83 (s, 2H), 0.41 (s, 6H), −1.01 (s, 2H), −1.15

(s, 2H), −1.94 (s, 3H), −2.07 (s, 6H), −3.35 (s, 2H), −7.01 (s, 2H), −7.29 (s, 3H) ppm. One resonance integrating for 2H is missing, possibly under a THF resonance.

Synthesis of [(THF)I_2ZnOUO(THF)Zn(THF)(HL)]

To a mixture of [KOUO(THF)(KHL)] (183.2 mg, 0.17 mmol) and ZnI_2 (108.2 mg, 0.34 mmol) was added THF (10 mL).the suspension was stirred for 16 h and filtered. The volatiles were removed to afford **[(THF)I_2ZnOUO(THF)Zn(THF)(HL)]** as a yellow brown solid in 85 % (194.5 mg). Orange single crystals suitable for X-ray diffraction studies were grown form a saturated solution of THF with a few drops of C_6D_6 at room temperature.

^{1}H NMR (THF + C_6D_6, double presaturation): δ_H 65.80 (s, 1H), 25.51 (s, 3H), 11.81 (s, 1H), 9.46 (s, 1H), 8.53 (s, 3H), 8.02 (s, 1H), 6.23 (s, 1H), 5.48 (s, 1H), 5.34 (s, 3H), 2.54 (s, 3H), 1.92 (s, 1H), 1.14 (s, 1H), 0.86 (s, 3H), 0.59 (s, 1H), −0.07 (s, 1H), −0.19 (s, 1H), −0.36 (s, 1H), −0.67 (s, 1H), −0.92 (s, 1H), −1.07 (s, 3H), −1.71 (s, 1H), −3.52 (s, 1H), −4.57 (s, 1H), −5.54 (s, 3H), −14.93 (s, 1H) ppm.

Analysis. Found: C, 35.96; H, 3.76; N, 6.25 %$C_{54}H_{65}N_8I_2O_5UZn_2(KI)_2$ requires C, 35.67; H, 3.53; N, 5.94 %.

Reaction of [UO_2(THF)(H_2L)] with two equivalents of KN($SiMe_3$)$_2$ and two equivalents of ZnI_2; attempted synthesis of [(Me_3SiO)UO(THF)(ZnI)$_2$L]

To a mixture of **[UO_2(THF)(H_2L)]** (200 mg, 0.18 mmol) and KN($SiMe_3$)$_2$ (73.4 mg, 0.36 mmol) was added THF (10 mL) at −78 °C. The solution was stirred for 15 min, then was added to a suspension of ZnI_2 (117.46 mg, 0.36 mmol) in toluene (10 mL) at −78 °C. The suspension was stirred for 24h. The solution was filtered then the volatiles were removed under reduced pressure. The ^{1}H NMR shows a mixture of **[UO_2(THF)(H_2L)]**, **[(Me_3SiO)UO(THF)(ZnI)$_2$L]** (trace) and an unknown compound.

Reaction of [UO_2(py)(H_2L)] with two equivalents of KN($SiMe_3$)$_2$ and two equivalents of $ZnCl_2$

To a mixture of **[UO_2(py)(H_2L)]** (100 mg, 0.09 mmol) and KN($SiMe_3$)$_2$ (35.8 mg, 0.18 mmol) was added toluene (10 mL) at −80 °C. The solution was allowed to

warm to room temperature over 15 min then the solution was added to a suspension of $ZnCl_2$ (24.55 mg, 0.18 mmol) in toluene (5 mL) at −80 °C. The suspension was stirred at room temperature for 16h. The volatiles were removed under reduced pressure. The ^{1}H NMR shows a mixture of **[UO_2(py)(H_2L)]** and **[(py)I_2ZnOUO(py)Zn(py)(HL)]**

Reaction of [UO_2(THF)(H_2L)] with two equivalents of KN($SiMe_3$)$_2$ in THF to afford [UO_2(OHK)(KHL)]

To a solution of **[UO_2(THF)(H_2L)]** (100 mg, 0.084 mmol) in THF (10 mL) at −78 °C was added a solution of KN($SiMe_3$)$_2$ (33.7 mg, 0.168 mmol) in THF (5 mL) at −78 °C. The solution was allowed to warm to room temperature for 16h. The volatiles were removed to afford **[UO_2(OHK)(KHL)]** as a brown solid in 60% yield (68 mg).

^{1}H NMR (THF + drops of C_6D_6, double presaturation): δ_H 10.36 (s, 1H) 8.93 (s, 2H), 8.72 (s, 1H), 8.33 (s, 2H), 7.03 (s, 2 x 2H), 6.59 (s, 2 x 2H), 6.51 (s, 2H), 5.99 (s, 2H), 2.43 (s, 6H), 2.38 (s, 6H), 1.08 (s, 3H), 0.27 (s, 3H) ppm. Two resonances integrating for 3H each are missing, they are obscured by the THF resonances.

Reaction of [UO_2(py)(H_2L)] with two equivalents of KN($SiMe_3$)$_2$ in pyridine to afford [UO_2(OHK)(KHL)]

To a solution of **[UO_2(py)(H_2L)]** (100 mg, 0.084 mmol) in pyridine at −35 °C was added slowly a solution of KN($SiMe_3$)$_2$ (33.7, 0.168 mmol) at −35 °C in pyridine. The solution was stirred for 15 min at −35 °C and the volatiles were removed to afford a red solid. Single crystals of [UO_2(OHK)(KHL)] suitable for X-ray diffraction studies were grown by slow diffusion of hexane into pyridine at room temperature.

^{1}H NMR (d_5-pyridine): δ_H 12.57 (s, 1H), 9.22 (s, 1H), 9.06 (s, 2H), 8.19 (s, 2H), 7.28 (m, 2 x 2H), 6.88 (m , 2 x 2H), 6.36 (s, 2H), 5.96 (s, 2H), 2.19 (d, 2 x 6H), 2.14 (s, 3H), 2.03 (s, 3H), 1.44 (s, 3H), 0.74 (s, 3H) ppm.

Synthesis of [{UO_2(OH)K(η^2-C_6H_6)(H_2L)}$_2$], Reaction of [UO_2(THF)(H_2L)] with one equivalent of KOH

THF (20 ml) was added to an equimolar mixture of **[UO_2(THF)(H_2L)]** (0.089 g, 0.089 mmol) and dry KOH (0.005 g, 0.089 mmol) at 25°C. The resulting solution was stirred for 16 h, and the volatiles removed under vacuum. The resulting pink-red solid was recrystallised from benzene to yield **[{UO_2(OH)K(η^2-C_6H_6)(H_2L)}$_2$]** as orange rectangular block-shaped crystals (0.024 g, 25 %). Red single crystals suitable for X-ray diffraction studies were grown from a saturated solution of C_6D_6.

^{1}H NMR (THF + drops of C_6D_6, double presaturation): δ_H 11.19 (s, 1H, OH), 9.17 (s, 2H, imine), 9.08 (s, 2H, NH), 8.59 (s, 2H, imine), 7.40 (s, 2H, aryl), 7.32 (s, 2H, aryl), 7.22 (d, 2H, pyrrole), 6.84 (d 2H, pyrrole), 6.68 (m, 2H, pyrrole), 6.22 (m, 2H, pyrrole), 2.72 (s, 6H, 2 x methyl), 2.68 (s, 6H, 2 x methyl), 1.34 (s, 3H, methyl), 0.55 (s, 3H, methyl); ^{1}H NMR ($CDCl_3$): δ_H 9.96 (s, 1H, OH), 9.00 (s, 2H, imine), 8.35 (s, 2H, NH), 8.25 (s, 2H, imine), 7.29 (d, 2H, pyrrole), 7.07(s, 2H, aryl), 6.89 (s, 2H, aryl), 6.69 (d 2H, pyrrole), 6.52 (m, 2H, pyrrole), 6.05 (m, 2H, pyrrole), 2.50 (s, 6H, 2 x methyl), 2.39 (s, 6H, 2 x methyl), 2.25 (s,3H,methyl), 2.13 (s,3H, methyl),1.68 (s, 3H, methyl), 1.09 (s, 3H, methyl).

Synthesis of [(py)$_2$IZnOUO(py)(H_2L)]

To a mixture of **[(py)$_3$LiOUO(py)Li(py)(HL)]** (50 mg, 0.04 mmol) and one equivalent of ZnI_2 (27 mg, 0.04 mmol) was added pyridine (5 mL). The solution was stirred for 4 h then the volatiles were removed to afford **[(py)$_2$IZnOUO(py)(H_2L)]** with one LiI incorporated as a yellow-brown solid in 75% (45 mg).

Orange single crystals suitable for X-ray diffraction studies were grown from a saturated pyridine solution of **[(py)$_2$IZnOUO(py)(H_2L)]** at −35 °C.

^{1}H NMR (d_5-pyridine): δ_H 75.11 (s, 2H), 26.00 (s, 3H), 12.86 (s, 2H), 10.47 (s, 2H), 9.18 (s, 3H), 6.67 (s, 2H), 3.27 (s, 2H), 2.92 (s, 3H), 0.43 (s, 6H), −0.23 (s, 2H), −0.70 (s, 2H), −1.72 (s, 2H), −1.83 (s, 6H), −5.04 (s, 2H), −5.83 (s, 3H) ppm.

Synthesis of [UO_2(py)Zn(py)ZnI(py)(L)]

To a mixture of **[(py)$_3$LiOUO(py){Li(py)}$_2$(L)]** (24.2 mg, 0.017 mmol) and three equivalents of ZnI_2 (16.2 mg, 0.05 mmol) in a Teflon-tapped NMR tube at room

temperature was added pyridine (0.5 mL). Single crystals of **[UO_2(py)Zn(py)ZnI(py)(L)]** suitable for X-ray diffraction studies were grown from a saturated solution of pyridine at −35 °C.

^{1}H NMR (d_5-pyridine): δ_H 29.26 (s, 3H), 12.51 (s, 1H), 11.59 (s, 1H), 10.30 (s, 1H), 9.24 (s, 3H), 8.05 (s, 1H), 6.76 (s, 1H), 5.04 (s, 1H), 2.51 (s, 3H), 2.12 (s, 1H), 2.02 (s, 1H), 2.02 (s, 3H), 1.96 (s, 1H), 1.12 (s, 1H), 0.34 (s, 1H), 0.04 (s, 1H), −0.34 (s, 3H), −0.70 (s, 1H), −1.75 (s, 3H), −2.04 (s, 3H), −2.17 (s, 1H), −2.65 (s, 1H), −2.95 (s, 1H), −3.45 (s, 1H), −4.79 (s, 1H), −4.97 (s, 1H), −6.32 (s, 3H) ppm.

IR (Nujol mull, cm^{-1}): ν 1565, 1262, 1098, 1024, 892, 876, 803, 724.

6.6. Crystallographic details

X-ray diffraction data for **[$(py)_3$LiOUO(py)Li(py)(HL)]**, **[(Me_3SiO)UO(THF)$(ZnCl)_2$(L)]** and **[(py)I_2ZnOUO(THF)Zn(py)(HL)]** were collected at 100 K on an Oxford Diffraction Supernova diffractometer using mirror monochromated Cu-Kα radiation (λ = 1.54178 Å), X-ray diffraction data for **[$(py)_3$LiOUO(py){Li(py)}$_2$(L)]** and **[Li(THF)][$(THF)_2(Me_3Si)_2$NLiOUO(THF){Li(THF)}$_2$(L)]** were collected at 150 K on a Bruker SMART 1000 diffractometer equipped with a CCD area detector using graphite monochromated using Mo Kα radiation (λ = 0.71073 Å) and X-ray data for **[(Me_3SiO)UO(py)(H_2L)]**, **[(^{t}BuMe$_2$SiO)UO(py)(H_2L)]**, **[(py)$_2$IZnOUO(py)(H_2L)]**, **[UO_2(py)Zn(py)ZnI(py)(L)]**, **[UO_2(OHK)(HKL)]** and **[(py)Cl_2ZnOUO(py)Zn(py)(HL)]** were collected at 170 K using an Oxford Cryosystems low temperature device attached to an Oxford Diffraction Xcalibur Eos diffractometer equipped with an Eos detector and operating graphite monochromated Mo*K*α radiation (λ = 0.71073 Å). The following structures **[$(py)_3$LiOUO(py){Li(py)}$_2$(L)]**, **[Li(THF)][$(THF)_2(Me_3Si)_2$NLiOUO(THF){Li(THF)}$_2$(L)]**, **[(^{t}BuMe$_2$SiO)UO(py)(H_2L)]**, **[(Me_3SiO)UO(THF)$(ZnCl)_2$(L)]**, **[(py)Cl_2ZnOUO(py)Zn(py)(HL)]**, **[(py)$_2$IZnOUO(py)(H_2L)]**, **[UO_2(py)Zn(py)ZnI(py)(L)]**, **[(py)I_2ZnOUO(THF)Zn(py)(HL)]** were solved by SIR-92 and **[(Me_3SiO)UO(py)(H_2L)]** and **[UO_2(OHK)(HKL)]** structures were

solved by SHELXS-97, using the WinGX suite of programs, all structure were solved using direct methods and refined using a full-matrix least square refinement on $|F|^2$ using SHELX-97.Unless otherwise stated, all non-hydrogen atoms were refined with anisotropic displacement parameters and hydrogen atoms were placed using a riding model and refined with fixed isotropic displacement parameters. All hydrogen atoms were palced at calculated postion and were included as part of a riding model. The solvent of crystallisation in **$[UO_2(py)Zn(py)ZnI(py)(L)]$** was diffused and could not be modelled accurately so the corresponding electron density was accounted for using the SQUEEZE routine of PLATON. Two voids were found which equated to 5 molecules of pyridine in the unit cell. The solvent of crystallisation **$[(Me_3SiO)UO(THF)(ZnCl)_2(L)]$** was diffuse and could not be modelled accurately so the corresponding electron density was accounted for using the SQUEEZE routine of PLATON. Two voids were found which equated to 7 molecules of benzene in the unit cell. The structure of **$[(py)_3LiOUO(py)Li(py)(HL)]$** is disordered and has been solved by Prof Simon Parsons. The complex is disordered by a 180 deg rotation about the [010] direction. The Pacman ligand and one of the oxo ligands are common to both disorder components, but the U, Li, associated pyridine ligands and the second oxo ligand are all disordered. The relative weights of the two components are 0.78:0.22. One of the part-weight lithium sites (Li2 and Li2') is also at variance with the pseudo 2-fold symmetry. The U and ligand atoms of the main component were all refined freely with anisotropic displacement parameters. The Li atoms were both refined isotropically. Within the minor component only the U-atom was refined with apds, all other atoms were refined isotropically. The pyridine ligands of the minor component were all refined as rigid hexagons with a common isotropic displacement parameter applied to all six atoms. The O2-Li1'distance in the minor component was lightly restrained to 2.00(5) Ang. The Li1'-N(pyridine) bond distances were also lightly restrained to be equal, and the three Li1'-pyridine moieties restrained to be planar.

There is considerable overlap between the pyridine ligands attached to Li2 and Li2'. Similarly, there is overlap between two pairs of pyridine molecules (one pair based on N17 and N1H and another on N1C and N1C') which act as ligands is one component and solvent of crystallisation in the other.

The refinement statistics were insensitive to assignment of the C and N atoms of the non-ligating pyridine molecules. The model presented is based on location of some H-atoms in difference maps and minimisation of short H¨¨H contacts. The pyridine molecule based on N1B appears to 'point' into the cavity of the pacman ligand, which is suggestive of an alternative site for Li2'.There is, however, no evidence from Fourier difference syntheses to support this: there are no peaks within the ligand cavity which could be assigned as lithium, while the H-atom attached to C5B was clearly visible in the maps.

6.7. Raman spectroscopy

A couple of drops of Cu_2L (~1 mg, ~0.01 mmol) dissolved in pyridine (< 1 mL) were dropped onto a Klarite on a microscope slide. The pyridine was allowed to evaporate to leave a thin layer of Cu_2L on the slide. Complexes **[UO_2(py)(H_2L)]** (11 mg, 0.01 mmol) and **[(py)$_3$LiOUO(py)Li(py)(HL)]** (2.5 mg, 0.002 mmol) were prepared using the same methodology in an argon-filled glovebox. The lowering of the $D_{\infty h}$ symmetry of free uranyl group to C_i upon complexation and desymmetrisation should lead to a splitting of the uranyl symmetric stretch. The fluorescence of the ligand has previously hampered the acquisition of good quality Raman data, but the use of Klarite substrates has allowed the acquisition of the data shown below. We tentatively assign the strong absorption at 818 cm^{-1} in the starting material [**UO_2(py)(H_2L)]** and the split bands 796 and 817 cm^{-1} in the doubly lithiated complex **[(py)$_3$LiOUO(py)Li(py)(HL)]** as the symmetric $\nu^{s}_{U=O}$ stretch.

6.8. DFT calculations

Uranium was treated with a Stuttgart–Dresden pseudopotential in combination with the appropriate basis set. In all cases, the basis set was augmented by a set of polarization function (g for U). Carbon, oxygen, nitrogen, lithium and hydrogen atoms were described with a 6–31G(d,p) polarized double–ζ basis set. Calculations were carried out at the DFT level of theory using the hybrid functional

B3PW91. Geometry optimisations were carried out without any symmetry restrictions and the nature of the extrema (minima) was verified with analytical frequency calculations. For all transition states, the intrinsic reaction coordinate was followed to verify the direct connection between the transition state and adducts. All these computations were performed with the Gaussian 03 suite of programs. Gibbs free energies were obtained at 298.15 K within the harmonic approximation. The electronic density was analyzed using the Natural Bonding Analysis (NBO) technique.

Real Macrocycle: **Model used of Macrocycle**

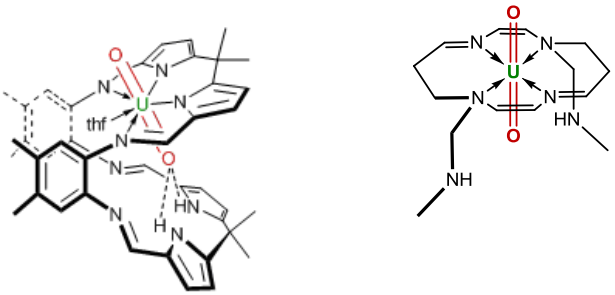

macrocycle used for the calculations

In the equatorial plane of uranyl, the real macrocycle and the model are quite similar with two nitrogens of deprotonated pyrrole groups and two nitrogens of macrocycle backbone in interaction with uranium of uranyl. The macrocycle model is closed in the equatorial plane with oxygen in order to model the interaction between one molecule of THF and the uranium in the real system. The bottom pocket of the real macrocycle is modelled by two arms with a secondary amine group in each arm. The two secondary amines groups of the macrocycle model corresponding to the two pyrroles in the bottom of the real macrocycle. This model has been used successfully in the modelling of the silylation reaction of uranyl.

Direct reduction of the [(OUO)Li_2L] intermediate by a lithium amide to form complex **4** was also investigated by computing the free energy of the reaction [(OUO)Li_2L] + $LiN(SiMe_3)_2$ $\rightarrow$ **4** + •$N(SiMe_3)_2$. The free energy of reaction is

computed to be 38.1 kcal.mol^{-1}, which is only 5.9 kcal.mol^{-1} more favourable than the formation of the C-H activation product. Thus, the two processes are indistinguishable from a computational viewpoint.

The pathway for the reaction of **2** with one equivalent of $LiN(SiMe_3)_2$ is show below; the difference between deprotonation and reduction pathways is too close to distinguish the two.

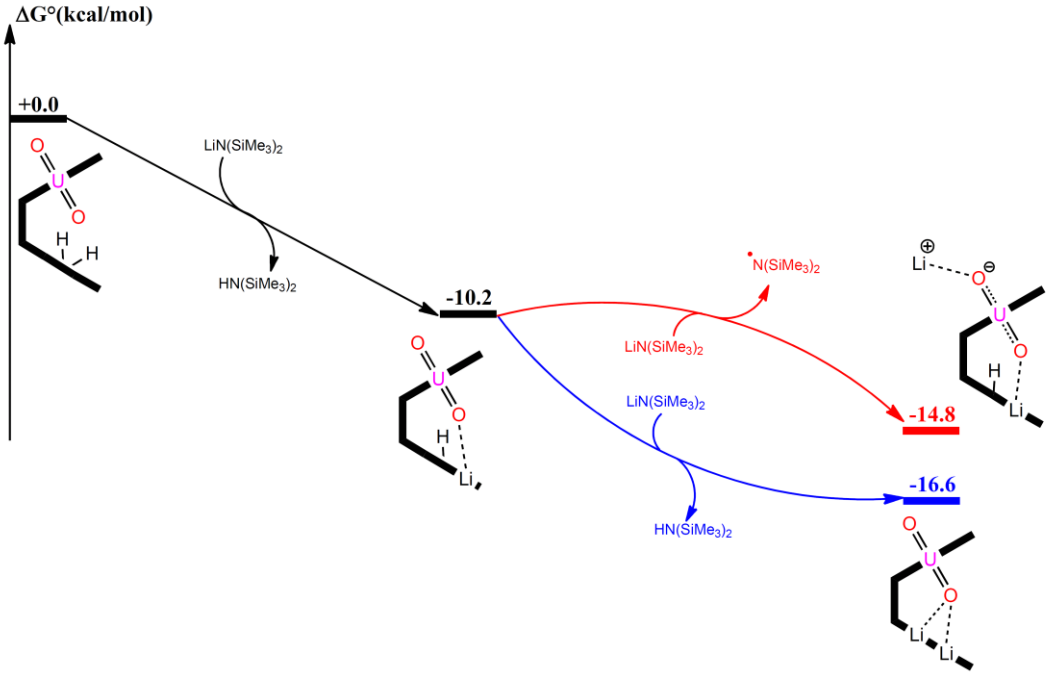

First lithiation, then either reduction or deprotonation (Paths A or B respectively)

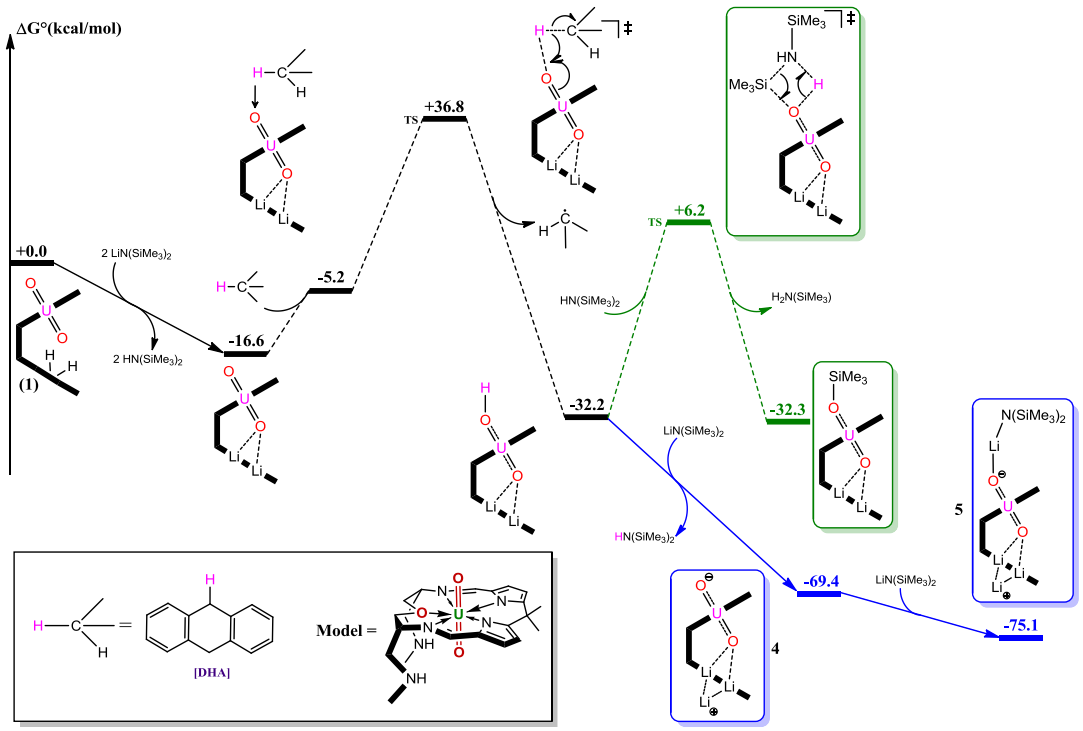

Full pathway with oxo-C-H activation computed.

A molecular picture of the transition state calculated for the C-H abstraction mechanism, best described as a proton transfer between DHA and the exo-oxo group of uranyl(VI), is shown in the figure below.

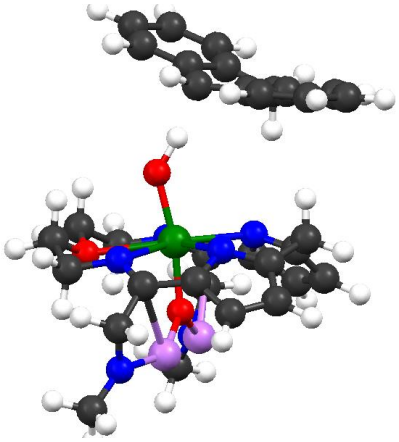

Calculated structure of the transition state of C-H activation of DHA. Green = U; purple = Li; red = O; blue = N; grey = C; white = H.

Optimised structures

DHA

HF=-540.5478773
G=-540.365224

C	0.030349	0.000000	0.045456
C	0.051500	0.000000	1.446945
C	1.247420	0.000000	2.151951
C	2.443925	0.000000	0.065736
C	2.456316	0.000000	1.453970
C	1.240980	0.000000	-0.653626
C	1.293269	0.000000	-2.161210
C	-0.038379	0.000000	-2.868771
C	-0.059770	0.000000	-4.270316
C	-1.255598	0.000000	-4.975321
C	-2.464530	0.000000	-4.277341
C	-2.452137	0.000000	-2.889113
C	-1.249270	0.000000	-2.169716
C	-1.301769	0.000000	-0.662586
H	-1.881566	0.872107	-0.327516
H	-1.881566	-0.872107	-0.327516
H	-0.892940	0.000000	1.987636
H	1.239830	0.000000	3.238344
H	3.400902	0.000000	1.990689
H	3.384436	0.000000	-0.481792
H	0.884735	0.000000	-4.810936
H	-1.247763	0.000000	-6.061714
H	-3.409228	0.000000	-4.813901
H	-3.392672	0.000000	-2.341640
H	1.873384	-0.872046	-2.495979
H	1.873384	0.872045	-2.495979

DHA radical

HF=-539.918053
G=-539.748917

C	-0.004254	-0.016154	0.066293
C	0.047968	0.025804	1.457180
C	1.264243	0.007465	2.138839
C	2.433265	-0.095522	0.035431
C	2.462145	-0.054440	1.418328
C	1.207462	-0.076439	-0.671888
C	1.175003	-0.112095	-2.093404
C	-0.040228	-0.076137	-2.832125
C	-0.040024	-0.095213	-4.247214
C	-1.223290	-0.054426	-4.963822
C	-2.445951	0.007371	-4.286394
C	-2.463540	0.025898	-2.892091
C	-1.285134	-0.015910	-2.151426
C	-1.336537	-0.005716	-0.643015
H	-1.913032	0.870189	-0.309842
H	-1.925355	-0.871584	-0.303036
H	-0.881984	0.073163	2.020523
H	1.279278	0.041136	3.224302
H	3.413518	-0.069839	1.942731
H	3.360573	-0.142497	-0.530451
H	0.913524	-0.142000	-4.767692
H	-1.201545	-0.069770	-6.049931
H	-3.378757	0.040865	-4.841675
H	-3.416464	0.073480	-2.368525
H	2.115459	-0.159349	-2.636754

LiN(SiMe3)2

HF=-309.595098
G=-309.408429

N	0.272498	0.000000	0.195764
Si	0.051370	0.000000	1.907502
Si	1.672584	0.000000	-0.787373
Li	-0.876900	0.000000	-1.202126
C	0.972120	0.000000	-2.609781
C	2.789004	1.535425	-0.681451
C	2.789004	-1.535424	-0.681451
H	1.806907	0.000000	-3.317691
H	0.387189	-0.900056	-2.865449
H	0.387189	0.900055	-2.865449
H	3.589905	-1.509139	-1.429249
H	3.258745	-1.598592	0.305854
H	2.210318	-2.453201	-0.829743
H	3.589905	1.509139	-1.429249
H	2.210318	2.453201	-0.829743
H	3.258745	1.598593	0.305853
C	1.671983	0.000000	2.910737
C	-0.945531	1.531082	2.451572
C	-0.945532	-1.531082	2.451572
H	-1.129310	-1.535476	3.532140
H	-1.921125	-1.565313	1.951130
H	-0.410871	-2.452483	2.196270
H	1.463831	0.000000	3.986878
H	2.278878	-0.885611	2.693023
H	2.278878	0.885610	2.693023
H	-1.129310	1.535476	3.532140
H	-0.410870	2.452483	2.196270
H	-1.921124	1.565314	1.951130

HN(SiMe3)2

HF=-302.667305
G=-302.470110

N	0.300598	0.000000	0.172266
Si	0.037853	0.000000	1.914574
Si	1.710071	0.000000	-0.886579
H	-0.564824	0.000000	-0.356613
C	1.034082	0.000000	-2.657270
C	2.786004	1.538906	-0.634841
C	2.786004	-1.538907	-0.634841
H	1.855268	0.000000	-3.381750
H	0.421442	-0.886790	-2.851871
H	0.421443	0.886791	-2.851871
H	3.621773	-1.543529	-1.343636
H	3.209542	-1.579065	0.373654
H	2.202495	-2.451563	-0.792202
H	3.621774	1.543528	-1.343635
H	2.202496	2.451563	-0.792201
H	3.209543	1.579064	0.373654
C	1.705090	0.000001	2.806081
C	-0.948572	1.538393	2.418056
C	-0.948571	-1.538394	2.418056
H	-1.158789	-1.539745	3.493410
H	-1.909574	-1.584798	1.893907
H	-0.393584	-2.451006	2.178560
H	1.542465	0.000001	3.889410
H	2.297206	-0.887138	2.562154
H	2.297206	0.887139	2.562154
H	-1.158790	1.539745	3.493410
H	-0.393585	2.451006	2.178560
H	-1.909575	1.584797	1.893907

H2N(SiMe3)

HF=-179.602021
G=-179.497083

N	0.447345	-0.057674	0.264183
H	-0.358708	0.136230	0.845106
H	3.501846	0.014864	-0.459196
Si	1.392563	1.330235	-0.270045
C	2.921817	0.642707	-1.142217
C	0.472929	2.495541	-1.455329
H	2.650885	0.034274	-2.011996
H	0.169619	1.975472	-2.370489
H	-0.429282	2.906687	-0.989591
H	1.109708	3.338387	-1.747651
H	3.568999	1.451780	-1.496904
C	1.874048	2.288348	1.286471
H	0.990515	2.628194	1.837785
H	2.468096	1.659455	1.956318
H	2.465467	3.175039	1.035054
H	0.189124	-0.734204	-0.443218

(1)

HF=-1344.9971186
G=-1344.609840

N	3.551963	-1.404270	-0.178348
C	3.159687	-0.600796	0.825197
C	1.750263	-0.518744	0.834992
C	1.285018	-1.285152	-0.237378
C	2.425382	-1.814568	-0.881540
C	4.157910	0.049298	1.766851
C	5.315819	0.808209	1.142830
C	5.785748	2.106697	1.437103
C	6.870570	2.354417	0.590933
C	7.034309	1.199631	-0.205856
N	6.087406	0.261645	0.188058
U	5.456486	-1.192471	-1.575909
O	6.223860	-1.844104	-3.905372
C	5.630739	-3.130808	-4.180750
C	4.108995	-3.053635	-3.992539
H	3.666453	-2.371436	-4.729469
C	7.811831	0.968714	-1.391466
N	7.587056	-0.120812	-2.092106
C	8.133024	-0.412179	-3.405663
C	7.666027	-1.794782	-3.882840
C	2.577469	-2.455410	-2.158350
N	3.787919	-2.616356	-2.645417
O	6.297992	-2.609158	-0.949774
O	4.659815	0.180478	-2.328731
H	7.832136	0.362599	-4.122254
H	0.250187	-1.427010	-0.522744
H	1.148414	0.033408	1.546151
H	5.379205	2.778314	2.183096
H	7.456139	3.264247	0.548696
H	3.614003	0.733298	2.425088
H	4.573897	-0.734171	2.418983
C	1.339432	-2.824712	-2.947360
C	8.785177	2.031633	-1.853437
H	3.713076	-4.057985	-4.211991
H	5.861744	-3.419541	-5.214608
H	6.063294	-3.873111	-3.495754
H	8.035325	-2.576522	-3.204839
H	8.048643	-1.986471	-4.893990
H	9.234486	-0.434131	-3.406378
H	1.469411	-3.839149	-3.350181
H	0.467171	-2.868657	-2.274126
N	1.169832	-1.910570	-4.069429
H	1.118990	-0.961655	-3.710268
C	-0.010895	-2.204162	-4.863366
H	-0.118439	-1.451486	-5.649703
H	0.108184	-3.178348	-5.351803
H	-0.951935	-2.236658	-4.285132
H	9.727166	1.543246	-2.140568
N	8.257757	2.719689	-3.025049
H	9.028691	2.705304	-1.014905
H	7.350833	3.112578	-2.790050
C	9.140974	3.767418	-3.507985
H	8.667015	4.287340	-4.345520
H	9.415104	4.518644	-2.745500
H	10.071174	3.321379	-3.878829

(2)

HF=-1358.878757
G=-1358.513047

C	5.453788	-0.942805	3.604185
C	5.302356	-0.609520	2.244569
N	6.157277	-1.337976	1.494472
C	6.836936	-2.206392	2.347690
C	6.420038	-1.954399	3.674385
C	4.297907	0.312368	1.587049
C	3.283956	-0.439561	0.751310
N	3.671583	-1.124958	-0.346788
C	2.571397	-1.846633	-0.807566
C	1.457769	-1.542552	0.008254
C	1.912567	-0.651281	0.989037
U	5.515725	-2.598428	-0.397467
O	6.450881	-1.672966	-1.554042
C	2.723386	-2.922580	-1.752775
N	3.947697	-3.248430	-2.137165
C	4.195146	-4.489163	-2.852245
C	5.695268	-4.734267	-2.943402
O	6.230942	-4.710694	-1.607699
C	7.652971	-4.902492	-1.492365
C	8.021888	-4.813922	-0.017682
N	7.547020	-3.554214	0.530351
C	7.573642	-3.331701	1.835626
C	8.060111	-4.361326	2.834162
N	6.930595	-5.241706	3.023568
C	7.343757	-6.512000	3.558043
O	4.550867	-3.658814	0.789050
C	1.518885	-3.808006	-1.995846
N	1.560454	-4.768593	-0.917340
C	0.816585	-5.955789	-1.245717
Li	2.620515	-4.077785	0.439610
Li	5.399685	-4.366107	2.453645
H	7.566782	-5.644209	0.545817
H	3.701826	-5.317103	-2.318604
H	6.782507	-2.456260	4.561787
H	4.923108	-0.492438	4.433557
H	1.325953	-0.200437	1.779602
H	0.455129	-1.931396	-0.111791
H	3.775714	0.886141	2.357408
H	4.829881	1.031067	0.949997

H 9.113487 -4.914084 0.067805
H 7.917863 -5.887933 -1.896064
H 8.165555 -4.124909 -2.075162
H 6.187030 -3.952042 -3.537627
H 5.898079 -5.712733 -3.396998
H 3.789675 -4.463610 -3.873895
H 8.945101 -4.874983 2.404703
H 8.437118 -3.859814 3.749380
H 6.479189 -7.181797 3.650282
H 8.093018 -7.040945 2.930864
H 7.800721 -6.442412 4.566790
H 1.621302 -4.274201 -2.997236
H 0.596692 -3.194100 -2.058741
H 0.908085 -6.694010 0.438725
H -0.268658 -5.774581 -1.389057
H 1.157997 -6.455426 2.177278

(3)DHA

HF=-1899.422516
G=-1898.860273

C 4.967560 -1.862390 1.115034
C 3.922493 -0.939989 1.192931
C 2.694597 -1.235150 0.581784
C 2.536928 -2.446180 0.094716
C 3.586872 -3.358897 0.176215
C 4.806628 -3.065944 0.431059
C 1.579730 -0.220488 0.677910
C 1.569620 0.479400 2.016274
C 2.798812 0.779528 2.623679
C 4.071035 0.378798 1.914479
C 0.380923 0.838263 2.655305
C 0.402580 1.499082 3.882607
C 1.623270 1.801260 4.484129
C 2.813300 1.437293 3.855875
O 4.722867 2.971516 0.854113
U 3.862777 4.373030 1.463637
O 3.007940 5.863315 2.177426
N 3.540534 5.388532 0.641582
C 2.326550 5.603032 1.194447
C 2.208875 6.952498 1.580367
C 3.395425 7.594136 1.204297
C 4.211296 6.610372 0.599519
C 1.287810 4.502969 1.228413
C 0.835070 4.097015 -0.157617
N 1.699099 3.530364 -1.029789
C 1.053707 3.428418 -2.262057
C -0.272351 3.895921 -2.117590
C -0.405690 4.313434 -0.787101
C 5.380146 6.795931 -0.219020
N 5.776261 5.787920 -0.981734
C 6.759186 5.994753 -2.031924
C 6.841533 4.750994 -2.906092
O 5.516769 4.457355 -3.385922
C 5.391201 3.288835 -4.217129
C 3.925329 3.140561 -4.599945
N 3.110290 3.106111 -3.397541
C 1.790618 3.182015 -3.474071
C 1.048223 3.343743 -4.784238
N 1.115757 4.760233 -5.059126
C 0.903605 5.032755 -6.455913
C 5.886960 8.211774 -0.397460
N 5.087595 8.747083 -1.475099
C 5.730153 9.879197 -2.087997
Li 3.557670 7.711831 -1.634099
Li 1.495323 5.647317 -3.474371
H 3.603793 3.985962 -5.228858
H 6.464326 6.869818 -2.633025
H -1.025959 3.923616 -2.893707
H -1.293033 4.722198 -0.320263
H 1.358745 7.399600 2.080061
H 3.650188 8.636992 1.339970
H 0.421787 4.844889 1.801039
H 1.693625 3.628141 1.751949
H 3.818020 2.222784 -5.195625
H 6.012103 3.414808 -5.113148
H 5.742486 2.412818 -3.655012
H 7.212360 3.889433 -2.334059
H 7.504981 4.926135 -3.762542
H 7.760899 6.193994 -1.624702
H 1.555023 2.726691 -5.554579
H 0.027090 2.916940 -4.702687
H 1.019216 6.106256 -6.653016
H 1.613274 4.505469 -7.128581
H -0.107693 4.750853 -6.815320
H 6.969257 8.169761 -0.638119
H 5.829028 8.763081 0.563847
H 5.132967 10.239660 -2.935351
H 5.860544 10.741251 -1.401642
H 6.745552 9.659976 -2.482033
H 4.327138 1.157756 1.179096
H 4.907393 0.339213 2.620515
H -0.570273 0.594395 2.187097
H -0.530125 1.768875 4.370747
H 1.650213 2.309725 5.444108
H 3.766698 1.662650 4.328768
H 1.580437 -2.676877 -0.559087
H 3.449519 -4.298704 -0.704237
H 5.627996 -3.775675 0.380326
H 5.915668 -1.635836 1.598220
H 0.610846 -0.692695 0.483424
H 1.716050 0.536958 -0.110572

(4)DHA

HF=-1899.352016
G=-1898.793212

C 5.111879 -1.042244 0.041253
C 3.995438 -0.369055 0.579351
C 2.696664 -0.823396 0.243148
C 2.553258 -1.932940 -0.586200
C 3.666560 -2.591921 -1.108105
C 4.950847 -2.138897 -0.792705
C 1.497588 -0.062442 0.748957
C 1.740463 0.699382 2.026357
C 3.050515 1.150665 2.321317
C 4.149053 0.773899 1.455940
C 0.696845 1.012357 2.894109
C 0.915587 1.784647 4.035860
C 2.200863 2.257084 4.317049
C 3.254353 1.942163 3.470667
O 4.521415 2.621936 -0.381528
U 3.654787 4.171380 -1.157115
O 3.027809 5.680683 -2.158798
N 3.210270 5.403913 0.805970
C 1.969155 5.736925 1.225643
C 1.923766 7.108328 1.538914
C 3.187149 7.637641 1.250527
C 3.975619 6.568221 0.771461
C 0.852680 4.713262 1.232756
C 0.488481 4.213252 -0.150202
N 1.383257 3.531416 -0.901120
C 0.821068 3.344402 -2.163982
C -0.487430 3.874203 -2.158088
C -0.693913 4.419332 -0.885438
C 5.222062 6.610911 0.050378
N 5.613763 5.525233 -0.588100
C 6.696292 5.556979 -1.560362
C 6.745728 4.234861 -2.321423
O 5.465379 4.010568 -2.939947
C 5.313404 2.763750 -3.642901
C 3.884530 2.677446 -4.172830
N 2.939812 2.830722 -3.075919
C 1.641997 2.955163 -3.280690
C 1.045381 3.034024 -4.669638
N 1.271334 4.394603 -5.097263
C 1.075290 4.538033 -6.511577
C 5.856051 7.963347 -0.204768
N 5.247584 8.459782 -1.416093
C 5.899249 9.658014 -1.861683
Li 3.720624 7.427187 -1.764599
Li 1.779073 5.402487 -3.592548
H 3.707731 3.457400 -4.928275
H 6.546133 6.399169 -2.254472
H -1.181448 3.872934 -2.988296
H -1.589375 4.911199 -0.526628
H 1.068474 7.645031 1.929946
H 3.502930 8.667153 1.357697
H -0.033881 5.158942 1.692295
H 1.146817 3.862465 1.860940
H 3.774674 1.703085 -4.670299
H 6.028084 2.728366 -4.475494
H 5.522730 1.937457 -2.950410
H 6.958050 3.401329 -1.638027
H 7.520425 4.273099 -3.098254
H 7.674513 5.698541 -1.077754
H 1.552092 2.286842 -5.316141
H -0.018976 2.723243 -4.653218
H 1.279533 5.570595 -6.820446
H 1.732322 3.881222 -7.120998
H 0.041252 4.303098 -6.839871
H 6.956797 7.834950 -0.288537
H 5.713187 8.617261 0.680581
H 5.442595 10.015847 -2.792819
H 5.840487 10.494358 -1.133133
H 6.983491 9.522849 -2.063691
H 4.275276 1.885309 0.407326
H 5.151506 0.946305 1.852126
H -0.304375 0.649120 2.672260
H 0.088926 2.016645 4.701379
H 2.378867 2.862462 5.201435
H 4.258230 2.294509 3.694669
H 1.553859 -2.287037 -0.830321
H 3.533520 -3.456183 -1.752690
H 5.822841 -2.650813 -1.190761
H 6.109171 -0.696221 0.303051
H 0.636939 -0.732578 0.859025
H 1.209003 0.670047 -0.023957

(5)

HF=-1359.5256488
G=-1359.154250

C 1.931206 -0.780661 0.993276
C 3.292074 -0.533657 0.713100
N 3.654563 -1.165520 -0.420938
C 2.560869 -1.895589 -0.865337
C 1.462914 -1.642983 -0.003159
C 4.317992 0.210100 1.550188
C 5.334537 -0.703533 2.211402
C 5.438308 -1.073930 3.568526
C 6.430463 -2.056820 3.645327
C 6.903258 -2.256034 2.323390
N 6.241398 -1.378110 1.475309
U 5.576126 -2.641321 -0.482100
O 4.530210 -3.837049 0.799342
C 7.641913 -3.382484 1.798609
C 8.093446 -4.435068 2.795112
N 6.950218 -5.273596 3.071538
C 7.293752 -6.395916 3.892749
C 2.723135 -2.970719 -1.816645
C 1.530665 -3.884887 -2.032981
N 1.503920 -4.814539 -0.927545
C 0.498272 -5.820675 -1.096138
O 6.761932 -1.636167 -1.940493
N 3.928507 -3.266026 -2.242732
C 4.249146 -4.479838 -2.978502
C 5.768193 -4.665906 -3.043105
O 6.291951 -4.767638 -1.706266
C 7.725648 -4.838910 -1.597832
C 8.123852 -4.813563 -0.118741
N 7.662254 -3.580511 0.501977
Li 5.382756 -4.367358 2.330434
Li 2.766059 -4.139613 0.410748
H 7.703796 -5.694569 0.387620
H 3.792340 -5.363155 -2.509471
H 6.767265 -2.570832 4.536721
H 4.859216 -0.669071 4.389344
H 1.363035 -0.374358 1.821046
H 0.461474 -2.043886 -0.096551
H 3.798591 0.783826 2.323518
H 4.844814 0.932469 0.913331
H 9.220227 -4.904478 -0.083332
H 8.077800 -5.770245 -2.061957
H 8.163493 -3.979634 -2.122789
H 6.233473 -3.805077 -3.541639
H 6.007947 -5.583412 -3.597705
H 3.890432 -4.435357 -4.018116
H 8.945255 -5.006455 2.379958
H 8.488618 -3.944799 3.706130
H 6.413658 -7.022384 4.072173
H 8.074506 -7.036787 3.437891
H 7.696443 -6.095547 4.880587
H 1.617798 -4.395636 -3.010572
H 0.603539 -3.283177 -2.100838
H 0.510966 -6.519516 -0.253214
H -0.523139 -5.396283 -1.162919
H 0.634371 -6.410592 -2.023725
H 7.112191 -0.744504 -2.036247

(6)

HF=-1662.158814
G=-1661.560813

N 3.591151 -1.380923 -0.554777
C 3.019393 -0.739351 0.491108
C 1.646910 -1.045685 0.549324
C 1.385086 -1.953473 -0.483483
C 2.611605 -2.172224 -1.150160
C 3.853284 0.086601 1.450485
C 4.854244 -0.731025 2.242205
N 5.862929 -1.383640 1.621925
C 6.504550 -2.173049 2.574067
C 5.903675 -1.940124 3.831221
C 4.863415 -1.026382 3.616845
U 5.562757 -2.710913 -0.315966
O 6.587546 -1.583466 -1.480313

C 7.366156 -3.265614 2.191701
C 7.765562 -4.248382 3.274013
N 6.683732 -5.203701 3.327097
C 7.096664 -6.407778 3.994286
C 2.967719 -3.242898 - 2.044875
C 1.892477 -4.247087 - 2.404022
N 1.936210 -5.239609 - 1.357762
C 1.260121 -6.440714 - 1.767400
N 7.529058 -3.525285 0.903756
C 8.074877 -4.808211 0.487062
C 7.896766 -4.997222 - 1.015111
O 6.503311 -4.841490 - 1.343667
C 6.169962 -4.917682 - 2.737381
C 4.665918 -4.719798 - 2.892164
N 4.253272 -3.454845 - 2.295822
O 4.511065 -3.876296 0.776965
Li 5.195020 -4.454385 2.499867
Li 2.836658 -4.573058 0.128428
N 5.861232 -0.468254 - 3.626347
Si 7.680581 -0.326145 - 2.560063
C 7.533807 1.176971 - 1.428919
Si 4.636417 0.883772 - 3.997636
C 4.009145 1.605067 - 2.388231
C 5.463880 2.182121 - 5.083161
C 3.249517 0.025191 - 4.945607
C 9.150977 -1.465809 - 2.107954
C 8.440252 0.326985 - 4.217385
H 7.562038 -5.607990 1.048021
H 4.117526 -5.538472 - 2.395772
H 6.188397 -2.400148 4.768125
H 4.188932 -0.622345 4.361513
H 0.936640 -0.654756 1.267217
H 0.438838 -2.422608 - 0.718529
H 3.184528 0.598637 2.148265
H 4.385235 0.866692 0.888924
H 9.149712 -4.892961 0.706308
H 8.225231 -6.002029 - 1.311403
H 8.476777 -4.251743 - 1.574666
H 6.732927 -4.143427 - 3.279935
H 6.461292 -5.901590 -3.128325
H 4.429983 -4.769564 -3.966084
H 8.735969 -4.705782 2.982207
H 7.980683 -3.713074 4.222968
H 6.279323 -7.141085 3.991943
H 7.973583 -6.906351 3.524642
H 7.382712 -6.256301 5.057130
H 2.133011 -4.662048 -3.408067
H 0.915277 -3.735885 -2.538508
H 1.330772 -7.202354 -0.979752
H 0.177817 -6.298108 -1.973372
H 1.675764 -6.898889 -2.692278
H 9.436945 0.727770 -3.999436
H 8.589379 -0.481464 -4.946155
H 7.865150 1.116495 -4.707274
H 8.548086 1.468060 -1.132600
H 7.085903 2.036524 -1.935161
H 6.969208 0.953780 -0.521509
H 10.094118 -0.939186 -2.292317
H 9.105465 -1.787465 -1.065415
H 9.156743 -2.358077 -2.745672
H 4.701987 2.907216 -5.391617
H 6.244438 2.730412 -4.548930
H 5.899129 1.756449 -5.992359
H 3.155139 2.257934 -2.599820
H 3.675197 0.807492 -1.718349
H 4.770704 2.197699 -1.876209
H 2.490071 0.757044 -5.241719
H 3.611793 -0.461577 -5.857221
H 2.758934 -0.728813 -4.322270
H 6.137955 -0.858588 -4.528356
H 5.351447 -1.213494 -3.140180

(7)

HF=-1482.593379
G=-1482.127359

C 2.167416 -0.449496 0.556046
C 3.553411 -0.391256 0.331919
N 3.891413 -1.225601 -0.679883
C 2.734957 -1.893142 -1.082922
C 1.646792 -1.400349 -0.331674
C 4.615239 0.364458 1.102866
C 5.577543 -0.546039 1.835452
C 5.744012 -0.729394 3.218559
C 6.649991 -1.784586 3.387428
C 7.018756 -2.213605 2.094617
N 6.373546 -1.407201 1.157125
U 5.614577 -2.818803 -0.564867
O 4.567402 -3.735940 0.757688
C 7.662334 -3.442391 1.708887
C 8.088179 -4.388186 2.812227
N 6.920294 -5.192435 3.081190
C 7.278067 -6.408171 3.761891
C 2.800707 -3.081021 -1.894394
C 1.534745 -3.898213 -2.044749
N 1.525959 -4.776106 -0.899086
C 0.653877 -5.899223 -1.116457
O 6.738072 -1.962822 -1.997315
N 3.993916 -3.545691 -2.233281
C 4.130386 -4.884263 -2.783266
C 5.602826 -5.268456 -2.844341
O 6.164228 -5.105018 -1.530654
C 7.562705 -5.410357 -1.397019
C 7.963459 -5.165167 0.051222
N 7.603562 -3.810768 0.437914
Li 5.407346 -4.357938 2.385780
Li 2.707915 -4.140178 0.391499
H 7.452438 -5.874808 0.722981
H 3.568851 -5.589785 -2.148846
H 6.994622 -2.208560 4.321208
H 5.256910 -0.159531 3.999797
H 1.614800 0.131894 1.283328
H 0.615855 -1.715611 -0.422242
H 4.126667 1.021298 1.827699
H 5.176932 1.009481 0.414235
H 9.044503 -5.346348 0.140880
H 7.730846 -6.460371 -1.668856
H 8.134886 -4.768217 -2.081374
H 6.150515 -4.626670 -3.548847
H 5.712326 -6.315049 -3.156359
H 3.718208 -4.955852 -3.800357
H 8.950498 -4.984110 2.443518
H 8.488559 -3.816675 3.675290
H 6.387776 -7.032010 3.915021
H 8.014747 -7.032477 3.210387
H 7.725815 -6.243394 4.764295
H 1.587911 -4.444770 -3.010736
H 0.654378 -3.230035 -2.146064
H 0.693682 -6.580644 -0.256586
H -0.411970 -5.617822 -1.248200
H 0.910912 -6.502800 -2.014387
Si 7.528856 -0.702275 -2.856421
C 7.168238 0.935615 -2.003635
C 9.371314 -1.098857 -2.826168
C 6.841807 -0.728540 -4.611108
H 9.944150 -0.323891 -3.347038
H 9.734685 -1.156697 -1.795614
H 9.577284 -2.055650 -3.316053
H 7.684752 1.757235 -2.511788
H 6.095078 1.148834 -2.016871
H 7.506181 0.910338 -0.963252
H 7.293880 0.063160 -5.218480
H 7.044846 -1.686233 -5.100219
H 5.758642 -0.573471 -4.600248

(8)

HF=-1366.521512
G=-1366.151837

N 6.276396 -1.243131 1.472526
C 5.360322 -0.571724 2.197638
C 5.434230 -0.969423 3.551577
C 6.423853 -1.960195 3.630814
C 6.920272 -2.139910 2.312897
C 4.350579 0.340054 1.526436
C 3.313784 -0.425532 0.724556
C 1.968482 -0.695343 1.040449
C 1.494638 -1.590067 0.069578
C 2.572820 -1.839812 -0.812286
N 3.663478 -1.080058 -0.402795
U 5.662507 -2.372028 -0.598031
N 7.771394 -3.374371 0.463330
C 8.326933 -4.571802 -0.154387
C 7.791330 -4.718126 -1.573984
O 6.346767 -4.755899 -1.509933
C 5.699864 -4.829642 -2.813947
C 4.203568 -4.581395 -2.686674
N 3.944007 -3.258230 -2.146006
C 2.733662 -2.962348 -1.710342
C 1.584535 -3.949575 -1.804824
N 1.782804 -4.858567 -0.695307
C 0.970735 -6.033662 -0.851353
C 7.613432 -3.288871 1.765043
C 7.757937 -4.500657 2.667655
N 6.496443 -5.229032 2.500578
C 6.487621 -6.379700 3.384316
O 4.739015 -3.569852 0.680886
O 6.545985 -1.414839 -1.812290
Li 5.740416 -5.214986 0.679765
Li 2.823218 -3.878153 0.485976
H 8.107417 -5.488598 0.415848
H 3.724773 -5.331717 -2.030204
H 6.762882 -2.467335 4.526455
H 4.859559 -0.558523 4.372560
H 1.408515 -0.278482 1.868543
H 0.502513 -2.017507 0.003559
H 3.845136 0.939734 2.288925
H 4.881299 1.035781 0.864580
H 9.421079 -4.496614 -0.227455
H 8.160127 -5.644407 -2.032634
H 8.092065 -3.863088 -2.192949
H 6.163276 -4.068582 -3.455396
H 5.889295 -5.823053 -3.238602
H 3.777219 -4.714704 -3.692779
H 8.653689 -5.089898 2.390163
H 7.937846 -4.181865 3.710912
H 5.540755 -6.927400 3.285540
H 7.300023 -7.103667 3.175702
H 6.591926 -6.112804 4.454835
H 1.640020 -4.449319 -2.796488
H 0.610611 -3.416948 -1.812759
H 1.140667 -6.726463 -0.016300
H -0.120425 -5.824836 -0.871513
H 1.174896 -6.603782 -1.784712
Li 5.230875 -3.662938 2.553391

(9)

HF=-1676.1420001
G=-1675.569284

N 2.314367 -2.185818 -0.294674
C 1.519642 -2.016463 0.784592
C 0.473175 -2.956481 0.761433
C 0.668443 -3.757032 -0.374066
C 1.835977 -3.278145 -1.012610
C 1.891924 -1.017989 1.863827
C 3.136299 -1.428266 2.626748
N 4.349672 -1.421237 2.035663
C 5.253125 -2.029598 2.896940
C 4.577040 -2.360877 4.099166
C 3.238739 -1.980849 3.921907
U 4.673851 -2.306787 -0.186879
O 5.046892 -0.753010 -1.071580
C 6.505618 -2.552249 2.393632
C 7.153731 -3.672582 3.185008
N 6.495367 -4.885756 2.687217
C 6.985530 -6.035880 3.426939
C 2.665121 -3.967420 -1.973767
C 2.200151 -5.333850 -2.439446
N 2.681076 -6.247278 -1.423055
C 2.673756 -7.601915 -1.907365
N 6.841193 -2.301282 1.147002
C 8.026034 -2.906878 0.547989
C 7.837827 -3.027671 -0.958066
O 6.610052 -3.760826 -1.196834
C 6.285795 -3.909012 -2.611254
C 4.870632 -4.439393 -2.779538
N 3.905515 -3.547113 -2.159734
O 4.359075 -4.024772 0.716963
Li 2.903215 -5.191069 0.078512
Li 6.095781 -4.909122 0.762389
Li 4.603468 -4.221719 2.651997
H 8.255175 -3.897172 0.971674
H 4.760062 -5.442539 -2.327581
H 5.016013 -2.790227 4.991993
H 2.439853 -2.059857 4.648707
H -0.334623 -3.032621 1.478508
H 0.053650 -4.583854 -0.704736
H 1.058710 -0.916937 2.564604
H 2.054565 -0.032555 1.409778
H 8.907781 -2.274085 0.717218
H 8.677259 -3.569388 -1.410729
H 7.757663 -2.039642 -1.426884
H 6.392446 -2.922748 -3.080911
H 7.009818 -4.598085 -3.061945
H 4.701253 -4.552998 -3.860806
H 8.251033 -3.669032 3.043216
H 7.003911 -3.512177 4.268024
H 6.491630 -6.951487 3.075177
H 8.075521 -6.196924 3.318687
H 6.797642 -5.970061 4.516429
H 2.639159 -5.524708 -3.441503
H 1.103489 -5.339546 -2.604887
H 3.065510 -8.281049 -1.138743
H 1.662496 -7.974040 -2.173057
H 3.292408 -7.758665 -2.817472

Li 5.616863 1.045332 -1.223839
N 6.582935 2.588633 -1.550673
Si 8.158421 2.503446 -2.215249
Si 5.602788 3.930440 -1.124720
C 5.227943 5.150144 -2.542346
C 3.908435 3.221896 -0.558650
C 6.249179 4.971462 0.337984
C 8.295337 3.103511 -4.022012
C 9.507338 3.426604 -1.229281
C 8.689655 0.657873 -2.236100
H 10.505219 3.250271 -1.648386
H 9.331982 4.508036 -1.238561
H 9.515261 3.104018 -0.182517
H 9.686264 0.517993 -2.669993
H 8.707803 0.262557 -1.212469
H 7.982233 0.064688 -2.830796
H 9.302854 2.949235 -4.426719
H 7.585951 2.567751 -4.662541
H 8.064514 4.171307 -4.100826
H 3.216373 4.022923 -0.275300
H 3.418918 2.649041 -1.358121
H 4.014613 2.572566 0.321761
H 4.522073 5.928403 -2.228936
H 6.141604 5.649630 -2.883511
H 4.797503 4.627004 -3.403097
H 5.535140 5.753987 0.621068
H 6.427130 4.340314 1.215624
H 7.196688 5.460366 0.087031

6.9. References

(1) Becke, A. D. *The Journal of Chemical Physics* **1993**, *98*, 5648.
(2) Reed, A. E.; Curtiss, L. A.; Weinhold, F. *Chem. Rev.* **1988**, *88*, 899.
(3) Littler, B. J.; Miller, M. A.; Hung, C.-H.; Wagner, R. W.; O'Shea, D. F.; Boyle, P. D.; Lindsey, J. S. *The Journal of Organic Chemistry* **1999**, *64*, 1391.
(4) Love, J. B.; Blake, A. J.; Wilson, C.; Reid, S. D.; Novak, A.; Hitchcock, P. B. *Chem. Commun.* **2003**, 1682.
(5) Givaja, G.; Volpe, M.; Leeland, J. W.; Edwards, M. A.; Young, T. K.; Darby, S. B.; Reid, S. D.; Blake, A. J.; Wilson, C.; Wolowska, J.; McInnes, E. J. L.; Schröder, M.; Love, J. B. *Chemistry – A European Journal* **2007**, *13*, 3707.
(6) Wilkerson, M. P.; Burns, C. J.; Paine, R. T.; Scott, B. L. *Inorg. Chem.* **1999**, *38*, 4156.
(7) Barnhart, D. M.; Burns, C. J.; Sauer, N. N.; Watkin, J. G. *Inorg. Chem.* **1995**, *34*, 4079.
(8) Arnold, P. L.; Patel, D.; Wilson, C.; Love, J. B. *Nature* **2008**, *451*, 315.

Appendix 1: Crystal data for the uranyl Pacman complexes

	[OUO(THF){Li(THF)(HL)]	**[(py)$_3$LiOUO(py)Li(py)(HL)]**	**[(py)$_3$LiOUO(py){Li(py)}$_2$(L)]**
Chemical formula	$C_{50}H_{57}LiN_8O_4U \cdot C_{20}H_{40}O_5$	$[UO_2(C42H40N_8)Li_2(C5H5N)_5].4C5H5N$	$C_{92}H_{90}Li_3N_{18}O_2U$
M_r	1439.53	1653.64	1738.67
Crystal system, space group	Triclinic, $P\bar{1}$	Monoclinic, *Cc*	Triclinic, $P\bar{1}$
Temperature (K)	150	100	150
a, *b*, *c* (Å)	12.9187 (6), 16.9057 (7), 17.0274 (7)	14.0928 (3), 24.2786 (3), 22.7601 (4)	15.0681 (4), 15.9581 (4), 19.1549 (5)
α, β, γ (°)	107.186 (3), 96.271 (3), 106.235 (3)	90.769 (1)	94.953 (1), 90.628 (1), 114.436 (1)
V (Å^3)	3335.6 (2)	7786.7 (2)	4172.17 (19)
Z	2	4	2
Radiation type	Mo *K*α	Cu *K*α	Mo *K*α
μ (mm^{-1})	2.50	6.34	2.01
Crystal size (mm)	0.25 × 0.14 × 0.08	0.17 × 0.11 × 0.05	0.41 × 0.22 × 0.19
Diffractometer	Bruker Smart Apex CCD diffractometer	SuperNova, Dual, Cu at zero, Atlas diffractometer	Bruker Smart Apex CCD diffractometer
Absorption correction	Multi-scan *SADABS*	Analytical + multiscan, CrysAlisPro, Oxford Diffraction Ltd., Version 1.171.33.55 (release 05-01-2010 CrysAlis171.NET) (compiled Jan 5 2010,16:28:46) Analytical numeric absorption correction using a multifaceted crystal model based on expressions derived by R.C. Clark & J.S. Reid. (Clark, R. C. & Reid, J. S. (1995). Acta Cryst. A51, 887-897)	Multi-scan *SADABS*
T_{min}, T_{max}	0.574, 0.825	0.703, 0.728	0.586, 0.745
Measured, independent and observed [$I > 2\sigma(I)$] reflections	56425, 13655, 11637	141013, 15090, 14111	73522, 17009, 14818
R_{int}	0.070	0.071	0.051
$R[F^2 > 2\sigma(F^2)]$, $wR(F^2)$, *S*	0.049, 0.118, 1.07	0.033, 0.084, 1.04	0.044, 0.089, 1.07
No.	13655	15090	17009

reflections			
No. parameters	802	1016	1045
No. restraints	0	18	0
H-atom treatment	riding	Riding	riding
$\Delta\rho_{max}$, $\Delta\rho_{min}$ (e Å^{-3})	2.92, -1.18	0.80, -1.18	1.21, -1.39
Absolute structure		Flack H D (1983), Acta Cryst. A39, 876-881	
Flack parameter		0.478 (4)	

	[(THF)({Me_3Si}$_2$N)LiOUO(THF){Li(THF)}$_2$(L)]	**[(Me_3SiO)UO(py)(H_2L)]**	**[(Bu^tMe_2SiO)UO(py)(H_2L)]**
Chemical formula	$C_{76}H_{114}Li_4N_9O_9Si_2U$	$C_{240}H_{264}N_{44}O_8Si_4U_4$	$C_{54}H_{62.67}N_6O_{1.33}Si_{0.67}U_{0.67}$
M_r	1619.73	4957.43	994.51
Crystal system, space group	Triclinic, $P\bar{1}$	Orthorhombic, $Pna2_1$	MONOCLINIC, $P1_21/n1$
Temperature (K)	150	171	171
a, *b*, *c* (Å)	12.2088 (3), 16.2176 (5), 20.9697 (6)	22.2907 (12), 15.3718 (9), 16.4959 (9)	17.0122 (9), 14.8055 (7), 30.004 (2)
α, β, γ (°)	75.391 (2), 86.593 (2), 80.083 (2)	5652.3 (5)	98.532 (5)
V (Å^3)	3957.13 (19)	1	7473.7 (7)
Z	2	Mo *K*α	6
Radiation type	Mo *K*α	2.95	Mo *K*α
μ (mm^{-1})	2.14	0.23 × 0.18 × 0.09	2.24
Crystal size (mm)	0.39 × 0.31 × 0.31		0.50 × 0.19 × 0.18
Diffractometer	Bruker Smart Apex CCD diffractometer	Xcalibur, Eos diffractometer	Xcalibur, Eos diffractometer
Absorption correction	Multi-scan *SADABS*	Multi-scan	Multi-scan
T_{min}, T_{max}	0.637, 0.745	0.935, 1	0.846, 1.000
Measured, independent and observed [$I > 2\sigma(I)$] reflections	60613, 16142, 14798	30982, 12445, 9470	75119, 19611, 14687
R_{int}	0.035	0.047	0.060
$R[F^2 > 2\sigma(F^2)]$, $wR(F^2)$, *S*	0.035, 0.089, 1.07	0.040, 0.095, 1.07	0.091, 0.164, 1.30
No. reflections	16142	12445	19611
No.	921	687	855

parameters			
No. restraints	2	9	0
H-atom treatment	riding	riding	Riding
$\Delta\rho_{max}$, $\Delta\rho_{min}$ (e Å^{-3})	2.19, -0.93	1.75, −2.08	$w = 1/[\sigma^2(F_o^2) + (0.P)^2 + 56.4224P]$ where $P = (F_o^2 + 2F_c^2)/3$
Absolute structure		Flack H D (1983), Acta Cryst. A39, 876-881	7.37, −6.59
Flack parameter		−0.016 (5)	

	[(Me$_3$SiO)UO(THF)(ZnCl)$_2$(L)]	**[Cl$_2$Zn(py)OUO(py)Zn(py)(HL)]**	**[I$_2$Zn(py)OUO(THF)Zn(py)(HL)]**
Chemical formula	$C_{61}H_{69}Cl_2N_8O_3SiUZn_2$	$C_{48}H_{47.33}Cl_{1.33}N_{9.33}O_{1.33}U_{0.67}Zn_{1.33}$	$C_{45.33}H_{55.33}I_{1.33}N_{6.67}O_4U_{0.67}Zn_{1.33}$
M_r	1430.00	1069.40	1172.68
Crystal system, space group	Monoclinic, $P12_1/n1$	TRICLINIC, $P1$	Triclinic, $P1$
Temperature (K)	171	171	100
a, b, c (Å)	12.7074 (3), 17.2090 (5), 28.218 (1)	12.3734 (4), 15.4162 (6), 20.7285 (8)	12.7534 (2), 15.2777 (2), 20.2051 (3)
α, β, γ (°)	100.156 (3)	69.800 (3), 77.258 (3), 72.537 (3)	95.737 (1), 106.854 (1), 111.132 (2)
V (Å^3)	6074.1 (3)	3509.4 (2)	3420.89 (9)
Z	4	3	3
Radiation type	Mo $K\alpha$	Mo $K\alpha$	Cu $K\alpha$
μ (mm^{-1})	3.60	3.11	14.95
Crystal size (mm)	0.38 × 0.11 × 0.10	0.51 × 0.14 × 0.10	0.06 × 0.02 × 0.02
Diffractometer	Xcalibur, Eos diffractometer	Xcalibur, Eos diffractometer	SuperNova, Dual, Cu at zero, Atlas diffractometer
Absorption correction	Multi-scan	Multi-scan	Multi-scan
T_{min}, T_{max}	0.732, 1.000	2.810, 26.674	0.513, 1.000
Measured, independent and observed [$I > 2\sigma(I)$] reflections	45336, 15834, 10853	44968, 14828, 12028	69699, 13587, 12464
R_{int}	0.069	0.049	0.040
$R[F^2 > 2\sigma(F^2)]$, $wR(F^2)$, S	0.053, 0.124, 1.03	0.039, 0.080, 1.03	0.032, 0.086, 1.03
No. reflections	15834	14828	13587
No. parameters	707	842	805
No.	0	0	0

restraints			
H-atom treatment	Riding	Riding	Riding
$\Delta\rho_{max}$, $\Delta\rho_{min}$ (e Å^{-3})	3.50, −1.52	1.05, −0.59	$w = 1/[\sigma^2(F_o^2) + (0.0401P)^2 + 13.420P]$ where $P = (F_o^2 + 2F_c^2)/3$
Absolute structure Flack parameter			1.77, −1.63

	$[UO_2(OHK)(KHL)]$	**$[\{UO_2(OH)K(C_6H_6)(H_2L)\}_2]$**	**$[IZn(py)_2OUO(py)(H_2L)]$**
Chemical formula	$C_{42}H_{42}K_{1.33}N_{8.33}O_2U_{0.67}$	$C_{72}H_{73}KN_8O_3U$	$C_{51.20}H_{52}I_{0.80}N_{8.80}O_{1.60}U_{0.80}Zn_{0.80}$
M_r	906.33	1375.51	1160.46
Crystal system, space group	TRICLINIC, *P*1	Triclinic, $P\bar{1}$	Orthorhombic, $P2_12_12_1$
Temperature (K)	171	150	171
a, *b*, *c* (Å)	13.2105 (8), 13.8360 (11), 19.3782 (12)	13.864 (5), 15.187 (5), 18.151 (5)	13.5592 (7), 16.3675 (6), 27.6618 (10)
α, β, γ (°)	70.118 (6), 78.215 (5), 70.549 (6)	92.186 (5), 105.716 (5), 116.998 (5)	
V (Å^3)	3124.2 (4)	3219.7 (18)	6139.0 (4)
Z	3	2	5
Radiation type	Mo *K*α	Mo *K*α	Mo *K*α
μ (mm^{-1})	2.79	2.64	3.58
Crystal size (mm)	0.42 × 0.25 × 0.11	0.35 × 0.33 × 0.32	0.18 × 0.14 × 0.13
Diffractometer	Xcalibur, Eos diffractometer	Bruker x8 diffractometer	Xcalibur, Eos diffractometer
Absorption correction	Multi-scan	Multi-scan (*SADAB*)*S*	Multi-scan
T_{min}, T_{max}	0.421, 1.000	0.459, 0.486	0.944, 1.000
Measured, independent and observed [$I > 2\sigma(I)$] reflections	76378, 16728, 9993	73027, 17777, 15880	34572, 14347, 11137
R_{int}	0.074	0.032	0.056
$R[F^2 > 2\sigma(F^2)]$, $wR(F^2)$, *S*	0.045, 0.112, 0.92	0.029, 0.071, 1.07	0.088, 0.236, 1.01
No.	16728	17777	14347

reflections			
No. parameters	752	731	726
No. restraints	0	0	0
H-atom treatment	Riding	Riding	Riding
$\Delta\rho_{max}$, $\Delta\rho_{min}$ (e Å^{-3})	2.94, −0.83		$w = 1/[\sigma^2(F_o^2) + (0.1191P)^2 + 99.7964P]$ where $P = (F_o^2 + 2F_c^2)/3$
Absolute structure			3.66, −1.11
Flack parameter			Flack H D (1983), Acta Cryst. A39, 876-881 1.003 (12)

	$[UO_2(py)Zn(py)ZnI(py)(L)]$
Chemical formula	$C_{35.08}H_{33.85}I_{0.62}N_{6.77}O_{1.23}U_{0.62}Zn_{1.23}$
M_r	874.95
Crystal system, space group	Monoclinic, *C*12/*c*1
Temperature (K)	171
a, *b*, *c* (Å)	28.8095 (9), 20.1946 (4), 27.7238 (7)
α, β, γ (°)	95.439 (3)
V (Å^3)	16057.0 (7)
Z	13
Radiation type	Mo *K*α
μ (mm^{-1})	3.03
Crystal size (mm)	0.36 × 0.15 × 0.11
Diffractometer	Xcalibur, Eos diffractometer
Absorption correction	Multi-scan
T_{min}, T_{max}	0.890, 1.000
Measured, independent and observed [$I > 2\sigma(I)$] reflections	52443, 16923, 11829
R_{int}	0.066
$R[F^2 > 2\sigma(F^2)]$, $wR(F^2)$, *S*	0.633
No. reflections	16923

No. parameters	675
No. restraints	0
H-atom treatment	Riding
$\Delta\rho_{max}$, $\Delta\rho_{min}$ (e Å^{-3})	1.71, −1.13
Absolute structure	
Flack parameter	

Computer Programmes: *Bruker SMART version 5.624* and 5.625 (Bruker, 2001); *Bruker SAINT version 6.36a* (Bruker, 2002); *Bruker SHELXTL* (Bruker, 2001); *SHELXL-97* (Sheldrick, 1997); *PLATON* (Spek,2003); WinGX (Farrugia, 1999).

Appendix 2: EPR data of $[(py)_3LiOUO(py)Li(py)(HL)]$

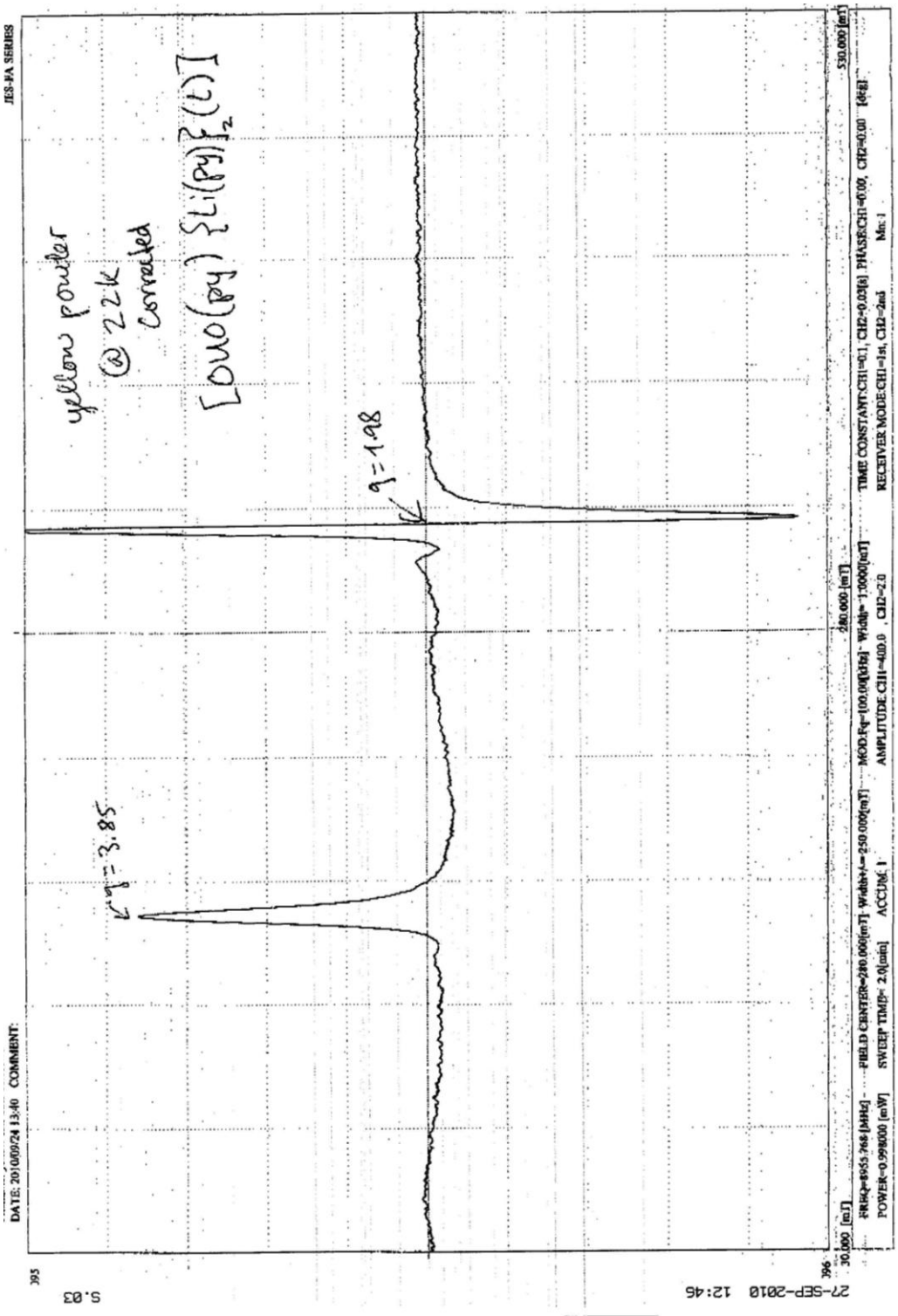
JES-FA SERIES
DATE: 2010/09/24 13:40 COMMENT:
yellow powder
@ 22K
corrected
[Lu(O)(py)5Li(py)]2(2)
g=3.85
g=1.98
S.03
27-SEP-2010 12:45

Appendix 3: Publications based on the work presented

PAPER www.rsc.org/dalton | Dalton Transactions

Equatorial ligand substitution by hydroxide in uranyl Pacman complexes of a Schiff-base pyrrole macrocycle†

Polly L. Arnold,*[a] Dipti Patel,[a] Anne-Frédérique Pécharman,[a] Claire Wilson[b] and Jason B. Love*[a]

Received 22nd October 2009, Accepted 12th February 2010
First published as an Advance Article on the web 2nd March 2010
DOI: 10.1039/b922115h

The synthesis of the mono-uranyl complex $[UO_2(THF)(H_2L^{Me})]$ of a ditopic Schiff-base pyrrole macrocycle is described and is shown to adopt a Pacman wedge-shaped structure in which the uranyl dication is desymmetrised and sits solely in one N_4-donor compartment to leave the other vacant. While investigating the mechanism of the previously reported, base-initiated, reductive silylation chemistry of $[UO_2(THF)(H_2L^{Me})]$, we found that uranyl hydroxide complexes could be isolated. As such, the reaction between $[UO_2(THF)(H_2L^{Me})]$ and KH in THF generated the dimeric cation-cation hydroxide $[\{UO_2(OH)K(C_6H_6)(H_2L^{Me})\}_2]$ when crystallised from C_6H_6, or alternatively, when crystallised from THF, the monomeric THF-adducted cation-cation complex $[UO_2(OH)K(THF)_2(H_2L^{Me})]$ was isolated. These compounds result formally from the substitution of the equatorial THF molecule by hydroxide, and it was also shown that the reaction between dry KOH and $[UO_2(THF)(H_2L^{Me})]$ generated $[\{UO_2(OH)K(C_6H_6)(H_2L^{Me})\}_2]$.

Introduction

The uranyl dication, $[UO_2]^{2+}$ is the most prevalent form of uranium in solution chemistry and in the environment, and is characterised by strong and inert uranium oxo multiple bonding, with a rigorously linear O=U=O geometry and a formal U–O bond order of approximately 2.5 as a result of relativistic effects on the energies of the uranium valence orbitals.[1] Accordingly, ligand chemistry takes place almost exclusively in the equatorial plane.[2] We described recently the synthesis of mononuclear uranyl complexes of the macrocycle H_4L (Scheme 1), and showed that a folded, Pacman structure in solution and in the solid state was adopted and that substitution of the THF molecule that occupies the fifth, equatorial position by pyridine to form $[UO_2(C_5H_5N)(H_2L)]$ was straightforward.[3]

Significantly, we also found that reactions between $[UO_2(THF)(H_2L^{Me})]$, an analogue of $[UO_2(THF)(H_2L)]$, in which the aryl hinge groups are methylated, and $KN(SiMe_3)_2$ in the presence of two molar equivalents of a divalent transition metal halide, *e.g.* FeI_2 or ZnI_2 resulted in the remarkably selective reductive silylation of the uranyl dication, so forming the U^V complexes $[UO(OSiMe_3)(THF)(MI)_2(L^{Me})]$ (M = Fe, Zn; Scheme 1).[4] The use of KH as the base in the presence of either N–Si or C–Si substrates resulted in E–Si bond cleavage (E = N, C) and O–Si bond formation, with the generation of the same U^V reductively-silylated complexes. Therefore, we reasoned that the deprotonation of the vacant N_4-donor cavity by the potassium base caused the bonding in the $[UO_2]^{2+}$ group to be disrupted such that the *exo*-U=O bond was able to participate in radical abstraction reactions. This mechanism has been corroborated recently by theoretical calculations that show that the deprotonation of macrocyclic uranyl model complexes results firstly in the highly exergonic formation of an intermediate in which two potassium cations are bound to one U=O only. This activating-interaction then promotes an S_N2 radical reaction between the *exo* U=O group and silanes to form initially the reductively-silylated species which is then stabilised by addition of transition metal cations.[5]

The interactions of the oxo groups of the uranyl dication with other metal cations are known as cation-cation interactions, or CCI's. Sullivan pioneered the study of CCI's, first noting the unusual interaction of the $[UO_2]^{2+}$ ion with the pentavalent $[NpO_2]^+$ cation in acidic solution,[6] and recognising that CCI's form much more readily in f^1 systems such as pentavalent uranyl, and also in neptunyl, and plutonyl salts that incorporate a more Lewis basic oxo group.[7] Weak interactions have been seen in a handful of X-ray structures of f^0 uranyl complexes such as $[Na(THF)_2][UO_2\{N(SiMe_3)_2\}_3]$,[8] and $Li_4[(UO_2)_{10}O_{10}(Mo_2O_8)]$.[9] CCI's change the solubilities of the actinyl salts in solution, and have important implications for the PUREX process that has been used for the last few decades by the nuclear industry to separate the dissolved components of spent nuclear fuel.[10] The precise interactions of solvated hydroxyl uranyl complexes with other cations is also attracting interest in the study of nuclear waste behaviour.[11]

Herein, we describe the full details of the synthesis and crystal structure of the uranyl complex $[UO_2(THF)(H_2L^{Me})]$ and its reaction with KH and K that generate complexes arising formally from addition of KOH to $[UO_2(THF)(H_2L^{Me})]$, isolated as two different solvates, $[\{UO_2(OH)K(C_6H_6)(H_2L^{Me})\}_2]$ and $[\{UO_2(OH)K(THF)_2(H_2L^{Me})\}_2]$. The single crystal X-ray structures of these solvates contain a variety of CCIs with potassium cations; as such, structural features of these complexes are compared with those in $[\{UO_2(O)K_2(C_6H_6)(H_2L)\}_2]$, the structure of which we communicated previously.[12]

[a]*EaStCHEM School of Chemistry, University of Edinburgh, The King's Buildings, West Mains Road, Edinburgh, UK EH9 3JJ. E-mail: polly.arnold@ed.ac.uk, jason.love@ed.ac.uk; Fax: +44 131 6504743; Tel: +44 131 6504762*
[b]*Rigaku Europe, Unit B6, Chaucer Business Park, Watery Lane, Sevenoaks, Kent, UK TN15 6QY*

† CCDC reference numbers 752122, 752123, 752124. For crystallographic data in CIF or other electronic format see DOI: 10.1039/b922115h

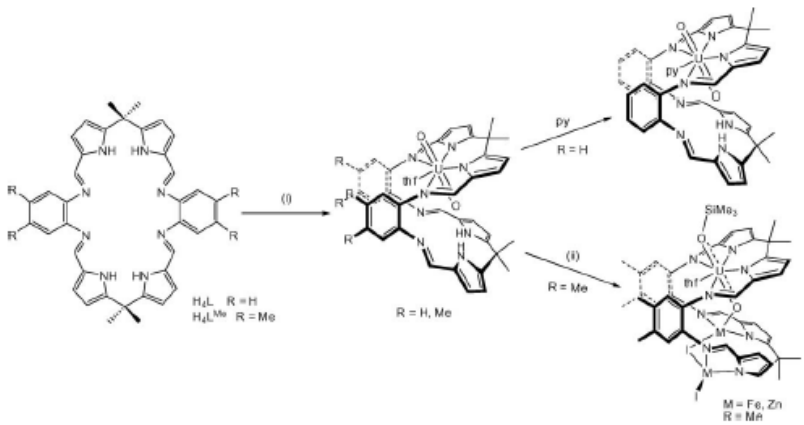

Scheme 1 Synthesis and reactions of the macrocyclic uranyl complexes. Conditions: (i) $[UO_2(THF)_2\{N(SiMe_3)_2\}_2]$, -78 °C, THF, 88%; (ii) $KN(SiMe_3)_2$, MI_2, -78 °C, THF, M = Fe, 81%, M = Zn, 46% (alternatively: KH, $N(SiMe_3)_2$, MI_2 -78 °C, THF).

Results and discussion

Formation and characterisation of the uranyl complex $[UO_2(THF)(H_2L^{Me})]$

In a manner similar to that described by us previously,[3] the transamination reaction between the uranyl silylamide $[UO_2(THF)_2\{N(SiMe_3)_2\}_2]$ and H_4L^{Me} in THF at low temperature resulted in the sole formation of the mono-uranyl complex $[UO_2(THF)(H_2L^{Me})]$ as an analytically-pure, dark brown solid in high yield (Scheme 1). Dark red columnar crystals suitable for X-ray diffraction studies were grown by the slow diffusion of hexane into a THF solution and the solid state structure was determined by X-ray diffraction (Fig. 1); selected bond lengths and angles are detailed in Table 1, with crystal data shown in Table 2. In a manner similar to that shown by us previously, one N_4-donor set of the macrocycle is sufficiently flexible to accommodate the large uranyl ion in a pentagonal bipyramidal geometry. The N-donors are found to occupy four equatorial sites with the fifth occupied by an oxygen atom of a bound THF molecule; the axial positions contain the two *trans*-oxo ligands. The second N_4-donor compartment of the macrocyclic ligand remains metal free with the pyrrole nitrogens protonated and results in a wedge-shaped geometry that differentiates between the two uranyl oxo groups. The uranyl-oxo bond lengths (U1-O1 1.787(3), U1-O2 1.770(3) Å) are similar to those in the related complex $[UO_2(THF)(H_2L)]$ (U1-O1 1.790(4), U1-O2 1.766(4) Å),[3] and show an elongation in the *endo* U=O bond distance of similar magnitude (0.017 Å) due to hydrogen bonding interactions with the pyrrole hydrogens of the vacant compartment.[13]

The uranyl complex was characterised further by ^1H and $^{13}C\{^1H\}$ NMR spectroscopy, which revealed that the solid state structure is retained in solution. Discrete resonances are observed in the ^1H NMR spectrum for the metal free and complexed N_4-donor compartments, *e.g.* two distinct resonances at 8.74 and 7.99 ppm attributable to the Schiff base imine protons were

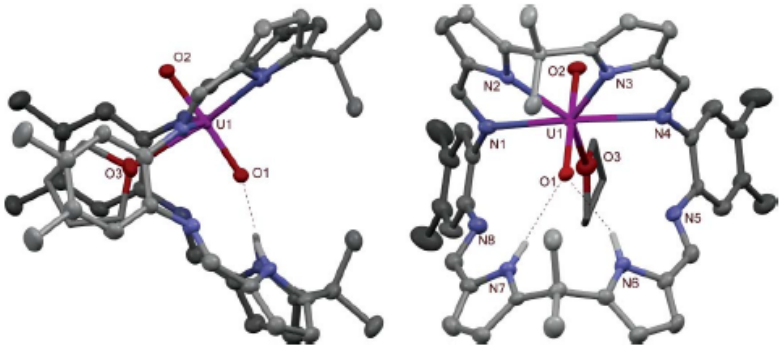

Fig. 1 Side-on and face-on views of the solid state structure of the mono-uranyl complex $[UO_2(THF)(H_2L^{Me})]$. For clarity, solvent of crystallisation and all hydrogens except those on the pyrrole nitrogens are omitted (50% probability displacement ellipsoids).

Table 1 Selected bond length (Å) and angles (°) for $[UO_2(THF)(H_2L^{Me})]$, $[\{UO_2(OH)K(C_6H_6)(H_2L^{Me})\}_2]$, and $[UO_2(OH)K(THF)_2(H_2L^{Me})]$

$[UO_2(THF)(H_2L^{Me})]$		$[\{UO_2(OH)K(C_6H_6)(H_2L^{Me})\}_2]$		$[UO_2(OH)K(THF)_2(H_2L^{Me})]$	
U1–O1	1.787 (3)	U1–O1	1.7956 (16)	U1–O2	1.788 (6)
U1–O2	1.770 (3)	U1–O2	1.8027 (16)	U1–O1	1.821 (6)
U1–O3	2.457 (3)	U1–O3	2.1863 (18)	U1–O3	2.186 (8)
U1–N1	2.557 (4)	U1–N1	2.531 (2)	U1–N1	2.598 (8)
U1–N2	2.473 (4)	U1–N2	2.476 (2)	U1–N2	2.499 (8)
U1–N3	2.443 (4)	U1–N3	2.504 (2)	U1–N3	2.519 (9)
U1–N4	2.583 (4)	U1–N4	2.603 (2)	U1–N4	2.550 (8)
		U1–K1	3.7853 (11)	U1–K1	3.966 (2)
		U1–K1^{i}	4.1083 (11)	K1–O3	2.574 (7)
		K1–O3	2.6610 (19)	K1–O4	2.688 (15)
		K1–O2	2.8127 (19)	K1–O5	2.758 (14)
		K1–O2^{i}	2.8382 (18)	K1–N8	2.900 (9)
		K1–N3^{i}	3.133 (2)	K1–N5	3.027 (9)
		O2–K1^{i}	2.8382 (18)	K1–O1	3.194 (7)
				K1–N6	3.254 (10)
				K1–N7	3.265 (9)
O1–U1–O2	176.97 (16)	O1–U1–O2	179.16 (7)	O1–U1–O2	178.5 (3)
O1–U1–O3	92.82 (13)	O1–U1–O3	94.51 (7)	O1–U1–O3	89.0 (3)
N1–U1–N2	66.25 (14)	N1–U1–N2	67.92 (7)	N2–U1–N1	65.5 (3)
N1–U1–N4	152.42 (14)	N1–U1–N4	153.28 (7)	N1–U1–N4	154.5 (2)
N2–U1–N3	70.86 (13)	N2–U1–N3	70.29 (7)	N2–U1–N3	70.0 (3)
N3–U1–N4	66.46 (13)	N3–U1–N4	65.71 (7)	N3–U1–N4	65.6 (3)
N1–U1–O3	79.72(13)	N1–U1–O3	79.14 (7)	N1–U1–O3	78.6 (3)
N4–U1–O3	75.64(13)	N4–U1–O3	76.04 (6)	N4–U1–O3	80.0 (3)
		O1–U1–K1	135.93 (6)	O2–U1–K1	126.3 (2)

Symmetry code/s: (i) $-x+1, -y+1, -z+1$.

Table 2 Crystal data for $[UO_2(THF)(H_2L^{Me})]$, $[\{UO_2(OH)K(C_6H_6)(H_2L^{Me})\}_2]$, and $[UO_2(OH)K(THF)_2(H_2L^{Me})]$. Experiments were carried out with Mo-Kα radiation

	$[UO_2(THF)(H_2L^{Me})]$	$[\{UO_2(OH)K(C_6H_6)(H_2L^{Me})\}_2]$	$[UO_2(OH)K(THF)_2(H_2L^{Me})]$
Chemical formula	$C_{46}H_{50}N_6O_5U{\cdot}C_4H_8O$	$C_{72}H_{73}KN_6O_7U$	$C_{55}H_{66}KN_6O_{5.50}U$
M_r	1073.07	1375.51	1204.29
Crystal system, space group	Orthorhombic, $P2_12_12_1$	Triclinic, $P\bar{1}$	Orthorhombic, $P2_12_12$
a, b, c/Å	13.3919 (7), 14.7012 (8), 26.5250 (14)	13.864 (5), 15.187 (5), 18.151 (5)	22.7824 (11), 23.0693 (10), 10.9145 (5)
α,β,γ (°)	90, 90, 90	92.186 (5), 105.716 (5), 116.998 (5)	90, 90, 90
V/Å^3	5222.2 (8)	3219.7 (18)	5736.4 (5)
Z	4	2	4
μ/mm^{-1}	3.16	2.64	2.95
Crystal size/mm	0.28 × 0.13 × 0.13	0.35 × 0.33 × 0.32	0.26 × 0.13 × 0.13
Diffractometer	Bruker *SMART APEX* CCD area detector	Bruker *SMART APEX* CCD area detector	Bruker *SMART APEX* CCD area detector
Absorption correction	Multi-scan *SADABS*	Multi-scan *SADABS*	Multi-scan *SADABS*
T_{min}, T_{max}	0.712, 1.000	0.459, 0.486	0.514, 0.700
No. of measured, independent and observed [$I > 2\sigma(I)$] reflections	33639, 11976, 11239	73027, 17777, 15880	60407, 11782, 11517
R_{int}	0.040	0.032	0.074
$R[F^2 > 2\sigma(F^2)]$, $wR(F^2)$, S	0.037, 0.087, 1.05	0.029, 0.071, 1.07	0.053, 0.138, 1.09
No. of reflections	11976	17777	11782
No. of parameters	576	731	563
No. of restraints	51	0	10
H-atom treatment	Riding model $w = 1/[\sigma^2(F_o^2) + (0.044P)^2 + 4.411P]$ where $P = (F_o^2 + 2F_c^2)/3$	Riding $w = 1/[\sigma^2(F_o^2) + (0.0393P)^2 + 1.2907P]$ where $P = (F_o^2 + 2F_c^2)/3$	Riding $w = 1/[\sigma^2(F_o^2) + (0.0726P)^2 + 28.6785P]$ where $P = (F_o^2 + 2F_c^2)/3$
$D\rho_{max}$, $D\rho_{min}$/e Å^{-3}	1.14, -0.67	2.22, -0.72	2.22, -3.38
Flack parameter	0.084 (6)	–	0.052 (11)

Computer programs: Bruker *SMART* version 5.625 (Bruker, 2001), *SMART* (Siemans, 1993), Bruker *SAINT* version 6.36a (Bruker, 2000), *SAINT* (Siemans, 1995), Bruker *SAINT*; Bruker *SHELXTL* (Bruker, 2001), *SAINT* (Sienmansm 1995), *SHELXS97* (Sheldrick, 1990), *SHELXL97* (Sheldrick, 1997), *ORTEP-3 for Windows* (Farrugia, 1997), *enCIFer* (Allen *et al.*, 2004); *PLATON* (Spek, 2003), *WinGX* publication routines (Farrugia, 1999).

seen, and also for the uranium-bound molecule of THF with four separate resonances at 4.83, 3.94, 0.86, 0.71 ppm. This equatorially-bound THF molecule is labile and undergoes fast exchange, as the ^{1}H NMR spectrum in d_8-THF no longer contains resonances due to coordinated THF. Furthermore, it has been shown previously by us that this THF molecule can be displaced by pyridine (Scheme 1).[3] The IR spectrum exhibits a strong absorption at 908 cm^{-1} that is attributed to the uranyl asymmetric stretch, is similar to that seen in $[UO_2(pyr)(H_2L)]$ (ν 910 cm^{-1}) and is indicative of a weakened U=O bond.

Reactions of $[UO_2(THF)(H_2L^{Me})]$ with KH, KOH, and K

While probing the mechanism of the reductive silylation of $[UO_2(THF)(H_2L^{Me})]$ (Scheme 1), in particular in an attempt to isolate and identify compounds such as $[UO_2(THF)K_2(L^{Me})]$ formed by deprotonation using a potassium base, we instead found that the reaction between $[UO_2(THF)(H_2L^{Me})]$ and some samples of KH in the absence of a silyl substrate formed a brown solid that, on crystallisation from benzene, generated the U^{VI} dimeric hydroxo complex $[\{UO_2(OH)K(C_6H_6)(H_2L^{Me})\}_2]$ in moderate yield (Scheme 2). Furthermore, recrystallisation of this material from a mixture of THF and benzene generated quantitatively the monomeric THF adduct $[UO_2(OH)K(THF)_2(H_2L^{Me})]$.

It therefore appears likely that the incorporation of KOH in these complexes has resulted through either the use of impure KH (*i.e.* some KOH is present) or from the decomposition of the potassium salt $[UO_2(THF)(K_2L^{Me})]$ by reaction with adventitious water. To corroborate the presence of KOH and to find a reproducible route to these complexes, the reaction between dry KOH and $[UO_2(THF)(H_2L^{Me})]$ was carried out and was found to form $[\{UO_2(OH)K(C_6H_6)(H_2L^{Me})\}_2]$ after crystallisation from benzene in moderate isolated yield (effectively quantitative by ^{1}H NMR spectroscopy); X-ray quality crystals were grown and were found to have the same unit cell parameters as material derived from KH reactions.

The ^{1}H NMR spectrum of $[\{UO_2(OH)K(C_6H_6)(H_2L^{Me})\}_2]$ in a mixture of C_6D_6 and THF supports the presence of the OH group with a characteristic broad resonance at 10.15 ppm and also suggests that the Pacman solid state structure is retained in solution with two separate resonances for the imine protons at 8.75 and 7.89 ppm associated with different N_4-donor compartments. The ^{1}H NMR spectrum of this complex derived from the reaction between $[UO_2(THF)(K_2L^{Me})]$ and KOH is very similar with subtle differences which is likely due to facile THF solvent exchange and the difficulty encountered in accurately defining concentrations and solvent mixture ratios. The IR spectrum shows an absorption at 894 cm^{-1} and is attributed to the uranyl asymmetric stretch. This vibration lies within the expected range for the uranyl asymmetric stretch and is shifted to lower energy compared to that of the uranyl macrocyclic precursor $[UO_2(THF)(H_2L^{Me})]$ which may indicate slight elongation of the U=O bond (see below for solid state structure). There are also absorptions at 3608 and 3360 cm^{-1}, consistent with OH and NH stretches respectively that support further the presence of the hydroxo ligand and the metal-free N_4-donor compartment.

Dissolution of $[\{UO_2(OH)K(C_6H_6)(H_2L^{Me})\}_2]$ in a mixture of THF and benzene resulted in the quantitative deposition of red-orange rectangular block shaped crystals of the THF adduct $[UO_2(OH)K(THF)_2(H_2L^{Me})]$. Elemental analysis of this material supported its formulation, and the ^{1}H NMR spectrum is similar to that of $[\{UO_2(OH)K(C_6H_6)(H_2L^{Me})\}_2]$ in that the spectrum is diamagnetic and discrete resonances are observed for the separate uranyl-containing and metal-free N_4 compartments; as such this indicates that a Pacman structure is adopted in solution. Notable features in the ^{1}H NMR spectrum of the complex are the imine resonances at 8.73 and 7.88 ppm, the broad resonance for the OH proton at 10.41 ppm, and the NH protons at 8.66 ppm. The IR spectrum of $[UO_2(OH)K(THF)_2(H_2L^{Me})]$ shows an absorption at 895 cm^{-1} that is similar to that seen for $[\{UO_2(OH)K(C_6H_6)(H_2L^{Me})\}_2]$. Also, there are absorptions at 3626 and 3329 cm^{-1} that support

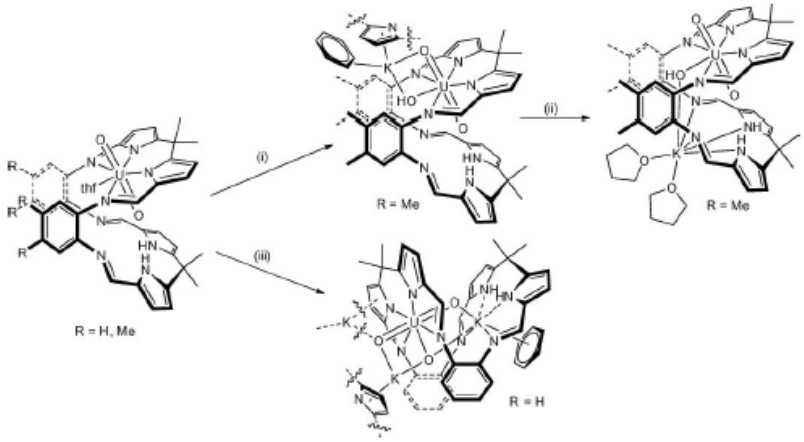

Scheme 2 Reactions of $[UO_2(THF)(H_2L^{Me})]$ with KH, KOH, and K. Conditions: (i) KH, -78 °C, THF, recrystallise from C_6H_6, 35% (alternatively: KOH, THF, recrystallise from C_6H_6, 25%), (ii) THF–C_6H_6, 100%; (iii) K, C_6H_6, 10% (ref. 12).

further the presence of a hydroxo ligand and a metal-free N_4-donor compartment.

X-ray crystallography

X-ray quality crystals of $[\{UO_2(OH)K(C_6H_6)(H_2L^{Me})\}_2]$ were grown from C_6H_6 and $[UO_2(OH)K(THF)_2(H_2L^{Me})]$ from a mixture of THF and C_6H_6; the solid state structures are shown in Fig. 2, with selected bond lengths and angles detailed in Table 1 and crystal data listed in Table 2. We have also attempted previously the chemical reduction of $[UO_2(THF)(H_2L)]$ with an excess of potassium metal (Scheme 2), but only isolated a small quantity of orange crystalline material (*ca.* 10% yield) characterised as the dimeric potassium oxide adduct $[\{UO_2(O)K_2(C_6H_6)(H_2L)\}_2]$ by single crystal X-ray diffraction (Fig. 2, bottom, for comparison).[12]

The presence of KOH in $[\{UO_2(OH)K(C_6H_6)(H_2L^{Me})\}_2]$ does not disrupt the general Pacman structural motif, and the uranyl fragment remains complexed by the four nitrogen atoms (U1-N1 2.532(2), U1-N2 2.476(2), U1-N3 2.505(2), U1-N4 2.604(2) Å) in one half of the macrocycle. The uranium-oxo bond distances (U1-O1 1.7949(16), U1-O2 1.8029(16) Å) are longer than those reported for $[UO_2(THF)(H_2L^{Me})]$ although they are still consistent with the hexavalent oxidation state.[14] The pentagonal bipyramidal coordination sphere of the uranium metal centre is completed in the equatorial plane by a hydroxo ligand, which resides in the same fifth equatorial site as the oxygen atom of the usually bound THF molecule, in-between the macrocyclic aryl rings. The uranyl-hydroxo U1-O3 bond length of 2.1854(19) Å is significantly shorter than those found in $(UO_2)_2(\mu\text{-OH})$ complexes (range 2.29-2.51 Å, mean 2.34 Å)[15] with a relatively acute U1-O3-K1 angle of 102.25(6) ° (range for $(UO_2)_2(\mu\text{-OH})$ complexes 102.0-145.4°, mean 113.4°);[15] there are no structurally-characterised hydroxyl bridged uranyl-alkali metal complexes for comparison.

The potassium cation resides above the plane of the macrocycle at a distance approximately equidistant from the *exo*-oxo atom (K1-O2 2.8130(19) Å) and the oxygen atom of the hydroxo ligand (K1-O3 2.657(2) Å) and leads to a slight elongation of the *exo*-oxo-uranium bond length compared to that of $[UO_2(THF)(H_2L^{Me})]$ (*ca.* 0.03 Å). Hexavalent uranyl complexes with CCI interactions to a potassium cation are rare, and only a handful of calixarene and carboxylate complexes of the uranyl ion with potassium CCIs have been structurally characterised. For example, Thuéry and Masci reported the complex $[(UO_2)K_2(L)(H_2O)_2(NC_5H_5)]$ (L = *p*-*tert*-butyltetrahomodioxacalix[4]arene) derived from the combination of uranyl nitrate, the free base calixarene and KOH. This complex incorporates potassium cations bridging pairs of uranyl cations to form polymeric chain structures, with the potassium–oxo interactions similar to those in $[\{UO_2(OH)K(C_6H_6)(H_2L^{Me})\}_2]$.[16] The mean O–K distance in U=O···K CCI structures reported to date is 2.788 Å.[17] The presence of the potassium cation in $[\{UO_2(OH)K(C_6H_6)(H_2L^{Me})\}_2]$ results in dimerisation as K1 not only interacts strongly with O3 of the hydroxyl ligand and the O2 oxo group, but also with O2′ of an adjacent complex in a symmetric bridging arrangement (K1-O2′ 2.8389(18) Å); this is reinforced by an intermolecular η^5-interaction to a pyrrole ring of the adjacent macrocycle. The coordination sphere of K1 is completed by an η^2-interaction with a molecule of benzene solvent of crystallisation. The bottom compartment of the macrocycle remains metal-free, and both the pyrrolic nitrogens are protonated. As in $[UO_2(THF)(H_2L^{Me})]$, the *endo*-oxo ligand forms hydrogen bonds with the hydrogen atoms on the pyrroles (N6···O1 3.056 Å, N7···O1 3.202 Å), interactions that presumably help stabilise the complex. The structure of $[\{UO_2(OH)K(C_6H_6)(H_2L^{Me})\}_2]$ is clearly related to that of the previously communicated K_2O adduct $[\{UO_2(O)K_2(C_6H_6)(H_2L)\}_2]$ through exchange of (O)-H with (O)-K (Fig. 2, bottom).[12] This latter complex adopts a similar dimeric structural motif in which the two macrocycles are conjoined by K cations (Fig. 2, bottom), and the second K cation (K1) is bound to both the *endo*-uranyl oxygen and the oxo O3; the coordination sphere of K1 is completed through complexation by the macrocyclic imine nitrogens and an η^6-benzene.

In the X-ray crystal structure of $[UO_2(OH)K(THF)_2(H_2L^{Me})]$ (Fig. 2, middle), it is clear that the addition of THF has caused the scission of the intermolecular K-macrocycle interactions in the dimer of $[\{UO_2(OH)K(C_6H_6)(H_2L^{Me})\}_2]$ with the migration of the potassium cation K1 to the U-free half of the macrocyclic wedge. The geometry of the uranyl dication remains pentagonal bipyramidal with the oxo ligands *trans* (O1-U1-O2 178.5(3)°) and the equatorial coordination occupied by one N_4 donor compartment and the hydroxo group; the bond distances between these donor atoms and U1 are similar to those seen in the structure of $[\{UO_2(OH)K(C_6H_6)(H_2L^{Me})\}_2]$. The potassium cation again adopts a bridging geometry, although in this case K1 bridges the hydroxo group O3 (K1-O3 2.547(5) Å) and the oxo ligand O1 (K1-O1 3.194(7) Å) in an asymmetric manner within the macrocyclic cleft. The remaining coordination sphere of K1 is completed by coordination with pyrrole and imine nitrogens of the vacant donor compartment and by two molecules of THF. This structural mode clearly affects the bonding in the uranyl fragment, as significant elongation of the *endo*-U1-O1 bond distance is seen (1.821(6) Å) compared to the *exo*-U1-O2 distance (1.788(6) Å) and also to the U–O bond distances in $[\{UO_2(OH)K(C_6H_6)(H_2L^{Me})\}_2]$ (1.8029(16) and 1.7949(16) Å). In a similar manner to $[UO_2(THF)(H_2L^{Me})]$ and $[\{UO_2(OH)K(C_6H_6)(H_2L^{Me})\}_2]$, a hydrogen bonding interaction between the *endo*-oxo group O1 and the pyrrole hydrogens is observed (N6···O1 3.046 Å, N7···O1 3.079 Å).

Conclusions

We have shown that reactions between the uranyl Pacman complex $[UO_2(THF)(H_2L^{Me})]$ and the potassium-based reagents K metal, KH, and KOH result in the isolation of KOH or K_2O adducts that have been characterised in the solid state and in solution. Structural data show that these complexes retain their overall Pacman structural motif in which the O-atoms at the uranyl are arranged in a T-shape. The K cations are coordinated either outside or within the macrocyclic framework which results in cation-cation interactions with the oxo-groups of the uranyl dication and bridging interactions with the equatorial hydroxide or oxide ligand.

Experimental details

All manipulations were carried out under a dry, oxygen-free dinitrogen atmosphere using standard Schlenk techniques or in MBraun Unilab or Vacuum Atmospheres OMNI-lab gloveboxes unless otherwise stated. THF and hexane were degassed and

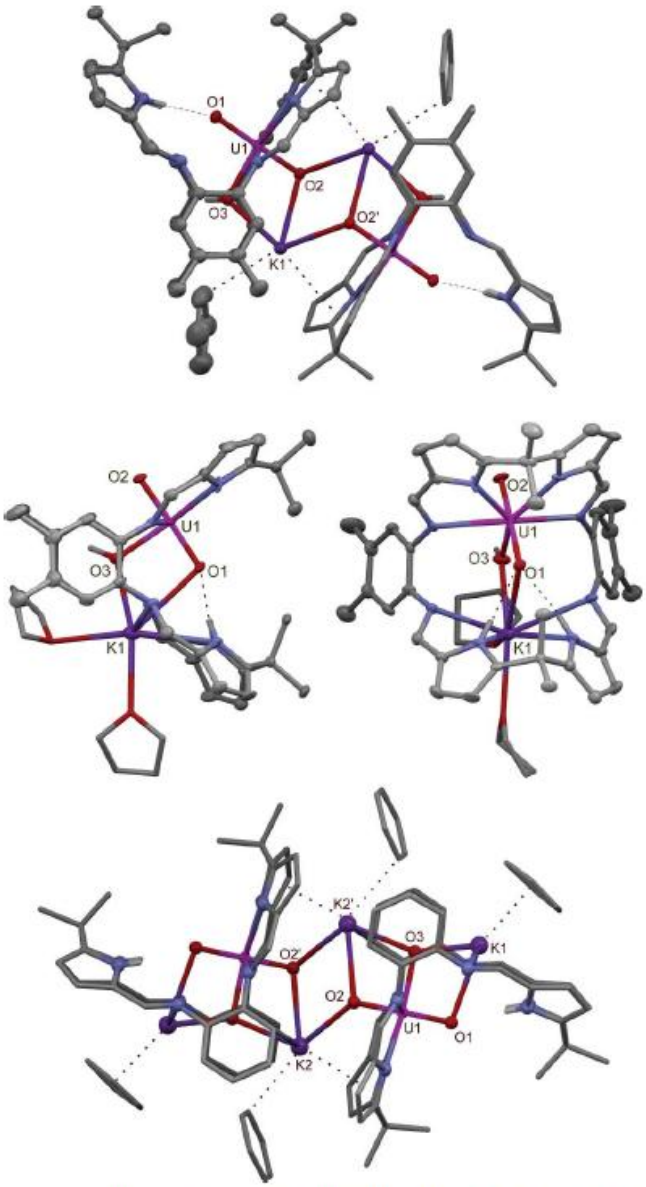

Fig. 2 Solid state structures of the KOH uranyl adducts $[\{UO_2(OH)K(C_6H_6)(H_2L^{Me})\}_2]$ (top), $[UO_2(OH)K(THF)_2(H_2L^{Me})]$ (middle), and $[\{UO_2(O)K_2(C_6H_6)(H_2L)\}_2]$ (bottom, mixed 50 : 50 disorder between K2 and H, only oxo complex is shown). For clarity, all hydrogens except those on the pyrrole nitrogens, and solvent of crystallisation are omitted (where present, displacement ellipsoids are drawn at 50% probability).

purified by passage through activated alumina towers prior to use, while benzene was boiled over K and distilled. All deuterated solvents were boiled over potassium, vacuum transferred, and freeze-pump-thaw degassed three times prior to use. The compounds H_4L^{Me} and $[UO_2(THF)_2\{N(SiMe_3)_2\}_2]$ were synthesised according to literature procedures,[18] and KOH

was prepared by the addition of degassed water to potassium in toluene; all other reagents were used as purchased without further purification. ^{1}H and ^{13}C NMR spectra were recorded on Bruker DPX 300 and Avance 360 MHz NMR spectrometers at 300 K. Chemical shifts are reported in parts per million, and referenced to residual proton resonances calibrated against external TMS. Infrared spectra were recorded on Nicolet 210 and Jasco 410 spectrophotometers. Elemental analyses were carried out by Mr. Stephen Boyer at London Metropolitan University. Solutions for UV-vis spectrophotometry were made in a nitrogen filled glovebox and spectra were recorded in either a Teflon-tapped 10 mm quartz cell or a 1 mm quartz cell sealed by a tight fitting Subaseal on a Unicam UV1 spectrophotometer. Mass spectra were recorded by Mr. Tony Hollingsworth at the University of Nottingham on a VG Autospec instrument.

Synthesis of $[UO_2(THF)(H_2L^{Me})]$

A solution of H_4L^{Me} (2.64 g, 4.0 mmol) in THF (20 mL) was added slowly to a stirred solution of $[UO_2(THF)_2\{N(SiMe_3)_2\}_2]$ (2.94 g, 4.0 mmol) in THF (20 mL) at -78 °C. The resulting solution was allowed to warm to room temperature over 16 h, after which the volatiles were removed under vacuum and the residual solids redissolved in THF (15 mL). Addition of hexane (20 mL) to this solution resulted in a precipitate that was isolated by filtration, washed with hexane (2 × 10 mL), and dried under vacuum to yield $[UO_2(THF)(H_2L^{Me})]$ as a brown/red solid (3.76 g, 88%).

Analysis found: C 56.00, H 5.55, N 10.51%; $C_{50}H_{58}N_8O_4U$ requires: C 55.96, H 5.46, N 10.44%; ^{1}H NMR (C_6D_6): δ_H 8.74 (s, 2H, imine), 8.49 (s, 2H, N*H*), 7.99 (s, 2H, imine), 7.18 (s, 2H, aryl), 6.81 (s, 2H, aryl), 6.78 (d, 2H, pyrrole), 6.71 (d, 2H, pyrrole), 6.27 (d, 2H, pyrrole), 5.86 (d, 2H, pyrrole), 4.83 (m, 2H, THF), 3.94 (m, 2H, THF), 2.23 (s, 3H, methyl), 2.13 (s, 6H, 2 × methyl), 2.08 (s, 3H, methyl), 2.00 (s, 6H, 2 × methyl), 1.31 (s, 3H, methyl) 0.86 (m, 2H, THF), 0.71 (m, 2H, THF), 0.52 (s, 3H, methyl); ^{1}H NMR (d_8-THF): δ_H 8.87 (s, 2H, imine), 8.21 (s, 2H, imine), 8.09 (s, 2H, N*H*), 7.13 (s, 2H, aryl), 7.08 (s, 2H, aryl), 6.84 (d, 2H, J = 3.5 Hz, pyrrole), 6.34 (d, 2H, J = 3.5 Hz, pyrrole), 6.19 (d, 2H, pyrrole), 5.71 (d, 2H, pyrrole), 2.32 (s, 6H, 2 × methyl), 2.23 (s, 6H, 2 × methyl), 1.99 (s, 3H, methyl), 1.79 (s, 3H, methyl), 1.42 (s, 3H, methyl), 0.83 (s, 3H, methyl); ^{13}C{^{1}H} (C_6D_6): δ_C 164.9 (q), 161.0 (q), 148.1 (imine), 146.5 (imine), 144.1 (q), 143.2 (q), 139.3 (q), 134.0 (q), 132.0 (q), 124.5 (q), 122.2 (aryl), 117.8 (pyrrole), 114.7 (pyrrole), 109.8 (aryl), 105.7 (pyrrole), 75.6 and 78.0 (THF), 40.8 (q), 35.7 (methyl), 34.4 (quaternary), 29.1 (methyl), 27.7 (methyl), 26.2 and 25.7 (THF), 25.0 (methyl), 18.9 (methyl), 18.8 (methyl); EIMS: m/z 928.3 (3.87%, M^+), 913.2 (6.61%, M-O^+); IR (Nujol): ν 3373(br, NH), 1619, 1601, 1583, 1281(s), 1263, 1214, 1181, 1049(s), 1019, 959, 908 (s, U=O asymmetric stretch), 895, 780, 766 cm^{-1}; UV-vis (THF, 25 °C): 322 nm (ε = 42048 dm^{3}mol^{-1}cm^{-1}).

Reaction between $[UO_2(THF)(H_2L^{Me})]$ and KH: isolation of $[\{UO_2(OH)K(C_6H_6)(H_2L^{Me})\}_2]$

THF (20 mL) was added to a stirred mixture of $[UO_2(THF)(H_2L^{Me})]$ (0.10 g, 0.09 mmol) and KH (11 mg, 0.18 mmol) at -78 °C and was allowed to warm to room temperature over 16 h. After this time, the mixture was filtered by cannula, the residual solids washed with THF (5 mL) and the washings and filtrate combined. The volatiles were removed under vacuum leaving a brown solid that was recrystallised from benzene to yield $[\{UO_2(OH)K(C_6H_6)(H_2L^{Me})\}_2]$, (0.034 g, 35%). Orange hexagonal block-shaped crystals suitable for X-ray diffraction studies were grown from a saturated benzene solution.

Analysis. Found: C 54.22, H 4.60, N 10.47. $C_{48}H_{49}KN_8O_3U$ requires C 54.22, H 4.65, N 10.54%; ^{1}H NMR (C_6D_6 + THF, double presaturation): δ_H 10.15 (s, 1H, O*H*), 8.75 (s, 2H, imine), 8.62 (s, 2H, N*H*), 7.89 (s, 2H, imine), 7.05 (d, 2H, pyrrole), 6.89 (s, 2H, aryl), 6.68 (d, 2H, pyrrole), 6.63 (s, 2H, aryl), 6.14 (m, 2H, pyrrole), 5.72 (m, 2H, pyrrole), 2.17 (s, 6H, 2 × methyl), 2.10 (s, 6H, 2 × methyl), 2.04 (s, 3H, methyl), 0.71, (s, 3H, methyl), 0.18 (s, 3H, methyl). The remaining 1 × methyl resonance is under the THF resonance of the solvent; IR (Nujol mull): ν 3608 (br, OH), 3360 (br, NH), 1620, 1601 (s), 1584, 1353, 1286 (s), 1267, 1214, 1179, 1047 (s), 1016, 960, 894 (U=O asymmetric), 860 (s), 779, 688 cm^{-1}.

Synthesis of $[UO_2(OH)K(THF)_2(H_2L^{Me})]$

Dissolution of the crystals of $[\{UO_2(OH)K(C_6H_6)(H_2L^{Me})\}_2]$ in a mixture of THF and C_6H_6 resulted in the quantitative deposition of X-ray quality, red-orange rectangular block shaped crystals of $[UO_2(OH)K(THF)_2(H_2L^{Me})]$

Analysis. Found: C 53.18, H 5.27, N 9.95. $C_{50}H_{59}KN_8O_5U$ requires: C 53.18, H 5.27, N 9.92%; ^{1}H NMR (C_6D_6 + THF double presaturation): δ_H 10.41 (s, 1H, O*H*), 8.73 (s, 2H, imine), 8.66 (s, 2H, N*H*), 7.88 (s, 2H, imine), 7.06 (d, 2H, pyrrole), 6.71 (m, 4H, aryl), 6.66 (d, 2H, pyrrole), 6.15 (m, 2H, pyrrole), 5.75 (m, 2H, pyrrole), 2.19 (s, 6H, 2 × methyl), 2.08 (s, 6H, 2 × methyl), 2.06 (s, 3H, methyl), 0.64 (s, 3H, methyl), 0.22 (s, 3H, methyl); IR (Nujol): ν 3626 (br, OH), 3329 (br, NH), 1601 (s), 1583 (s), 1562 (sh), 1352, 1284 (s), 1269, 1215, 1184, 1153, 1043 (s), 1018, 960, 895 (U=O asymmetric), 866 (s), 795, 777, 760, 621, 594 cm^{-1}.

Direct synthesis of $[\{UO_2(OH)K(C_6H_6)(H_2L^{Me})\}_2]$

THF (20 ml) was added to an equimolar mixture of $[UO_2(THF)(H_2L^{Me})]$ (0.089 g, 0.089 mmol) and dry KOH (0.005 g, 0.089 mmol) at 25 °C. The resulting solution was stirred for 16 h, and the volatiles removed under vacuum. The resulting pink red solid was recrystallised from benzene to yield $[\{UO_2(OH)K(C_6H_6)(H_2L^{Me})\}_2]$ as orange rectangular block-shaped crystals (0.024 g, 25%). The crystals were analysed by X-ray crystallography and were found to have the same unit cell parameters as those formed using the above alternative route.

^{1}H NMR:(C_6D_6+THF double presaturation): δ_H 11.19 (s, 1H, OH), 9.17 (s, 2H, imine), 9.08 (s, 2H, NH), 8.59 (s, 2H, imine), 7.40 (s, 2H, aryl), 7.32 (s, 2H, aryl), 7.22 (d, 2H, pyrrole), 6.84 (d 2H, pyrrole), 6.68 (m, 2H, pyrrole), 6.22 (m, 2H, pyrrole), 2.72 (s, 6H, 2 × methyl), 2.68 (s, 6H, 2 × methyl), 1.34 (s, 3H, methyl), 0.55 (s, 3H, methyl); ^{1}H NMR ($CDCl_3$): δ_H 9.96 (s, 1H, OH), 9.00 (s, 2H, imine), 8.35 (s, 2H, NH), 8.25 (s, 2H, imine), 7.29 (d, 2H, pyrrole), 7.07(s, 2H, aryl), 6.89 (s, 2H, aryl), 6.69 (d 2H, pyrrole), 6.52 (m, 2H, pyrrole), 6.05 (m, 2H, pyrrole), 2.50 (s, 6H, 2 × methyl), 2.39 (s, 6H, 2 × methyl), 2.25 (s,3H,methyl), 2.13 (s,3H, methyl),1.68 (s, 3H, methyl), 1.09 (s, 3H, methyl).

Crystallographic details†

X-Ray diffraction data from single crystals of $[UO_2(THF)(H_2L^{Me})]$, $[UO_2(OH)K(THF)_2(H_2L^{Me})]$ and $[\{UO_2(OH)K(C_6H_6)(H_2L^{Me})\}_2]$ were collected at 150 K using graphite monochromated Mo-Kα radiation ($\lambda = 0.71073$ Å) on a Bruker SMART APEX diffractometer equipped with a CCD detector. Details of the individual data collections and refinements are given in Table 2. All structures were solved by direct methods and refined using full-matrix least square refinement on $|F|^2$ using SHELXL-97. Unless otherwise stated, all non-hydrogen atoms were refined with anisotropic displacement parameters while hydrogen atoms were placed at calculated positions and included as part of a riding model. In $[UO_2(THF)(H_2L^{Me})]$, two half-occupied THF solvent molecules per asymmetric unit were refined isotropically using distance and similarity restraints. In $[\{UO_2(OH)K(C_6H_6)(H_2L^{Me})\}_2]$, some of the benzene solvent of crystallisation was disordered over two sites and was refined isotropically with 50 : 50 occupancy. In $[UO_2(OH)K(THF)_2(H_2L^{Me})]$, the twin law (0 -1 0, -1 0 0, 0 0 -1) was applied and the twin component fraction refined to 0.1198(11). The two molecules of THF bound to the K, and one THF solvent of crystallisation could not be modelled accurately and so were refined isotropically. Furthermore, the two molecules of benzene that lie on crystallographic mirror planes could not be modelled accurately and so were also refined isotropically using distance and similarity restraints.

Acknowledgements

We thank the Universities of Edinburgh and Nottingham for funding.

References

1 R. G. Denning, *J. Phys. Chem. A*, 2007, **111**, 4125.
2 C. Clavaguera-Sarrio, S. Hoyau, N. Ismail and C. J. Marsden, *J. Phys. Chem. A*, 2003, **107**, 4515; P. C. Burns, R. C. Ewing and F. C. Hawthorne, *Can. Mineral.*, 1997, **35**, 1551.
3 P. L. Arnold, A. J. Blake, C. Wilson and J. B. Love, *Inorg. Chem.*, 2004, **43**, 8206.
4 P. L. Arnold, D. Patel, C. Wilson and J. B. Love, *Nature*, 2008, **451**, 315.
5 A. Yahia, P. L. Arnold, J. B. Love and L. Maron, *Chem. Commun.*, 2009, 2402.
6 J. C. Sullivan, J. C. Hindman and A. J. Zielen, *J. Am. Chem. Soc.*, 1961, **83**, 3373.
7 C. Den Auwer, A. C. Gregoire-Kappenstein and P. Moisy, *Radiochim. Acta*, 2003, **91**, 773; H. Steele and R. J. Taylor, *Inorg. Chem.*, 2007, **46**, 6311; F. Burdet, J. Pecaut and M. Mazzanti, *J. Am. Chem. Soc.*, 2006, **128**, 16512; S. M. Cornet, L. J. L. Haller, M. J. Sarsfield, D. Collison, M. Helliwell, I. May and N. Kaltsoyannis, *Chem. Commun.*, 2009, 917; J. J. Berard, G. Schreckenbach, P. L. Arnold, D. Patel and J. B. Love, *Inorg. Chem.*, 2008, **47**, 11583.
8 C. J. Burns, D. L. Clark, R. J. Donohoe, P. B. Duval, B. L. Scott and C. D. Tait, *Inorg. Chem.*, 2000, **39**, 5464.
9 E. V. Alekseev, S. V. Krivovichev, T. Malcherek and W. Depmeier, *Inorg. Chem.*, 2007, **46**, 8442.
10 J. E. Birkett, M. J. Carrott, O. D. Fox, C. J. Jones, C. J. Maher, C. V. Roube, R. J. Taylor and D. A. Woodhead, *Chimia*, 2005, **59**, 898.
11 J. P. Austin, M. Sundararajan, M. A. Vincent and I. H. Hillier, *Dalton Trans.*, 2009, 5902.
12 P. L. Arnold, J. B. Love, A. J. Blake and C. Wilson, *Recent Adv. Actinide Sci.*, 2006, **305**, 228.
13 T. S. Franczyk, K. R. Czerwinski and K. N. Raymond, *J. Am. Chem. Soc.*, 1992, **114**, 8138; P. H. Walton and K. N. Raymond, *Inorg. Chim. Acta*, 1995, **240**, 593.
14 P. L. Arnold, J. B. Love and D. Patel, *Coord. Chem. Rev.*, 2009, **253**, 1973.
15 D. A. Fletcher, R. F. McMeeking and D. Parkin, *J. Chem. Inf. Comput. Sci.*, 1996, **36**, 746.
16 P. Thuery and B. Masci, *Dalton Trans.*, 2003, 2411.
17 B. Masci and P. Thuery, *Cryst. Growth Des.*, 2008, **8**, 1689; B. Masci and P. Thuéry, *CrystEngComm*, 2007, **9**, 582; P. Thuéry, B. Masci, M. Takimoto and T. Yamato, *Inorg. Chem. Commun.*, 2007, **10**, 795; W. Zhang and J. Zhao, *Inorg. Chem. Commun.*, 2006, **9**, 397; W. H. Zhang and H. S. Zhao, *J. Mol. Struct.*, 2006, **789**, 177.
18 G. Givaja, M. Volpe, J. W. Leeland, M. A. Edwards, T. K. Young, S. B. Darby, S. D. Reid, A. J. Blake, C. Wilson, J. Wolowska, E. J. L. McInnes, M. Schröder and J. B. Love, *Chem.–Eur. J.*, 2007, **13**, 3707; R. A. Andersen, K. Faegri, Jr., J. C. Green, A. Haaland, M. F. Lappert, W. P. Leung and K. Rypdal, *Inorg. Chem.*, 1988, **27**, 1782.

ARTICLES
PUBLISHED ONLINE: 23 NOVEMBER 2010 | DOI: 10.1038/NCHEM.904
nature chemistry

Uranyl oxo activation and functionalization by metal cation coordination

Polly L. Arnold[1]*†, Anne-Frédérique Pécharman[1], Emmalina Hollis[1], Ahmed Yahia[2], Laurent Maron[2], Simon Parsons[1] and Jason B. Love[1]*†

The oxo groups in the uranyl ion $[UO_2]^{2+}$—one of many oxo cations formed by metals from across the periodic table—are particularly inert, which explains the dominance of this ion in the laboratory and its persistence as an environmental contaminant. In contrast, transition metal oxo (M=O) compounds can be highly reactive and carry out difficult reactions such as the oxygenation of hydrocarbons. Here we show how the sequential addition of a lithium metal base to the uranyl ion constrained in a 'Pacman' environment results in lithium coordination to the U=O bonds and single-electron reduction. This reaction depends on the nature and stoichiometry of the lithium reagent and suggests that competing reduction and C–H bond activation reactions are occurring.

Chemical reactions of the oxo ligands of the uranyl dication $[UO_2]^{2+}$ are rare owing to the strongly covalent and linear O=U=O bonding. As a consequence, over 50% of known uranium compounds incorporate this highly stable motif[1]. In contrast, the oxo groups of the transition metal congeners $[MO_2]^{2+}$ (M=Cr, Mo, W) can be highly reactive, and undergo a myriad of oxidation and oxygenation reactions with substrates as inert as hydrocarbons[2,3]. Nevertheless, reduction and oxo-functionalization reactions of the uranyl are becoming increasingly important, particularly as there is a need to understand the chemical reactions and mechanisms that occur during the immobilization of uranium in the environment and as a result of photoactivation of the ion, upon which it becomes a potent oxidant[4,5]. The singly reduced uranyl ion $[UO_2]^{+}$ is thought to be produced in all of these reactions and is unstable with respect to disproportionation to the uranyl dication and insoluble tetravalent uranium phases.

Depending on the substrate available, different mechanisms, including unimolecular electron transfer and hydrogen-atom abstraction have been identified[6], but the instability of the pentavalent state hampers a better understanding of these processes[7]. Significantly, the recent renaissance in actinide science[8] has included new anaerobic studies on uranyl reduction by reagents such as cobaltocene, $K_2(C_8H_8)$ or potassium metal[9–13], but the majority of pentavalent complexes isolated to date remain unstable with respect to disproportionation.

We have previously reported a new type of chemical reaction of the uranyl ion, in which the asymmetric, macrocyclic uranyl complex **1** cleaved N–Si and C–Si bonds to form the singly reduced and oxo-silylated compound **A** (Fig. 1)[14]. This transformation was initiated by the reaction between **1** and potassium bases, and density functional theory (DFT) calculations have shown that model compounds in which potassium cations bond to a uranyl oxo group can undergo S_N2-type homolytic bond cleavage reactions with silanes and aminosilanes[15]. Now we report that the use of lithium bases allows the synthesis and characterization of a series of unique oxo-lithiated, hexa- and pentavalent uranyl complexes that adopt wedged, 'Pacman' geometries and that provide insight into the mechanism of reduction.

Results and Discussion

Reaction of 1 with one equivalent of lithium base. The addition of one equivalent of $LiN(SiMe_3)_2$ to **1thf** in THF at 25 °C generates the red–brown, diamagnetic, mono-lithiated complex, [OUO(THF){Li(THF)}(HL)] **2thf**, denoted [(OUO)LiHL] **2** in Fig. 1 (L is the tetraanionic, wedge-shaped macrocycle drawn fully in Fig. 1). Isolated in 51% yield, **2thf** has been fully characterized; the results of X-ray diffraction are shown in Fig. 2. This structure shows that the lithium cation is four-coordinate and bound in the bottom pocket to one imine–pyrrolide group, the *endo*-uranyl oxo, and one molecule of THF. The U1–O1 (1.794(3) Å) and U1–O2 (1.767(3) Å) bond distances are similar to other $[UO_2]^{2+}$ complexes, including **1thf**, and are commensurate with the diamagnetic nature of **2thf**. The formation of **2thf** is always accompanied by quantities of doubly and triply lithiated complexes but it was isolated as a pure material in small quantities by fractional crystallization. In similar reactions in pyridine solution, the pyridine-solvated, mono-lithiated analogue **2py** can be identified in the ^{1}H NMR spectrum but has proved difficult to isolate.

Reaction of 1 with two equivalents of lithium base. Reactions between **1** and two equivalents of $LiN(SiMe_3)_2$ in cold pyridine or THF afford a mixture of diamagnetic and paramagnetic complexes, including the majority product **4py** in pyridine (see later). However, reactions in pyridine in the presence of dihydroanthracene (DHA), which contains weak C–H bonds (bond dissociation energy (BDE) = 79 kcal mol^{-1}), leads to the preferential generation of a single paramagnetic product, which is characterized as the U(v) complex [$(py)_3$LiOUO(py)Li(py)(HL)] **3py** (see Fig. 1), viewed formally as the lithium salt of the singly reduced $[UO_2]^{+}$. The number and integrals of the paramagnetically shifted resonances in the ^{1}H NMR spectrum of **3py** support an asymmetric ligand arrangement. It is likely that the most paramagnetically shifted and broadened resonance integrating as 1H at 60.1 ppm is due to the remaining pyrrole NH. The ^{7}Li{^{1}H} NMR spectrum of **3py** displays a single

[1]EaStCHEM School of Chemistry, University of Edinburgh, Edinburgh EH9 3JJ, UK, [2]LPCNO, UMR 5215, INSA, Université Paul Sabatier Toulouse III, CNRS, 135, avenue de Rangueil, 31077 Toulouse cedex 4, and ICSM, UMR 5257, CEA, CNRS, ENSCM, Université Montpellier II, centre de Marcoule, BP17171, 30207 Bagnols sur Cèze cedex, France; †These authors contributed equally to this work. *e-mail: Polly.Arnold@ed.ac.uk; Jason.Love@ed.ac.uk

NATURE CHEMISTRY DOI: 10.1038/NCHEM.904 ARTICLES

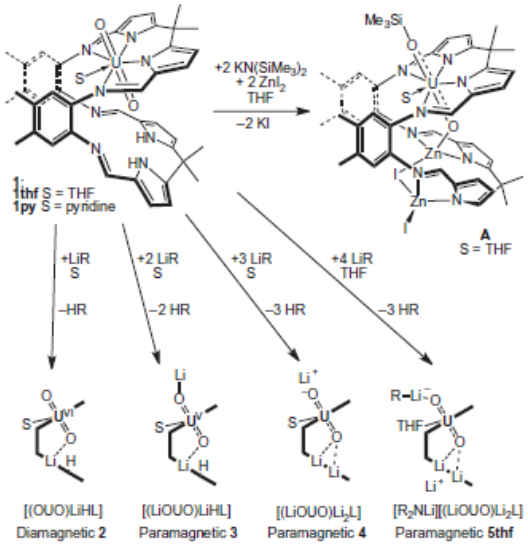

Figure 1 | Synthetic procedures to produce diamagnetic and paramagnetic uranyl Pacman complexes. The reactions between the mono-uranyl complex $[UO_2(S)(H_2L)]$ **1** and one of a variety of lithium bases LiR (R = H, NH_2, N^iPr_2, $N(SiMe_3)_2$, CPh_3, C_5H_5) or $KN(SiMe_3)_2$ in the presence and absence of ZnI_2 (S = THF, pyridine) form the oxo-silylated uranyl complex **A** or mono-, doubly, triply or tetra-lithiated uranyl complexes. At least two equivalents of lithium or potassium base are required to form a pentavalent uranyl complex.

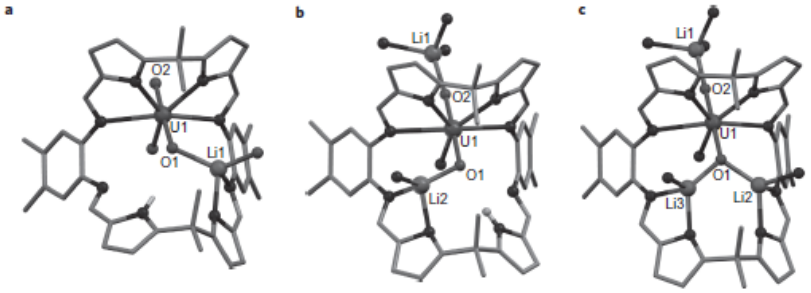

Figure 2 | X-ray crystal structure determination of mono-, doubly and triply lithiated uranyl complexes. a, Mono-lithiated **2thf**. **b**, Doubly lithiated **3py**. **c**, Triply lithiated **4py**. For clarity, hydrogen atoms, carbon atoms associated with coordinated THF or pyridine, solvents of crystallization, and a minor disorder component of **3py** are omitted. The molecules are shown face-on. Selected bond distance (Å) and angles (°): **a**, U1–O1 1.794(3); U1–O2 1.767(3); Li1–O1 2.060(11); O1–U1–O2 176.09(17); **b**, U1–O1 1.834(4); U1–O2 1.879(5); Li1–O2 1.927(13); Li2–O1 1.94(2); O1–U1–O2 174.82(15); Li1–O2–U1 167.3(4); **c**, U1–O1 1.894(2), U1–O2 1.859(2), O1–Li2 1.979(7), O1–Li3 1.976(7), O2–Li1 1.914(7), O1–U1–O2 174.21(10), Li1–O2–U1 169.2(3).

resonance at 92 ppm and suggests that the lithium cations are fluxional in solution. On cooling to the lowest available temperature (238 K) an additional broad new resonance at 128 ppm appears, suggesting that two lithium environments are present at the low temperature limit. The asymmetric structure observed in the ^{1}H NMR spectrum is supported by a single-crystal X-ray diffraction study of **3py** (Fig. 2), which shows that both lithium cations are four-coordinate, one bound similarly to that in **2thf** (that is, within the cleft to the *endo*-oxo) whereas the other coordinates to the *exo*-oxo with its tetrahedral coordination completed by three molecules of pyridine. The U1–O1 (1.834(4) Å) and U1–O2 (1.879(5) Å) bond distances are elongated substantially compared with those in diamagnetic **2thf** and support single-electron reduction to $[UO_2]^+$. The Fourier transform infrared (FTIR) spectrum of **3py** contains a weak and very broad band at 3,310 cm^{-1}, which could result from a pyrrole NH, and an absorption at 709 cm^{-1} assigned to the asymmetric $[UO_2]^+$ stretch, which is weakened substantially compared with that in the U(VI) starting material **1py** ($\nu_{U=O}$ = 908 cm^{-1}). The observation that treatment of the $[UO_2]^{2+}$ dication with a lithium base yields a product of single-electron reduction was a great surprise owing to the inertness of the uranyl dication and the known instability of the reduced monocation $[UO_2]^+$ towards disproportionation[13,16]. The pentavalent $[UO_2]^+$ complex **3py** was also isolated from reactions between **1py** and two equivalents of LiN^iPr_2 (LDA), LiC_5H_5, $LiCPh_3$, $LiNH_2$, or LiH in the absence of

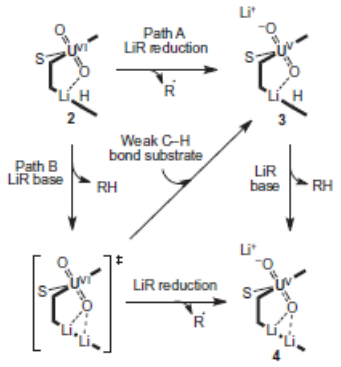

Figure 3 | Possible mechanisms that generate pentavalent uranyl $[UO_2]^+$ by reaction with a lithium reagent LiR. Two routes are proposed involving either Path A in which LiR (R = H, NH_2, N^iPr_2, $N(SiMe_3)_2$, CPh_3, C_5H_5) acts as a reducing agent or Path B in which LiR acts as a base.

DHA in essentially quantitative yield. The reactions with $LiNH_2$ and LiH initially form a mixture of **4py**, **2py** and **1py**, but on heating convert completely to **3py**. Similar reactions in THF lead to mixtures of paramagnetic products. Furthermore, reaction between $[Li_4(L)]$ and $[UO_2Cl_2(THF)_3]$ in pyridine generates **3py** slowly as the sole product at room temperature, a reaction that is accelerated by heating to 110 °C. The reaction between **1py** and two equivalents of LDA in pyridine is the cleanest reaction. Furthermore, if it is carried out at −30 °C, a new complex with C_s symmetry (identified by ^{1}H NMR spectroscopy) is isolated. As with **3py**, this new complex contains a broad paramagnetically shifted resonance at low field (86 ppm), which integrates for 1H and is probably due to an NH or OH proton, the latter suggested by C_s symmetry. It is likely that this material is an isomer of **3py** as bulk crystallization forms crystals of the same unit cell as **3py** and slow conversion into **3py** is observed in solution over prolonged periods at elevated temperatures.

Reaction of 1 with three or four equivalents of lithium base. Reaction of **1** with three equivalents of $LiN(SiMe_3)_2$ in pyridine at 25 °C rapidly affords the triply lithiated U(v) complex $[(LiOUO)Li_2L]$ **4py** (see Fig. 1). A similar reaction in THF again forms mixtures of paramagnetic compounds, but the use of four equivalents of $LiN(SiMe_3)_2$ generates the stable U(v) adduct $[R_2NLi][(LiOUO)Li_2L]$ **5thf**. Both **4py** and **5thf** are significantly more straightforward to isolate than the singly and doubly lithiated complexes, and have been fully characterized, including by X-ray crystallography (see Supplementary Information for **5thf**). In the X-ray structure of **4py**, all of the lithium cations are four-coordinate, with Li1 interacting with the *exo*-uranyl oxo atom O2, and Li2 and Li3 bound symmetrically within the cleft and to the *endo*-oxo O1. These interactions elongate the U1–O1 (1.894(2)Å) and U1–O2 (1.859(2) Å) bond distances significantly compared with **1thf**, and again support the presence of functionalized $[UO_2]^+$. A variable-temperature, solid-state magnetic study of **5thf** (see Supplementary Information) also supports the presence of a single *f*-electron and no further reduction to U(iv) (ref. 17). The FTIR spectrum of **4py** displays an absorption at 704 cm^{-1}, which is assigned to the asymmetric stretch of the $[UO_2]^+$ group[5].

Reactions to probe the mechanism of formation of the pentavalent uranyl complexes. It is clear from the above data that the sequential addition of lithium reagents to the uranyl complex **1** ultimately leads to single-electron reduction and lithium functionalization of the oxo groups. The most important mechanistic step of this process is the addition of the second equivalent of lithium reagent as this is the point at which reduction of U(vi) to U(v) occurs; as such, we have carried out a series of experiments to probe this transformation.

The reaction between **1py** and two equivalents of LDA in D_5-pyridine was monitored by ^{1}H NMR spectroscopy and cleanly generates **3py**. The N–H resonance of the by-product amine HN^iPr_2 could not be located in the ^{1}H NMR spectrum, but the ^{2}H NMR spectrum of the residues redissolved in H_5-pyridine shows that deuterium is incorporated at multiple sites in the ligand, notably at 60.1 ppm (N–H) and 1.4 ppm (a *meso*-CH_3 group). The reaction between two equivalents of LiC_5H_5 and **1py** in D_5-pyridine produces **3py** cleanly as well as two equivalents of HC_5H_5, identified by integration of the ^{1}H NMR spectrum; deuterium incorporation was observed at 1.5 ppm, corresponding to ligand deuteriation, but no radical-coupled products were present.

In contrast, the reaction between **1py** and two equivalents of $LiN(SiMe_3)_2$ forms mixtures of paramagnetic **4py** and diamagnetic **2py** and **1py** unless a substrate containing a weak C–H bond such as dihydroanthracene is present, upon which the formation of **3py** is favoured. The reaction between **1py** and two equivalents of $LiN(SiMe_3)_2$ in D_5-pyridine in the presence of DHA was monitored by ^{1}H NMR spectroscopy. Rapid and clean formation of **3py** was observed, and significantly, two equivalents of $HN(SiMe_3)_2$ were identified by integration of N–H (1.46 ppm) and $SiMe_3$ (0.08 ppm) resonances. No $DN(SiMe_3)_2$ was observed in the ^{2}H NMR spectrum. Furthermore, a stoichiometric quantity of radical-coupled 9,9′,10,10′-tetrahydro-9,9′-bianthracene is seen as the dominant hydrogen-abstracted product along with a small amount of anthracene[18,19]. With D_4-DHA in H_5-pyridine, the reaction is less clean, with the formation of a small quantity of **4py** and **3py**, but two equivalents of $HN(SiMe_3)_2$ are again seen in the ^{1}H NMR spectrum. Deuterium incorporation into **3py** was seen in the ^{2}H NMR spectrum at a few resonances corresponding to ligand deuteriation, and observation of a broad resonance at 1.46 ppm suggests that a small quantity of $DN(SiMe_3)_2$ is also formed during this reaction. The reaction between **1py** and two $LiN(SiMe_3)_2$ in D_5-pyridine in the presence of xanthene, another substrate containing a weak C–H bond, gives a more complex mixture of products, forming **4py** (13%), **3py** (55%), **2py** and **1py** (total 28%), radical-coupled xanthene (28%) and two equivalents of $HN(SiMe_3)_2$ according to integration of the ^{1}H NMR spectrum. Interestingly, equal quantities of **3py** and radical-coupled bi-xanthene arising from hydrogen abstraction are produced,

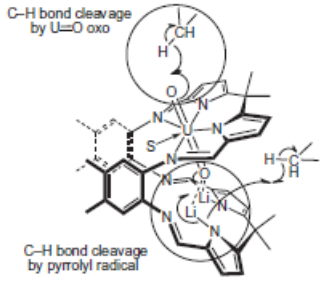

Figure 4 | Mechanistic insight into the formation of doubly lithiated uranyl complexes. Two mechanisms that involve C–H bond cleavage to form doubly lithiated **3py** are postulated and involve either the uranyl oxo group, highlighted by the upper circle, or a pyrrolyl radical, highlighted by the lower circle.

NATURE CHEMISTRY DOI: 10.1038/NCHEM.904

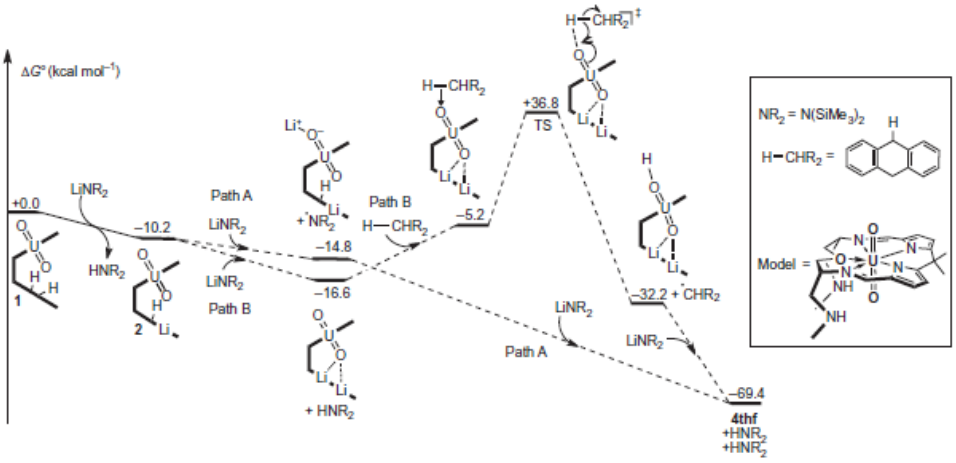

Figure 5 | Computed energy profile for the reduction and oxo-group C–H activation by a model of a Pacman uranyl complex. The calculations show that the formations of all of the lithiated uranyl complexes are exergonic and that the transition states involving oxo-group C–H activation are thermodynamically accessible. They do not show significant differences in energy between the path A and path B mechanisms. TS: transition state.

suggesting that **4py** is formed by a different mechanism to **3py**. Indeed, the reaction of **1py** with three equivalents of $LiN(SiMe_3)_2$ in D_5-pyridine produces only **4py** along with two equivalents of $HN(SiMe_3)_2$ and one equivalent of $DN(SiMe_3)_2$, identified by integration of N–H and $SiMe_3$ resonances in the ^1H NMR spectrum; the presence of $DN(SiMe_3)_2$ is supported by a resonance at 1.46 ppm in the ^2H NMR spectrum.

Plausible mechanisms that can account for the isolation of the paramagnetic doubly and triply lithiated complexes **3py** and **4py** are outlined in Fig. 3, and arise from the lithium reagent acting either as a reductant (Path A) or a base (Path B). The U(VI)/U(V) reduction potential of **1thf** in THF is −0.54 V (versus standard hydrogen electrode (SHE)), and therefore only strongly reducing lithium reagents such as lithium alkyls and hydrides would be expected to effect the direct reduction of **1py**. However, Hayton and co-workers have shown that formation of an adduct between the Lewis acid $B(C_6F_5)_3$ and one of the uranyl oxo-groups in the complex $[UO_2(Acnac)_2]$ results in a 0.57 V shift of the U(VI)/U(V) couple to a more positive potential[13]. By analogy, it is therefore likely that both the singly lithiated U(VI) complex **2py** and the postulated doubly deprotonated U(VI) intermediate $[UO_2(Li_2L)]$ are easier to reduce than **1py**. Unfortunately, we have been unable to measure with certainty the U(VI)/U(V) reduction potential of **2py** owing to reaction with the electrolyte.

If it is assumed that lithium-cation coordination to the uranyl oxo results in a shift of the reduction potential to a more positive value it is likely that LDA (oxidation potential, $E_{ox} = -0.59$ V versus SHE in THF/HMPA at −25 °C, HMPA = hexamethylphosphoramide) and perhaps LiC_5H_5 ($E_{ox} = -0.03$ V versus SHE in DMSO) are capable of reducing **2py**[20,21]. The formation of two equivalents of HC_5H_5—combined with incorporation of deuterium into the ligand in the latter reaction—can occur if the resulting cyclopentadienyl radical reacts with ligand C–H bonds within a radical cage complex.

In contrast however, the significantly more positive oxidation potential of $LiN(SiMe_3)_2$ ($E_{ox} = +0.32$ V versus SHE in THF at −25 °C)[22] combined with the observation that two equivalents of $HN(SiMe_3)_2$ are produced during the reaction suggests that $LiN(SiMe_3)_2$ is acting solely as a base. The formation of the more reducing Li(DHA) carbanion ($E_{ox} = -0.83$ V versus SHE in DMSO) during reactions in the presence of DHA is possible but unlikely as the pK_a of DHA (30.1) is significantly greater than that of $HN(SiMe_3)_2$ (25.8), and no Li(DHA) is seen in the NMR spectrum of the control reaction between DHA and $LiN(SiMe_3)_2$. The generation of triply lithiated **4py** can be explained if it is assumed that the U(VI)/U(V) reduction potential of the doubly deprotonated U(VI) intermediate $[UO_2(Li_2L)]$ has shifted to a much more positive potential (>+ 0.4 V versus SHE), upon which the addition of a third equivalent of $LiN(SiMe_3)_2$ can effect reduction. This would result in the formation of $\cdot N(SiMe_3)_2$, which in D_5-pyridine generates a mixture of $HN(SiMe_3)_2/DN(SiMe_3)_2$ in a 2:1 ratio, as is observed. The involvement of DHA or xanthene in the mechanism of formation of **3py** from **1py** is more difficult to understand, but the observation of products of hydrogen-atom abstraction suggests that cleavage of the weak C–H bond in DHA or xanthene (BDE < 80 kcal mol^{-1})[23] is an important step. Significantly, the inclusion of other benzylic substrates containing stronger C–H bonds, such as toluene (BDE = 89 kcal mol^{-1}) or cyclohexene (BDE = 85 kcal mol^{-1}), does not favour the formation of **3py** and results in the mixtures described above.

Mechanisms in which the intermediate $[U^{VI}O_2(Li_2L)]$ can cleave C–H bonds could involve the uranyl oxo-group acting in a manner similar to a transition metal, undergoing intermolecular hydrogen-atom abstraction to form U–OH. Although thermally induced C–H bond activation by uranyl is unknown, photo-excited uranyl $[^*UO_2]^{2+}$ is known to cleave C–H bonds during the photochemical destruction of hydrocarbons. Alternatively, internal reduction could occur with the formation of a pyrrolyl radical that is sufficiently reactive to abstract a hydrogen atom from the substrate (Fig. 4)[24].

In the reaction of **1py** with $LiN(SiMe_3)_2$ in the presence of D_4-DHA in H_5-pyridine, both U=O oxo and pyrrolyl radical mechanisms would be expected to result in deuterium incorporation in **3py**. The ^2H NMR spectra of these reactions show some incorporation of deuterium into ligand CH and CH_3 bonds of the macrocycle, but not clearly the expected N–H (or O–H) resonance. Furthermore, the solution structure of **3py** correlates to the solid-state structure. An oxo-mechanism, which would be expected to

form a C_s-symmetric uranyl hydroxide, therefore appears unlikely. However, it is seen that the lithium cations in **3py** exchange on the ^{7}Li NMR timescale and that intermolecular reactions between uranyl species can occur as evidenced by the conversion of mixtures of **4py**/**2py**/**1py** into **3py** at elevated temperatures. As such, we cannot rule out an oxo-based C–H bond cleavage mechanism.

A pyrrolyl radical formed through an internal reduction mechanism would result, after hydrogen abstraction, in **3py** but its formation would necessitate a shift in the U(VI)/ U(V) reduction potential to a value more positive than that of Li(pyrrolide) (E_{ox} +0.40 V versus SHE in DMSO). It is known that pyrrole anion radicals adopt a α-pyrrolenine tautomeric form, indicating that the radical should be able to delocalize throughout the pyrrole-imine framework; deuterium abstraction from the substrate may then lead to deuterium incorporation at various sites on the macrocyclic ligand as evidenced in the ^{2}H NMR spectrum. We have also found previously that the pyrrole–imine moiety can tautomerize to azafulvene-amine on metal coordination[25]. The need for a weak C–H bond is less clear in a mechanism involving internal reduction and formation of a pyrrolyl radical, as the reaction between Li_4L and $[UO_2Cl_2(THF)_3]$ in D_5-pyridine generates **3py** cleanly in the absence of DHA. However, it has been shown that rhodium-stabilized aminyl radical complexes can be isolated and react as nucleophilic radicals to abstract hydrogen atoms from substrates such as $^nBu_3SnH$ (BDE 74 kcal mol^{-1}) and PhSH (BDE 83 kcal mol^{-1}), which contain C–H bonds weaker than in the precursor amine complex (BDE 86 kcal mol^{-1})[26]. It is therefore plausible that a pyrrolyl radical generated through an internal reduction process is only weakly oxidizing and quenched by weak C–H bonds to afford **3py**.

To further investigate these mechanisms, DFT calculations were carried out and the computed steps involved in the proposed paths A and B were found to be both kinetically and thermodynamically accessible at room temperature (Fig. 5; see Supplementary Information for computational details). The reduction of **2** by $LiN(SiMe_3)_2$ (Path A) is computed to be exergonic by −14.8 kcal mol^{-1}, whereas the deprotonation route (Path B), is −16.6 kcal mol^{-1}; the differences in these values are too small to show any preference from a computational perspective. Of the two possible C–H abstraction possibilities shown in Fig. 4, the abstraction by the oxo-group from DHA has been computed and is found to be kinetically accessible with a barrier of 36.8 kcal mol^{-1}—similar to that calculated for the analogous oxo silylation process[15]. Based on the geometry (the U–O bond is still short), the transition state is best described as a proton transfer between DHA and the *exo*-oxo group of $[UO_2]^{2+}$, with the reduction of the metal occurring immediately after the proton transfer, leading to **3**. DFT calculations for the energetics of the alternative mechanism involving internal reduction and formation of a pyrrolyl radical (Path B) were not possible as they would not give the same product observed in the experiment and DFT cannot localize the electron. From **3**, the formation of the triply lithiated complexes **4** is computed to be highly favourable.

Conclusions

In the reductive uranyl silylation chemistry to make **A** we proposed that the direct interaction between the activated U(VI) complex $[UO_2(K_2L)]$ and the silyl substrate resulted in homolytic Si–N (BDE = 111 kcal mol^{-1}) or Si–C (BDE ≈ 90 kcal mol^{-1}) bond cleavage[14]. Similarly, the results presented in this work suggest that endogenous bonding of a lithium cation to the uranyl oxo group facilitates reduction chemistry. The sensitivity of this chemistry towards the lithium reagent implies that more than one mechanism operates during the formation of the singly reduced uranyl complex **3**. The lithium reagents LDA, $LiNH_2$, $LiCPh_3$, LiH or LiC_5H_5 appear to act as reductants with the release of a radical, which is quenched by the ligand through hydrogen abstraction. However, for $LiN(SiMe_3)_2$ we can eliminate this mechanism, and invoke instead hydrogen-atom abstraction by the uranyl complex, although it has not been possible to identify whether a U=O group or a ligand-centred radical in the complex cleaves the C–H bond. Unfortunately, DFT calculations have been unable to distinguish between the two mechanisms. Although the chemistry of **1** takes place in the dark, the fact that photochemically activated uranyl dications are capable of the destruction of organic compounds by hydrogen-atom abstraction[27,28] via a substrate-dependent mechanism is notable in light of these results. The contrast to the silylation chemistry observed for the doubly potassiated uranyl macrocyclic analogue suggests that the nature of the metals incorporated into the bottom pocket of the macrocycle are an important variable in expanding the scope of this reaction, and that these complexes should offer access to a wide range of new covalent bond-forming reactions of the uranyl oxo group.

Methods

Working under a dry, oxygen-free dinitrogen atmosphere, with reagents dissolved or suspended in aprotic solvents, and combined or isolated using cannula and glove box techniques, we first treated the hinged macrocydic complex $[UO_2(S)(H_2L)]$—in which one compartment binds the uranyl dication and the other still contains two pyrrolic H atoms (S = tetrahydrofuran or pyridine)—with 1, 2, 3, and 4 equivalents of lithium base. In each case, soluble, isolable complexes were formed, which contained increasing quantities of lithium cations coordinated to the uranium oxo groups. The second equivalent of base resulted in the formation of complexes in which the uranium was singly reduced. Repetition of the reaction with different bases, and in the presence of substrates with weak benzylic C–H bonds showed, by analysis of the NMR spectra, that thermal, homolytic C–H bond cleavage had occurred in the cases where a less reducing lithium base was used. All compounds were characterized by elemental analysis, FTIR spectroscopy, variable temperature magnetic moment measurements, NMR spectroscopy and single crystal X-ray diffraction studies to confirm their identity. Full details of all experiments can be found in the Supplementary Information, along with rotating images of some of the molecules. X-ray crystallographic coordinates for **2thf**, **3py**, **4py**, and **5thf** have been deposited at the Cambridge Crystallographic Database, numbers 768618, 782912, 768619 and 743941.

Received 11 March 2010; accepted 7 October 2010; published online 23 November 2010

References

1. Denning, R. G. Electronic structure and bonding in actinyl ions and their analogs. *J. Phys. Chem. A.* **111,** 4125–4143 (2007).
2. Limberg, C. On the trail of CrO_2Cl_2 and its reactions with organic compounds. *Chem. Eur. J.* **6,** 2083–2089 (2000).
3. Que, Jr L. & Tolman, W. B. Biologically inspired oxidation catalysts. *Nature* **455,** 333–340 (2008).
4. Fortier, S. & Hayton, T. W. Oxo ligand functionalization in the uranyl ion (UO_2^{2+}). *Coord. Chem. Rev.* **254,** 197–214 (2010).
5. Arnold, P. L., Love, J. B. & Patel, D. Pentavalent uranyl complexes. *Coord. Chem. Rev.* **253,** 1973–1978 (2009).
6. McCleskey, T. M., Foreman, T. M., Hallman, E. E., Burns, C. J. & Sauer, N. N. Approaching zero discharge in uranium reprocessing: photochemical reduction of uranyl. *Environ. Sci. Tech.* **35,** 547–551 (2000).
7. Renshaw, J. C. *et al.* Bioreduction of uranium: Environmental implications of a pentavalent intermediate. *Environ. Sci. Tech.* **39,** 5657–5660 (2005).
8. Fox, A. R., Bart, S. C., Meyer, K. & Cummins, C. C. Towards uranium catalysis. *Nature* **455,** 341–349 (2008).
9. Natrajan, L., Burdet, F., Pecaut, J. & Mazzanti, M. Synthesis and structure of a stable pentavalent-uranyl coordination polymer. *J. Am. Chem. Soc.* **128,** 7152–7153 (2006).
10. Mougel, V., Horeglad, P., Nocton, G., Pecaut, J. & Mazzanti, M. Stable pentavalent uranyl species and selective assembly of a polymetallic mixed-valent uranyl complex by cation-cation interactions. *Angew. Chem. Int. Ed.* **48,** 8477–8480 (2009).
11. Berthet, J. C., Siffredi, G., Thuery, P. & Ephritikhine, M. Easy access to stable pentavalent uranyl complexes. *Chem. Commun.* 3184–3186 (2006).
12. Berthet, J. C., Siffredi, G., Thuery, P. & Ephritikhine, M. Synthesis and crystal structure of pentavalent uranyl complexes. The remarkable stability of UO2X (X=I, SO3CF3) in non-aqueous solutions. *Dalton Trans.* 3478–3494 (2009).
13. Hayton, T. W. & Wu, G. Exploring the effects of reduction or Lewis acid coordination on the U=O bond of the uranyl moiety. *Inorg. Chem.* **48,** 3065–3072 (2009).
14. Arnold, P. L., Patel, D., Wilson, C. & Love, J. B. Reduction and selective oxo-group silylation of the uranyl dication. *Nature* **451,** 315–317 (2008).

15. Yahia, A., Arnold, P. L., Love, J. B. & Maron, L. A DFT study of the single electron reduction and silylation of the U–O bond of the uranyl dication in a macrocyclic environment. *Chem. Commun.* 2402 (2009).
16. Nocton, G. *et al.* Synthesis, structure, and bonding of stable complexes of pentavalent uranyl. *J. Am. Chem. Soc.* **132,** 495–508 (2010).
17. Gamp, E., Edelstein, N. M., Khan Malek, C., Hubert, S. & Genet, M. Anisotropic magnetic susceptibility of single crystal UCl_4. *J. Chem. Phys.* **79,** 2023–2026 (1983).
18. Lucas, R. L., Powell, D. R. & Borovik, A. S. Preparation of iron amido complexes via putative Fe(IV) imido intermediates. *J. Am. Chem. Soc.* **127,** 11596–11597 (2005).
19. Zdilla, M. J., Dexheimer, J. L. & Abu-Omar, M. M. Hydrogen atom transfer reactions of imido manganese(v) corrole: one reaction with two mechanistic pathways. *J. Am. Chem. Soc.* **129,** 11505–11511 (2007).
20. Bordwell, F. G., Zhang, X. & Cheng, J.-P. Comparisons of the acidities and homolytic bond dissociation energies of acidic N-H and C-H bonds in diphenylmethanes and carbazoles. *J. Org. Chem.* **56,** 3216–3219 (1991).
21. Bordwell, F. G., Harrelson, Jr J. A. & Satish, A. V. Oxidation potentials of carbanions and homolytic bond dissociation energies of their conjugate acids. *J. Org. Chem.* **54,** 3101–3105 (1989).
22. Renaud, P. & Fox, M. A. Electrochemical behaviour of lithium dialkylamides: the effect of aggregation. *J. Am. Chem. Soc.* **110,** 5702–5705 (1988).
23. McMillen, D. F. & Golden, D. M. Hydrocarbon bond dissociation energies. *Ann. Rev. Phys. Chem.* **33,** 493–532 (1982).
24. Kasai, P. H. & McLeod, D. Electron spin resonance study of heterocycles. II. Pyrrole, pyrazole, imidazole, and indole anion radicals. *J. Am. Chem. Soc.* **95,** 27–31 (1973).
25. Reid, S. D., Wilson, C., Blake, A. J. & Love, J. B. Tautomerisation and hydrogen-bonding interactions in four-coordinate metal halide and azide complexes of N-donor-extended dipyrromethanes. *Dalton Trans.* **39,** 418–425 (2010).
26. Büttner, T. *et al.* A stable aminyl radical metal complex. *Science* **307,** 235–238 (2005).
27. Jørgensen, C. K. & Reisfeld, R. Uranyl photophysics. *Struct. Bond.* **50,** 121–171 (1982).
28. McCleskey, T. M., Burns, C. J. & Tumas, W. Uranyl photochemistry with alkenes: Distinguishing between H-atom abstraction and electron transfer. *Inorg. Chem.* **38,** 5924–5925 (1999).

Acknowledgements
We thank the EPSRC(UK), EaStCHEM, the University of Edinburgh and the CEA, CNRS and UPS for support. L.M. is grateful to Institut Universitaire de France. CalMip (CNRS, Toulouse, France), CINES (CNRS, Montpellier, France) and CCRT (CEA, France) are acknowledged for calculation facilities. The authors are grateful to D. Graham, I. Lamour, R. E. Mulvey and S. Robertson for help with obtaining the Raman spectroscopic measurements.

Author contributions
A.-F.P. and E.H. synthesized and characterized the compounds, and solved the crystal structure data; A.Y. and L.M. carried out the DFT calculations; and S.J.P. solved and refined the disorder components for the crystal structure of **3py**. P.L.A. and J.B.L. generated and managed the project, helped characterize the compounds, analysed the data and wrote the manuscript.

Additional information
The authors declare no competing financial interests. Supplementary information and chemical compound information accompany this paper at www.nature.com/naturechemistry. Reprints and permission information is available online at http://npg.nature.com/reprintsandpermissions/. Correspondence and requests for materials should be addressed to P.L.A. and J.B.L.

Uranyl Reactivity

DOI: 10.1002/anie.201104359

Oxo Group Protonation and Silylation of Pentavalent Uranyl Pacman Complexes**

Polly L. Arnold, Anne-Frédérique Pécharman, and Jason B. Love**

The chemical reactivity of the oxo group of the uranyl dication, $[UO_2]^{2+}$, the most prevalent aqueous and environmental form of uranium and by far the most chemically inert, has been transformed in recent years.[1,2] For example, new routes to the singly reduced, pentavalent uranyl have been developed and have facilitated fascinating new Lewis acid–base interactions between the oxo groups and alkali metals,[3,4] boranes,[5–7] transition metals,[8] rare earth metals,[9] and other uranyl cations.[10] In some cases it is evident that oxo group functionalization can modify the U^{VI}/U^{V} reduction potential such that reduction is facilitated.[3,6,7]

While the above cation–cation interactions (CCIs) in $[UO_2]^{+}$ compounds are becoming increasingly understood, reactions of $[UO_2]^{2+}$ that result in covalent bond formation at one or both oxo groups are extremely rare and at present limited to reductive silylation that forms a UO–Si bond. We showed recently that uranyl Pacman complexes, in which the uranyl oxo groups are in different spatial environments, underwent reduction and oxo group silylation reactions on treatment with potassium bases and transition metal halides.[11,12] Subsequently, perfluoroaryl borane-functionalized uranyl complexes have been shown to undergo reductive silylation reactions with tertiary silanes,[6] while the direct reaction of uranyl complexes with Me_3SiI results in U^{V} and U^{IV} oxo-silylated complexes.[13] Furthermore, complete deoxygenation of $[UO_2]^{2+}$ can be realized by reaction with trimethylsilyl halides, forming U^{IV} halides and $(Me_3Si)_2O$, presumably through a reduced, oxo-silylated intermediate.[14] These reactions can be contrasted to those of the photochemically generated $*[UO_2]^{2+}$ ion which, in aqueous solution, can abstract an H-atom from alkanes and arenes to form carbon radicals and transient $[UO_2H]^{2+}$ which contains a new O–H bond.[15]

We recently reported the synthesis of a variety of lithium-functionalized, pentavalent uranyl Pacman complexes that result from either direct reduction of the hexavalent, uranyl Pacman complex **1** (Scheme 1) or by a C–H activation process.[3] The ready availability of the thermally stable, doubly lithiated pentavalent uranyl complex **2** has now allowed us to probe reactions at the uranyl oxo groups.

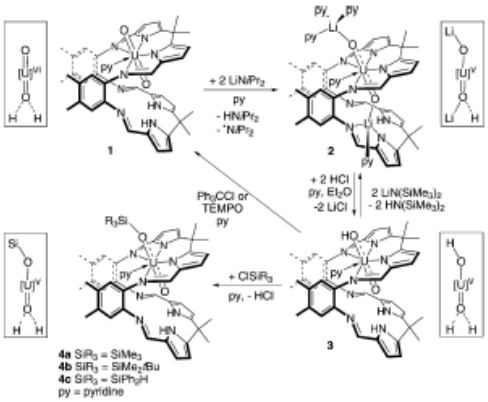

Scheme 1. Synthesis of protonated and silylated pentavalent uranyl Pacman complexes **3** and **4**.

Here we describe protonation and silylation reactions of **2** that lead to new, covalently functionalized uranyl complexes.

The reaction between **2** and two equivalents of HCl in pyridine/diethyl ether resulted in the clean formation of the protonated pentavalent uranyl complex **3** as a poorly soluble yellow-brown solid (Scheme 1). We have, as yet, been unable to crystallize **3** and unequivocally determine its structure in the solid state, but the NMR and IR spectroscopic, and microanalytical data of **3** and its deuterated analogue **[D_2]-3**, in which 2 D's are incorporated (formed from the reaction between **2** and two molar equivalents of DCl) fully support its formulation. The IR spectrum of **3** confirms the retention of the U^{V} oxidation state with a UO_2 stretch observed at 765 cm^{-1} (cf. $\nu_3 = 908$ for **1** and 709 cm^{-1} for **2**).[2] The OH and two NH groups have overlapping absorptions in the range 3378–3108 cm^{-1} (Supporting Information, Figure S1) while the NH stretch in **1** is at 3368 cm^{-1}, and in **2** is at 3310 cm^{-1}. The OH/NH absorptions shift on deuteriation to 2478–2269 cm^{-1}, in accordance with reduced mass calculated values between 2465 and 2259 cm^{-1}. Complete deuteration was not observed, and likely indicates that a H/D exchange process operates between the OH and NH protons.

The ^{1}H NMR spectrum of **3** reveals the presence of paramagnetically shifted resonances between $\delta = +90$ and -10 ppm, the number and integrals of which are consistent with the retention of a wedged, Pacman structure in solution of C_s symmetry (Figure S2). The most strongly paramagnetically contact-shifted resonance at $\delta = 86.4$ ppm integrates as a

[*] Prof. P. L. Arnold, A.-F. Pécharman, Dr. J. B. Love
EaStCHEM School of Chemistry, University of Edinburgh
West Mains Road, Edinburgh, EH9 3JJ (UK)
E-mail: polly.arnold@ed.ac.uk
jason.love@ed.ac.uk

[**] We thank the University of Edinburgh and EPSRC (UK) for funding.
Supporting information for this article is available on the WWW under http://dx.doi.org/10.1002/anie.201104359.

single proton and is assigned to the UOH group. The ^{2}H NMR spectrum of **[D$_2$]-3** shows deuterium incorporation at this resonance, and also at $\delta = 7.3$ ppm. This latter resonance is therefore assigned as pyrrolic N–D (Figure S3) and is obscured by pyridine solvent in the related ^{1}H NMR spectrum. Complex **3** is remarkably stable, showing no signs of disproportionation or decomposition in solution at room or elevated temperatures by ^{1}H NMR spectroscopy.

To confirm the pentavalent oxidation state of **3**, the stoichiometric reaction between **3** and trityl chloride was carried out [Eq. (1) and Figure S4]. The ^{1}H NMR spectrum of the reaction mixture showed a 2:1 ratio of the single-electron oxidized product **1** and Gomberg's dimer, the latter formed as a result of single-electron reduction.[16] Furthermore, reaction between **3** and TEMPO ((2,2,6,6-tetramethylpiperidine-1-yl)oxyl) cleanly regenerated **1** through H-abstraction, while reaction of **3** with two molar equivalents of LiN(SiMe$_3$)$_2$ reformed **2**. It is also clear that **3** is not a monolithiated species as no paramagnetic Li environments are seen in the ^{7}Li NMR spectrum and its reaction with two equivalents of LiN(SiMe$_3$)$_2$ generates **2** and not the triply lithiated compound [Li(py)$_3$OUO(py)Li$_2$(py)$_2$(L)] reported by us previously.[3]

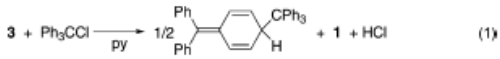

(1)

H-atom functionalization of the uranyl oxo group is important to aqueous uranyl chemistry. At high pH, equatorial hydroxide ligands are formed at $[UO_2]^{2+}$ from the five equatorially bound water ligands. The deprotonation of one equatorial OH group and proton-shuttling to an axial oxo has been suggested as key to the exchange of axial and equatorial O-ligands and suggests the existence of interesting T-shaped UO_3 and *cis*-uranyl cations, which are as yet unobserved uranium geometries.[17,18] Indeed, the spectroscopic data for **3** and its derivatives may provide insight into the speciation of complex aqueous uranyl oxo–hydroxo mixtures.[19]

Reactions between **3** and the chlorosilanes Me$_3$SiCl, *t*BuMe$_2$SiCl, or Ph$_2$HSiCl in pyridine resulted in the clean formation of the oxo-silylated products **4a**, **4b**, and **4c**, respectively (Scheme 1) and the loss of HCl to the pyridine solvent. To our knowledge, this is the first time that metathesis of a functional group that is covalently bound to the uranyl oxo has been seen. While the direct salt elimination reaction between **2** and a molar equivalent of Me$_3$SiCl resulted in the possible formation of monolithiated **4a** (by ^{1}H NMR spectroscopy), pure samples could not be isolated due to the presence of other, as yet unidentified paramagnetic complexes. As with **3**, the ^{1}H NMR spectrum of **4a** shows the presence of paramagnetically shifted resonances between $\delta = +60$ and -10 ppm, the number and integrals of which are consistent with a wedged, Pacman structure in solution (Figure S5). Significantly, the resonance at $\delta = 86.4$ ppm, assigned as the OH proton in **3**, is absent in **4a**. Furthermore, a single resonance for the SiMe$_3$ protons is seen at $\delta = 15.0$ ppm and the NH resonance has shifted from $\delta = 7.3$ in **3** to 58.1 ppm in **4a**. In the *t*BuMe$_2$Si-functionalized analogue **4b**, the SiMe$_2$ and NH protons resonate at $\delta = 14.8$ and 56.6 ppm, respectively, while the SiH and NH protons in **4c** appear at $\delta = 37.2$ and 54.1 ppm (Figure S6, S7). To confirm the assignment of the NH protons in **4a**, the reaction between **[D$_2$]-3** and Me$_3$SiCl was carried out to form **[D$_2$]-4a**, which displayed a resonance at $\delta = 58$ ppm in the ^{2}H NMR spectrum (Figure S8). In the IR spectra of **4a–c** (Figure S9, S10), U=O stretches are found between 860–823 cm^{-1} and ca. 700 cm^{-1}, respectively,[2] whilst the NH stretches are seen at ca. 3290 cm^{-1}. In order to confirm the gross structure and O–Si bond formation, crystals of **4a** and **4b** were grown and their solid-state structures determined by X-ray crystallography (Figure 1). The X-ray data for **4b** showed problems consistent with multiple twinning. As such, only the connectivity was established (Figure S11), but it is clear from these data that **4a** and **4b** have the same core structure.

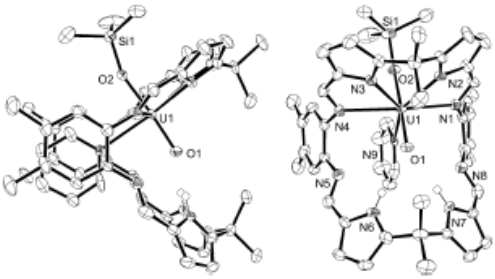

Figure 1. X-ray crystal structure of the trimethylsilylated pentavalent uranyl complex **4a**. For clarity, all hydrogen atoms except those involved in hydrogen bonding and solvent of crystallization are omitted (displacement ellipsoids drawn at 50% probability). Selected distances [Å] and angles [°]: U1–O1 1.854(4), U1–O2 2.034(4), Si1–O2 1.667(5), N6···O1 3.043(6), N7···O1 3.037(6), O1-U1-O2 176.00(19), U1-O2-Si1 160.2(3).

In the structure of **4a** the uranium adopts a distorted pentagonal bipyramidal geometry in which the oxygen ligands are linear and co-axial and the five equatorial sites are made up from the N$_4$-donor set of the macrocycle and a molecule of pyridine, sandwiched between the two macrocyclic aryl hinges. The vacant, lower macrocyclic N$_4$-donor compartment is oriented such that hydrogen bonds are evident between the pyrrole NH groups and the endogenous uranyl oxo group; the N···O separations are slightly shorter in **4a** than in the analogous U^{VI} complex **1** (N···O 3.078(3)/3.103(3) Å). It is clear from the structure that silylation has occurred and that the pentavalent uranium oxidation state is retained. The silylated oxo–uranium bond distance U1–O2 2.034(4) Å and the endogenous U1–O1 distance 1.854(4) are similar to those seen in related uranyl siloxides and pentavalent uranyl complexes (1.97 to 2.04 Å);[2,6,11,13] in contrast, U^{IV} and U^{III} siloxide bonds are significantly longer (2.06 to 2.20 Å).[20]

In summary, we have shown that it is possible to carry out new OH and OSi bond-forming reactions and interconversions from a pentavalent uranyl complex without the occur-

rence of deleterious redox processes such as disproportionation. Work is also in progress to identify whether modification of the fifth equatorial solvent site in **3** will enable us to identify possible adducts of **3** that can help better define uranyl oxo ion exchange processes.

Experimental Section

Synthetic procedures and characterizing data. **3**: To a solution of **2** (250 mg, 0.21 mmol) in pyridine was added 1.9 equivalents of HCl in Et_2O (2.0 mL, 0.4 mmol). The resulting suspension was stirred for 2 h, after which the precipitate was isolated and dried under vacuum, to afford 152 mg, 71% of **3** as a brown-yellow solid. Elemental analysis (%) for $C_{49}H_{46}N_9O_2Li_2U$, found: C 56.19, H 4.93, N 12.56; calcd: C 55.95, H 4.80, N 12.49. IR (Nujol mull): $\tilde{\nu}$ = 3376, 3189, 1623, 1600, 1583, 1288, 1265, 1218, 1103, 1045, 1020, 892, 782, 765 (UO stretch), 725, 709 cm^{-1}; ^1H NMR ([D_5]pyridine): δ_H = 86.39 (s, 1H), 32.47 (s, 3H), 13.94 (s, 2H), 10.73 (s, 3H + 2H), 5.66 (s, 2H), 3.30 (s, 3H), 2.05 (s, 2H), 1.74 (s, 2H), 0.49 (s, 6H), −1.89 (s, 2H), −2.39 (s, 6H), −2.56 (s, 2H), −3.67 (s, 2H), 7.01 (s, 3H), −8.75 ppm (s, 2H).

4a–c: To a solution of **3** in pyridine was added neat silyl chloride. The mixture was stirred for 2 h after which the suspension was filtered and the volatiles evaporated from the filtrate to afford silylated **4a–c** as brown-yellow solids.

4a: **3** (75 mg, 0.074 mmol), Me_3SiCl (9.4 μL, 0.074 mmol), Yield 63 mg, 78%. Elemental analysis (%) for $C_{50}H_{56}N_9O_2SiU$, found: C 53.28, H 4.79, N 11.93; calcd: C 55.55, H 5.22, N 11.66; IR (Nujol mull): $\tilde{\nu}$ = 3286 (NH), 1621, 1602, 1583, 1284, 1263, 1216, 1186, 1045, 1033, 1016, 894, 860 (UO stretch), 802, 781, 767, 744, 703 cm^{-1} (UO stretch); ^1H NMR ([D_5]pyridine): δ_H = 58.10 (s, 2H), 15.02 (s, 9H), 14.58 (s, 3H), 11.13 (s, 2H), 10.04 (s, 2H), 8.63 (s, 2H), 6.65 (s, 3H), 3.60 (s, 2 × 2H), 3.19 (s, 2H), 2.48 (s, 2H), 1.87(s, 2H), 0.14 (s, 6H), −0.46, (s, 6H), −2.95 (s, 3H), −8.40 ppm (s, 3H).

4b: **3** (100 mg, 0.09 mmol), $BuMe_2SiCl$ (14.9 mg, 0.09 mmol), Yield 70 mg, 63%. Elemental analysis (%) for $C_{53}H_{62}N_9O_2SiU$, found: C 56.06, H 5.69, N, 9.90; calcd; C 56.67, H 5.56, N 11.22; IR (Nujol mull): $\tilde{\nu}$ = 3290 (NH), 1622, 1583, 1282, 1263, 1217, 1182, 1047, 1020, 893, 831 (UO stretch), 769, 725, 694 cm^{-1} (UO stretch); ^1H NMR ([D_5]pyridine): δ_H = 56.56 (s, 2H), 14.79 (s, 6H), 13.33 (s, 3H), 11.00 (s, 2H), 10.09 (s, 2H), 9.23 (s, 9H), 9.01 (s, 2H), 6.26 (s, 3H), 3.60 (s, 2 × 2H), 2.98 (s, 2H), 1.28 (s, 2H), 1.09 (s, 2H), −0.16 (s, 6H), −0.38 (s, 6H), −2.80 (s, 3H), −8.59 ppm (s, 3H).

4c: **3** (75 mg, 0.074 mmol), Ph_2HSiCl (14.6 μL, 0.074 mmol), 60 mg, Yield 67%. IR (Nujol mull): $\tilde{\nu}$ = 3291, 2142 (Si-H), 1619, 1600, 1583, 1282, 1261, 1218, 1184, 1118 (Si-Ph), 1047, 1022, 894, 823 (UO stretch), 771, 734, 700 cm^{-1} (UO stretch); ^1H NMR ([D_5]pyridine): δ_H = 54.13 (s, 2H, NH), 37.21 (s, 1H, SiH), 17.65 (m, 4H, PhSi), 12.79 (s, 3H), 10.70 (s, 2H), 9.87 (m, 4H, SiPh), 9.79 (s, 2H), 9.15 (m, 2H, SiPh), 8.67 (s, 2H), 6.04 (s, 3H), 4.35 (s, 2H), 3.91 (s, 2H), 3.51 (s, 4H), 1.49 (s, 2H), 0.10 (s, 6H), −0.25 (s, 6H), −2.44 (s, 3H), −8.28 ppm (s, 3H).

Reaction between **3** and Ph_3CCl: Pyridine was added to a mixture of **3** (25 mg, 0.02 mmol) and trityl chloride (6.1 mg, 0.02 mmol) in a Teflon-tapped NMR tube at room temperature. After a few minutes the solution was dark brown. The reaction mixture was analyzed by ^1H NMR spectroscopy from which it was evident that Gomberg's dimer $Ph_2C{=}(C_6H_5)CPh_3$ and $[UO_2(py)(H_2L)]$ (**1**) had formed in a 0.5:1.0 ratio.

Received: June 23, 2011
Published online: August 26, 2011

Keywords: actinides · oxo functionalization · pentavalent uranyl · schiff-base macrocycle · uranyl hydroxide

[1] P. L. Arnold, *Chem. Commun.* **2011**, *47*, 9005; S. Fortier, T. W. Hayton, *Coord. Chem. Rev.* **2010**, *254*, 197; C. R. Graves, J. L. Kiplinger, *Chem. Commun.* **2009**, 3831.
[2] P. L. Arnold, J. B. Love, D. Patel, *Coord. Chem. Rev.* **2009**, *253*, 1973.
[3] P. L. Arnold, A.-F. Pécharman, E. Hollis, A. Yahia, L. Maron, S. Parsons, J. B. Love, *Nat. Chem.* **2010**, *2*, 1056.
[4] L. Natrajan, F. Burdet, J. Pecaut, M. Mazzanti, *J. Am. Chem. Soc.* **2006**, *128*, 7152; J. C. Berthet, G. Siffredi, P. Thuery, M. Ephritikhine, *Chem. Commun.* **2006**, 3184; J. C. Berthet, G. Siffredi, P. Thuery, M. Ephritikhine, *Dalton Trans.* **2009**, 3478.
[5] M. J. Sarsfield, M. Helliwell, *J. Am. Chem. Soc.* **2004**, *126*, 1036.
[6] D. D. Schnaars, G. Wu, T. W. Hayton, *Inorg. Chem.* **2011**, *50*, 4695.
[7] T. W. Hayton, G. Wu, *Inorg. Chem.* **2009**, *48*, 3065.
[8] P. L. Arnold, D. Patel, A. J. Blake, C. Wilson, J. B. Love, *J. Am. Chem. Soc.* **2006**, *128*, 9610.
[9] P. L. Arnold, E. Hollis, F. J. White, N. Magnani, R. Caciuffo, J. B. Love, *Angew. Chem.* **2011**, *123*, 917; *Angew. Chem. Int. Ed.* **2011**, *50*, 887.
[10] M. P. Wilkerson, C. J. Burns, H. J. Dewey, J. M. Martin, D. E. Morris, R. T. Paine, B. L. Scott, *Inorg. Chem.* **2000**, *39*, 5277; V. Mougel, P. Horeglad, G. Nocton, J. Pecaut, M. Mazzanti, *Chem. Eur. J.* **2010**, *16*, 14365; G. Nocton, P. Horeglad, V. Vetere, J. Pecaut, L. Dubois, P. Maldivi, N. M. Edelstein, M. Mazzanti, *J. Am. Chem. Soc.* **2010**, *132*, 495; G. Nocton, P. Horeglad, J. Pecaut, M. Mazzanti, *J. Am. Chem. Soc.* **2008**, *130*, 16633; F. Burdet, J. Pecaut, M. Mazzanti, *J. Am. Chem. Soc.* **2006**, *128*, 16512.
[11] P. L. Arnold, D. Patel, C. Wilson, J. B. Love, *Nature* **2008**, *451*, 315.
[12] A. Yahia, P. L. Arnold, J. B. Love, L. Maron, *Chem. Commun.* **2009**, 2402; A. Yahia, P. L. Arnold, J. B. Love, L. Maron, *Chem. Eur. J.* **2010**, *16*, 4881.
[13] J. L. Brown, G. Wu, T. W. Hayton, *J. Am. Chem. Soc.* **2010**, *132*, 7248; J. L. Brown, C. C. Mokhtarzadeh, J. M. Lever, G. Wu, T. W. Hayton, *Inorg. Chem.* **2011**, *50*, 5105.
[14] J. C. Berthet, G. Siffredi, P. Thuery, M. Ephritikhine, *Eur. J. Inorg. Chem.* **2007**, 4017.
[15] A. Bakac, J. H. Espenson, *Inorg. Chem.* **1995**, *34*, 1730; W. L. Waltz, J. Lilie, X. Xu, P. Sedlak, H. Mockel, *Inorg. Chim. Acta* **1999**, *285*, 322.
[16] P. L. Arnold, Z. R. Turner, N. Kaltsoyannis, P. Pelekanaki, R. M. Bellabarba, R. B. Tooze, *Chem. Eur. J.* **2010**, *16*, 9623.
[17] M. Bühl, G. Schreckenbach, *Inorg. Chem.* **2010**, *49*, 3821.
[18] G. A. Shamov, G. Schreckenbach, *J. Am. Chem. Soc.* **2008**, *130*, 13735; H. P. Hratchian, J. L. Sonnenberg, P. J. Hay, R. L. Martin, B. E. Bursten, H. B. Schlegel, *J. Phys. Chem. A* **2005**, *109*, 8579.
[19] K. Müller, V. Brendler, H. Foerstendorf, *Inorg. Chem.* **2008**, *47*, 10127; S. Tsushima, A. Rossberg, A. Ikeda, K. Müller, A. C. Scheinost, *Inorg. Chem.* **2007**, *46*, 10819; G. S. Groenewold, A. K. Gianotto, M. E. McIlwain, M. J. Van Stipdonk, M. Kullman, D. T. Moore, N. Polfer, J. Oomens, I. Infante, L. Visscher, B. Siboulet, W. A. de Jong, *J. Phys. Chem. A* **2008**, *112*, 508.
[20] G. Zi, L. Jia, E. L. Werkema, M. D. Walter, J. P. Gottfriedsen, R. A. Andersen, *Organometallics* **2005**, *24*, 4251; I. Korobkov, S. Gambarotta, G. P. A. Yap, *Angew. Chem.* **2002**, *114*, 3583; *Angew. Chem. Int. Ed.* **2002**, *41*, 3433; M. Porchia, N. Brianese, U. Casellato, F. Ossola, G. Rossetto, P. Zanella, R. Graziani, *J. Chem. Soc. Dalton Trans.* **1989**, 677.

